

Dankwoord

Mijn oprechte dank gaat in de eerste plaats uit naar mijn promotor Carlo. Hij heeft zonder twijfel het grootste aandeel in het helpen landen van deze thesis. Het was onder zijn impuls dat ik ben gestart als doctoraatsstudent aan de UHasselt. Ons vierjarig onderzoek heeft veel uitdagende onderwerpen opgeleverd waaraan ik met veel interesse gewerkt heb. Gaandeweg kon ik altijd beroep doen op zijn dagelijkse hulp en suggesties. Om mijn resultaten te situeren in een bredere fysieke context, kon ik steeds rekenen op zijn aanzienlijke fysieke achtergrond.

Vervolgens bedank ik graag mijn collega's van de theoretische onderzoeksgroep voor de onberispelijke werksfeer: Mieke, Gert, Christian, Tim, Stefanie, Marc. Bart, voor de samenwerking bij het geven van de lessen kwantummechanica; mijn kennis over dit vak was anders al lang teloor gegaan. Thijs, Karel en Jan, voor het nodige vertier, de hulp bij fysieke en esthetische vragen, de heftige doch verhelderende discussies, maar vooral voor het immer paraat staan als er iets geprint moest worden.

Ook enkele collega's aan andere universiteiten – Enrico, Jean-Charles, Takahiro, Michiel en Pieter – wil ik bedanken voor de productieve discussies over ons gemeenschappelijk onderzoeksdomein.

En dan is er de G6, een culinair oord van olijk jolijt, intense meningsverschillen (al dan niet oprecht), flauwe en heel flauwe moppen, merkwaardige weetjes, hachelijke weddenschappen en bijgevolg veel taart. Deze riante sfeer werd mede mogelijk gemaakt door de volgende onvergetelijke personages: Michel, Rik, Marcel, Rob, Tim, Dieter, Dorine, Robin, Cedric, Wim, René, Eli, Koen, Jarda, Sali en vele anderen.

Als laatste, maar niet als minste, wil ik mijn familie en vrienden bedanken. In het bijzonder mijn ouders, mijn zus Eef, mijn schoonbroer David en Felix, voor hun jarenlange steun, goede raad en het steevast huiselijk onthaal. San, Koen en Anne-Marie, voor de talrijke, plezierige uitstappen en avonden. En al mijn scoutsmakkers, die menig weekend erin slaagden om de maandagochtend extra moeizaam te maken.

De rekeninfrastructuur en dienstverlening gebruikt in dit werk, werd voorzien door het VSC (Vlaams Supercomputer Centrum), gefinancierd door het FWO en de Vlaamse regering – departement EWI.

Samenvatting

In deze thesis onderzoeken we de dynamica van verscheidene systemen die zich in een actief viscoelastisch bad bevinden. Wat deze baden zo interessant maakt, is hun complexiteit en het feit dat ze niet in evenwicht zijn. De complexiteit van deze baden vindt zijn oorsprong in hun viscoelastische eigenschap die, anders dan viskeuze baden, persistente beweging verhindert. Deze eigenschap komt tot stand door geheugenefecten die zowel de wrijving als de thermische agitatie, inwerkende op het systeem, beïnvloeden. Deze effecten leveren vaak anomale dynamica op; dit impliceert een deviatie van normale diffusie. Een bad dat enkel viscoelastisch is, voldoet aan de fluctuatie-dissipatie relatie. In zulk een bad zal een systeem altijd thermaliseren. De baden die wij onderzoeken zijn ook actief; hierdoor zijn ze uit evenwicht. Deze actieve eigenschap wordt gemodelleerd door stochastische krachten met een tijdsafhankelijke correlatie. Er wordt verondersteld dat deze krachten in een bepaalde, doch willekeurige, richting duwen gedurende een karakteristieke tijdsschaal. Na deze tijd veranderen ze hun richting willekeurig. Om de evolutie van het systeem te beschrijven, stellen we een veralgemeende Langevin-vergelijking voor die de gereduceerde dynamica bepaalt. De motivatie voor dit onderzoek is het vermogen van actieve viscoelastische baden om de interne vloeistof van een biologische cel te modelleren. Deze vloeistof noemt men het cytosol en is zeer complex en ongetwijfeld niet in evenwicht.

Het eerste systeem dat we bestuderen is een één-dimensionaal deeltje in een potentiaal. We beschouwen drie verschillende potentialen. De eerste is een constante potentiaal dat een vrij deeltje impliceert. We verschaffen de exacte oplossing van de veralgemeende Langevin-vergelijking en concluderen dat het vrij deeltje zowel super- als subdiffusie vertoont. We passen deze resultaten toe op experimenten van getagde deeltjes in een levende cel. We vinden dat ze, tenminste kwalitatief, de geobserveerde dynamica kunnen beschrijven. De tweede potentiaal is een kwadratische; dit resulteert in een harmonische oscillator. Opnieuw berekenen we de exacte tijdsevolutie van de dynamica maar we passen ook ons numeriek schema toe op dit systeem; hierdoor kunnen we de betrouwbaarheid van het algoritme testen. We vinden dat de initiële dynamica van de harmonische oscillator identiek is aan die van het vrij deeltje. Voor lange tijden echter, bereikt het systeem een tijdsafhankelijke toestand die een interessante afhankelijkheid van de viscoelasticiteit vertoont. De resultaten van de harmonische oscillator gebruiken we om te voorspellen hoe moleculaire motoren zich zullen gedragen in een complexe, niet-evenwicht omgeving. We vinden onder andere dat hun mobiliteit verhoogt. De derde potentiaal is een dubbele put, of met andere woorden, twee lokale minima gescheiden door een energiebarrière. De veralgemeende Langevin-vergelijking van dit systeem kan niet analytisch opgelost worden; daarom doen we volledig beroep op ons algoritme om de dynamica te bestuderen. Op basis van empirische argumenten stellen we een mogelijke uitdrukking voor die de ontsnapingsgraad in een geëquilibreerd viscoelastisch bad beschrijft. Wanneer het bad ook actief is, observeren we een interessante afhankelijkheid tussen de stationaire toestand en de viscoelasticiteit. We bespreken ook het mogelijk bestaan van een effectieve potentiaal. De ontsnapingsgraad in een niet-evenwicht bad blijkt zeer tegen-intuïtief

te zijn. We gebruiken de dubbele put als een model voor de ploidynamica van DNA-haarspelden.

Het tweede systeem dat we bestuderen is de Rouse-keten; dit is een simpel model voor een polymeer. De Rouse keten bestaat uit massa's die lineair verbonden zijn door harmonische veren. Na het bespreken van het gedrag van de keten in een viscoelastisch bad in evenwicht – de massa's vertonen drie subdiffusieve regimes – stellen we deze bloot aan twee verschillende niet-evenwichtsprocessen. Het eerste proces is een constante kracht die inwerkt op een uiteinde van de keten. Vermits deze kracht conservatief is, zal de keten na enige tijd thermaliseren. Maar kort na de activatie van de kracht, ondervindt de keten een niet-evenwichts transiënte fase. Het is deze fase die hoofdzakelijk onze interesse geniet. We observeren hoe de rotationele symmetrie van de keten gebroken wordt ten gunste van een langwerpige vorm. We leiden de evolutie van zowel de gemiddelde lengte als de specifieke trompetvorm af. We bestuderen ook hoe het krachtfrent door de keten propageert. Bij het tweede proces brengt het bad actieve fluctuaties toe aan de Rouse-keten. Vermits deze krachten niet conservatief zijn, zal het systeem zich voor altijd in een niet-evenwichtstoestand bevinden. We vinden dat het diffusieprofiel van de massa's verscheidene nieuwe regimes vertoont in vergelijking met de dynamica in een geëquilibreerd viscoelastisch bad. Deze nieuwe regimes kunnen zowel super- als subdiffusief zijn. Door de actieve krachten zal de keten eveneens zwellen; dit zwellen is sterk afhankelijk van de viscoelasticiteit van het bad. We vergelijken kwalitatief onze resultaten van de Rouse-keten met recente experimenten. Om te besluiten stellen we enkele potentialen voor die het realisme van de Rouse-keten moeten verhogen. Deze potentialen zorgen voor zelf-vermijding, eindig uitrekbare veren en buigstijfheid. Om de eigenschappen van deze complexe ketens te onderzoeken, moeten we terugvallen op simulaties vermits een analytische benadering niet voor handen is. We vinden dat de lengte-kracht relatie voor een zelf-vermijdende, eindig rekbare keten niet meer lineair is en twee verschillende regimes vertoont. Een semi-flexibele keten in een actief viscoelastisch bad heeft andere exponenten voor zijn anomale diffusie (deze kunnen deels voorspeld worden met een benaderende theorie). Naast zwellen kan een semi-flexibele keten ook krimpen in deze baden.

Om te besluiten construeren we de veralgemeende Langevin-vergelijking voor de middelste massa in een Rouse-keten. De gereduceerde dynamica die deze vergelijking inhoudt, vindt zijn oorsprong in de projectie van de vrijheidsgraden van het omringende viskeuze warmtebad en de rest van de keten op de middelste massa. Eerst overlopen we de afleiding van deze veralgemeende Langevin-vergelijking wanneer het warmtebad in evenwicht is. Daarna introduceren we twee aandrijvende processen die het systeem uit evenwicht zullen trekken. Het eerste proces is een constante kracht op de eerste massa. We vinden een uitdrukking voor de effectieve kracht op de middelste massa die resulteert uit deze perturbatie. Het tweede proces is een warmtebad dat aangedreven wordt door stochastische actieve krachten. De toevoeging van deze actieve krachten produceert een frenetieke bijdrage bij de tweede fluctuatiedissipatie relatie. Voor exponentieel gecorreleerde actieve krachten leiden we een uitdrukking in gesloten vorm af voor de frenetieke bijdrage. Deze uitdrukking is geanalyseerd voor specifieke gevallen.

Abstract

In this thesis we investigate the dynamics of various systems that reside in an active viscoelastic bath. What makes these baths particularly interesting is that they are both complex and not in equilibrium. The complexity of the baths is found in their viscoelastic nature that, other than in viscous baths, hinder persistent motion. This characteristic is achieved by memory effects that influence both the friction and the thermal agitation that the bath inflicts on the system. These effects often yield anomalous dynamics, which implies a deviation from normal diffusion. A solely viscoelastic bath obeys the fluctuation-dissipation relation. The system will, in such a bath, always thermalise. The baths we consider, however, are also active, making them a nonequilibrium environment. This active forcing is modelled by stochastic forces with a time dependent correlation. They are assumed to push in a particular, yet random, direction for some characteristic time-scale. After this time, they change their direction randomly. To describe the evolution of the system, we propose a generalised Langevin equation that governs its reduced dynamics. The motivation to study active viscoelastic baths is their ability to model the interior fluid of a biological cell. This fluid is called the cytosol and it is very complex and certainly not in equilibrium.

The first system we study is the one-dimensional particle in a potential. We consider three potentials. The first is a constant potential resulting in a free particle. We provide the exact solution to its generalised Langevin equation and conclude that the free particle displays both super- and subdiffusion. We apply these results on experiments of tracer particles inside living cells and find that they can, at least qualitatively, explain the observed dynamics. The second potential is a quadratic one, constituting to a harmonic oscillator. Again, we compute the exact time-evolution of its dynamics, but we also apply our numerical scheme on this system to check the algorithm's validity. We find that the initial dynamics of the harmonic oscillator is identical to those of the free particle. For long times however, the system reaches a steady state with an interesting dependence on the viscoelasticity. The results of the harmonic oscillator are used to predict how the behaviour of molecular motors is altered in a complex, nonequilibrium environment. We find that their mobility is increased. The third potential is a double well, i.e. two local minima separated by an energy barrier. The generalised Langevin equation of this system can not be solved analytically, we therefore relied on our algorithm to study its dynamics. On the basis of empirical arguments, we propose a possible expression for the escape rate in an equilibrated viscoelastic bath. When the bath is active, we observe an interesting dependency of the steady state probability distribution on the viscoelasticity. We also discuss the possible existence of an effective potential. The escape rate in this nonequilibrium bath proved to be non-intuitive. We use the double well as a model for the folding dynamics of DNA-hairpins.

The second system we study is the Rouse chain, it is a simple model for a polymer. It consists of beads, linearly connected by harmonic springs. After discussing how a Rouse chain behaves in an equilibrated viscoelastic bath – the beads display three subdiffusive regimes – we expose it to two different nonequilibrium processes. In

the first, we apply a constant force on one end of the chain. Because this force is conservative, the chain will thermalise after some time. But shortly after the activation of the force, the chain will experience a nonequilibrium transient phase. It is mainly this transient phase we investigate. We observe how the rotational symmetry of the chain is broken in favour of an elongated shape. We derive the evolution of both the average length and the particular trumpet shape. We also investigate how the force-front propagates the chain. In the second, the bath delivers active fluctuations to the Rouse chain. Since this is nonconservative forcing, the chain will remain out-of-equilibrium indefinitely. We find that the diffusion profile of the beads acquires several new regimes compared to the purely viscoelastic case, these new regimes are both super- and subdiffusive. Due to these active forces the chain will swell, this swelling is heavily dependent on the viscoelasticity of the bath. We qualitatively compare our results of the Rouse chain to recent experiments. To conclude, we propose some potentials to increase the realism of the Rouse chain. These include self-avoidance, finite extendible springs and bending rigidity. To investigate the properties of these more complex chains we use the algorithm since an analytic treatment is not at hand. We find that the length-force relation for a self-avoiding, finite extendible chain is no longer linear and displays two distinct regimes. A semi-flexible chain in an active viscoelastic bath has different exponents for its anomalous diffusion (which can also be partly predicted using an approximated theory). Apart from swelling, a semi-flexible chain can also shrink in these baths.

To conclude, we construct the generalised Langevin equation for the middle bead of a Rouse chain. The reduced dynamics this equation entails originates from the projection of the degrees-of-freedom of the surrounding viscous heat bath and the rest of the chain on the middle bead. We first review the derivation of this generalised Langevin equation when the heat bath is in equilibrium. Thereafter, we introduce two driving agents that will pull the system away from equilibrium. Firstly, a constant force on the first bead. We find the expression for the effective force on the middle bead resulting from this perturbation. Secondly, we consider the heat bath to be driven by stochastic active forces. The inclusion of these active forces produces a frenetic contribution to the second fluctuation-dissipation relation. When the active forces are exponentially correlated, a closed form for the expression of the frenetic contribution is derived. This expression is analysed for some specific cases.

Contents

Dankwoord	i
Samenvatting	iii
Abstract	v
Contents	vii
1 Introduction	3
1.1 Nonequilibrium statistical mechanics	3
1.2 Particles and polymers	6
1.3 Motivation for our work	10
1.4 Outline of this thesis	11
2 Generalised Langevin Equation	13
2.1 A brief history of Brownian motion	13
2.2 Langevin equation	17
2.3 Generalisation	23
2.4 Viscoelastic bath	27
2.5 Active processes	31
2.5.1 Motor-activated network	31
2.5.2 Self-propelled particle	33
2.6 Active viscoelastic bath	34
3 Numerical Algorithm	37
3.1 Coloured noise	37
3.1.1 Power-law correlated noise	38
3.1.2 Exponentially correlated noise	39
3.2 Fractional differential equation	40
4 Particle in a Potential	43
4.1 Free particle	43
4.1.1 Anomalous diffusion	44
4.1.2 Motion of tracer particles	47
4.2 Harmonic oscillator	49
4.2.1 Anomalous diffusion and steady state	50
4.2.2 Velocity correlation	57

4.2.3	Stepping of molecular motors	60
4.3	Double well	63
4.3.1	Kramers' escape rate	65
4.3.2	Anomalous escape rate	66
4.3.3	Folding of DNA-hairpins	73
5	Polymer Dynamics	79
5.1	The Rouse model	79
5.1.1	From random walk to Rouse model	80
5.1.2	Normal coordinates	84
5.1.3	Dynamic properties	87
5.2	The Rouse chain in a viscoelastic bath	91
5.3	Dragging through a viscoelastic bath	95
5.3.1	Mean position	97
5.3.2	Shape of the polymer	98
5.3.3	Mean velocity	103
5.3.4	Front propagation	105
5.4	Dynamics in an active viscoelastic bath	106
5.4.1	Anomalous diffusion	108
5.4.2	Swelling of the polymer	115
5.5	Toward a more realistic model	119
5.5.1	Potentials	120
5.5.2	Dragging a real chain	123
5.5.3	Semi-flexible polymer in an active viscoelastic bath	126
6	Generalised Langevin Equation: Middle Bead	137
6.1	System plus bead-bath	137
6.1.1	Eigenvectors of the bath-bath coupling	138
6.1.2	Normal coordinates	141
6.1.3	Overview	142
6.2	Equation of motion	143
6.2.1	Motion of the normal coordinates	143
6.2.2	Motion of the middle bead	145
6.3	Generalised Langevin equation	149
6.4	Extension to driven baths	150
6.4.1	Constant force	150
6.4.2	Active forces	151
7	Conclusion and Perspective	159
	Appendices	163
A	Functions and Transformations	163
A.1	Mittag-Leffler function	163
A.2	Gamma function	165
A.3	Beta function	167
A.4	Hurwitz zeta function	168
A.5	Polylogarithm	168

A.6 Laplace transform	169
A.7 Fractional derivative	170
B Derivation of $\langle \xi(t)\xi(0) \rangle$	172
C Velocity Correlation	174
D Thermalised Worm-like Chain	176
E Derivation of K_+	180
Publications and Presentations	183
Bibliography	185

1 | Introduction

It's the job that's never started as takes longest to finish.

John R. R. Tolkien

In this introductory chapter we give an elementary and concise background of the topics that are investigated in this document. First, we discuss the field of nonequilibrium statistical mechanics, this is the framework on which our work is build. Second, some important biological concepts are explained, they are the main subjects to which our results are applied. Then we briefly comment on the motivation for our work and why it is relevant in the context of biological physics. Lastly, the general outline of this thesis is given.

1.1 Nonequilibrium statistical mechanics

The language of this document is that of *nonequilibrium statistical mechanics*. We give here a very basic overview of this subject. A clarifying way to describe this concept, is to explain its name word by word. Starting with the last.

Mechanics

Mechanics in its classical sense (we do not consider quantum or relativistic effects) is one of the oldest topics in physics. In general, it is concerned with the motion of objects with mass subjected to external forces. Some preliminary work on falling bodies was done by Galileo Galilei in the beginning of the 17th century but the first clear theory was devised by Isaac Newton in his famous *Principia* published in 1687 [1]. In this work he formulated his three laws of motion. Perhaps the most important law is the second, it states that the mass times acceleration of an object is equal to the total force that acts upon this object. This is, in fact, a second order differential equation of the object's position. Since it dictates the evolution of this position, it is also known as an equation of motion. To solve it one needs to know, apart from the mass and total force, the initial position and momentum (or velocity) of the object. The solution is the deterministic trajectory of the object.

An easy example of this is that of a ball which is thrown in the air. If one knows all the previously mentioned parameters, with gravity and air-friction as the external

forces, then the path the ball will take and its final position on the ground can be calculated. Next, we consider a somewhat more difficult example of two objects that interact with each other, namely the Sun and the Earth. At a specific moment, they both have a well-defined position and momentum. They also pull on each other with the force of gravity. Using Newton's second law one can create a set of two coupled equations of motion that perfectly predict where the Earth will be relative to the Sun at any moment in the future¹. Now, if we add a third interacting object to this problem, say for example Earth's Moon, then it can be proven that the resulting set of three coupled equations of motion can not be solved exactly. However, the set of equations does hold all the information necessary to fully describe the system and computer simulations can extract this information. One can solve this set of differential equations numerically to very high precision. So every dynamic property of this system can be known.

A hypothetical extension to all objects in the universe was made by Pierre-Simon Laplace in 1814 [2]. He stated that "*An intellect which at a certain moment would know all forces that set nature in motion, and all positions of all items of which nature is composed, if this intellect were also vast enough to submit these data to analysis, it would embrace in a single formula the movements of the greatest bodies of the universe and those of the tiniest atom; for such an intellect nothing would be uncertain and the future just like the past would be present before its eyes.*" Such an intellect is called *Laplace's demon*, and it might appear that with the rate at which our computing power grows, mankind can eventually become such a demon. There are, however, several flaws in his hypothesis. One of which arises from statistical mechanics².

Statistical mechanics

In our discussion of classical mechanics we mentioned that a system with three interacting objects is not exactly solvable. Now imagine a volume filled with a gas. This gas consists of molecules whose number is of the order of 10^{23} . They interact with each other through non-trivial quantum mechanical effects. If a system with three planets is not exactly solvable then finding the trajectory of every molecule in a gas is certainly futile. What is more, obtaining the initial position and momentum of 10^{23} objects is an impossible task in itself. Even the most advanced computer in the future will most likely not be able to perform a simulation of such a scale. Knowing the motion of every molecule is therefore beyond our grasp but luckily this information is also not very interesting. When studying a gas, or any macroscopic system that consist of a huge number of constituents, one is mainly interested in its global characteristics, for example its temperature or pressure. The precise behaviour of the individual molecules is of less importance.

The first complete theory on this subject was fully developed in the 19th century by people such as James P. Joule, Rudolf Clausius and Nicolas L. S. Carnot to name a few. It is called *thermodynamics*. It concerns itself with the concepts of heat and temperature, and how they relate to energy and work. It does so without the assumption that matter is made up of numerous components (at that time the existence of atoms

¹This problem was in fact first worked out by Isaac Newton himself, thereby providing an exact derivation of the laws of planetary motion that Johannes Kepler found empirically. It was published in the same Principia as his three laws of motion.

²Another is the stochastic nature of quantum mechanics, unknown to Laplace at the time.

was still controversial). The laws of thermodynamics were formulated on an empirical basis and although these laws stood the test of time, they give no explanation on how the internal structure of an object gives rise to its thermal properties.

At the end of the 19th century a new theory emerged that did account for the microscopic motion of the gas molecules obeying the laws of classical mechanics. This *kinetic theory* was mainly developed by James C. Maxwell, Ludwig Boltzmann and Josiah W. Gibbs. They argued that the macroscopic observables of a system should not depend on the precise motion of every microscopic particle but rather on their average collective dynamics that obscure the microscopic features. The kinetic theory is based on the *ensemble concept*, which assumes that specific macroscopic properties can be achieved by different microscopic configurations (or micro-states). To illustrate this, imagine two glasses of water at the same temperature. The trajectories of the molecules in one glass are obviously different than those in the other glass but they still yield the same macroscopic observable, i.e. the same temperature. To put it the other way around, a system typically has countless micro-states, each of which has its own resulting macroscopic properties (or macro-state), yet many of these macro-states are very similar. The ensemble concept provides a link between the microscopic and macroscopic realms by taking averages over such an ensemble to find the thermodynamic quantities. It can also explain the fluctuations around this average value, which is something that thermodynamics does not provide. This theory is therefore called *statistical mechanics*.

The simplest way to understand the ensemble concept is through the study of isolated systems. In thermodynamics, a system is isolated when it is contained by immovable walls through which neither mass nor energy can pass. An ensemble of an isolated system whose macroscopic properties do not evolve in time is called an equilibrium ensemble¹. To grasp the concept of equilibrium one assumes that every possible micro-state is equally likely for an isolated system. The most probable resulting macro-state will then be that which has the most corresponding micro-states. For many physical systems the amount of micro-states is enormous but most of them correspond to the same macro-state (or one that is very similar). This state is called the equilibrium state. A system that starts in a micro-state that does not correspond to the equilibrium state will quickly evolve to it, because being in a corresponding micro-state is much more likely. The amount of micro-states that yield the same macro-state is characterised by a concept called *entropy*. A macro-state with many corresponding micro-states has high entropy while a macro-state with few corresponding micro-states has low entropy. This results in the second law of thermodynamics which states that the total entropy of an (isolated) system will always increase over time. The tendency to increase entropy creates an “arrow of time”: the past holds less entropy than the future. There is a sense of irreversibility in this statement, a macroscopic system that has increased its entropy will not be able to go back to its previous, low entropy, state. For example, the likeliness of your ice cream to reform in its cone after it melted on a hot day is essentially non-existing.

According to R. Ulanowicz [3], this notion of irreversibility is one of the arguments against Laplace’s demon (although perhaps the weakest), since the demon relies on the reversibility of classical mechanics. From an irreversible thermodynamic viewpoint one cannot recreate past positions and momenta from a current state.

¹For a non-isolated system to be in equilibrium, there should be no net flows of matter or energy.

Nonequilibrium statistical mechanics

From the previous discussion one can conclude that a system always goes to a state of maximum entropy, the equilibrium state. The behaviour of systems in equilibrium is well understood in the framework of 19th century statistical mechanics. Through the concept of Boltzmann statistics, where every micro-state is given a statistical weight according to its total energy, the calculation of averages is tractable.

But what about a system that is not yet in a maximum entropy state, but is still increasing its entropy? Such a system is not in equilibrium and the formalism of Boltzmann statistics can not be applied. Without such a guiding principle, the treatment of these *nonequilibrium* systems is very difficult. To this day, no unified theory, like the one for equilibrium processes, on nonequilibrium processes is at hand. While some researchers try to achieve such a theory, others investigate very specific nonequilibrium systems to explain certain phenomena. All this research is situated in the field of nonequilibrium statistical mechanics.

What makes nonequilibrium systems very attractive is that, since they increase their entropy, they have some sense of the passing of time. Whereas an equilibrium system shows no time-dependence in its macroscopic properties, a nonequilibrium system will see an evolution in its properties¹. In the natural world around us almost everything is constantly changing, nothing seems to be in equilibrium. This makes the study of nonequilibrium systems, non-trivial as it might be, truly a subject on *everyday physics*.

1.2 Particles and polymers

In this section we discuss some concepts from biology that are used throughout this work. They will always have something to do with the biological cell, whether they be the cell itself or some molecular process inside the cell. A cell (from Latin *cella*, meaning “small room”) is often called the building block of life, capable of independently reproducing itself. We give here a short impression of the cell’s make-up, more detailed information on this subject can be found in any standard textbook on cell biology (for example [4]).

The cell’s interior is protected from the outside world by a plasma membrane. This membrane also provides a way to exchange substances between the outside and inside of the cell. The cell’s interior is a very complex environment. It is filled with a gel-like medium, called the cytosol. Giving the cell structure and rigidity is the stiff cytoskeleton, which also provides internal transportation. Suspended in the cytosol, we find a whole arsenal of ions, macromolecules and organelles² fulfilling diverse tasks. The features and functions of the macromolecules is explained later. Some of the responsibilities of the organelles are the creation of chemical energy (mitochondrion), the storage of macromolecules (Golgi apparatus) and locomotion (flagellum). But the most important organelle is the cell’s nucleus. It encloses the genetic material of

¹This statement is actually not strictly true, a nonequilibrium system can also be in a steady-state. None of its properties will change but the system does possess some time-asymmetry. For example, a stream of water will flow in the opposite direction when time is reversed.

²An organelle is a functional subunit of the cell. It forms a compartment with its own membrane where it performs specific tasks. Together with the cytosol, it forms the cytoplasm.

the cell that comes in the form of *deoxyribonucleic acid* or DNA. This DNA molecule provides the blueprint of the cell, regulating almost every function and characteristic of the cell. We will soon discuss DNA in more detail.

In this document we will often use the terms *particle* and *polymer*. Sometimes we deem them to be abstract, physically idealised entities. Other times we interpret them as real biological concepts. Here we will explain how we relate these two terms to biology.

Particles

In classical physics, the term “(point) particle” is used to denote a body without spacial extension, i.e. it has zero dimensions. These point particles have a well-defined position and can have a mass and/or a charge. It goes without saying that this is an extreme idealisation, but it is often used as an approximate description for a realistic body. When the volume of a body is irrelevant for its investigated properties, this approximation is permitted. This is often the case when the body can be studied from a long distance, making it essentially point-like. Examples are the Earth in the context of the large solar system or a molecule diffusing through a gas.

Often, a biological phenomenon can be described by assuming it behaves like a point particle. For example, to investigate the diffusive properties inside a cell, experimentalists often use tracer particles. These particles can be artificial (for example silica beads) whose position can be tracked by optical measurements. Non-artificial tracer particles also exist, they are macromolecules that are fluorescently tagged. Important here is that these macromolecules have a compact global structure. It is also possible that a macromolecule has an elongated structure, such molecules will be discussed below. One can also consider the cell itself as a particle, and especially the single-celled organism called *bacteria*. When investigating how a bacteria moves through its environment, one can disregard its complex inner structure and only focus on the approximated position of the bacteria viewed as a particle.

When investigating a particle, its position is defined by three coordinates. But the evolution of coordinates can also depict something other than the position of a particle. When a chemical reaction takes place, some properties of a substance will change. This change can sometimes be represented by a one-dimensional coordinate, called a reaction coordinate. Examples of such reactions are the conformational change of a macromolecule, the production of certain substances and the (un)binding of molecules. A reaction coordinate is not always a function of time, often one measures it as a function of the free energy of the system.

Polymers

In the above discussions we often mentioned the term macromolecule. As its name suggests, it is a very large molecule, consisting of thousands of atoms or more. The most prominent macromolecules in a cell are polymers. The word polymer consists of two Greek words, *poly-* meaning “many” and *-mer* meaning “parts”. A polymer thus consists of many subunits called *monomers*. These monomers are covalently bound together through a process called polymerisation. The total number of monomers in a single polymer is called the degree of polymerisation, and can be very large, over 10^8 . The linking of monomers can be linear (i.e. one after the other) resulting in a

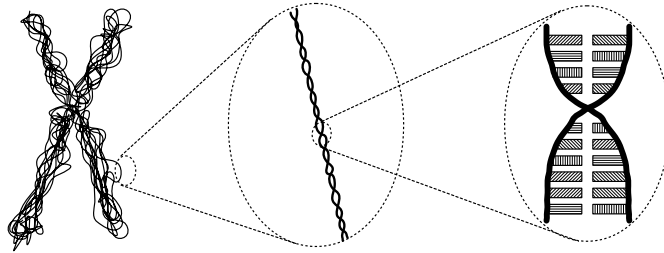


Figure 1.1: A schematic representation of the DNA polymer that zooms in on specific features of the DNA. From left to right we have: the whole chromosome (the packed version of DNA), the DNA double helix and the bonds between the two DNA strands where different nucleotides are indicated with a specific pattern.

polymer that resembles a long chain. Some polymers are non-linear, having several branch points giving them a complex geometry (we do not consider them here).

There are many man-made synthetic polymers (such as plastics), but we will not focus on them. Nature has its own set of biopolymers which are more relevant for our work. We give here the four types of biopolymers with, between brackets, the monomers that make them up. Lipids (glycerol and fatty acids), proteins (amino acids), carbohydrates (monosaccharides), nucleic acids (nucleotides). When a polymer is submerged in a liquid at a specific temperature, it does not keep an elongated structure. It collapses to a coiled-up formation, like a ball of yarn. This collapsed state is not random but depends heavily on the specific sequence of the monomers and the weak interaction between them, attracting and repulsing each other. This results in a very definite structure for all identical polymers. For a biopolymer this unique structure is essential to perform its tasks inside the cell. The ability to collapse to its natural structure depends on temperature, too high or too low temperatures are harmful for cells since its polymers will lose their structure and become idle. Clearly, understanding how a polymer behaves in a cell is a very fascinating topic. Even more so because, due to its elongated nature, a polymer has special dynamics that a simple particle does not show. Some pioneers in the field of polymer physics are Paul Flory [5], Pierre-Gilles de Gennes [6], Samuel Edwards [7] and Alexander Grosberg [8].

In this document, our main interest lies in the dynamics of proteins and nucleic acids. There exists a vast array of different kinds of protein, they perform essential and diverse actions in the cell. These include: transportation, catalysis, managing the inheritable information, etc. Because the amount of different kinds of protein is enormous, we will explain the specifics of a studied protein when we encounter it in the main text. The two most important nucleic acids are DNA (deoxyribonucleic

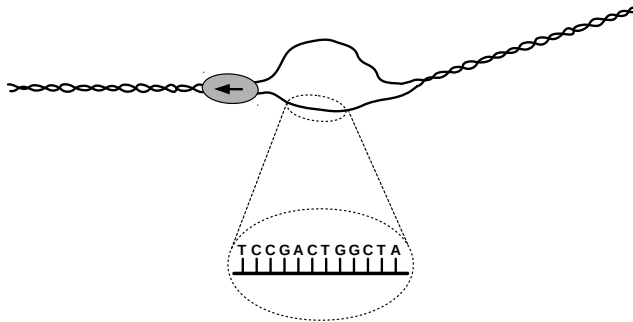


Figure 1.2: A schematic representation of how a DNA molecule is unzipped. The grey structure is a *helicase* protein that slides over the DNA molecule (indicated by the arrow) and breaks the weak bonds between the two DNA-polymer-strands. When the strands separate, their monomer sequence is exposed, as the detailed inset shows.

acid) and RNA (ribonucleic acid). Our work focusses on the dynamics of DNA, we will therefore give here a brief overview of its features.

If one had to elect a “molecule-of-life” it would, without a doubt, be DNA. This molecule holds the genetic material of an organism, called *genes*. These genes dictate all characteristics of the organism, ranging from its appearance to its behaviour, and they are inherited by the offspring of the organism¹. The discovery of DNA ended the search for the substance which guided our inheritable traits. A DNA molecule was first isolated by Friedrich Miescher in 1869. More than hundred years later, in 1953, the double helical structure of DNA was identified by James Watson and Francis Crick [10] using the *X*-ray diffractions of the molecule, provided by Rosalind Franklin. The DNA molecule actually consists of two weakly bound polymer-strands that can have a length of the order of meters. These strands are connected and winded-up along their length, giving the DNA-chain a helical structure (see Fig. 1.1). The weak (hydrogen) bonds between the DNA-polymer-strands are made by the individual monomers of each strand. A monomer of such a strand is called a *nucleotide*, it consists of a nitrogenous base, a five-carbon sugar, and a phosphate group. The latter two connect to other nucleotide monomers, creating the DNA-polymer-strand backbone. The nitrogenous base forms weak hydrogen bonds with a nitrogenous base of the other DNA-polymer-strand and holds the genetic information. Four types of nitrogenous bases exist: cytosine (C), guanine (G), adenine (A) and thymine (T). The weak links between strands only occur between cytosine and guanine or between adenine and thymine (see Fig. 1.1). This makes the two DNA-polymer-strands complementary (e.g. a sequence of $-AATGGCTGATCGTA-$ in one strand will correspond to a

¹Through random mutations during the inheritance of these genes, and the subsequent natural selection of the resulting offspring, the evolution of species [9] can occur.

sequence $-TTACCGACTAGCAT-$ in the other strand). All DNA molecules reside mostly in the cell's nucleus. The long DNA molecules can fit in this small organelle because they are neatly packed into a structure called a *chromosome* (see Fig. 1.1). This chromosome also provides the needed organisation enabling the cell to quickly access the needed instructions. To access this information, the cell uses specialised machinery that temporarily breaks the weak bonds between the DNA-polymer-strands, exposing the monomer sequence. The cell can then read out this sequence and use this information to create a specific protein that will fulfil its specialised task for the cell. The process of separating the DNA-polymer-strands is called the “*unzipping*” of the DNA, because of its resemblance to the zipper on a jacket (see Fig. 1.2). The reverse process, where the DNA-polymer-strands are rejoined, is called “*zipping*”.

From this discussion, it is clear that DNA dictates the workings of a cell and, by extension, life. Understanding the behaviour of DNA in its natural cellular environment is therefore crucial knowledge.

1.3 Motivation for our work

In this document we investigate how a particle or a polymer diffuses through an active viscoelastic bath. The detailed characteristics of such a bath are explained in the next chapter. Simply put, “active” means that some process is pulling the system out of equilibrium. And “viscoelastic” implies that the bath is a complex medium, unlike a viscous bath (like liquid water). In the case of the particle, we subject it to three different potentials and study how it behaves in each one. This model appears to be applicable to several cellular processes. For the polymer, we investigate properties that are often measured in experiments. The motivation for this work is twofold.

First, the mathematical models we construct and solve, although they are quite specific, contribute to the contemporary development of nonequilibrium statistical mechanics. We mentioned before that a general theory on this matter is still lacking. While our work will not provide such a theory, it does give an insight into the particular nonequilibrium physics of complex active systems. It builds on previous works by C. Marchetti [11], P. Hänggi [12], A. Grosberg [13], T. Sakaue [14], N. Gov [15] and A. Spakowitz [16]. Our work can be a guideline for solving similar problems or provide a background for finding a general theory for out-of-equilibrium diffusive processes. The interior of a biological cell is an excellent example of a nonequilibrium and complex environment. We use this natural system to interpret our results. This gives a means to subject them to the test of experiment. Some existing experiments that inspired our research include those of R. Di Leonardo [17], N. Fakhri [18], A. Javer [19], D. Goldstein [20] and F. MacKintosh [21].

Almost everything in our thermodynamic world is irreversible, and the most permanent to us is perhaps death. Therefore, the Darwinistic purpose of all living things is to stay alive long enough in order to produce offspring that carries on its genes. To stay alive, an organism must be capable to react to a large range of external and internal impulses. It must be able to locate food, move toward it and process it to generate energy. It should sense danger and move away from it. It needs to adapt itself in order to react to natural phenomena such as weather, diseases, etc. And it must find a suitable mate. All these things require the organism to process information and

change itself accordingly. Because systems that are in equilibrium can not change by themselves (for example rocks), a living organism must be out-of-equilibrium in order to make the necessary changes. Once it has reached a state of equilibrium, it will be dead. Therefore we can state that *life must resist equilibrium*. This statement is the second, somewhat poetic, motivation for our work. By combining the physics of nonequilibrium systems with the biology of a cell, we hope to better understand some of the processes a cell uses to stay alive. A meaningful example is the difference in activity between healthy and cancerous cells [20], which we will study in more detail.

1.4 Outline of this thesis

The structure of this thesis is as follows.

In Chapter 2, we explain the concept of the generalised Langevin equation. It is the physical framework on which we build our models. We start with a historical note on the creation of this equation. Thereafter, the original and generalised Langevin equation are discussed. Then, we point out a specific example of a generalised Langevin equation, namely that which describes a viscoelastic bath. Lastly, we introduce a relevant extension to the equation that will describe a system which is out-of-equilibrium. Throughout this chapter we illustrate how the generalised Langevin equation can be used as a model for the interior of a biological cell.

In Chapter 3, we reveal the important features of the algorithm we devised to simulate several systems that could not be solved analytically. These features are the generation of non-white noise and the integration of fractional differential equations.

In Chapter 4, we investigate the dynamics of a particle that is subjected to a potential and submerged in an active viscoelastic bath. The potentials considered are a constant potential, a harmonic oscillator and a double well. We use the results to explain some biological phenomena, including the motion of tracer particles, the stepping of a kinesin molecular motor and the folding of DNA-hairpins.

In Chapter 5, we review the construction of the original Rouse model, which is used to describe polymer dynamics. Then we study how this chain behaves in a viscoelastic bath, which mimics the natural cellular environment of a polymer. Thereafter we discuss the nonequilibrium dynamics that emerge when a Rouse chain in a viscoelastic bath is subjected to a constant force or active forces. These nonequilibrium processes should describe the natural cellular environment even better than the viscoelasticity alone. Lastly, we introduce more realistic features to the Rouse chain and numerically analyse how the previously found dynamics are influenced by these features.

In Chapter 6, we develop the generalised Langevin equation of the middle bead in a Rouse chain in a viscous bath. Once we found this equation, we examine how it changes when the heat-bath is provided with a driving agent that possibly spoils the fluctuation-dissipation relation and can pull the system away from equilibrium.

In Chapter 7, we give the concluding remarks and discuss some interesting topics that qualify for future research.

In the Appendices, we show some mathematical functions and calculations that were too lengthy to include in the main text.

We highlight here a convention we used when plotting our results. Analytically acquired results are always shown in black, while simulated data is presented in colour.

2 | Generalised Langevin Equation

One is always forced to let something to chance.

Napoléon Bonaparte

This chapter gives a concise overview of the origin and concept of the Langevin equation. We first discuss the extraordinary history of a kinetic process called Brownian motion where the Langevin equation finds its origin. Then we explain how the Langevin equation was constructed from a phenomenological perspective and its connection to the fluctuation-dissipation relation. Thereafter we reveal a more rigorous way to derive the (generalised) Langevin formalism. We consider a specific example of a generalised Langevin equation which describes a viscoelastic bath. Then, we discuss a nonequilibrium phenomenon called active processes and explain how they can be included in the Langevin formalism. To conclude, we give a summary of the characteristics of the generalised Langevin equation that describes an active viscoelastic bath. For a more complete account of the topics in this chapter we recommend the following works: [7, 22] on the Langevin equation, [23–25] on its history and [26, 27] on its generalisation.

2.1 A brief history of Brownian motion

During the 19th century the existence of the atom – and subsequently the kinetic theory of heat – was heavily disputed and generally not recognized as a reality. At best it was seen as a hypothetical entity which could indeed explain some observations but not to be preferred over the, at that time, conventional caloric theory of heat (where heat is thought of as a self-repellent fluid called *caloric* that flows from hotter to colder bodies). It is therefore striking that at the beginning of that century experiments were being performed that are now seen as one of the best illustrations of the existence of molecular motion. These experiments observed the rapid and irregular motion of minute particles (e.g. pollen) suspended in a fluid. This motion of so called “organic molecules”¹ was first attributed to a vital/biological cause by Buffon and Needham.

¹This terminology should not be confused with the modern meaning of organic molecules. Before modern biology, it was believed that plants and animals developed out of a supply of interchangeable parts, “the organic molecules”, that formed a particular organism by following an “interior mold”.

It was one of England's leading botanists Robert Brown who, in 1827, first recognised that this irregular motion was a feature of all kinds of small particles, organic and inorganic alike [28]. To prove his conjecture, he went as far as observing small fragments of the Sphinx which are clearly not alive but displayed the motion all the same. He therefore moved this topic from biology to physics. Brown himself proposed that the motion of the particles, which he called *active molecules*, finds its origin in the particles themselves and not the surrounding fluid¹. Although it was later shown that the opposite was true, his detailed work and innovative insights on the subject certainly earned him the honour of lending his name to the phenomenon. Brown's scientific nature is nicely illustrated by a recollection from the 1830's of Charles R. Darwin: "*He seemed to me to be chiefly remarkable for the minuteness of his observations and their perfect accuracy*" [29].

In the three decades that followed Brown's observations, attempts to conduct further experiments or formulate a theory were largely abandoned. Even the great founders of statistical mechanics, i.e. Rudolf Clausius, Ludwig Boltzmann and James Maxwell, appeared to not recognize the relevance of Brownian motion in the development of the kinetic theory of gases. Some early theories on the cause of Brownian motion did exist, such as unequal temperatures in the strongly illuminated water, evaporation, air currents, motions caused by the hands of the observer, heat flow, capillarity and so forth. But many of them were found to be unsatisfactory, some of them were even disproved by Brown himself.

In the second half of the 19th century, Brownian motion began to attract more researchers and its connection with heat slowly became accepted. In 1863, Christian Wiener argued that the motion was not caused by an external influence, but had to be attributed to internal motions in the fluid [30]. This was a big step in the right direction but he based his argument on the existence of *material* and *aether* atoms, causing his theory ultimately to fail. Giovanni Cantoni came perhaps closest to having discovered the true cause of Brownian motion. He also suggested that the motion was due to the thermal motions in the fluid and that it was important evidence for the mechanical theory of heat [31]. However, at the end of the century there was still no clear and quantitative theory to which experiments could be compared. Even worse, many if not all experimentalists were measuring the wrong quantity. At the time, the speed of the particle was considered to characterise its erratic motion, but none of the results agreed with the theoretical predictions of the (Waterston-Maxwell) equipartition theorem². It was up to a particularly talented theoretician to identify the relevant quantity.

There is perhaps no other physicist who had such a tremendous impact on so many different fields than Albert Einstein. During his *Wunderjahr* of 1905 he published four groundbreaking papers that cleared the way for the age of modern physics. One of these works was on the theory of Brownian motion [32] (the other three being on the photoelectric effect [33], special relativity [34] and the mass-energy equivalence [35]). It took his brilliant mind to combine two, then seemingly unrelated, topics. The first being Stokes' hydrodynamic formula for the force F on a sphere moving

¹As an interesting side note: a large part of this document concerns itself with *active particles* that do generate their own motion. Although these are not the particles that Brown studied, the similar terminology and description is striking.

²The equipartition theorem predicts: $\langle v^2 \rangle = 3k_B T/m$, with $\langle v^2 \rangle$ the particle's average velocity squared, m its mass, T the fluid's temperature and k_B the Boltzmann constant (see Section 2.2).

through a viscous fluid, i.e. $F = \gamma v$, with v its velocity and γ the friction coefficient. The second topic was van 't Hoff's law which is the thermodynamic prediction for the osmotic pressure of dissolved molecules. This law is now known as the ideal gas law, i.e. $pV = Nk_B T$, with p the osmotic pressure, V the volume, N the number of particles in the volume, k_B the Boltzmann constant and T the temperature. Einstein argued that no distinction should be made between the "invisible" fluid particles and the visible suspended particle regarding this osmotic pressure. By applying these theories on the motion of the suspended particle he was able to express the diffusion constant in terms of the temperature and the friction coefficient. What he found was

$$D = \frac{k_B T}{\gamma}. \quad (2.1)$$

Today we call this the Einstein or Einstein-Smoluchowski relation. He then went on to derive the diffusion equation which he applied to a single particle, assuming the particles do not influence each other. From this he found the probability distribution of finding the particle at location x at time t . He concluded that, on average, the particle is found at its initial location x_0 but its mean-squared displacement from it is non-zero and scales linearly with time

$$\langle (\Delta x)^2 \rangle = 2Dt, \quad (2.2)$$

where $\Delta x = x - x_0$. His theory thus predicted that the kinetic theory was capable to describe Brownian motion. Max Born declared that Einstein's work did "*more than any other work to convince physicists of the reality of atoms and molecules, of the kinetic theory of heat, and of the fundamental part of probability in the natural laws*" [36]. What is even more remarkable in all this, is that Einstein admittedly had never even observed Brownian motion himself. Along with his theory, he provided an answer to the essential question of what should be measured in an experiment on Brownian motion. The answer: the particle's mean-squared displacement, not its velocity!¹ To give credit where credit is due, five years prior to Einstein's paper, Louis Bachelier, doctoral student of Henri Poincaré, already modelled Brownian motion. In his PhD thesis "*The Theory of Speculation*" from 1900 [38], he used Brownian motion to investigate the movement of the stock exchange. His work remained unnoticed for several decades before Andrey Kolmogorov recognized its pioneering significance.

Although Einstein's paper was revolutionising, being quite abstract and based on the not yet widely known statistical mechanics, the appreciation for it was at first relatively low. In later papers Einstein clarified his reasoning for a wider audience, but the year after his first paper on the subject Marian von Smoluchowski published his approach to the problem [39]. His derivation was based on combinatorics and the mean-free-path approximation of kinetic theory, it was therefore considered more direct, simpler and more convincing. He nevertheless came to the same conclusions as Einstein. Smoluchowski's main point was to correct the conventional believe that collisions from all sides average out and can therefore not be able to generate Brownian motion. He argued that these collisions in fact advocate for the observable and

¹The reason why the measured velocity deviated so strongly from the equipartition theorem was because the true velocity between collisions is obscured by the perpetual change in the particle's direction due to the all-direction bombardment of the fluid on a longer time-scale. Measurements on a short enough time-scale were not possible in those days. Recently however, these experiments were successfully performed, showing agreement with the equipartition theorem [37].

irregular motion of the particle. Although not in his 1906 paper, the Smoluchowski equation is a widely used generalisation of the diffusion equation for describing a particle performing Brownian motion. It reads

$$\frac{\partial \Psi}{\partial t} = \frac{\partial}{\partial x} \left(D \frac{\partial \Psi}{\partial x} + \frac{1}{\gamma} \frac{\partial U}{\partial x} \Psi \right), \quad (2.3)$$

where $\Psi(x, t)$ is the probability distribution that a particular particle is found at point x at time t . The function $U(x)$ is an external potential on the particle which, for the original Brownian motion, is equal to zero.

Arguably the most comprehensible formulation of Einstein's theory was proposed by Paul Langevin in 1908, calling it himself "*infinitely more simple*" [40]. He derived the equation of motion for the Brownian particle which provided a more dynamical point-of-view for the Brownian motion. He achieved this by applying Newton's second law, where the mass m times the acceleration of the particle should be equal to the total force acted upon it. First he considered this force to be Stokes' friction force also used by Einstein, which is a systematic interaction between the particle and the fluid. In one dimension it is proportional but opposite to the velocity of the particle with the friction coefficient as the proportionality constant, i.e. $-\gamma v$. Then he argued that due to the irregular impacts of the surrounding molecules this systematic friction force is only a mean and that the true value should fluctuate around this value. He therefore formulated the equation of motion in the direction x as follows

$$m \frac{d^2 x}{dt^2} = -\gamma \frac{dx}{dt} + X. \quad (2.4)$$

The complementary force X , he argued, is indifferently positive and negative. Its magnitude should be so that it represents the constant agitation of the particle which would die out due to the friction force alone. The above expression is now known as the Langevin equation. Langevin himself used it to calculate the mean-squared displacement of the particle, confirming the result Einstein found three years earlier. The term X is now known as a stochastic variable because of its constant fluctuation. Having written down the first stochastic differential equation, makes Langevin also the founder of that mathematical topic.

As mentioned before, the first quantitative experiments on Brownian motion attempted to measure the velocity of the particle and compare it to the equipartition theorem. But because the path of the particle is not smooth, differentiating with respect to time will not yield the correct velocity. After the theoretical treatment of Einstein and Smoluchowski and later Langevin, it was clear that the mean-squared displacement of the particle was the relevant quantity that should be measured. Initial experiments by Svedberg [41] and Henri [42] showed that indeed the mean-squared displacement scaled linearly with time, but the diffusion constants they found did not agree with the theoretical prediction. The pivotal experiments on the subject were done by Jean Perrin in 1908. Earlier, he had expressed interest in Brownian motion by giving a lecture on how this phenomenon revealed the limits of the second law of thermodynamics on small scales. But it was after a presentation of Langevin in 1908, that Perrin got determined to verify the theory of Brownian motion experimentally. Perrin later recalled: "*ever since I became, through M. Langevin, acquainted with the theory, it has been my aim to apply to it the test of experiment*". He proposed that the

main point of failure of the previous experiments was the validity of Stokes' law. Perrin therefore first thoroughly tested that Stokes' law did apply to the small particles of gamboge he used [43]. At last, he and his students found that their experiments completely agreed, within the error margin, with Einstein's theory [44]. To fit the acquired data, they took $N_A = 64 \cdot 10^{22}$ for Avogadro's number which came quite close to the today's accepted value of $N_A \approx 60 \cdot 10^{22}$. Perrin's efforts in popularising his results dealt the defining blow to the caloric theory of heat from which it never recovered. His experiments marked the advent of the universal acceptance of *atomism*. For his achievements, he was awarded the Nobel Prize for Physics in 1926.

We end this account on the history of Brownian motion with a perspicuous summary formulated by Ralph Fowler (1929) on the main insights the early research on Brownian motion provided: *“By the study of suitable particles suspended in a fluid (1) we can see the manifestations of the molecular motions going on before our eyes, (2) we can check the assumptions of statistical mechanics in a rather detailed way by proving that the characteristics of the Brownian movement agree with the demands of the theory, and (3) we obtain a direct, though not very accurate method of measuring molecular magnitudes.”* [45]

2.2 Langevin equation

The Langevin equation was first formulated by Paul Langevin (see Fig. 2.1) in 1908 as a simplified version of Einstein's theory on Brownian motion (see Section 2.1). Here we will discuss the construction and consequences of this equation. Our argumentation is closely related to the original paper by Langevin [40], but we do adopt a more modern notation (and sometimes interpretation) of the subject.

The Langevin equation provides the equation of motion of a minute particle of mass m suspended in a fluid. It does so by evaluating the Newton's second law of motion where the mass times acceleration is equal to total force acted upon the object

$$m \frac{d^2 \vec{x}}{dt^2} = \vec{F}_{tot}(t), \quad (2.5)$$

where $\vec{x}(t)$ indicates the evolution (through time t) of the location of the particle in three dimensions. This equation conveys the need to identify all the forces that contribute to \vec{F}_{tot} . First, we discuss the forces originating from the interaction of the particle with its surrounding fluid (which also consists of smaller particles, i.e. molecules). These *internal* forces can be subdivided into two classes: the systematic force $\vec{f}_{sys}(t)$ and the fluctuating force $\vec{\xi}_T(t)$.

The systematic force comes from the head-on collisions the particle experiences when moving through the fluid molecules. The most elementary formula for this force is Stokes' law, which assumes the friction force to be proportional to the particle's velocity $\vec{v} = d\vec{x}/dt$ but points in the opposite direction

$$\vec{f}_{sys}(t) = -\gamma \vec{v}(t), \quad (2.6)$$

where γ is the friction coefficient. For a spherical particle in a viscous fluid we have $\gamma = 6\pi\eta R$, with η the viscosity of the fluid and R the radius of the particle. If this friction force was the only contribution to the total force, it would gradually “absorb”



Figure 2.1: Paul Langevin (1872-1946). Photograph by Henri Manuel.

the particle's initial velocity and the particle would eventually grind to a halt. This is not what is observed from a Brownian particle. What is more, the equipartition theorem would be violated because in equilibrium we should find $\langle \vec{v}^2 \rangle = 3k_B T/m$, where k_B is the Boltzmann constant and T the temperature of the fluid. (In this work, $\langle \cdot \rangle$ always stands for an ensemble average of the quantity between the brackets.)

Keeping the system "alive" is the fluctuating force¹. It represents the perpetual and (approximately) uncorrelated impacts of the fluid molecules on the particle. They come from all directions and have different magnitudes. The fluctuating force is therefore modelled by a random function. Because it is not influenced by the state of the particle, nor the collisions that happened in the past we call it *Markovian*. In other words, this force has no "memory"². Due to these characteristics we will draw the fluctuating force from a Gaussian distribution with zero mean and variance $2S$. The value S determines the characteristic strength of the impacts. We therefore have

$$\langle \vec{\xi}_T(t) \rangle = 0, \quad (2.7)$$

$$\langle \vec{\xi}_T(t) \cdot \vec{\xi}_T(t') \rangle = 2S\delta(t-t'). \quad (2.8)$$

The second line is the autocorrelation of the fluctuating force which reflects the fact that the collisions are not related at different times. The function $\delta(t)$ represents the Dirac delta function. Because both the systematic force and the fluctuating force find their origin in the fluid, we will later reveal that these forces are indeed coupled.

The other contribution to the total force is a possible *external* influence $\vec{f}_{ext}(t)$. This could be, for example, gravity that pulls on the particle or an optical trap which restricts the particle's movement. If this external force is conservative it can be derived from a potential $U(\vec{x})$ acting on the particle as a function of its position

$$\vec{f}_{ext}(t) = -\vec{\nabla}U, \quad (2.9)$$

with $\vec{\nabla}$ the gradient operator. To obtain ordinary Brownian motion, this potential should be equal to zero.

All the contributions to the total force are now known: $\vec{F}_{tot} = \vec{f}_{ext} + \vec{f}_{sys} + \vec{\xi}_T$. If we put this into the equation of motion, Eq. (2.5), we arrive at

$$m \frac{d^2 \vec{x}}{dt^2} = -\vec{\nabla}U - \gamma \frac{d\vec{x}}{dt} + \vec{\xi}_T(t), \quad (2.10)$$

this is the famous Langevin equation. It is a stochastic differential equation for the position of the particle. Without knowing the expression of $U(\vec{x})$ we can not solve this equation. For the remainder of this section, we assume the external potential to be constant, i.e. $U = \text{constant}$. If the equation is then solved for the velocity $\vec{v} = d\vec{x}/dt$, we find

$$\vec{v}(t) = \vec{v}(0)e^{-\gamma t/m} + \frac{1}{m} \int_0^t d\tau \vec{\xi}_T(\tau) e^{\gamma(\tau-t)/m}. \quad (2.11)$$

¹This force goes by many names, it is also called random force, stochastic force or, simply, noise.

²This is only an approximation because the fluid molecules and the particle do, in fact, all influence each other, especially on very short time-scales. Later we will introduce memory effects to the fluctuating force, making it *non-Markovian* (see Section 2.3).

A particle in equilibrium should obey the equipartition theorem, we will shortly discuss this theorem in full. In short, it predicts the value of the average squared velocity of the particle (in equilibrium). It is therefore instructive that we take the square and ensemble average of the above expression. We use Eq. (2.8) and the fact that $\vec{v}(0)$ and $\vec{\xi}_T(t)$ are mutually uncorrelated. After some straightforward calculations one finds

$$\langle \vec{v}^2(t) \rangle = \langle \vec{v}^2(0) \rangle e^{-2\gamma t/m} + \frac{S}{\gamma m} \left[1 - e^{-2\gamma t/m} \right]. \quad (2.12)$$

We now briefly deviate from our discussion of the Langevin equation to give a short overview of theory behind the equipartition theorem.

Equipartition theorem

As its name already suggests, the equipartition theorem states that, in thermal equilibrium, the energy is equally distributed among its various forms. It relates the temperature of a system with the average value of its energy. The system can be a large collection (e.g. a gas) or a particular part (e.g. a single particle). The theorem can make a quantitative prediction when the system has a generalised degree-of-freedom which occurs in the Hamiltonian only as a square term. Then this energy term makes a $k_B T/2$ contribution to the mean energy of the system. The Hamiltonian can here be understood as the function that defines the total energy (potential plus kinetic) of the system.

This claim can easily be proven. Take λ to be a degree-of-freedom of the system (it can be a position or momentum coordinate). When a system is in thermal equilibrium it obeys Boltzmann statistics. The probability distribution $P(\lambda)$ for finding the system between λ and $\lambda+d\lambda$ is given by its Boltzmann factor divided by the partition function

$$P(\lambda) = \frac{e^{-\beta H(\lambda)}}{\int d\lambda e^{-\beta H(\lambda)}}, \quad (2.13)$$

where $\beta = 1/k_B T$ is the inverse temperature and the integration range is (always) from $-\infty$ to ∞ . The Hamiltonian H should be a quadratic function of λ

$$H = A\lambda^2 + H', \quad (2.14)$$

where A and H' do not depend on λ , but can depend on other coordinates. Using this Hamiltonian in Eq. (2.13) produces a Gaussian distribution for $P(\lambda)$, peaked around $\lambda = 0$. The average value for the quadratic energy term is thus

$$\langle A\lambda^2 \rangle = \int d\lambda A\lambda^2 P(\lambda) = \frac{\int d\lambda A\lambda^2 e^{-\beta(A\lambda^2 + H')}}{\int d\lambda e^{-\beta(A\lambda^2 + H')}}. \quad (2.15)$$

This expression can be rewritten as a derivative to the inverse temperature

$$\langle A\lambda^2 \rangle = -\frac{\partial}{\partial \beta} \ln \int d\lambda e^{-\beta A\lambda^2} = -\frac{\partial}{\partial \beta} \ln \sqrt{\frac{\pi}{\beta A}}. \quad (2.16)$$

From this relation we can obtain the result which we call the equipartition theorem

$$\langle A\lambda^2 \rangle = \frac{k_B T}{2}. \quad (2.17)$$

Of course we assumed here that all the other coordinates (all but λ) were kept constant, because A can depend on them. But since the result is independent of A , we can assume that it is the average of $A\lambda^2$ over the total probability distribution.

We can obtain an especially interesting relation when we apply the equipartition theorem to the kinetic energy of a particle. The kinetic contribution to the Hamiltonian of a particle is $mv^2/2$ with $v^2 = v_x^2 + v_y^2 + v_z^2$. Plugging this into Eq. (2.17), we easily find

$$\langle v^2 \rangle = \frac{3k_B T}{m}. \quad (2.18)$$

This implies that, in thermal equilibrium, a heavier particle has a lower average speed than a lighter particle. We can also state that the average total kinetic energy of an ideal gas of N particles is $3Nk_B T/2$.

Fluctuation-dissipation relation

Now we return to our discussion of the Langevin equation and its special relation with the (second) fluctuation-dissipation relation [46, 47]. Most generally, the fluctuation-dissipation relation states that for a system that obeys detailed balance¹, the linear response of it to an external perturbation is equivalent to a small and spontaneous fluctuation away from thermal equilibrium. Or to put it in other words, when there is a process that dissipates energy from the system into heat, there is a (related) reverse process that, with thermal fluctuations, delivers energy to the system.

Now we derive the relationship between the Langevin equation and the fluctuation-dissipation relation. For this, we take the long time limit, $t \rightarrow \infty$, of the mean-squared velocity of the Brownian particle, i.e. Eq. (2.12). We find that this quantity approaches a constant

$$\lim_{t \rightarrow \infty} \langle \bar{v}^2(t) \rangle = \frac{S}{\gamma m}. \quad (2.19)$$

Because of the long time limit, the system will surely have reached thermal equilibrium. We can therefore apply the equipartition theorem, Eq. (2.18), to the average squared velocity. From this we find a formula for the strength of the fluctuating force

$$S = 3\gamma k_B T. \quad (2.20)$$

This is the fluctuation-dissipation relation for Brownian motion. We already mentioned that the systematic force and the fluctuating force are related, and now we have proven it. That is because γ is a characteristic of the friction force which now also appears in the collision force. The fact that they are related is perhaps not surprising because they both originate from the same process, namely the interaction of

¹Simply put, detailed balance means that for a system in equilibrium, all elementary processes are equilibrated by their reverse process.

the particle with the surrounding fluid molecules. Also notice that the strength of the collisions are related to the temperature of the fluid. The higher the temperature the harder the impacts, which is quite obvious since the temperature is a measure for the average velocity of the particle. Therefore we will often refer to $\vec{\xi}_T$ as the thermal force, hence the subscript T . To be complete we give here again the statistical characteristics of the thermal force in their final form

$$\langle \vec{\xi}_T(t) \rangle = 0, \quad (2.21)$$

$$\langle \vec{\xi}_T(t) \cdot \vec{\xi}_T(t') \rangle = 6\gamma k_B T \delta(t - t'). \quad (2.22)$$

Remember that $\vec{\xi}_T$ is Gaussian distributed, so the first and second moment, given above, fully describe this thermal force. In terms of the general concept of the fluctuation-dissipation relation, one can state that the friction the particle experiences dissipates energy into heat, while the thermal fluctuation maintain the perpetual Brownian motion of the particle, effectively converting heat into kinetic motion.

Langevin's derivation of Einstein's result

Here we will show how Langevin used his formula to derive the Einstein relation for the mean-squared displacement of a Brownian particle, Eq. (2.2). For this we will use the one dimensional version of the Langevin equation, Eq. (2.10). For Brownian motion we also should take $U = 0$. This equation, multiplied by x , may be written as

$$\frac{m}{2} \frac{d^2 x^2}{dt^2} - mv^2(t) = -\frac{\gamma}{2} \frac{dx^2}{dt} + x\xi_T(t), \quad (2.23)$$

with $v = dx/dt$. Now we take the ensemble average of this expression. The average of $x\xi_T$ is evidently zero, because the location of the particle is uncorrelated with the thermal force. Or to put it differently, if the particle moved a certain positive distance, there is not reason why the thermal force should also be in that direction. Taking $z = \langle dx^2/dt \rangle$, we can write

$$\frac{m}{2} \frac{dz}{dt} - k_B T = -\frac{\gamma}{2} z, \quad (2.24)$$

here we also used the (one-dimensional) equipartition theorem on the average squared velocity, i.e. Eq. (2.18). The general solution to this differential equation is

$$z(t) = \frac{2k_B T}{\gamma} + c e^{-\gamma t/m}, \quad (2.25)$$

with c the constant of integration. This solution enters a constant regime for times where Brownian motion is observable. This constant is equal to the first term of the right-hand side. One therefore has in thermal equilibrium

$$\left\langle \frac{dx^2}{dt} \right\rangle = \frac{2k_B T}{\gamma}. \quad (2.26)$$

Hence, for a time interval t we find

$$\langle x^2 \rangle - \langle x_0^2 \rangle = \frac{2k_B T}{\gamma} t, \quad (2.27)$$

with x_0 the particle's initial position. He then argued that the displacement Δx , given by $x = x_0 + \Delta x$, is indifferently positive and negative, therefore $\langle x_0 \Delta x \rangle = 0$. Langevin was then able to retrieve the relation that Einstein derived:

$$\langle (\Delta x)^2 \rangle = \frac{2k_B T}{\gamma} t = 2D t. \quad (2.28)$$

Overdamped limit

The last thing we will discuss here is the overdamped limit of the Langevin equation. The overdamped Langevin equation is an approximation of the original equation where one assumes that the mass of the particle is very small and/or the friction is very large, i.e. $m/\gamma \ll 1$. The inertia term drops out of the Langevin equation, Eq. (2.10), and it becomes

$$\gamma \frac{d\vec{x}}{dt} = -\vec{\nabla}U + \vec{\xi}_T(t), \quad (2.29)$$

By taking this limit, the velocity of the particle is thermally relaxed at all time. Yet the equipartition theorem, Eq. (2.18), appears to become nonsensical. However, while the mass goes to zero, the average squared velocity becomes infinite. This implies that the mean kinetic energy can still be finite and equal to $3k_B T/2$. This approximation is mostly suitable for the motion in a fluid with a low *Reynolds number*. This number is the ratio of the inertial forces to viscous forces. At the scale of a Brownian particle a fluid is often characterised by a low Reynolds number [48], which results in a smooth laminar fluid flows (high Reynolds number fluids produce turbulent flows).

2.3 Generalisation

Until now we have focussed on Langevin's original formulation which is based on phenomenological arguments. The friction and fluctuating force in his equation of motion, Eq. (2.10), originate from an understanding of how the fluid molecules behave collectively. Yet the true dynamics of the particle depend on its explicit interaction with every fluid molecule. The number of molecules in a typical fluid suspension is of the order of 10^{23} , writing down every interaction is an impossible task and the subsequent set of equations would not even be analytically solvable anyway. There is however a path we can take that leads from a full description of a complex many-body system to the final equation of motion of a single component without the need to keep track of all other components. This assumes that one can project the dynamics of fast evolving variables onto the subspace of one (or several) slowly evolving variable(s). This process involves integrating out the degrees-of-freedom of these fast variables in favour of those of the slow variables, effectively creating the *reduced dynamics* of the slow variable. In the case of a Brownian particle, the slow variable is obviously the position and velocity of the particle and the fast variables are the positions and velocity of all the fluid molecules. When one acquires the equation of motion via this route, it is known as a *generalised Langevin equation*. We will see that, equating the Newtonian inertial term, it will typically produce three effective forces: the derivative of a mean force's potential, a random force and a friction force, the latter two forces

are almost always memory dependent. This all sounds promising but, as is often the case in physics, this projection is only exactly solvable for some very specific and simple systems. However, the general idea behind the generalised Langevin equation provides us with a new view on the original Langevin equation and its applicability to different systems, other than a particle suspended in a viscous fluid.

To illustrate how a generalised Langevin equation can be constructed, we will briefly discuss a simple example where the projection of the degrees-of-freedom can be performed completely, the system is called *Brownian motion in a harmonic oscillator bath* or Caldeira-Leggett model [49]. This model was initially introduced by R. Feynman and F. Vernon as a model for quantum dissipation [50]. In Chapter 6 we will discuss in more depth another example where a generalised Langevin equation can be obtained. The system we will consider here assumes that the particle of interest, referred to as the *system*, is connected to all the bath particles via harmonic springs. Every bath particle is also connected by a harmonic spring to all other bath particles. We will characterise the system, with mass m , by its coordinate x and its conjugate momentum p . The bath, of masses m_i , is described by the set of coordinates x_i and their conjugate momenta p_i . The full Hamiltonian H is given by the sum of the system's Hamiltonian H_s plus the bath Hamiltonian H_b plus the system-bath coupling Hamiltonian H_c , i.e. $H = H_s + H_b + H_c$.

Deriving these Hamiltonians is quite elaborate, two important techniques are applied. First, the fact that the potential of the harmonic springs is purely quadratic significantly simplifies the problem. One can construct a matrix that defines the interaction between all particles. Second, changing the bath coordinate system using a linear combination of the original coordinates will diagonalise the interaction matrix. The coupling between the new coordinates has no cross-terms, apart from the cross-coupling with the system and new bath coordinates. The self-interaction of these coordinates is characterised by the eigenvalues of the matrix. This new coordinate system is used in further calculations (because of the linear relation between the two coordinate systems, going back to the original coordinates is straightforward. We therefore keep the notation x_i for the new bath coordinates). One can find the full derivation in [27] or read Chapter 6 for a very analogous version of the derivation. The final result for the system's Hamiltonian is

$$H_s = \frac{p^2}{2m} + U(x), \quad (2.30)$$

where $U(x)$ is an arbitrary external potential on the system alone, it is present even without the bath. The bath Hamiltonian is

$$H_b = \sum_i \left[\frac{p_i^2}{2m_i} + \frac{m_i \omega_i^2}{2} x_i^2 \right], \quad (2.31)$$

where the sum is always over all the bath particles. The Hamiltonian that characterises the coupling between the system and the bath is

$$H_c = x \sum_i \epsilon_i x_i. \quad (2.32)$$

Notice that this Hamiltonian implies a bilinear interaction between the system and the bath. The frequency of the i^{th} oscillator is given by ω_i and ϵ_i characterises the

strength of the coupling with this oscillator. The equations of motion for the full Hamiltonian H can be found using Hamilton's equations

$$\frac{dx}{dt} = + \frac{\partial H}{\partial p} = \frac{p}{m}, \quad (2.33)$$

$$\frac{dp}{dt} = - \frac{\partial H}{\partial x} = - \frac{dU}{dx} - \sum_i \epsilon_i x_i, \quad (2.34)$$

$$\frac{dx_i}{dt} = + \frac{\partial H}{\partial p_i} = \frac{p_i}{m_i}, \quad (2.35)$$

$$\frac{dp_i}{dt} = - \frac{\partial H}{\partial x_i} = -m_i \omega_i^2 x_i - \epsilon_i x. \quad (2.36)$$

These equations can be coupled into a set of second-order differential equations

$$m \frac{d^2 x}{dt^2} = - \frac{dU}{dx} - \sum_i \epsilon_i x_i, \quad (2.37)$$

$$m_i \frac{d^2 x_i}{dt^2} = -m_i \omega_i^2 x_i - \epsilon_i x \quad \forall i. \quad (2.38)$$

Assuming that the evolution of the system $x(t)$ is known, one can easily solve the second set of differential equations using Laplace transforms (see Appendix A.6). Also applying integration by parts, to obtain a more pleasing form, one arrives at

$$\begin{aligned} x_i(t) = & x_i(0) \cos(\omega_i t) + p_i(0) \frac{\sin(\omega_i t)}{m_i \omega_i} - \frac{\epsilon_i}{m_i \omega_i^2} (x(t) - x(0) \cos(\omega_i t)) \\ & + \frac{\epsilon_i}{m_i \omega_i^2} \int_0^t d\tau \frac{p(\tau)}{m} \cos(\omega_i(t - \tau)). \end{aligned} \quad (2.39)$$

Substituting this equation into Eq. (2.37), we find an expression of the following form

$$m \frac{d^2 x}{dt^2} = - \frac{dW}{dx} - \int_0^t d\tau K(t - \tau) \frac{dx(\tau)}{dt} + \xi(t). \quad (2.40)$$

Here we have carefully grouped some original terms into three new variables, namely an effective potential $W(x)$, a memory kernel $K(t)$ and a random force $\xi(t)$. Notice that this equation of motion does not appear to depend on the bath degrees-of-freedom $\{x_i, p_i\}$ nor its parameters $\{m_i, \omega_i, \epsilon_i\}$. This is of course because we absorbed their dependencies into the three new variables. It might look like we cheated quite a bit by doing this but for many specific systems the expression of these variables can be simplified yielding properties that do not depend on the bath variables. We can also show that some of these new variables are related. We call Eq. (2.40) the generalised Langevin equation, it represents the reduced dynamics of the system.

The effective potential is given by the following expression

$$W(x) = U(x) - \sum_i \frac{\epsilon_i^2}{2m_i \omega_i^2} x^2. \quad (2.41)$$

The first term is just the external potential on the system and the second term is the potential of the mean force that the bath exerts on the system. In this case of

the harmonic oscillator bath the extra term in the potential is quite simple and its origin is clear. However, when the generalised Langevin equation is used in a more phenomenological context, the potential of the mean force can be more tricky to find. Because this issue will not pose itself in our work, we will not go into further detail on this subject.

The memory kernel has the following form

$$K(t) = \sum_i \frac{\epsilon_i^2}{m_i \omega_i^2} \cos(\omega_i t). \quad (2.42)$$

In the generalised Langevin equation, Eq. (2.40), this memory kernel is convoluted with the entire history of the velocity dx/dt . Because the bath can not instantaneously interact with the system, its responds to the dynamics of the system needs a finite time to “reach” the system. To put it more simple, there is a delay in the responds of the bath to the system. The memory integral is often viewed as a friction force, this implies that the friction at present is dependent on how the system behaved in the past. These history dependent dynamics are therefore called *non-Markovian*.

The random force is a linear combination of initial values

$$\xi(t) = - \sum_i \epsilon_i \left(x_i(0) \cos(\omega_i t) + p_i(0) \frac{\sin(\omega_i t)}{m_i \omega_i} + x(0) \frac{\epsilon_i \cos(\omega_i t)}{m_i \omega_i^2} \right). \quad (2.43)$$

Calling this function random is perhaps strange at first sight. Indeed, it only contains the initial values of the positions and momenta, and these are in principle known. From this one could conclude that $\xi(t)$ is a deterministic function. But the sheer number of bath particles makes it impossible to catalogue all initial values. Furthermore, because most of these large baths are chaotic¹ in nature, we should know the initial values with infinite precision (which is impossible). However, the large (deterministic) bath is so complex that its resulting influence appears to be random. And from statistical physics we know that many-body systems can be described by their average behaviour. Therefore we will treat $\xi(t)$ using Boltzmann statistics, and because of the central limit theorem the statistics of the random function should not be too complicated. We should expect from a random bath that it is not correlated with the initial conditions of the system, i.e. $\langle \xi(t)x(0) \rangle = \langle \xi(t)p(0) \rangle = 0$. These relations are fulfilled but their derivation is not given here (see [27] for the derivation). In Appendix B we calculate the autocorrelation of the random function, we find

$$\langle \xi(t)\xi(0) \rangle = k_B T K(t). \quad (2.44)$$

This is the more general form of the (second) fluctuation-dissipation relation. Like we stated previously, it reflects the close relationship between the systematic friction and the random fluctuations. It also suggests that the random forces at different times can be related, just as the previous actions of the system influence the present behaviour of the bath, so does the history of the bath influence itself. This adds to non-Markovian nature of the generalised Langevin equation. When constructing a

¹Chaotic systems are extremely sensitive to their initial conditions. Although they are deterministic, starting values that are infinitesimally close together can yield fiercely diverging dynamics. This makes long-time predictions of chaotic systems impossible to obtain. For more info see [51].

generalised Langevin equation, great care should be taken when deciding which terms will contribute to the memory kernel and which to the random force. The distinction between systematic behaviour and random behaviour can be arbitrary, but in the end the fluctuation-dissipation relation should hold.

Finally we will show how the generalised Langevin equation can be reduced to the original Langevin equation. In the case of Brownian motion in a viscous fluid one can assume that the interaction between the heavy particle and the fluid molecules happens instantaneously. The bath can respond immediately and therefore no memory effects are introduced. This instantaneous interaction is represented by a Dirac delta memory kernel: $K(t) = 2\gamma\delta(t)$. We therefore find that

$$\int_0^t d\tau K(t - \tau) \frac{dx(\tau)}{dt} = 2\gamma \int_0^t d\tau \delta(t - \tau) \frac{dx(\tau)}{dt} = \gamma \frac{dx}{dt}. \quad (2.45)$$

Substituting this result into the generalised Langevin equation, Eq. (2.40), we arrive at the original Langevin equation, Eq. (2.10). Notice that with this memory kernel we retrieve the original fluctuation-dissipation relation, Eq. (2.22) (we actually find 1/3 of the original result, but that is because we considered only one coordinate here).

2.4 Viscoelastic bath

We mentioned in the previous section that the generalised Langevin equation can also be applied on a phenomenological basis rather than being an exact equation. In this section we will use it in this first sense to describe a complex fluid called a *viscoelastic fluid* (or bath). As its name suggests, this kind of fluid displays both elastic and viscous characteristics. A pure viscous fluid would be liquid water, while an example of an elastic material is rubber. A viscoelastic fluid is thus somewhere in between these two extremes. One of its main features is that a Brownian particle, submerged in such a bath, will experience anti-persistent motion. What is meant by this is that a displacement of the particle in a particular direction will bring about an increased chance to move in the opposite direction at a later time. This effect is due to the elastic stresses in the fluid that “pull” on the particle when it tries to move through it. Because of these time correlations in the particle’s trajectory, its dynamics is not an instantaneous process but it is influenced by past events. To put it simpler, the deformation of the viscoelastic fluid that the particle brought about in the past will yield a response to the particle in the present. From this description it is clear that a viscoelastic bath requires a non-Markovian treatment where memory effects are present. This is exactly what the generalised Langevin equation can provide us. Although we will discuss it at length in the next chapter, we will briefly mention that a Brownian particle in a viscoelastic bath will perform subdiffusive motion. Subdiffusion is characterised by a mean-squared displacement that is not linear in time (as is the case for normal diffusion) but goes as a power-law of time, where the exponent is positive but smaller than one.

Perhaps the most important application of a viscoelastic bath is its ability to describe the intracellular fluid, called *cytosol*, of a biological cell [4]. The cytosol, which is held together by the plasma membrane, consists mostly of water with dissolved solutes (such as ions) and macromolecules. It can be seen as the liquid matrix

around the various organelles that reside inside the cell. Also present throughout the interior of a cell is the cytoskeleton which forms a great mesh that is mainly responsible for the shape of the cell and the transport-processes within. It is clear that the cytosol is densely packed with different substances, we therefore consider it a *crowded* environment. The predominant “crowders” are the abundant (large) macromolecules, they restrict the diffusive motion of other substances such as tracer particles. This restriction arises from the macromolecules’ internal degrees-of-freedom and the fact that they have a similar size as the tracer particle. To understand this one can imagine that the motion of the particle will squeeze the macromolecules, who in turn will provide an elastic (i.e. entropic) restoring stress. This results in the non-trivial subdiffusive motion that is observed [18, 52–54] when studying the movement of tracer particles in the cytosol. Many models have been devised to explain this anomalous behaviour, such as the continuous time random walk (with traps), hard disks simulations, obstructed diffusion, etc. However, it was recently shown that the language of the generalised Langevin equation best describes the observed motion [55]. In this study they used artificial crowded fluids to show that crowding renders fluids viscoelastic and that the observed subdiffusion has all the characteristics of one that originates from a generalised Langevin equation. In fact, the authors of [55] argued that fractional Brownian motion is the model that best describes the motion in a crowded fluid. Fractional Brownian motion, however, is a process that does not satisfy the fluctuation-dissipation relation. We therefore argue that the generalised Langevin equation provides a better description on the grounds that it is more physical. We can make this claim because, as we will soon show, the appropriate generalised Langevin equation satisfies the same conditions that were pursued in [55]. More information on fractional Brownian motion can be found in [56].

In order to describe a viscoelastic bath with the generalised Langevin equation, which is given by Eq. (2.40), we should specify the effective potential $W(x)$ and the memory kernel $K(t)$. First, we assume that no effective potential finds its origin in the bath itself. We will, however, allow an external potential $U(x)$ to act on the particle. The generalised Langevin equation, Eq. (2.40), thus becomes

$$m \frac{d^2 x}{dt^2} = -\frac{dU}{dx} - \int_0^t d\tau K(t - \tau) \frac{dx(\tau)}{dt} + \xi_T(t). \quad (2.46)$$

Notice that we added the subscript T to the noise term because here it resembles the kinetic (or thermal) impacts on the particle. Now we are left with the characterisation of the memory kernel, it will define both the non-Markovian friction force and the non-white thermal forces. The convolution between the memory kernel and the velocity profile in Eq. (2.46) starts at $t = 0$, we say that at this moment the memory is “born”. Before its birth ($t < 0$), we assume the system to be in equilibrium with the bath.

To find an expression for the memory kernel of a viscoelastic bath we adopt a model devised by J. Clerk Maxwell in 1867 [57]. To describe the viscosity of a fluid, Maxwell used a transient viscoelastic theory where the elasticity relaxes to zero. To understand how his viscoelastic friction acts on a Brownian particle we consider the Maxwellian viscoelastic element from rheology. This element is connected to the particle and consists of a spring and dashpot¹ in series (see Fig. 2.2). The spring has elastic spring

¹A dashpot is a mechanical damper which resists motion via viscous friction. The force it generates is proportional but opposite to the velocity.

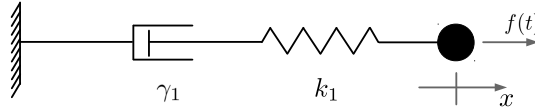


Figure 2.2: A Maxwellian viscoelastic element. It is on the left connected to a rigid wall and consists of a dashpot (viscous friction coefficient γ_1) and an elastic spring (elastic spring constant k_1) in series. The Brownian particle is attached on the right. Also indicated are the applied force $f(t)$ and the displacement of the particle x .

constant k_1 and T_1 is the Maxwell time of the elastic force relaxation. The coefficient of viscous friction is defined as $\gamma_1 = k_1 T_1$. Now suppose we apply a force $f(t)$ on the particle as indicated in Fig. 2.2. Due to this force, the particle is displaced from its initial position, indicated by x . This displacement subsequently induces an elongation of the spring x_s and the dashpot x_d , and we thus have $x = x_d + x_s$. A harmonic spring has the following relation between the applied force and its elongation: $f = k_1 x_s$. For a dashpot the next relation holds: $f = \gamma_1 \dot{x}_d$, where $\dot{x} = dx/dt$. If we now take the time derivative of the particle's displacement we get $\dot{x} = \dot{x}_d + \dot{x}_s$ or

$$\dot{x} = \frac{f}{\gamma_1} + \frac{\dot{f}}{k_1}. \quad (2.47)$$

This is a first-order linear ordinary differential equation of $f(t)$. Solving it with $f(0) = 0$ as boundary condition, results in the following expression

$$f(t) = k_1 \int_0^t d\tau \exp\left(-\frac{k_1}{\gamma_1}(t-\tau)\right) \frac{dx(\tau)}{dt}. \quad (2.48)$$

From Newton's third law, we conclude that the force the Maxwellian element exerts on the particle has the same magnitude as Eq. (2.48) but points in the opposite direction. Therefore the friction the element generates on the Brownian particle is equal to $-\int_0^t d\tau K_1(t-\tau)\dot{x}(\tau)$, where the memory kernel is given by $K_1(t) = k_1 \exp(-t/T_1)$.

The Maxwell model can be generalised to one where several Maxwellian viscoelastic elements are acting on the particle in parallel. This can reflect a complex viscoelastic bath – which the cytosol surely is – where distinct components contribute to the global viscoelasticity. The individual elements all have their own characteristic spring constant k_i and relaxation time T_i . It can be shown [58] that the resulting memory kernel $K(t)$ is equal to the sum over all the contributing memory kernels $K_i(t)$

$$K(t) = \sum_i k_i e^{-t/T_i}. \quad (2.49)$$

A sum over exponentials can be used to approximate a decaying power-law. This was used by Gemant [59] and later by Cole and Cole [60], to propose that the response of many viscoelastic baths is well described by the following strict power-law memory kernel

$$K(t) = \frac{\eta_\alpha}{\Gamma(1-\alpha)} t^{-\alpha}. \quad (2.50)$$

We introduced the generalised friction coefficient¹ $\eta_\alpha = \gamma\Gamma(3-\alpha)$, where $\Gamma(\cdot)$ is the gamma function (see Appendix A.2). The exponent α characterises the viscoelasticity of the bath. From this decreasing memory function it is clear that past events have less influence than more recent ones. Yet because the kernel does not drop down exponentially fast, the influence of the system's history will be long lasting. The value of α is always between zero and one, i.e. $0 \leq \alpha \leq 1$. When α is equal to one, we return to a viscous fluid. The memory kernel will become a Dirac delta function for this case and we retrieve the original Langevin equation, Eq. (2.10). On the other hand, when α is equal to zero, the bath becomes a purely elastic medium. The kernel is then a constant for $t > 0$ and the friction force will be $2\gamma[x(0) - x(t)]$. This effectively adds a harmonic term to the equation of motion and will cause the particle to become trapped in a process called *dynamic caging*². For all α -values in between zero and one the bath is viscoelastic.

In this document we are mostly concerned with very small and light particles. For such particles the inertial term (on the left-hand side of Eq. (2.46)) can be neglected, this will result in the overdamped generalised Langevin equation. Due to the specific form of the memory kernel of a viscoelastic bath we can write Eq. (2.46) in a more mathematically pleasing form using the fractional derivative formalism (see Appendix A.7). With this formalism the integral term in Eq. (2.46) can be replaced by a Caputo fractional derivative of order α which is denoted by ${}_c\mathcal{D}^\alpha$. The equation of motion for an overdamped particle, at position x , in a viscoelastic bath becomes

$$\eta_\alpha {}_c\mathcal{D}^\alpha x(t) = -\frac{dU}{dx} + \xi_T(t), \quad (2.51)$$

where $U(x)$ is some external potential. To be complete we also give the autocorrelation of the thermal force in full. Using the fluctuation-dissipation relation, Eq. (2.44), results in

$$\langle \xi_T(t)\xi_T(t') \rangle = \frac{\eta_\alpha k_B T}{\Gamma(1-\alpha)} |t-t'|^{-\alpha}. \quad (2.52)$$

Because of the time dependence of its autocorrelation, the random force is classified as coloured noise. To be more specific it is related to fractional Gaussian noise [61] (see Section 3.1.1). It still has zero mean however,

$$\langle \xi_T(t) \rangle = 0. \quad (2.53)$$

¹Although we used the same symbol γ , it does not have the same time-dimension as in Eq. (2.6).

²An example of such caging is a bath with large, heavy particles and one smaller tracer particle. The tracer particle will become trapped in the slowly moving spaces between the heavy particles and will only rarely escape, only to become trapped in another location.

2.5 Active processes

Until now, the (generalised) Langevin equations we considered all described a system that is – or eventually will be – in equilibrium with the surrounding bath. Because they obey the fluctuation-dissipation relation, the origin of the fluctuating force and the systematic force is the same. This implies that the system dissipates any energy back to the bath which it gained from the bath’s fluctuations. This, however, need not be the case for all physical systems. Consider, for example, a second source of fluctuating forces that is introduced to the system. Also assume that this force does not have a complementary systematic force. The fluctuating force will deliver energy to the system and without a complementary dissipative sink to extract this extra energy the total energy of the system will increase. According to the second law of thermodynamics, this increase in energy yields an increase in entropy and where there is entropy production there cannot be equilibrium. In other words, adding an extra fluctuating term, that does not comply with the fluctuation-dissipation relation, to a system’s (generalised) Langevin equation pulls it out-of-equilibrium.

This example of adding an extra fluctuating force is relevant for the generalised Langevin description of a cell’s cytosol that was introduced in the previous subsection. Apart from being viscoelastic, the cytosol is also an *active* medium. By this we mean that inside a cell there are many biological processes that consume energy to generate persistent motion that would not occur in a thermalised state. This is one of many mechanisms a cell can utilise to keep itself away from equilibrium, which is (as we discussed in Section 1.3) essential for it to stay alive. For a particle (or a larger structure) suspended in the cell’s cytosol this activity is external. We also consider here a different system where the activity is internal. Such a system is, for example, a motile bacteria, capable of generating its own directed propulsion. We will now discuss the origin of the activity of these two cases (external and internal) and how it effects the generalised Langevin equation.

2.5.1 Motor-activated network

Throughout the cytosol inside a cell is a complex mesh of stiff, interlinking filaments and tubules that are called the *cytoskeleton*. It is the main provider of the cell’s structure and its inner mechanics. Actin filaments are one of the dominant components of the cytoskeleton, being flexible and strong polymers. When a *molecular motor*, called myosin-II, attaches to an actin filament it can generate a force and effectively “walk” from one end of the filament to the other (the direction of this walk is predetermined by the composition of the actin filament). It is capable to perform this motion by consuming the energy source called adenosine triphosphate, more commonly known by its abbreviation *ATP*. When such a molecular motor is attached to two actin filaments it can exert transient contractile stresses. By this we mean that the motor pulls the two filaments past itself in opposite directions (see Fig. 2.3). Because the cytoskeleton is a large and intertwined structure, these stresses can influence parts of the cell that are far away from the actual molecular motor itself. Naturally, when many of these motors perform these forces at different sites on the cytoskeleton, they induce (non-thermal) forces throughout the cytosol. These fluctuations are one of many active processes that occur in a cell.

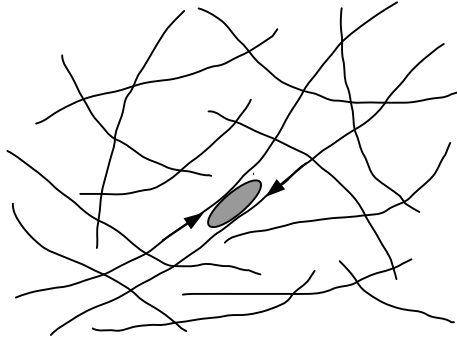


Figure 2.3: Schematic representation of the actin filaments (black lines) and the myosin-II molecular motor (grey structure). Also indicated, with arrows, are the opposite forces the molecular motor exerts on the filaments.

To describe these active fluctuations mathematically we assume they can be represented by a stochastic function¹ $\xi_A(t)$. We also assume this function is Gaussian distributed, so only its mean and autocorrelation need to be determined. Because the cytoskeleton is rather uniform throughout the cell and the molecular motors can bind on it anywhere, the fluctuations have no preferred direction. Therefore the mean of $\xi_A(t)$ is equal to zero. Experiments [18, 62, 63] on these fluctuations have shown that its power spectrum $S(\omega)$ is like that of white-noise for low frequencies: $S(\omega) \sim \text{constant}$. And for high frequencies it follows a power-law: $S(\omega) \sim \omega^{-2}$. These properties are contained in a Lorentzian power spectrum, which means it is proportional to $S(\omega) \sim 1/(1 + A\omega^2)$, with A constant. The Wiener-Khinchin theorem [22] states that the power spectrum of a stationary random process is equal to the Fourier transform of the autocorrelation function of this process. The inverse Fourier transform of a Lorentzian can be written as an exponential of the absolute value of its argument². Inspired by these experiments, we use exponentially correlated noise as a model for the active forces in the cytosol,

$$\langle \xi_A(t) \rangle = 0, \quad (2.55)$$

$$\langle \xi_A(t)\xi_A(t') \rangle = C \exp(-|t - t'|/\tau_A). \quad (2.56)$$

The autocorrelation is coloured and can be understood as a process where a force of average strength \sqrt{C} is directed in a particular orientation for an average persistence time τ_A . Adding the active forces $\xi_A(t)$ to the generalised Langevin equation of a viscoelastic bath, Eq. (2.51), is a model for the dynamics of a particle in the cytosol inside a cell with some potential U acting upon it.

¹For simplicity we restrict ourselves here to the one dimensional case, generalising to three dimensions is straightforward and will be done in a later section.

²This can be easily proved when one uses the fact that $c_1 e^{-|t|/c_2}$ is an even function:

$$\int_{-\infty}^{\infty} dt c_1 e^{-|t|/c_2} e^{-2\pi i t \omega} = 2c_1 \int_0^{\infty} dt e^{-t/c_2} \cos(2\pi t \omega) = \frac{2c_1 c_2}{1 + (2\pi c_2 \omega)^2}. \quad (2.54)$$

We should note here that experiments [64–66] have shown that the displacement of a particle in an artificial actin-myosin network has a Gaussian distribution with exponential tails superimposed. However, in a very recent work [67], it was found that at low myosin concentrations the distribution is purely Gaussian. In our work we will always assume that $\xi_A(t)$ is a Gaussian random variable. Though we acknowledge that this is an approximation.

2.5.2 Self-propelled particle

In the previous subsection we discussed how active forces can originate from an external source. Here we look at a system where they manifest themselves internally. We will, however, find that the generalised Langevin equation of this system is identical to the external one. The system considered here is called a *self-propelled particle* [11]. Such a particle is submerged in a solvent and is capable to generate its own propulsion velocity v . The direction of its movement is randomised, this randomisation can be done in two ways. First we consider the *roll-and-tumble particles*. They move (“roll”) in a straight line until they choose (“tumble”) a new direction, this new direction is completely uncorrelated with its previous direction (see Fig. 2.4a). The average length the particle covers before tumbling is determined by its tumbling rate μ . The second type of self-propelled particle are the *active Brownian particles*. They also generate a constant velocity v , but their direction is changed continuously using rotational Brownian motion (see Fig. 2.4b). We can describe the position \vec{r} of an active Brownian particle in a viscous fluid with the following coupled Langevin equation (this equation only holds for two dimensions, in three dimensions it becomes much more complicated)

$$\frac{d\vec{r}}{dt} = v \vec{e}(\theta) + \frac{1}{\gamma} \vec{\xi}_T(t), \quad (2.57)$$

$$\frac{d\theta}{dt} = \xi_R(t). \quad (2.58)$$

The first equation is an overdamped Langevin equation of the position where the thermal noise $\vec{\xi}_T$ is the same as in Section 2.2. The first term on the right-hand side represents the propulsion with velocity v , where vector \vec{e} determines the direction in which the particle moves. We have that, in two dimensions, $\vec{e} = (\cos(\theta), \sin(\theta))$. This couples the first equation to the second where the angle θ is changed through a diffusion equation. The random (non-thermal) torque ξ_R is a Gaussian variable with zero mean and autocorrelation $\langle \xi_R(t) \xi_R(t') \rangle = 2D_R \delta(t - t')$, where D_R is the rotational diffusion coefficient. It can be shown [68] that Eqs. (2.57) and (2.58) can be combined into one Langevin equation

$$\gamma \frac{d\vec{r}}{dt} = \vec{\xi}_T(t) + \vec{\xi}_A(t). \quad (2.59)$$

Here we introduced the active noise $\vec{\xi}_A$, each component of this vector has the same properties as the active forces of the previous subsection, i.e. Eqs. (2.55) and (2.56). We have that the persistence time is equal to $\tau_A = 1/D_R = 1/\mu$, it represents the characteristic time-scale in which the particle moves in a straight line. Also the strength of the active noise is determined by $C = (\gamma v)^2/2$.

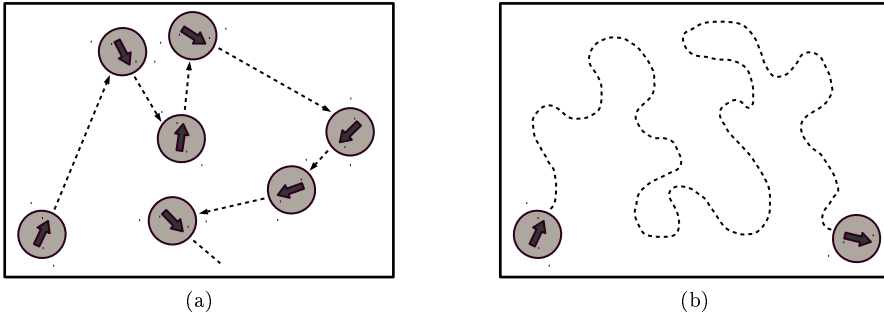


Figure 2.4: Schematic representation of the two types of self-propelled particles that move with propulsion speed v . (a) The roll-and-tumble particle, characterised by its tumbling rate μ . (b) The active Brownian particle, characterised by its rotational diffusion constant D_R .

When we add this active noise term to the generalised Langevin equation in a viscoelastic bath, Eq. (2.51), it becomes a good model for a motile bacteria in a complex fluid, experiencing potential U . A motile bacteria has the ability to “swim” through a fluid with for example its flagella. It can change its direction depending on external stimuli. An example of such a motile bacteria is the famous *Escherichia coli*. For an experimental and theoretical treatment of motile bacteria in a viscous ($\alpha = 1$) bath, we refer to [17].

2.6 Active viscoelastic bath

In this short section, we combine all the concepts discussed above into one. The equation we conceive here is a model for the dynamics of a coordinate $x(t)$ in an active viscoelastic bath, subjected to an external potential. One can use it, for example, to describe dynamic processes in the cytosol of a cell or the motion of motile bacteria through a complex fluid. The equation of motion reads

$$\eta_\alpha {}_c\mathcal{D}^\alpha x(t) = -\frac{dU}{dx} + \xi_T(t) + \xi_A(t) \quad (2.60)$$

This is a stochastic fractional differential equation of order α . The viscoelasticity of the bath is characterised by α . The generalised friction coefficient is given by $\eta_\alpha = \gamma\Gamma(3 - \alpha)$ and $U(x)$ symbolises the external potential. The first stochastic term represents the thermal random forces. They are Gaussian distributed and are characterised by

$$\langle \xi_T(t) \rangle = 0, \quad (2.61)$$

$$\langle \xi_T(t)\xi_T(t') \rangle = \frac{\eta_\alpha k_B T}{\Gamma(1 - \alpha)} |t - t'|^{-\alpha}. \quad (2.62)$$

The thermal energy is measured by $k_B T$, where k_B is the Boltzmann constant and T the temperature of the bath. The second stochastic term depicts the active random

forces. They too are Gaussian variables, with

$$\langle \xi_A(t) \rangle = 0, \quad (2.63)$$

$$\langle \xi_A(t) \xi_A(t') \rangle = C \exp(-|t - t'|/\tau_A). \quad (2.64)$$

The strength of the active random forces is determined by C and the time over which their direction persists is given by the persistence time τ_A .

This model can easily be extended to three dimensions. The coordinate and stochastic forces become vectors. The derivative of the external potential is replaced by the gradient of the potential.

$$\boxed{\eta_{\alpha c} \mathcal{D}^\alpha \vec{x}(t) = -\vec{\nabla} U(x) + \vec{\xi}_T(t) + \vec{\xi}_A(t)} \quad (2.65)$$

We assume that the stochastic forces do not correlate between dimensions. Therefore, the thermal random forces become

$$\langle \vec{\xi}_T(t) \rangle = 0, \quad (2.66)$$

$$\langle \vec{\xi}_T(t) \cdot \vec{\xi}_T(t') \rangle = \frac{3\eta_\alpha k_B T}{\Gamma(1 - \alpha)} |t - t'|^{-\alpha}. \quad (2.67)$$

While the active random forces are characterised by

$$\langle \vec{\xi}_A(t) \rangle = 0, \quad (2.68)$$

$$\langle \vec{\xi}_A(t) \cdot \vec{\xi}_A(t') \rangle = 3C \exp(-|t - t'|/\tau_A). \quad (2.69)$$

3 | Numerical Algorithm

Computers are useless, they can only give you answers.

Pablo Picasso

The three-dimensional overdamped Langevin equation is given by Eq. (2.29). The stochastic thermal noise is Gaussian white noise defined by Eqs. (2.21) and (2.22). The methods used for solving this standard Langevin equation numerically are well known and, in general, straightforward [69]. By integrating the equation discretely one can find an iterative expression from which $x(t+\Delta t)$ is calculated using $x(t)$, where $\Delta t > 0$ is a small time difference. This time step is chosen small for large accuracy but not so small as to severely slow the algorithm down. Due to the stochastic nature of an equation that includes Gaussian white noise, uncorrelated random numbers need to be generated. Modern computers can provide these fast and accurately.

The one-dimensional overdamped generalised Langevin equation with active noise is defined by Eq. (2.60). The time-dependent correlation of both of its noise terms is given in Section 2.6. Finding a numerical solution of this stochastic fractional differential equation is not such a trivial problem, the standard techniques used to simulate the ordinary Langevin equation are inadequate. The difficulty here is twofold. First there are two stochastic terms whose correlation is a function of time, meaning that generated noise depends on previously generated noise. Second, due to the non-local nature of a fractional differential equation the numerical integration of it should be done with care. The solution to both difficulties will be addressed here.

3.1 Coloured noise

The active and the thermal noise, represented collectively by ξ without subscript, in our model are Gaussian distributed with zero mean and a correlation that is a function of the absolute difference in time. So in general we have

$$\langle \xi(t)\xi(t') \rangle = f(|t - t'|). \quad (3.1)$$

The algorithm should generate a string of random numbers that comply with this correlation and that are Δt separated in time. We denote the i^{th} random number as $\xi[i] = \xi(i\Delta t)$. The different correlations require different techniques to be generated.

3.1.1 Power-law correlated noise

It can be shown that the concept of fractional Gaussian noise [70, 71] is equivalent to the power-law correlated thermal noise of our model, i.e. Eq. (2.62). Fractional Gaussian noise can be derived from a process called fractional Brownian motion. Reintroduced by Mandelbrot and van Ness [71], fractional Brownian motion $B_H(t)$ is a generalisation of Brownian motion where the increments are not independent of each other. This stochastic process is defined by the following criteria

- $B_H(t)$ has stationary increments
- $B_H(0) = 0$ and $\langle B_H(t) \rangle = 0$ for $t \geq 0$
- $\langle B_H^2(t) \rangle = t^{2H}$ for $t \geq 0$
- $B_H(t)$ has a Gaussian distribution with

$$\langle B_H(t)B_H(t') \rangle = \frac{1}{2} \left(t^{2H} + t'^{2H} - |t - t'|^{2H} \right) \quad (3.2)$$

The Hurst exponent $H \in [0, 1]$ determines the raggedness of the motion, larger values for H make smoother motions. When $H < 1/2$, the increments are negatively correlated while for $H > 1/2$ they are positively correlated. For $H = 1/2$ we recover classical Brownian motion, the so-called Wiener process. We can define fractional Gaussian noise $X_H(t)$ as the ratio of the increment difference and the time step over which this increment occurred

$$X_H(t) = \frac{B_H(t + \Delta t) - B_H(t)}{\Delta t}. \quad (3.3)$$

Using the second property, one immediately finds that the mean of this noise is zero, i.e. $\langle X_H(t) \rangle = 0$. Since the motion is Gaussian distributed, the noise is also a Gaussian variable. Thus if we also calculate its second moment, it is fully described

$$\begin{aligned} \langle X_H(t)X_H(t') \rangle &= \frac{1}{\Delta t^2} \left(\langle B_H(t)B_H(t') \rangle - \langle B_H(t)B_H(t' + \Delta t) \rangle \right. \\ &\quad \left. - \langle B_H(t')B_H(t + \Delta t) \rangle + \langle B_H(t + \Delta t)B_H(t' + \Delta t) \rangle \right). \end{aligned} \quad (3.4)$$

The fourth property, Eq. (3.2), is used to find

$$\langle X_H(t)X_H(t') \rangle = \frac{1}{2\Delta t^2} \left(|t - t' + \Delta t|^{2H} + |t - t' - \Delta t|^{2H} - 2|t - t'|^{2H} \right). \quad (3.5)$$

Now we let the time step Δt approach zero, $\Delta t \rightarrow 0$. The first and second term in Eq. (3.5) can be expanded using Taylor series

$$|t - t' \pm \Delta t|^{2H} = |t - t'|^{2H} \left(1 \pm 2H \frac{\Delta t}{|t - t'|} + H(2H - 1) \frac{\Delta t^2}{|t - t'|^2} + \mathcal{O}(\Delta t^3) \right). \quad (3.6)$$

Putting this in Eq. (3.5), we find

$$\langle X_H(t)X_H(t') \rangle \approx H(2H - 1)|t - t'|^{2H-2}. \quad (3.7)$$

If we now multiply this by $2\gamma k_B T$ and take $H = (2 - \alpha)/2$, then it becomes equal to Eq. (2.62), the thermal noise of our model. In other words, our thermal noise is equivalent to fractional Gaussian noise.

To generate this fractional Gaussian noise we use the algorithm conceived by Hosking in 1984 [72]. The Hosking algorithm produces a collection of numbers from a stationary process with a normal marginal distribution and correlation function $\rho[i] = \rho(i\Delta t)$. For our purpose this correlation function is $\rho[i] = \langle X_H(0)X_H(i\Delta t) \rangle$. Using Eq. (3.5) brings us to

$$\rho[i] = \frac{1}{2} \left(|i+1|^{2-\alpha} + |i-1|^{2-\alpha} - 2|i|^{2-\alpha} \right). \quad (3.8)$$

The scheme below produces fractional Gaussian noise $X[i]$ with Δt unity. It requires the production of Gaussian white noise $N(\mu, \sigma^2)$ with mean μ and variance σ^2 .

1. Set $v = 1$.
2. Generate a starting value $X[0] = N(0, v)$.
3. For every i^{th} time step do

$$\begin{aligned} \psi_k &= \phi_k \\ \phi_i &= v^{-1} \rho[i] - v^{-1} \sum_{j=1}^{i-1} \rho[i-j] \psi_j \\ v &= (1 - \phi_i^2) v \\ \phi_k &= \psi_k - \phi_i \psi_{i-k} \\ m &= \sum_{j=1}^i X[i-j] \phi_j \\ X[i] &= N(m, v). \end{aligned}$$

In every step, the indices k is always taken from 1 to $i-1$. For the scheme presented here we chose clarity above efficiency. For example, if several realisations of the same process are being performed, one could consider to calculate all needed values of ϕ beforehand. To rescale this process to one where $\Delta t \neq 1$, all $X[i]$ need to be multiplied by $\Delta t^{-\alpha/2}$. Then to make the transition from fractional Gaussian noise to our thermal noise, Eq. (2.62), we should multiply it by $\sqrt{2\gamma k_B T}$, thus we have

$$\xi_T[i] = \sqrt{2\gamma k_B T \Delta t^{-\alpha}} X[i]. \quad (3.9)$$

3.1.2 Exponentially correlated noise

The Hosking algorithm can surely be used to generate the active noise, which would have the following correlation function in the algorithm

$$\rho[i] = e^{-i\Delta t/\tau_A}. \quad (3.10)$$

The generated numbers should only be multiplied by \sqrt{C} , since the time-step Δt already appears explicitly in the correlation. But exponentially correlated noise can also be generated by a linear damping equation driven by Gaussian white noise. This method is much more time and memory efficient than the Hosking method. An integral algorithm for exponentially correlated noise was proposed by Fox *et al.* [73]. Its scheme is as follows, where again $N(\mu, \sigma^2)$ stands for Gaussian white noise with mean μ and variance σ^2

1. Set $E = e^{-\Delta t/\tau_A}$.
2. Generate a starting value $\xi_A[0] = N(0, C)$.
3. For every i^{th} time step do

$$\xi_A[i] = E \xi_A[i-1] + N(0, (1 - E^2)C). \quad (3.11)$$

3.2 Fractional differential equation

Here we seek the numerical integration of a differential equation of fractional order, in our work it always has the form of the following initial value problem

$${}_c\mathcal{D}^\alpha x(t) = g(t, x(t)), \quad x(0) = x_0, \quad (3.12)$$

with $0 < \alpha \leq 1$. The function g could be any nonlinear function, in our specific case, using Eq. (2.60), we have

$$g(t, x(t)) = \frac{1}{\eta_\alpha} \left(-\frac{dU}{dx} + \xi_T(t) + \xi_A(t) \right), \quad (3.13)$$

for $t > 0$. In order to solve Eq. (3.12) one can use the fact that this initial value problem is equivalent to the following Volterra integral [74]

$$x(t) = x_0 + \frac{1}{\Gamma(\alpha)} \int_0^t dy (t-y)^{\alpha-1} g(y, x(y)). \quad (3.14)$$

The algorithm developed to solve this integral is a generalisation of the classical Adams-Bashforth-Moulton integrator for first-order problems [75, 76]. The generalisation was done by Diethelm *et al.* [77] and optimised by Daftardar-Gejji *et al.* [78]. It will produce $x_{n+1} = x(t_{n+1})$ (with $t_i = i\Delta t$) a time step Δt further than x_n . Note that the integral in Eq. (3.14) goes from 0 to t which is a consequence of the non-locality of fractional differential equations. Therefore the iterative process of the algorithm will use all calculated solutions x_i instead of only the previous solution x_n , as is done in the integration of the ordinary Langevin equation. The algorithm uses the following predictor-corrector protocol where P_{n+1}^1 and P_{n+1}^2 are the predictors and x_{n+1} the corrector

$$P_{n+1}^1 = x_0 + \frac{\Delta t^\alpha}{\Gamma(\alpha+2)} \sum_{i=0}^n a_{i,n} g(t_i, x_i), \quad (3.15)$$

$$P_{n+1}^2 = \frac{\Delta t^\alpha}{\Gamma(\alpha+2)} g(t_{n+1}, P_{n+1}^1), \quad (3.16)$$

$$x_{n+1} = P_{n+1}^1 + \frac{\Delta t^\alpha}{\Gamma(\alpha+2)} g(t_{n+1}, P_{n+1}^1 + P_{n+1}^2). \quad (3.17)$$

The weight $a_{i,n}$ (which ultimately originates from the memory kernel, Eq. (2.62)) given to the previous solutions has the following form

$$a_{i,n} = \begin{cases} n^{\alpha+1} - (n - \alpha)(n + 1)^\alpha & \text{if } i = 0 \\ (n - i + 2)^{\alpha+1} + (n - i)^{\alpha+1} - 2(n - i + 1)^{\alpha+1} & \text{if } 1 \leq i \leq n. \end{cases} \quad (3.18)$$

The algorithm is now fully described. Note that for large n it will be increasingly intensive to calculate the next value of x_i due to the summation in Eq. (3.15). One also has to store all calculated values of $g(t_i, x_i)$ in the memory which could overflow for large n . We only presented the algorithm for one particle in one dimension, the extension to many (interacting) particles in three dimensions is relatively straightforward and not given here. Note that care should be taken in the case of the Rouse chain (see Section 5.1) where the dU/dx term in g is dependent on other integrated variables. Correctly updating it during the predictor-corrector protocol is essential.

4 | Particle in a Potential

Nothing is particularly hard if you divide it into small jobs.

Henry Ford

In this chapter we will employ the analytical model and numerical scheme, discussed in the previous chapters, to investigate a particle that resides in an active viscoelastic bath. The particle will be subjected to three different potentials, namely a constant potential, a harmonic oscillator and a double well. We only consider one-dimensional dynamics, meaning that the particle can only move along one direction. As we discussed in Chapter 2, the model of an active viscoelastic bath can be used to describe the internal environment of a biological cell, called the cytosol. We will therefore use our results to illustrate several cellular processes. The study of one particle also provides a stepping stone to the next chapter where we investigate the dynamics of a Rouse chain, which consists of many interacting particles. The results presented in this chapter were first published in [79].

4.1 Free particle

A free particle, with position $x(t)$, is not bound by the influence of an external force. Or, in other words, it is located in a region where the potential energy does not vary. The external potential $U(x)$ on a free particle can therefore be assumed constant

$$U(x) = \text{constant}. \quad (4.1)$$

If the free particle is surrounded by an active viscoelastic bath, we can describe its dynamics by the one-dimensional generalised Langevin equation from Section 2.6. After filling in the external potential, the equation of motion becomes

$$\eta_{\alpha} {}_c\mathcal{D}^{\alpha} x(t) = \xi_T(t) + \xi_A(t)H(t). \quad (4.2)$$

We added the *Heaviside function*¹ $H(t)$ to the active forces. This will turn the active forces on at $t = 0$. For times smaller than zero, the system is assumed to be thermally

¹Also known as the step function, the Heaviside function is a discontinuous function, defined as

$$H(t) = \begin{cases} 0 & \text{if } t < 0 \\ 1 & \text{if } t \geq 0 \end{cases} \quad (4.3)$$

relaxed. After $t = 0$, the particle will enter a nonequilibrium regime. To evaluate the particle's dynamics we need to solve Eq. (4.2), which is a stochastic fractional differential equation. We will find that the position $x(t)$ is a Gaussian variable and therefore characterised completely by its first and second moments.

4.1.1 Anomalous diffusion

In order to solve the equation of motion, Eq. (4.2), we start by taking its Laplace transform (see Appendix A.6). The result is

$$\eta_\alpha s^{\alpha-1} [s\tilde{x}[s] - x(0)] = \tilde{\xi}_T[s] + \tilde{\xi}_A[s], \quad (4.4)$$

where $\tilde{f}[s]$ represents the Laplace transform of a function $f(t)$. After some elementary algebra one finds

$$\tilde{x}[s] = s^{-1}x(0) + \frac{s^{-\alpha}}{\eta_\alpha} (\tilde{\xi}_T[s] + \tilde{\xi}_A[s]). \quad (4.5)$$

To transform this expression back to the time-domain, again the formulas from Appendix A.6 are used. It can be easily shown that the following relation characterises the evolution of the free particle's displacement

$$\Delta x(t) = \frac{1}{\Gamma(\alpha)\eta_\alpha} \int_0^t dt' (\xi_T(t-t') + \xi_A(t-t')) t'^{\alpha-1}, \quad (4.6)$$

where the displacement is given by $\Delta x(t) = x(t) - x(0)$. From this expression it is clear that the displacement is a linear combination of Gaussian variables, making it itself Gaussian distributed. We therefore search for its first and second moment. Taking the ensemble average of Eq. (4.6) immediately demonstrates that the mean of the displacement is zero, i.e. $\langle \Delta x(t) \rangle = 0$. To obtain this results one only uses the fact that the average of both noise terms is zero.

Next, we calculate the mean-squared displacement¹ of the particle, expressed as $\Delta^2(t) = \langle (\Delta x(t))^2 \rangle$. This quantity is a measure for the spacial exploration of the particle. To obtain this we take the square of Eq. (4.6) after which we perform the ensemble average.

$$\begin{aligned} \Delta^2(t) &= \frac{1}{\Gamma^2(\alpha)\eta_\alpha^2} \frac{\eta_\alpha k_B T}{\Gamma(1-\alpha)} \int_0^t dt' \int_0^t dt'' \frac{t'^{\alpha-1} t''^{\alpha-1}}{|t' - t''|^\alpha} \\ &\quad + \frac{C}{\Gamma^2(\alpha)\eta_\alpha^2} \int_0^t dt' \int_0^t dt'' e^{-|t' - t''|/\tau_A} t'^{\alpha-1} t''^{\alpha-1}. \end{aligned} \quad (4.7)$$

Here we used the autocorrelation of the thermal noise and the active noise, Eq. (2.62) and Eq. (2.64) respectively. Both terms in this expression can be simplified. For the first term notice that the double integral can be rewritten as follows

$$2 \int_0^t dt' \int_0^{t'} dt'' \frac{t'^{\alpha-1} t''^{\alpha-1}}{(t' - t'')^\alpha} = 2 \int_0^t dt' t'^{\alpha-1} \mathcal{B}(\alpha, 1 - \alpha) = \frac{2}{\alpha} \Gamma(\alpha) \Gamma(1 - \alpha) t^\alpha, \quad (4.8)$$

¹A more complete measure of the dynamics would be the variance in the displacement, which is defined as $\sigma^2(t) = \langle (\Delta x(t))^2 \rangle - \langle \Delta x(t) \rangle^2$. But since the mean displacement is zero, the variance is identical to the mean-squared displacement.

where $\mathcal{B}(\cdot, \cdot)$ is the beta-function (see Appendix A.3). The double integral in the second term of Eq. (4.7) can be written as

$$2 \int_0^t dt' \int_{t'}^t dt'' e^{-(t''-t')/\tau_A} t'^{\alpha-1} t''^{\alpha-1} = 2\tau_A^{2\alpha} \int_0^{t/\tau_A} dy e^y y^{\alpha-1} \Gamma(\alpha; y, t/\tau_A), \quad (4.9)$$

where $\Gamma(\cdot; \cdot, \cdot)$ is the difference between two incomplete gamma functions (see Appendix A.2). If we put the previous two calculations together we find that the mean-squared displacement of the free particle obeys the following expression

$$\Delta^2(t) = \frac{2D_\alpha}{\Gamma(\alpha+1)} t^\alpha + \frac{2\tau_A^{2\alpha} C}{\Gamma^2(\alpha)\eta_\alpha^2} \mathcal{A}_\alpha(t/\tau_A), \quad (4.10)$$

with

$$\mathcal{A}_\alpha(t) = \int_0^t dy e^y y^{\alpha-1} \Gamma(\alpha; y, t). \quad (4.11)$$

We have introduced here the anomalous diffusion coefficient $D_\alpha = k_B T / \eta_\alpha$, it conforms with the generalised Einstein relation. The mean-squared displacement consists of two terms. The first indicates the anomalous diffusion in a (non-active) viscoelastic bath. It is called anomalous because this diffusion is not a linear function of time (like normal diffusion in a viscous bath), instead it goes as a power-law. Since we have that $0 < \alpha \leq 1$, the diffusion will be slower in a viscoelastic bath. This slow diffusion is called *subdiffusion*. When $\alpha = 1$, the first term becomes normal diffusion, defined by Eq. (2.2). The second term in the mean-squared displacement is called the *active addition*, and it only exists when active forces are present, i.e. $C \neq 0$. The behaviour it gives to the particle is not clear from the expression itself. But by approximating this term for different time regimes, it will reveal its characteristics.

To approximate the active addition at early times, $t \ll \tau_A$, we use its original form from Eq. (4.7). For such small t , the exponential in the integrand will be almost equal to one, so $\exp(-|t' - t''|/\tau_A) \approx 1$. Applying this approximation decouples the integrals and solving them becomes trivial. The active addition for early times is

$$\frac{C}{\Gamma^2(\alpha+1)\eta_\alpha^2} t^{2\alpha}. \quad (4.12)$$

For long times, $t \gg \tau_A$, we have that t/τ_A is very large. This is the upper limit of the difference of gamma functions in Eq. (4.11), because this limit now becomes large we can do the following approximation $\Gamma(\alpha; y, t/\tau_A) \approx \Gamma(\alpha; y)$. The latter being an incomplete gamma function (see Appendix A.2). So for $t/\tau_A \gg 1$, we do the following manipulation

$$\mathcal{A}_\alpha(t/\tau_A \gg 1) \approx \int_0^{t/\tau_A} dy e^y y^{\alpha-1} \Gamma(\alpha; y) \quad (4.13)$$

$$= \int_0^{y'} dy e^y y^{\alpha-1} \Gamma(\alpha; y) + \int_{y'}^{t/\tau_A} dy e^y y^{\alpha-1} \Gamma(\alpha; y). \quad (4.14)$$

In the second line we divided the integral up at an arbitrary, but large, point $y' \gg 1$. The first term is a constant for a particular value of y' and thus not a function of

time. For the second term we use approximation (A.23) of the incomplete gamma function which is correct for large y . A large y is ensured because both y' and t/τ_A are chosen large. After this approximation is applied, the integral is straightforward to solve. Because t is still much larger than y' , we find

$$\mathcal{A}_\alpha(t/\tau_A \gg 1) \approx \frac{1}{2\alpha - 1} \left(\frac{t}{\tau_A} \right)^{2\alpha - 1}. \quad (4.15)$$

Plugging this result back into Eq. (4.10) leads to the following active addition for times larger than τ_A

$$\frac{2\tau_A C}{(2\alpha - 1)\Gamma^2(\alpha)\eta_\alpha^2} t^{2\alpha - 1}. \quad (4.16)$$

We now have all time-relations that the free particle can exhibit. A free particle in a non-active viscoelastic bath ($C = 0$) will always perform subdiffusion with a t^α relation to time, i.e. the first term of Eq. (4.10). When active forces are present and they are more prevailing than the thermal fluctuation, i.e. $C \gg k_B T$, we can clearly distinguish all previously derived time-relations.

For very early times, the particle shows the non-active subdiffusive behaviour with exponent α . This is because $\mathcal{A}_\alpha(t \rightarrow 0)$ goes faster to zero than the first term in Eq. (4.10). For early times, the exponent of the active addition becomes double that of the non-active term. The particle will therefore diffuse as Eq. (4.12). When $\alpha > 1/2$, this will lead to *superdiffusion*, since the time exponent is larger than that of normal diffusion (i.e. one). When times reach values higher than the persistence time τ_A , the 2α regime will make room for the $2\alpha - 1$ behaviour, Eq. (4.16). This exponent of time will always yield subdiffusion (or normal diffusion when $\alpha = 1$). When $\alpha < 1/2$, however, the exponent becomes negative, making this regime practically non-existing. For $\alpha > 1/2$, this regime persists for many time decades. But since its exponent is smaller than that of the non-active contribution (first term of Eq. (4.10)), it will eventually disappear in favour this faster non-active subdiffusion. Therefore, for very long times the particle will again subdiffuse with exponent α , as if the viscoelastic bath were not active. The viscoelastic bath effectively damps the active forces on these long time-scales. Only for a viscous bath, $\alpha = 1$, is this statement not true. Indeed, we then have $2\alpha - 1 = \alpha$. So for times larger than τ_A , the free particle in an active viscous bath performs normal diffusion, but with a diffusion constant that is enhanced by a factor $(1 + \tau_A C / \gamma k_B T)$. The free particle in a viscous bath therefore feels the presence of the active forces for all times to come.

From the above discussion, it is important to realise that the viscoelasticity of the bath clearly plays a defining role in the particle's response to the active forces. It influences both the prefactor as well as the exponent of this response's relation to time. To summarize, we present all the possible time-regimes in the following sequence for the mean-squared displacement of a free particle through time

$$\begin{aligned} \Delta^2(t) &= \frac{2D_\alpha}{\Gamma(\alpha + 1)} t^\alpha \xrightarrow{\tau_\downarrow} \frac{C}{\Gamma^2(\alpha + 1)\eta_\alpha^2} t^{2\alpha} \xrightarrow{\tau_A} \frac{2\tau_A C}{(2\alpha - 1)\Gamma^2(\alpha)\eta_\alpha^2} t^{2\alpha - 1} \\ &\xrightarrow{\tau_\uparrow} \frac{2D_\alpha}{\Gamma(\alpha + 1)} t^\alpha. \end{aligned} \quad (4.17)$$

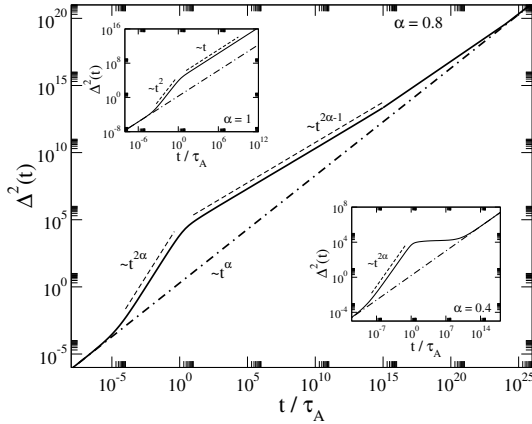


Figure 4.1: Log-log plot of the squared distance travelled by a free particle as a function of t/τ_A in a viscoelastic medium ($\alpha = 0.8$, $k_B T = \gamma = 1$) in the presence of active forces ($C = 10^4$, $\tau_A = 1$) (full line) compared to that without active forces (dashed-dotted line). Power-law behaviour is indicated with dashed lines. The insets share the same parameters apart from α . *Left inset:* $\alpha = 1$. *Right inset:* $\alpha = 0.4$.

The value above the arrows indicates the approximate time at which the transition happens. By equating the regimes, we found the early and late cross-over times, they are $\tau_\downarrow \sim (\eta_\alpha k_B T / C)^{1/\alpha}$ and $\tau_\uparrow \sim (\tau_A C / \eta_\alpha k_B T)^{1/(1-\alpha)}$. Figure 4.1 shows the mean-squared displacement of a free particle for large C and $\alpha = 0.4, 0.8$ and 1 . All regimes we discussed are clearly present. Also notice that the $2\alpha - 1$ behaviour for $\alpha = 0.4$ does not appear. The active curve rejoins relatively quickly with the non-active curve after $t = \tau_A$. For a viscous bath, the enhanced (normal) diffusion is evidently visible.

4.1.2 Motion of tracer particles

The results obtained from our model of a free particle in an active viscoelastic bath can be used to understand the dynamics of a tracer particle inside a cell (see Section 1.2). In several experiments it is observed that the motion of such a particle is superdiffusive at early times, but switches to being subdiffusive after a time of the order of seconds. In [80] it was, for example, found that the mean-squared displacement of a polystyrene microsphere, $3\mu\text{m}$ in diameter, inside a living cell performs superdiffusive motion, $\Delta^2(t) \sim t^{3/2}$, for times up to 10 seconds. On larger time scales, the particle had a subdiffusive motion, $\Delta^2(t) \sim t^{1/2}$.

In a study of breast-cancer cells [20, 81], the role of molecular motors and filaments of the cytoskeleton in active transport was investigated. These authors tracked the motion of tracer particles in cells with different metastatic¹ potential after chemical treatments that affect different cell components like myosin, actin and microtubules. While the precise value of the mean-squared displacement's exponent depended on

¹Metastasis means the spread of cancer or other disease from one tissue in the body to another. The affected tissue is considered not in contact with the affecting tissue.

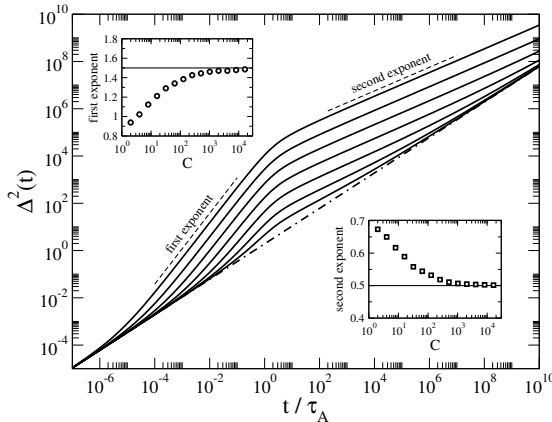


Figure 4.2: Log-log plot of the mean-squared displacement of a free particle as a function of t/τ_A in a viscoelastic medium ($\alpha = 3/4$, $k_B T = \gamma = 1$). The subdiffusion in a non-active bath is depicted by the dashed-dotted line. The full lines show the dynamics in an active bath ($\tau_A = 1$) for different values of C . We have $C = 2^i$ with $i = 2, 4, 6, 8, 10, 12$ and 14 . Higher lying curves have a larger value of C . The insets show the C -dependence of the exponents (determined by curve-fitting). *Left inset:* Shows the first exponent as a function of C in a lin-log plot, the asymptotic value 2α is indicated. *Right inset:* Shows the second exponent as a function of C in a lin-log plot, the asymptotic value $2\alpha - 1$ is indicated.

the treatment applied, in all cases it was found that the exponent decreased from a value in the range $1.2 - 1.4$ to a significant lower value of $0.8 - 1.0$ after approximately 3 seconds. So, this experiment also revealed a crossover between superdiffusive and subdiffusive motion.

In a recent work, Revere *et al.* [82] studied the motion of endogenous¹ particles in the protist *Acanthamoeba castellanii*. The cytoplasm of this organism has been called supercrowded, making it surely suitable to be modelled by a viscoelastic bath. In contrast to the earlier studies, the cells of *A. castellanii* have a non-zero motility. After subtraction of this motion, the dynamics of vesicles and granules (i.e. particles) was still found to superdiffuse with an exponent approximately equal to 1.8. For the times investigated (up to 10 seconds) no clear crossover to another exponent was observed. After treating the cells with latrunculin A or nocodazole (these substances decrease the activity of a cell by affecting the availability of actin filaments and microtubules respectively), the exponent decreased to a value around $1.5 - 1.6$ in an early time regime. Moreover, a cross-over to a decreased exponent after a few seconds can be observed in these cases, though the authors do not quote a value.

If we compare these experiments with our theory, we find that they are consistent. In the (theoretical) intermediate time regime, we found a crossover from superdiffusion to subdiffusion, as was observed in the experiments [20, 81, 82]. The drop in exponent in [80] from $3/2$ to $1/2$ suggests that the viscoelasticity of the cell's cytosol is

¹In this context, meaning naturally originating from within the cell.

characterised by $\alpha = 3/4$. Because these regimes are so clearly observable we conclude that the active forces are strong compared with the thermal ones, i.e. $C \gg k_B T$.

We need to make an important note here. When the active and thermal forces are of comparable strength, $C \approx k_B T$, the time-relations are not as evident as presented in Fig. 4.1. There is, however, still a clear cross-over between two effective exponents. The first effective exponent grows with growing C from α to 2α , while the second decreases from α to $2\alpha - 1$ with increasing C . This behaviour is presented in Fig. 4.2 for $\alpha = 3/4$. A specific example is the exponent 1.39 followed by 0.53, when $C = 128$. This implies that, for weak active forces, the diffusive exponents are not only related to the viscoelastic properties of the medium (i.e. α) but are also an (unknown) function of C . This could be the scenario behind the experiments on breast-cancer cells and *A. castellanii*. When applying rheological methods to determine the α -value of a cell, one needs to take into account this C -dependence of the exponents. Or one should be sure that the active forces are sufficiently strong. These C -dependent exponents can, however, explain the drop in the superdiffusive exponent measured by [82]. Here they inhibited the actin or microtubules, leaving the cell less active. This process can be linked to a decrease in C , which our model suggests will consequently decrease the (superdiffusive) exponent.

Another conclusion we can draw from comparing the experiments with our theory is that, for a living cell, the value of the persistence time τ_A is of the order of seconds. Indeed, the cross-over between a superdiffusive regime to a subdiffusive regime appears, in our results, at τ_A . If observed in the experiment, the cross-over happened at times ranging from 3 to 10 seconds. Although this value is bound to change when investigating different types of cells, it does give a sense of the time scales at which the active forces are persistent.

4.2 Harmonic oscillator

The obvious potential to study next would be a linear one, i.e. $U(x) \sim x$. This will generate a constant force on the particle and invoke a sedimentation process. However, due to its modest cellular relevance, we will not consider this potential here. Therefore the following potential is naturally a quadratic one, in physics commonly known as a harmonic oscillator

$$U(x) = \frac{k}{2} x^2. \quad (4.18)$$

This potential will inflict a *restoring force* on the particle toward the origin. This restoring force is proportional to the particle's displacement from the origin and its strength is measured by k . If the harmonic oscillator is surrounded by an active viscoelastic bath, the equation of motion for it will be (see Section 2.6)

$$\eta_\alpha {}_c \mathcal{D}^\alpha x(t) = -kx(t) + \xi_T(t) + \xi_A(t)H(t). \quad (4.19)$$

Again, we used the Heaviside function to turn the active forces on at $t = 0$, disturbing the thermalised state of the system. We will solve Eq. (4.19) to discover the behaviour of the harmonic oscillator. This equation is also studied numerically, with the algorithm discussed in Chapter 3. Because the exact solution is available, we can use it to test whether the performance of our numerical scheme is satisfactory.

4.2.1 Anomalous diffusion and steady state

Again, we take the Laplace transform of the equation of motion, Eq. (4.19), to find the evolution of x . Using the techniques from Appendix A.2, we find

$$\eta_\alpha s^{\alpha-1} [s\tilde{x}[s] - x(0)] = -k\tilde{x}[s] + \tilde{\xi}_T[s] + \tilde{\xi}_A[s]. \quad (4.20)$$

Somewhat rearranging the terms gives the following expression for the position in Laplace space

$$\tilde{x}[s] = s^{-1}x(0) \left[1 + \frac{k}{\eta_\alpha} s^{-\alpha}\right]^{-1} + \frac{s^{-\alpha}}{\eta_\alpha} (\tilde{\xi}_T[s] + \tilde{\xi}_A[s]) \left[1 + \frac{k}{\eta_\alpha} s^{-\alpha}\right]^{-1}. \quad (4.21)$$

The inverse Laplace transform of this equation can be done in terms of the *Mittag-Leffler function* $E_{\alpha,\beta}(\cdot)$ (see Appendix A.1). One finds that the position of the harmonic oscillator satisfies the following expression

$$x(t) = x(0)E_{\alpha,1}\left(- (t/\tau)^\alpha\right) + \frac{1}{\eta_\alpha} \int_0^t dt' (\xi_T(t-t') + \xi_A(t-t')) t'^{\alpha-1} E_{\alpha,\alpha}\left(- (t'/\tau)^\alpha\right). \quad (4.22)$$

It is clear that if we take $k = 0$, we retrieve the dynamics of the free particle, i.e. Eq. (4.6). We introduced the characteristic time τ of the oscillator, it is defined as

$$\tau = \left(\frac{\eta_\alpha}{k}\right)^{1/\alpha}. \quad (4.23)$$

Because the defining equation of $x(t)$, Eq. (4.20), is linear and both noise terms are Gaussian, also $x(t)$ is a Gaussian random variable. The average position of the harmonic oscillator is found by taking the ensemble average of Eq. (4.22). Because the potential is symmetric around $x = 0$ and the system is thermalised at $t = 0$, we have that $\langle x(0) \rangle = 0$. Both the noise terms are centered, it is therefore easy to find that $\langle x(t) \rangle = 0$ for all time t . From this it is straightforward to show that $\langle \Delta x(t) \rangle = 0$. We can now fully define $x(t)$ if we also find its second cumulant.

The mean-squared displacement of the harmonic oscillator is given by

$$\Delta^2(t) = \langle (\Delta x(t))^2 \rangle = \langle x^2(t) \rangle + \langle x^2(0) \rangle - 2\langle x(t)x(0) \rangle. \quad (4.24)$$

The system is thermalised at $t = 0$, therefore the second term on the right-hand side can be determined using the equipartition theorem (see Section 2.2). From this theorem we know that the average of the quadratic potential, $\langle kx^2/2 \rangle$, is equal to $k_B T/2$ in equilibrium. We thus find that $\langle x^2(0) \rangle = k_B T/k$. To evaluate the two remaining terms of Eq. (4.24), we first note that both the thermal and the active random forces are not correlated with the initial position of the harmonic oscillator, i.e. $\langle \xi_T(t)x(0) \rangle = \langle \xi_A(t)x(0) \rangle = 0$. Using this property and the equipartition result, it is straightforward to find the last term in Eq. (4.24). The correlation between the oscillators initial position with its position at a later time t is

$$\langle x(t)x(0) \rangle = \frac{k_B T}{k} E_{\alpha,1}\left(- (t/\tau)^\alpha\right). \quad (4.25)$$

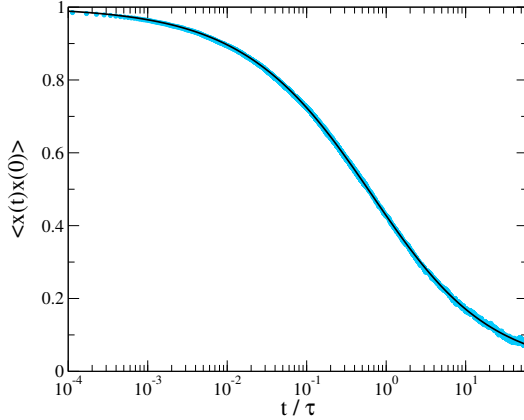


Figure 4.3: Lin-log plot of the correlation between the initial position and the position at time t , $\langle x(t)x(0) \rangle$, as a function of t/τ of a harmonic oscillator ($k = 1$) in an active ($C = \tau_A/\tau = 1$) viscoelastic ($\alpha = 0.5, k_B T = \gamma = 1$) bath. The blue dots are the simulated correlation (averaged over 10^5 histories) and the black line is the analytic expression, Eq. (4.25).

Notice that this correlation is not influenced by the active forces. It will therefore be the same in equilibrium and out of equilibrium. At $t = 0$ it is equal to the equipartition result, as it should be. Over time this correlation will decrease to zero. Figure 4.3 shows this correlation for a viscoelastic bath with $\alpha = 0.5$. For this particular value of α , the expression of the correlation can be written in closed form using the list provided in Appendix A.1. It becomes $\langle x(t)x(0) \rangle = (k_B T/k) \operatorname{erfc}(\sqrt{t/\tau}) e^{t/\tau}$. Also shown in this figure are the results of a numeric analysis of the system (using the algorithm discussed in Chapter 3). The performance of the simulation is clearly excellent on all the investigated time-scales. The final calculation, that of $\langle x^2(t) \rangle$, to acquire the mean-squared displacement is more involved. We square Eq. (4.22) and take its ensemble average. The cross-terms drop out due to reasons discussed above. Using the equipartition result and the noise correlations, Eqs. (2.62) and (2.64), give

$$\begin{aligned}
 \langle x^2(t) \rangle &= \frac{k_B T}{k} E_{\alpha,1}^2 \left(- (t/\tau)^\alpha \right) \\
 &+ \frac{k_B T}{\Gamma(1-\alpha)\eta_\alpha} \int_0^t dt' \int_0^t dt'' \frac{t'^{\alpha-1} t''^{\alpha-1}}{|t' - t''|^\alpha} E_{\alpha,\alpha} \left(- (t'/\tau)^\alpha \right) E_{\alpha,\alpha} \left(- (t''/\tau)^\alpha \right) \\
 &+ \frac{C}{\eta_\alpha^2} \int_0^t dt' \int_0^t dt'' e^{-|t'-t''|/\tau_A} t'^{\alpha-1} t''^{\alpha-1} E_{\alpha,\alpha} \left(- (t'/\tau)^\alpha \right) E_{\alpha,\alpha} \left(- (t''/\tau)^\alpha \right).
 \end{aligned} \tag{4.26}$$

This lengthy expression can be greatly simplified using property (A.10) of the Mittag-Leffler functions derived in Appendix A.1. The mean-squared position of the harmonic

oscillator then reads

$$\langle x^2(t) \rangle = \frac{k_B T}{k} + \frac{C}{k^2} A_\alpha(t; \tau, \tau_A), \quad (4.27)$$

with $A_\alpha(t; \cdot, \cdot) = A_\alpha(t, t; \cdot, \cdot)$ and

$$A_\alpha(t, t'; \tau_1, \tau_2) = \int_0^{t/\tau_1} dx \int_0^{t'/\tau_1} dy \left(\frac{E_{\alpha, \alpha}(-x^\alpha) E_{\alpha, \alpha}(-y^\alpha)}{x^{1-\alpha} y^{1-\alpha}} \right) e^{-\frac{\tau_1}{\tau_2} |x-y|}. \quad (4.28)$$

The mean-squared position consists of two terms. The first term is the equipartition result one finds if the oscillator were in equilibrium. The second term is the active addition which clearly disappears when no active forces are present, i.e. $C = 0$. We are now able to construct the mean-squared displacement of the harmonic oscillator. Adding the three derived terms of Eq. (4.24) gives

$$\Delta^2(t) = \frac{2k_B T}{k} \left[1 - E_{\alpha, 1} \left(- (t/\tau)^\alpha \right) \right] + \frac{C}{k^2} A_\alpha(t; \tau, \tau_A). \quad (4.29)$$

The first conclusion we can draw from this expression is that the diffusion in an active bath will be more rapid than in an equilibrated bath. This is because $A_\alpha(t; \tau, \tau_A)$ is a positive function for all positive time, making the fluctuations larger when $C \neq 0$. We will come back to this later. The specific dynamics that $\Delta^2(t)$ will exhibit is not clearly revealed by Eq. (4.29). We therefore approximate this expression for different time regimes to understand the dynamics it contains.

First notice that we can rewrite the first term of Eq. (4.29) using property (A.7) of the Mittag-Leffler functions. The first term becomes

$$\frac{2k_B T}{k} \frac{t^\alpha}{\tau^\alpha} E_{\alpha, \alpha+1} \left(- (t/\tau)^\alpha \right). \quad (4.30)$$

For very early times, $t \ll \tau$, we can approximate the above Mittag-Leffler function by $1/\Gamma(\alpha + 1)$. The first term of Eq. (4.29) is thus approximately equal to

$$\frac{2D_\alpha}{\Gamma(\alpha + 1)} t^\alpha. \quad (4.31)$$

This is the subdiffusion a free particle performs in a non-active viscoelastic bath. The second term of Eq. (4.29) can also be approximated for early times, $t \ll \tau_A$ and $t \ll \tau$. The exponential function in A_α can then be approximated by one and the Mittag-Leffler functions by $1/\Gamma(\alpha)$. By doing this, the integrals in A_α decouple and become trivial to solve. For these early times the second term in Eq. (4.29) becomes equal to Eq. (4.12), which is the $t^{2\alpha}$ anomalous diffusion of a free particle in an active viscoelastic bath. For times longer than τ_A , the free $t^{2\alpha-1}$ behaviour is retrieved when A_α is approximated by setting the Mittag-Leffler functions equal to $1/\Gamma(\alpha)$ and using Eq. (4.15). Both terms in Eq. (4.29) saturate when times become large, i.e. $t \gg \tau$. The system then reaches a nonequilibrium steady state, we will discuss this regime in more detail later. The sequence of time-relations that a harmonic oscillator in an active viscoelastic bath displays is given below (for $\tau_A \ll \tau$)

$$\Delta^2(t) = \frac{2D_\alpha}{\Gamma(\alpha + 1)} t^\alpha \xrightarrow{\tau_d} \frac{C}{\Gamma^2(\alpha + 1)\eta_\alpha^2} t^{2\alpha} \xrightarrow{\tau_A} \frac{2\tau_A C}{(2\alpha - 1)\Gamma^2(\alpha)\eta_\alpha^2} t^{2\alpha-1} \xrightarrow{\tau} nss, \quad (4.32)$$

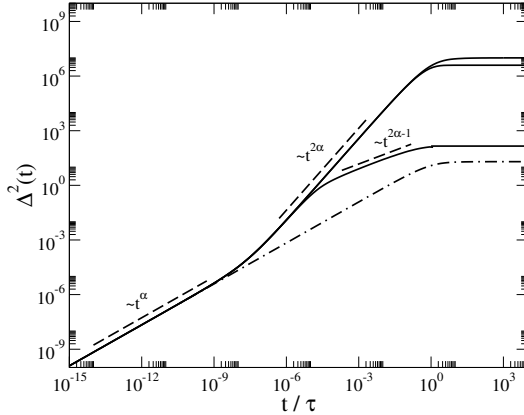


Figure 4.4: Log-log plot of the mean-squared displacement of a harmonic oscillator ($k = 10^{-1}$) as a function of t/τ in a viscoelastic medium ($\alpha = 3/4$, $k_B T = \gamma = 1$) in the presence of active forces with $C = 10^5$ and $\tau_A/\tau = 10^5$, 1 and 10^{-5} (full lines, top to bottom) compared to that without active forces (dashed-dotted line). The power-law behaviour is indicated with dashed lines.

where *nss* stands for nonequilibrium steady state. Figure 4.4 presents the mean-squared displacement of the harmonic oscillator, Eq. (4.29), for $\alpha = 3/4$ and different values of τ_A/τ . The harmonic oscillator in a non-active viscoelastic bath is also shown. The α and 2α regimes are clearly always present, but the $2\alpha - 1$ regime needs a low persistence time to reveal itself. In this figure the nonequilibrium steady state is also visible for times larger than τ . A comparison between the analytic results and the simulated data is given in Fig. 4.5 for a large variety of parameters. Again we can state that the algorithm performs extremely well, not showing any serious deviations from the exact result on all investigated time-scales.

We thus find that, between $t = 0$ and the steady state, the oscillator goes through a transient regime that is equal to that of a free particle. This can be understood by the fact that during these early times the particle does not feel it is bounded by a potential, it diffuses in an area where the potential is approximately constant. In other words, the particle is not yet aware it is an oscillator. The transient state is always dependent on α , also in equilibrium. But, interestingly, the steady state – which, in equilibrium, does not depend on the viscoelasticity – becomes α -dependent when the system is out-of-equilibrium. We will now investigate this further.

Steady state

Because the particle resides in a bounding potential, it cannot (on average) explore the whole space like the free particle could. Both in and out of equilibrium, the system will reach a steady state, in which it will cease to evolve in time. From here on we use the subscript *ss* to denote that the system is in a (nonequilibrium) steady state, this state is certainly reached when $t \rightarrow \infty$. We will focus on the steady state of the mean-squared position of the oscillator, i.e. $\langle x^2 \rangle_{ss} = \lim_{t \rightarrow \infty} \langle x^2(t) \rangle$, because of its

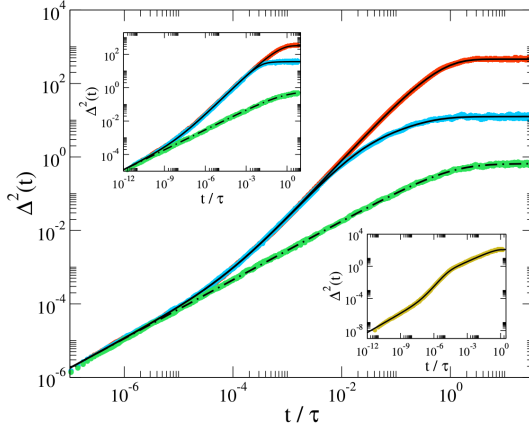


Figure 4.5: Log-log plot of the mean-squared displacement of a harmonic oscillator ($k = 3$) as a function of t/τ in a viscoelastic medium ($\alpha = 0.8$, $k_B T = \gamma = 1$) in the presence of active forces with $C = 10^4$ and $\tau_A/\tau = 1, 10^{-2}$ (full lines, top to bottom) compared to that without active forces (dashed-dotted line). The coloured dots are the simulated data (averaged over 10^3 histories) with green ($C = 0$), blue ($\tau_A/\tau = 10^{-2}$) and orange ($\tau_A/\tau = 1$). *Left inset*: Equivalent to the main graph but with $\alpha = 0.4$. *Right inset*: Equivalent to the main graph but with $k = 0.1$, $C = 10^5$ and $\tau_A/\tau = 10^{-5}$.

obvious relation to the equipartition theorem. Indeed, when the system is thermalised we have $\langle x^2(t) \rangle = k_B T/k$ for all time. The steady state for an oscillator that is driven out of equilibrium by active forces is given by the following expression

$$\langle x^2 \rangle_{ss} = \frac{k_B T}{k} + \frac{C}{k^2} A_\alpha^\infty(\tau/\tau_A). \quad (4.33)$$

Here we introduced the function $A_\alpha^\infty(\tau_1/\tau_2) = \lim_{t \rightarrow \infty} A_\alpha(t; \tau_1, \tau_2)$, which is a function of only the ratio τ_1/τ_2 , as can easily be seen from Eq. (4.28). In Fig. 4.6 we plot $A_\alpha^\infty(x)$ for different values of α . From it, it is immediately clear that the active addition to the steady state is always positive. This implies that, with the extra energy acquired from the active forces, the particle can diffuse further from the origin and therefore higher up the potential landscape. We will now discuss the properties of the two limit cases: when τ/τ_A is low and when it is high.

When $\tau/\tau_A \ll 1$, the exponential function in Eq. (4.28) will be approximately unity. Notice that this only holds when the integration variables are small. But since the tail of the integrand decreases rapidly to zero, it does not contribute much to the total integral, so the approximation still holds. The two integrals decouple and after using $\int_0^\infty dx x^{\alpha-1} E_{\alpha, \alpha}(-x^\alpha) = 1$ we conclude that $A_\alpha^\infty(\tau/\tau_A) \rightarrow 1$ when τ_A is much larger than τ . Figure 4.6 confirms this statement. We therefore find

$$\langle x^2 \rangle_{ss} = \frac{k_B T}{k} + \frac{C}{k^2}. \quad (4.34)$$

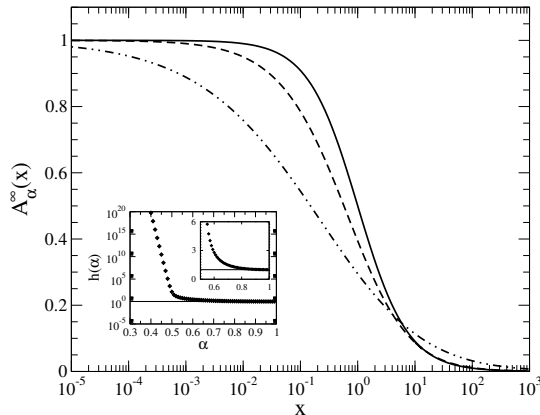


Figure 4.6: Lin-log plot of $A_\alpha^\infty(x)$ as a function of its argument x . With $\alpha = 1$ (solid line), $\alpha = 3/4$ (dashed line) and $\alpha = 0.4$ (dashed-dotted line). *Inset*: Log-lin plot of $h(\alpha)$ as a function of α . The horizontal line indicates $h(1) = 1$. *Inset's inset*: Lin-lin plot the original inset, with the α -axis starting at $1/2$.

We find that, just as in equilibrium, the steady state does not depend on the viscoelasticity (i.e. α) of the bath. In this bath, with large τ_A , the direction of the active forces stays, on average, the same over a long period of time. However, when k is very large, the steep potential will prevent this long persistent motion. We therefore see that the steady state then reduces to the original equipartition result. Building on this equipartition theorem we can associate an effective temperature T_* to this state, namely $k_B T_* = k_B T + C/k$. In Fig. 4.7 we show that our algorithm produces the correct steady state for τ/τ_A small.

When $\tau/\tau_A \gg 1$, the exponential function in Eq. (4.28) can be written as a Dirac delta function¹. It is then quite easy to work out that $A_\alpha^\infty(\tau/\tau_A) \rightarrow (\tau_A/\tau)h(\alpha)$ with $h(\alpha) = 2 \int_0^\infty dx x^{2\alpha-2} E_{\alpha,\alpha}^2(-x^\alpha)$. The steady state becomes

$$\langle x^2 \rangle_{ss} = \frac{k_B T}{k} + \frac{C}{k^2} \frac{\tau_A}{\tau} h(\alpha). \quad (4.36)$$

When the relaxation time of the oscillator is much larger than the persistence time of the active forces, the steady state depends on the viscoelasticity (i.e. α) of the bath. The function that quantifies this dependence is $h(\alpha)$. This is a decreasing function, reaching 1 when $\alpha = 1$. For $0.5 \leq \alpha \leq 1$, the value of $h(\alpha)$ is relatively low, with $h(0.5) \approx 141.2$. When we decrease α from 0.5 to zero, the value of $h(\alpha)$ explodes, going to infinity when $\alpha = 0$. This implies that, when $\alpha < 0.5$, the approximation of large τ/τ_A only holds when this value is extremely large, i.e. $\tau/\tau_A \gg \gg 1$. The effective temperature of this steady state is $k_B T_* = k_B T + (\tau_A C/\tau k)h(\alpha)$. For a bath

¹We used here the following definition of the Dirac delta function

$$\delta(x) = \lim_{\epsilon \rightarrow 0} \frac{1}{2\epsilon} \exp(-|x|/\epsilon). \quad (4.35)$$

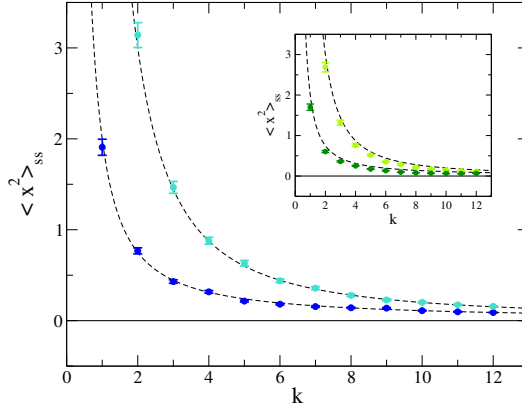


Figure 4.7: Lin-lin plot of the steady state value for the mean-squared position as a function of k of a harmonic oscillator in an active ($C = 1$ (dark dots) and 10 (light dots), $\tau/\tau_A = 10^{-5}$) viscoelastic ($\alpha = 0.8$, $k_B T = \gamma = 1$) bath. The coloured dots are the simulated data (averaged over 10^3 histories) and the dashed lines are the analytic expression (4.34). *Inset*: Equivalent to the main graph but with $\alpha = 0.4$.

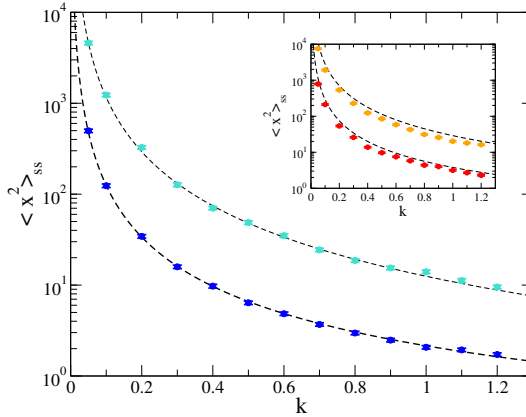


Figure 4.8: Log-lin plot of the steady state value for the mean-squared position as a function of k of a harmonic oscillator in an active ($C = 10^3$ (dark dots) and 10^4 (light dots), $\tau/\tau_A = 10^3$) viscoelastic ($\alpha = 0.8$, $k_B T = \gamma = 1$) bath. The coloured dots are the simulated data (averaged over 10^3 histories) and the dashed lines are the analytic expression (4.36). *Inset*: Equivalent to the main graph but with $\alpha = 0.6$.

with the same large τ/τ_A ratio, the effective temperature will be high in a low α bath and low in one with a high α -value. Adding active forces with small τ_A to a harmonic oscillator and letting it reach a steady state will enable one to determine α , which would not be possible in equilibrium or in low τ/τ_A steady state. Figure 4.8 proves that, when α is above 0.5, our algorithm performs satisfactory. For smaller α , the simulation results deviate somewhat from the analytic results. This is because low α systems take longer to reach steady state. These results are therefore not acquired from a fully steady state, since our algorithm has trouble simulating such long times (see Chapter 3).

Probability distribution

We already mentioned that the position of the oscillator $x(t)$ is a Gaussian variable. The probability to find the particle at time t in the small interval between x and $x + dx$ is therefore given by $P(x, t)dx$ with

$$P(x, t) = \frac{1}{\sqrt{2\pi\langle x^2(t) \rangle}} \exp\left(-\frac{x^2}{2\langle x^2(t) \rangle}\right), \quad (4.37)$$

and $\langle x^2(t) \rangle$ given by Eq. (4.27). The system is, as always, assumed to be in equilibrium at $t = 0$. So initially the variance of this normal distribution is $k_B T/k$. Notice that, independently of α , $A_\alpha(t; \tau, \tau_A)$ is always strictly positive and therefore the density $P(x, t)$ always broadens after the active forces have been turned on. This broadening through time is illustrated in Fig. 4.9 for a bath with $\alpha = 3/4$. For times larger than τ , the broadening stops and reaches a steady value. This steady variance is, of course, larger than in equilibrium and given by Eq. (4.33). The oscillator's fluctuations from the origin in an active bath are therefore larger than those in a non-active bath. Figure 4.10 shows the simulated distribution at different times. In these simulations, the system was not thermalised at $t = 0$, the particle always started in the origin. We therefore have $\langle x(0) \rangle = \langle x^2(0) \rangle = 0$. The initial distribution is then a Dirac delta peak: $P(x, 0) = \delta(x)$. The evolution of the distribution is still given by Eq. (4.37), but the mean-squared position is now expressed by

$$\langle x^2(t) \rangle_{x(0)=0} = \frac{k_B T}{k} \left[1 - E_{\alpha,1}^2\left(- (t/\tau)^\alpha\right) \right] + \frac{C}{k^2} A_\alpha(t; \tau, \tau_A), \quad (4.38)$$

rather than Eq. (4.27), where the system is in equilibrium at $t = 0$. The figure demonstrates that, again, the simulation produced the correct distribution results.

4.2.2 Velocity correlation

Because it resides in a viscoelastic bath, the velocity $v(t)$ of the oscillator at previous times has a direct influence on its present friction. Therefore the velocity correlation $\langle v(t_1)v(t_2) \rangle$ is a good measure to illustrate how the memory of the system relates past events with the present. Yet, great care has to be taken when considering the velocity because we applied the overdamped limit to the generalised Langevin equation (see Chapter 2). Difficulties arising from this limit will be addressed shortly.

The correlation of the velocity at time t_1 and t_2 is calculated using the Laplace transform. We have $\tilde{v}[s] = s\tilde{x}[s] - x(0)$, using Eq. (4.21) one finds the velocity's

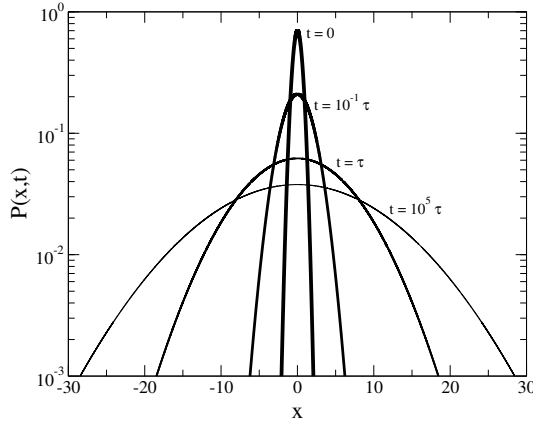


Figure 4.9: Log-lin plot of the probability distribution $P(x, t)$ for a harmonic oscillator ($k = 3$) in a viscoelastic bath ($\alpha = 3/4$, $k_B T = 1$, $\tau = 10^{-5}$) after active forces ($C = 10^3$, $\tau_A = 1$) are turned on at $t = 0$. At $t = 0$ the distribution is that of thermal equilibrium. The figure shows the broadening of the distribution as a function of time (the time corresponding to each curve is indicated).

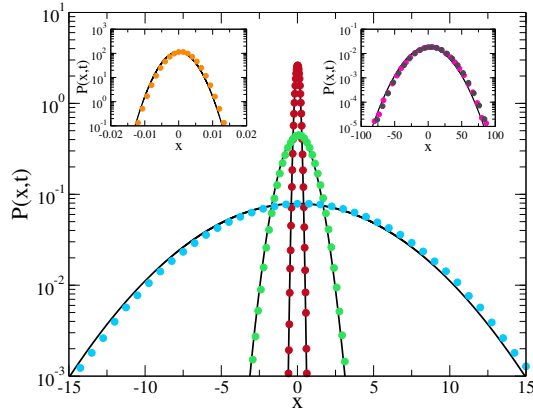


Figure 4.10: Log-lin plot of the probability distribution $P(x, t)$ for a harmonic oscillator ($k = 3$) in a viscoelastic bath ($\alpha = 0.8$, $k_B T = \gamma = 1$) after active forces ($C = 10^4$, $\tau_A/\tau = 1$) are turned on at $t = 0$. The initial position of the oscillator is in the origin, i.e. $x(0) = 0$. The coloured dots are the simulated distribution (averaged over 10^6 histories). The black lines are the analytic expression (4.37) using Eq. (4.38). The distribution is measured at different times: *Left inset*: $t/\tau = 10^{-6}$ (orange). *Main graph*: $t/\tau = 10^{-3}$ (red), 10^{-2} (green) and 10^{-1} (blue). *Right inset*: $t/\tau = 10$ (pink) and 10^2 (grey).

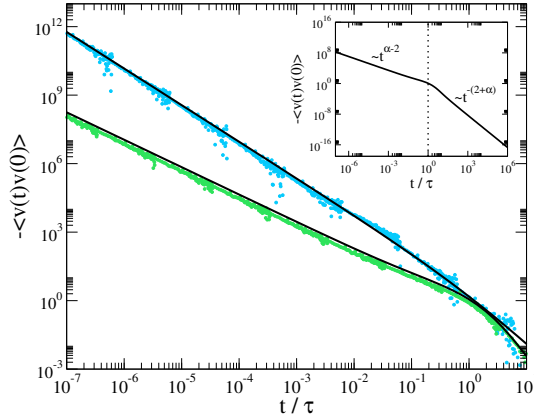


Figure 4.11: Log-log plot of minus the correlation between the initial velocity $v(0)$ and the velocity at time t as a function of (small) t/τ for a harmonic oscillator ($k = 3$) in an active ($C = 1$, $\tau_A/\tau = 10^{-2}$) viscoelastic ($\alpha = 0.4$ (blue), 0.8 (green), $k_B T = \gamma = 1$) bath. The coloured dots are the simulated correlation (averaged over 10^8 histories) and the black lines are the analytic expression (4.40). *Inset*: Shows the cross-over of power-law behaviour in the correlation, Eq. (4.40), at time τ .

Laplace transform

$$\tilde{v}[s] = -\frac{k s^{-\alpha}}{\eta_\alpha} x(0) \left[1 + \frac{k}{\eta_\alpha} s^{-\alpha} \right]^{-1} + \frac{s^{1-\alpha}}{\eta_\alpha} (\tilde{\xi}_T[s] + \tilde{\xi}_A[s]) \left[1 + \frac{k}{\eta_\alpha} s^{-\alpha} \right]^{-1}. \quad (4.39)$$

From this equation it is easy to see that the mean velocity of the oscillator is always zero, i.e. $\langle v(t) \rangle = 0$. This was expected since the stochastic forces have no preferred direction and the potential is symmetrical. We will now focus on the correlation between the initial velocity and the velocity at a later time t . In Appendix C we derive this relation, it reads

$$\langle v(t)v(0) \rangle = \frac{k_B T}{\eta_\alpha} t^{\alpha-2} E_{\alpha, \alpha-1} \left(-(t/\tau)^\alpha \right). \quad (4.40)$$

This correlation is always negative and increasing. Implying that, on average, the motion of the oscillator in a particular direction brings about a subsequent restoring motion in the opposite direction. This behaviour is due to the elastic response of a viscoelastic bath which is captured in the memory kernel, Eq. (2.50). Since this kernel goes to zero for long times, so does the resulting correlation. Also notice that $\langle v(t)v(0) \rangle$ is not influenced by the active forces, just as the correlation between the initial position and that on time t , Eq. (4.25). Figure 4.11 shows $-\langle v(t)v(0) \rangle$ for $\alpha = 0.4$ and 0.8 at times smaller than τ . For these short time-scales, the Mittag-Leffler function in Eq. (4.40) is approximately equal to $1/\Gamma(\alpha-1)$ (see Appendix A.1), causing the correlation to go as $t^{\alpha-2}$. Although this quantity inherently exhibits large fluctuations, the mean behaviour of the simulations clearly follows the analytic result.

For times larger than τ we use the asymptotic expansion, Eq. (A.4), of the Mittag-Leffler functions. In case of the Mittag-Leffler function in Eq. (4.40), the first term ($r = 1$) of this expansion is zero, because $1/\Gamma(-1) = 0$. Using the second term yields a correlation that goes as $t^{-(\alpha+2)}$ for long times. The initial decay thus crosses over to a faster decay after the characteristic time τ . This cross-over is clearly visible in the inset of Fig. 4.11, where the analytic solution of the velocity correlation is plotted for short and long time-scales. From Eq. (C.8) it is clear that $\langle v^2(t) \rangle \rightarrow -\infty$. This non-physical result comes from the fact that the instantaneous velocity is ill-defined in our model. The overdamped limit ($m \rightarrow 0$) assumes that the velocity is in thermal equilibrium for any time-scale. This would imply that $\langle v^2(0) \rangle = k_B T/m$ (see Section 2.2). This relation is spoiled by the overdamped limit because the inertia of the particle should not be neglected at very short time-scales. Therefore our model (and by extension our algorithm) is not suited to describe the instantaneous velocity, only the correlation of it between different times.

4.2.3 Stepping of molecular motors

Here we use the theory of a harmonic oscillator in an active viscoelastic bath to describe the dynamics of a *kinesin* macromolecule. Before going into its dynamics, we first give a short overview of the function and structure of this macromolecule. Kinesin is a protein found in eukaryotic cells, it belongs to the group of motor proteins. It can transport other proteins or organelles by attaching to it and subsequently moving along a microtubule filament. This movement is powered by ATP hydrolysis. A kinesin protein consists of two motor-heads that each have a neck-linker (see Fig. 4.12). These linkers are connected to a long coiled stalk that ends with the cargo-binding tail. When the kinesin is not bound to a microtubule filament, both motor-heads have an ADP (adenosine diphosphate) bound to their active site. The kinesin performs Brownian motion until it comes in contact with a microtubule filament. When one motor-head binds to the filament it releases its ADP, while the other motor-head trails behind it (Fig. 4.12: 1). After the bound motor-head has released its ADP, it binds ATP to its active site. This causes the neck-linker to quickly swing forward, positioning the loose motor-head in front of the bound motor-head (Fig. 4.12: 1 \rightarrow 2). The loose motor-head now needs to diffuse to the filament where it can weakly bind to it and release ADP (Fig. 4.12: 2). The bond between this motor-head and the filament becomes stronger when the (now) trailing bound motor-head hydrolyses its ATP. After the hydrolyses, the trailing motor-head lets go of the filament (Fig. 4.12: 3). This release causes the leading bound motor-head to bind ATP to its active site (Fig. 4.12: 4). From here on the whole process repeats. The kinesin can thus move step-by-step along the microtubule filament, each step one motor-head is placed before the other, effectively causing the kinesin to “walk”.

The phase where the forwardly swung motor-head needs to diffuse to reach the filament is the main interest of our discussion here. This phase (among others) determines the speed at which the kinesin can move along the filament. Detailed mechanochemical models have been introduced that successfully describe the velocity of the motor as a function of applied force, ATP-concentration, etc. It is less clear how to explain the large processivity of kinesin [83]. A crucial role in these models is played by the mechanical properties of the neck-linker. The diffusion of the motor-head depends on

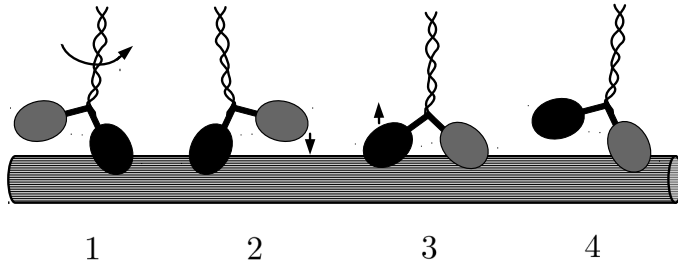


Figure 4.12: Schematic representation of the four stages one kinesin protein goes through when walking along a microtubule filament. The long horizontal cylinder represents the microtubule filament. The grey and black ovals are the motor-heads with a black neck-linker attached. The long twisted structure starting from the neck-linkers is the coiled stalk. In this picture there is no cargo bound to the tail.

the elastic properties of this neck-linker, which in the simplest approximation is often modelled as a Hookean spring (i.e. a linear relation between extension and force). A better approximation is to describe the linker as a worm-like chain (see Section 5.5) and use the latter's well known force-extension relation to determine the potential in which the motor-head diffuses [84]. Important properties are then the time it takes for the motor-head to diffuse in this potential over a distance of 4.1nm, i.e. the distance to the next binding site on the filament, and the probability p that the motor-head is within a small distance around that binding site. For example, in a model based on a Hookean spring, this probability was found to be rather small ($p = 0.058$) [84]. This model, however, did not incorporate active nor viscoelastic effects. Because these effects better characterise diffusive processes inside a cell, we investigate here if they can influence p , and preferably increase its value. We also study how the time to reach the binding site is changed in an active viscoelastic environment.

Because the diffusing motor-head is connected to a linker, which is modelled by a Hookean spring, inside the cytosol, it can be modelled as a harmonic oscillator in an active viscoelastic bath. The behaviour of this system was discussed above. We will follow [84] and choose $k = 1$ pN/nm. The thermal energy is calculated as follows, using $k_B = 0.0138$ pN nm/K and $T = 300$ K, one finds $k_B T \approx 4.14$ pN nm. From Eq. (4.23) it then follows that the characteristic time of the oscillating motor-head is $\tau \approx 50 \mu\text{s}$, which is much shorter than the persistence time of the active forces, which is of the order of seconds (see Section 2.5). Here, as a rough estimate we took $\gamma = 6\pi\eta a$ where for the cytosol we assumed the viscosity η to be thousand times that of water: $\eta_w = 8.90 \cdot 10^{-10}$ pN s/nm², and for the characteristic length-scale of a protein we took $a = 3$ nm. Hence we are in the regime where $\tau/\tau_A \ll 1$, so that

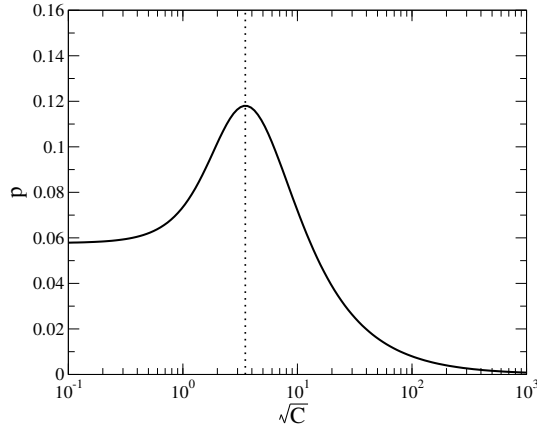


Figure 4.13: Lin-log plot of the probability p that the motor-head is in a region of 1 nm around the binding site at 4.1 nm as a function of the strength \sqrt{C} of the active forces. This figure is for the regime $\tau/\tau_A \ll 1$ where p only depends on C and not on α or τ_A . The dotted line indicates the value of \sqrt{C} where p reaches its maximum.

$\langle x^2 \rangle_{ss} = (k_B T/k) + (C/k^2)$. In the model of [84], it is assumed that the motor-head can attach to the microtubule when it is within one nano-meter from the binding site at 4.1 nm. The stationary state of the probability density is given by $P_{ss}(x) = \lim_{t \rightarrow \infty} P(x, t)$, in expression (4.37) one should replace $\langle x^2(t) \rangle$ with Eq. (4.34) to achieve this stationary distribution. The probability p that the motor-head is in the one nano-meter range of the binding site is then given by $p = \int_{3.1}^{5.1} dx P_{ss}(x)$.

$$p = \frac{1}{2} \left[\operatorname{erf} \left(\frac{5.1}{\sqrt{2\langle x^2 \rangle_{ss}}} \right) - \operatorname{erf} \left(\frac{3.1}{\sqrt{2\langle x^2 \rangle_{ss}}} \right) \right], \quad (4.41)$$

where $\operatorname{erf}(\cdot)$ is the error-function¹ and all distances are expressed in nm. In Fig. 4.13 we have plotted this probability as a function of the strength \sqrt{C} of the active forces (in pN). We see that upon increasing C , p increases from its initial value of $p = 0.058$ in absence of active forces, reaches a maximum of $p = 0.118$ around $\sqrt{C} \approx 3.5$ pN and then decreases again. The value where p reaches its maximum is indeed of the expected order for active forces in a cell. Hence, we conclude that active forces can double the probability that the free motor-head is near its binding site. Because we operated in the $\tau/\tau_A \ll 1$ regime, the viscoelasticity of the cytosol will not influence the result. That is because the steady state is independent of α , see Eq. (4.34).

Next, we investigate the possible influence of the dynamics of the mean-squared displacement on the motion of kinesin. For this we show in Fig. 4.14 the mean-squared displacement for a particle in a viscous environment ($\alpha = 1$) without active forces and

¹The error-function is defined as

$$\operatorname{erf}(x) = \frac{1}{\sqrt{\pi}} \int_{-x}^x dy e^{-y^2}. \quad (4.42)$$

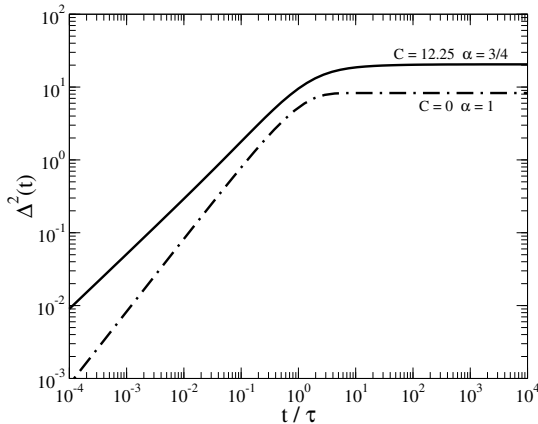


Figure 4.14: Log-log plot of the mean-squared distance travelled by a particle in a harmonic potential ($k = 1$ pN/nm, $k_B T = 4.14$ pN nm) in a viscous and non-active environment (dashed-dotted line) and in an active viscoelastic environment (full line) ($\alpha = 3/4$, $\sqrt{C} = 3.5$ pN, $\tau_A = 3$ s) and $\tau = 5 \cdot 10^{-5}$ s.

in a viscoelastic environment ($\alpha = 3/4$) in presence of active forces (the strength of which corresponds to the optimal value derived above, i.e. $\sqrt{C} = 3.5$ pN). We notice that in the latter situation, the mean-squared displacement is always larger. Given the uncertainty in the various parameters, we can conclude that the time to reach the binding site is of the same order in both situations. This suggests that active forces can help in overcoming the expected slowing down of a molecular motor in a complex environment and thus may provide the answer to why a motor in a cell moves with almost the same velocity as in an *in vitro* essay [85, 86].

It requires further research to investigate whether the effects found here (smaller time to reach the finding site, higher probability to be near the binding site) persists for more realistic models of the neck-linker and to quantify its impact on physical properties of the motor such as its velocity and processivity. Comparison with experiments on kinesin in a cellular environment can then be made [85, 86].

4.3 Double well

The last potential we investigate is a bistable one, meaning that it has two local equilibrium states separated by some energy barrier. A bistable potential surface can be modelled in various ways, from a cusp-shaped harmonic potential [12] to two wells of unequal depth [87]. Here we will use the symmetric double well given by the following expression

$$U(x) = \Delta U \left[\left(\frac{x}{b} - 1 \right)^2 - 1 \right]^2. \quad (4.43)$$

A schematic representation of this double well is given in Fig. 4.15. The potential has two minima, one at $x = 0$ and one at $x = 2b$, and a maximum at $x = b$ of height ΔU .

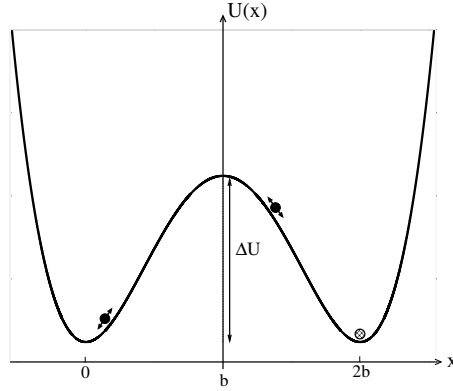


Figure 4.15: Schematic representation of the bistable potential surface. The height ΔU of the energy barrier, located at $x = b$, is indicated. The minima are at $x = 0$ and $x = 2b$. When measuring the survival probability, the particle starts “in equilibrium” in the left well and is free to move on this potential landscape until it reaches the bottom of the right well. When it does, it is eliminated from the system.

The choice for this potential is motivated by the fact that the approximate dynamics in the bottom of one well is that of a harmonic oscillator, which we investigated thoroughly in the previous section. If the double well is surrounded by an active viscoelastic bath, the dynamics of a particle moving on this potential landscape is governed by (see Section 2.6)

$$\eta_{\alpha} {}_c \mathcal{D}^{\alpha} x(t) = \frac{4}{b^4} \Delta U x(b-x)(2b-x) + \xi_T(t) + \xi_A(t)H(t). \quad (4.44)$$

This is a non-linear fractional differential equation, we will therefore not be able to solve it analytically. From here on we have to rely completely on our algorithm (see Chapter 3), which has proven its applicability in the previous section.

In order to make some predictions, we can apply the results of the previous section to describe the approximate dynamics in one of the wells. Indeed, expanding Eq. (4.43) around one of its minima to second order yields the harmonic approximation of both wells. This approximation has the form of potential Eq. (4.18), we can thus associate a k -value to the wells. Performing the expansion is easy and will give $k = 8\Delta U/b^2$. A particle that is located in one of the wells, and that has not yet had time to notice the presence of the energy barrier, will behave like the oscillator from the previous section with the before mentioned k . The characteristic time of a well is then given by Eq. (4.23), it reads

$$\tau_w = \left(\frac{\eta_{\alpha} b^2}{8\Delta U} \right)^{1/\alpha}. \quad (4.45)$$

For times greater than τ_w , the existence of a second well becomes apparent to the particle. In later discussions we often state that the particle is initially “in equilibrium” in the left well. By this we mean that the probability distribution at $t = 0$ of the

particle is that of a thermalised harmonic oscillator around $x = 0$, i.e. a Gaussian distribution with $\langle x \rangle = 0$ and $\langle x^2 \rangle = k_B T b^2 / 8 \Delta U$. Of course, the particle is not truly in equilibrium since its probability distribution does not correspond to the Boltzmann distribution of a double well.

A process that is often studied in a double well is the migration of a particle from one well to the other. Such a process is characterised by the *escape rate* R of the particle and it relates the height of the barrier and distance between the minima to the characteristic time to go from one well to the other. The first prediction of the escape rate was done by Hendrik Kramers in 1940 [88]. His calculations were based on a Brownian particle in a viscous bath. We will try to extend his work to an active viscoelastic bath. But before we do so, we briefly discuss how one can find his result, known as the Kramers' rate.

4.3.1 Kramers' escape rate

For his derivation, Kramers assumed that the energy barrier ΔU was high compared to the thermal energy $k_B T$. This implies that the particle spends a long time inside one well and only occasionally manages to completely climb the barrier as a result of thermal fluctuations. Once it has reached the top of the barrier, it has a chance of $1/2$ to fall in the neighbouring well. In the other case it just drops back into the initial well and has to start all over again. Here we attempt to predict the mean first passage time¹ \mathcal{T} from an initial position x_0 in the left well to the top of the barrier at b . The rate of arrival to the barrier is then the reciprocal to this mean first passage time. Multiplying this rate by one-half gives the Kramers' rate of a particle diffusing from one well to the other. The mean first passage time is given by the following formula (a derivation of this formula, based on the Smoluchowski equation (i.e. high friction) Eq. (2.3), can be found in [26])

$$\mathcal{T}(x_0) = \frac{1}{D} \int_{x_0}^b dy e^{U(y)/k_B T} \int_{-\infty}^y dz e^{-U(z)/k_B T}, \quad (4.46)$$

where $D = k_B T / \gamma$ is the diffusion constant. The integral over z is dominated by the harmonic approximation of the well's bottom $U(z) \approx U_m + \omega_m^2 z^2 / 2$, when $k_B T$ is small. Here we have $U_m = U(0)$ and $\omega_m = \sqrt{8 \Delta U / b^2}$ is the harmonic frequency around the minimum. When we fill this in into Eq. (4.46), and take $y \rightarrow \infty$ (which has little influence on the integral), we find after solving the trivial Gaussian integral

$$\mathcal{T}(x_0) = \frac{\sqrt{2\pi k_B T}}{D \omega_m} e^{-U_m/k_B T} \int_{x_0}^b dy e^{U(y)/k_B T}. \quad (4.47)$$

The remaining integral is dominated by the harmonic approximation of the energy barrier, one finds $U(y) \approx U_M - \omega_M^2 (y - b)^2 / 2$. Here we, naturally, have $U_M = U(b)$ and $\omega_M = \sqrt{4 \Delta U / b^2}$ is the (imaginary) harmonic frequency of the maximum. If we assume the initial position x_0 to be close to the minimum, which is very probable for small $k_B T$, we can take $x_0 \rightarrow -\infty$ because the integral is dominated by the small

¹The mean first passage time characterises the average time it takes a stochastic process, starting in some volume, to reach a specific threshold for the first time.

x_0 contribution anyway. Putting the approximation of $U(y)$ into Eq. (4.47) gives

$$\mathcal{T}(x_0) = \frac{\pi k_B T}{D \omega_m \omega_M} \exp\left(\frac{\Delta U}{k_B T}\right), \quad (4.48)$$

where $\Delta U = U_M - U_m$. This expression is independent of the initial position x_0 . This can be understood by the fact that, due to the low thermal energy, any initial position will first relax to the local equilibrium distribution near the minimum. Therefore any initial position will first evolve to a common starting configuration, yielding the exact value of x_0 irrelevant. As we mentioned before, the Kramers' rate is defined as $R_K = \mathcal{T}^{-1}/2$. Applying this to Eq. (4.48) and using the definition of the diffusion constant gives the Kramers' escape rate, which is correct for systems with high friction and a large barrier-to-temperature ratio

$$R_K = \frac{\omega_m \omega_M}{2\pi\gamma} \exp\left(-\frac{\Delta U}{k_B T}\right). \quad (4.49)$$

4.3.2 Anomalous escape rate

There is an extensive history [12, 87, 89–93] of research on the escape of a particle performing anomalous diffusion, but a general consensus has not yet been reached. We will not attempt to give a full analysis of this problem here, deriving the escape rate of an anomalous process is surely a challenging task and certainly a complete research-topic on its own. Therefore, we limit ourself to a more empiric treatment. In the first subsection we investigate how the escape rate changes when the particle is surrounded by a viscoelastic bath instead of a viscous one. In the next subsection we will also include the active forces.

Viscoelastic bath

One of the first generalisations of the escape rate problem was done by R. Grote and J. Hynes in 1980 [90], their theory was later refined by E. Pollak [91]. They used the generalised Langevin equation (with an undefined memory kernel) to formulate a non-Markovian rate theory. They concluded that the bath effectively modifies the imaginary frequency ω_M of the energy barrier. This effective barrier frequency ϕ_e depends on the memory kernel of the bath and if this kernel is positive for all time (as in our model) then $\phi_e < \omega_M$. This will slow the particle down in the vicinity of the barrier. The generalised escape rate reads

$$R_G = \frac{\omega_m \phi_e}{2\pi\omega_M} \exp\left(-\frac{\Delta U}{k_B T}\right). \quad (4.50)$$

In the overdamped limit, where $m \rightarrow 0$, one can derive¹ from equation (27) in [91] that $\phi_e \tilde{K}[\phi_e] = \omega_M^2$, where $\tilde{K}[\cdot]$ is the Laplace transform of our memory kernel,

¹In the notation of [91], the equation reads

$$M\lambda_0^{\#2} + \lambda_0^{\#} \tilde{\eta}(\lambda_0^{\#}) = \frac{d^2 V}{dq_{\#}^2}. \quad (4.51)$$

The mass is M (m in our notation), the effective barrier frequency is $\lambda_0^{\#}$ (ϕ_e in our notation), the Laplace transform of memory kernel is $\tilde{\eta}(\cdot)$ ($\tilde{K}[\cdot]$ in our notation) and the right-hand side depicts the imaginary barrier frequency (ω_M^2 in our notation).

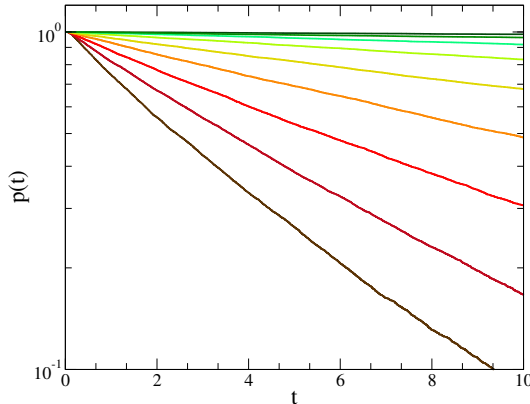


Figure 4.16: Log-lin plot of the survival probability as a function of time for a particle in a double well ($b = 1$), surrounded by a viscoelastic bath ($\alpha = 0.6$, $k_B T = \gamma = 1$). The coloured lines are the simulated data (averaged over 10^4 histories) for different ΔU values, they range from $\Delta U = 2$ (brown) to $\Delta U = 10$ (green) increased by unit increments. The particle was initially “in equilibrium” in the left well.

Eq. (2.50). Solving this equation is easy, it gives $\phi_e = (\omega_M^2/\eta_\alpha)^{1/\alpha}$, from which we define the characteristic time $\tau_e = 1/\phi_e$ of the effective barrier or

$$\tau_e = \left(\frac{\eta_\alpha b^2}{4\Delta U} \right)^{1/\alpha}. \quad (4.52)$$

When we also use $\omega_m = \sqrt{2}\omega_M$, the generalised escape rate in a viscoelastic bath thus becomes

$$R_G = \frac{\sqrt{2}}{2\pi} \frac{1}{\tau_e} \exp\left(-\frac{\Delta U}{k_B T}\right). \quad (4.53)$$

It is clear that when the bath is viscous, $\alpha = 1$, this generalised escape rate reduces to the Markovian Kramers’ rate R_K .

The question now is, can we apply this non-Markovian rate theory to our system? And if so, under what circumstances? To answer these questions, we first evaluate three typical conditions that need to be met. First, just as in Kramers’ approximation, the friction needs to be large. Because the friction is governed by the memory kernel, which diverges in the origin, we can safely assume that the friction is indeed sufficiently high. Second, in order to use the non-Markovian rate theory, the survival probability $p(t)$ in a well should, at least asymptotically, be exponential, i.e. $p(t) \sim \exp(-Rt)$, where R is the escape rate we would like to characterise. The survival probability measures the chance of still finding the particle inside the initial well after a time t . Naturally, we have $p(0) = 1$ and $p(t \rightarrow \infty) = 0$. Simulations have shown that this condition is clearly met for the investigated time-scales (provided that the height of the barrier is large). Figure 4.16 shows an example of this behaviour for $\alpha = 0.6$. One

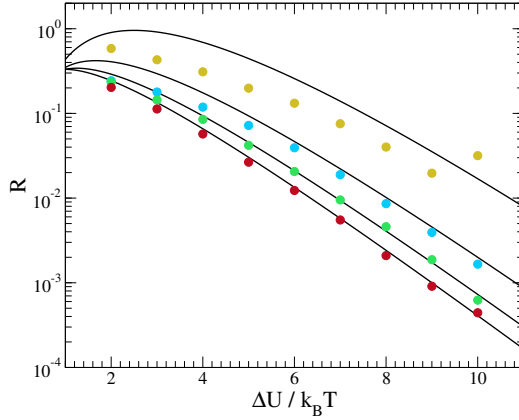


Figure 4.17: Log-lin plot of the escape rate as function of the barrier-to-temperature ratio for a particle in a double well ($b = 1$), surrounded by a viscoelastic bath ($k_B T = \gamma = 1$). The solid lines show the weighted generalised escape rate $R = \alpha R_G$. The coloured dots are the simulated data (averaged over 10^4 histories) for $\alpha = 0.4$ (yellow), 0.6 (blue), 0.8 (green) and 1 (red). The particle was initially “in equilibrium” in the left well.

sees that for low $\Delta U/k_B T$, the survival probability is not completely exponential, this was of course expected. When $\Delta U/k_B T$ is large, however, the lines in the log-lin plot of Fig. 4.16 become straight, implying an exponential behaviour for $p(t)$. Similar results were found for other values of α . However, to be sure that the exponential behaviour persists for many time-scales, one should simulate $p(t)$ for longer times than in Fig. 4.16. This can be a topic for future research. Third, and most importantly, the time-scales should be separated. We mentioned earlier that, for Kramers’ argument to hold, the time the particle spends inside the well should be much longer than the time it takes to leave the well. This implies a clear separation of time-scales, the relaxation time of the well τ_w should be smaller than the characteristic escape time τ_{esc} . Such a separation is also needed in the generalised model for the non-Markovian rate theory to hold. The relaxation time of the well is given by Eq. (4.45) and it is anomalously slow. Therefore, the characteristic escape time should be quite large. We have that $\tau_{esc} = 1/(2R)$. If we take for the escape rate $R = R_G$, then we find that $\tau_{esc}/\tau_w \sim \exp(\Delta U/k_B T)$. From this we conclude that when the energy barrier is sufficiently high the time-scales should separate and the non-Markovian rate theory can be applied. The three conditions are, for our kernel and large $\Delta U/k_B T$, satisfied.

We start with a particle “in equilibrium” in the left well. Then by simulating the survival probability $p(t)$ (see Fig. 4.16), and curve-fitting the result with $\exp(-Rt)$, we obtain the value of the escape rate R for a particular energy barrier ΔU . These escape rates are plotted in Fig. 4.17 as a function of the energy barrier for $\alpha = 1, 0.8, 0.6$ and 0.4 . We found that the escape rate follows the generalised escape rate R_G within a multiplicative factor. For larger values of α , this factor appears to agree well with α itself. We cannot argue why α appears to be a good value, we found it

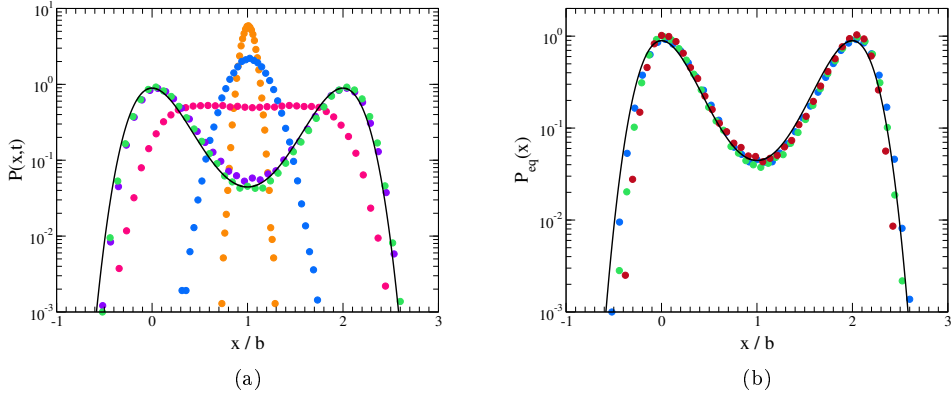


Figure 4.18: Log-lin plot of the probability distribution of a particle in a double well surrounded by a viscoelastic bath. The solid line in both figures represents the Boltzmann distribution, Eq. (4.55). The partition function Z was determined numerically by normalising $\exp(-U(x)/k_B T)$. (a) The distribution through time, with $P(x, 0) = \delta(x - b)$. Coloured dots are the simulated data for $\alpha = 0.8$, $b = 1$, $\Delta U = 3$, $k_B T = \gamma = 1$ and averaged over 10^5 histories. Measurements were at $t/\tau_e = 10^{-2}$ (orange), 10^{-1} (blue), 1 (pink), 10 (purple), 10^2 (green). (b) The equilibrium distribution measured at $t/\tau_e = 10^2$. The coloured dots are the simulated data with the same parameters as Fig. 4.18a, but with $\alpha = 0.4$ (red), 0.6 (green) and 0.8 (blue).

in an empirical manner and more analytic research should be done to determine the true multiplicative factor. Thus for large energy barriers we find that the “weighted” generalised escape rate follows

$$R = \alpha R_G = \frac{\sqrt{2}}{2\pi} \frac{\alpha}{\tau_e} \exp\left(-\frac{\Delta U}{k_B T}\right). \quad (4.54)$$

For $\alpha = 1$, this correctly reduces to the Kramers’ rate. Figure 4.17 shows that this proposed expression for R agrees quite well when $\alpha > 0.5$. For $\alpha < 0.5$, this assumption completely breaks down, although we found that R still lies within a multiplicative factor from R_G .

To conclude this section, we investigate the probability distribution $P(x, t)$ to find the particle at location x at time t . For long times this distribution should evolve into the equilibrium distribution $P_{eq}(x) = \lim_{t \rightarrow \infty} P(x, t)$, which is given by the Boltzmann distribution

$$P_{eq}(x) = \frac{1}{Z} \exp\left(-\frac{U(x)}{k_B T}\right), \quad (4.55)$$

where Z is the partition function, which for the double well potential can not be calculated analytically. It can, however, be easily determined numerically. Notice that this equilibrium distribution is independent of α , as was the case for the harmonic oscillator. In Fig. 4.18a the evolution of the probability through time is shown for

$\alpha = 0.8$. The initial nonequilibrium position of the particle is here always on top of the energy barrier, i.e. $P(x, 0) = \delta(x - b)$. It is clear that when $t > \tau_e$, the distribution reaches equilibrium. The simulated equilibrium distribution for different values of α can be seen in Fig. 4.18b, they all comply with the Boltzmann distribution. The independency of α is clearly visible. These figures give confidence that our algorithm performs well, not only for a harmonic oscillator but also for the double well.

Active viscoelastic bath

Naturally, when we turn on the active forces in the bath, the system will not thermalise to the Boltzmann distribution $P_{eq}(x)$. We can, however, expect that the probability distribution of finding the particle at position x will evolve to some steady state distribution, $P_{ss}(x) = \lim_{t \rightarrow \infty} P(x, t)$. This distribution does not depend on time, as was the case for the long time behaviour of a harmonic oscillator in an active bath. Also for the harmonic oscillator, we found that the steady state behaviour of the particle depended heavily on the value of the persistence time. When τ_A was small the steady state depended on α , while for large τ_A it did not (see Eqs. (4.36) and (4.34) respectively). We will therefore investigate the steady state distribution in a double well for these τ_A regimes. We use the characteristic time τ_e of the effective barrier as a measure for the value of the persistence time τ_A . The distributions are always measured at $t = 10^2 \tau_e$, ensuring that the system has reached its steady state.

For small persistence times, $\tau_e/\tau_A \gg 1$, Fig. 4.19 shows the steady state distribution for $\Delta U = 3$ and 8, the viscoelasticity ranges from $\alpha = 0.4, 0.6$ to 0.8. For both small and large ΔU , the most notable difference in the distribution occurs around the energy barrier itself. The active forces increase the chance to find the particle on top of the barrier. However, when α is small this probability is larger compared to when α is large. So again, small persistence times yield different steady states for distinct values of α . A probable explanation for the increased probability is the fact that the particle receives extra short “kicks” from the active forces through which it can climb the barrier more easily. The chance of being at the bottom of one of the wells is only slightly affected by these extra kicks. The increased anti-persistent diffusion in low α baths is a possible cause why the particle can reside longer on top of the barrier for these small α values.

A more curious behaviour is found when the persistence time is large, $\tau_e/\tau_A \ll 1$. From Fig. 4.20 it is immediately clear that, just as for the harmonic oscillator, the steady state probability distribution does not depend on the value of α , i.e. all viscoelastic baths reach the same state for long times when τ_A is large. For both a small and high energy barrier, Figs. 4.20a and 4.20b respectively, the particle is more likely to be found on the outer edges of the potential than in the bottom of the well as is the case for the equilibrium distribution. The reason for this behaviour is because the persistent active forces push the particle in one direction for a long time, helping the particle to climb the steep margins of the potential. The probability to be on top of the barrier is, for small ΔU , lower than in equilibrium. That is because the persistent active forces will push the particle up and across the low barrier with ease, causing few particles to actually reside on the top. When the barrier is, however, sufficiently high the active forces can just barely manage to get the particle on top of it before changing direction. This makes for a increased probability to be on top of

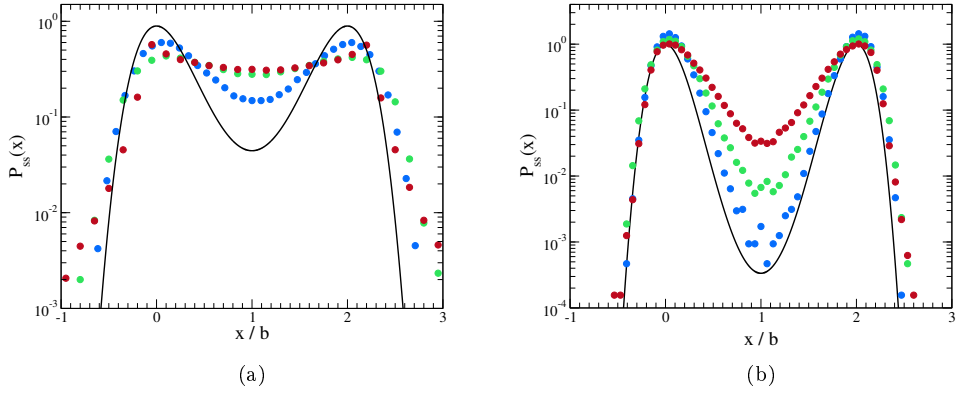


Figure 4.19: Log-lin plot of the steady state probability distribution of a particle in a double well ($b = 1$) surrounded by an active ($C = 10^3$, $\tau_A/\tau_e = 10^{-3}$) viscoelastic bath ($\alpha = 0.4$ (red), 0.6 (green), 0.8 (blue), $k_B T = \gamma = 1$). The solid line in both figures represents the Boltzmann distribution, Eq. (4.55). The partition function Z was determined numerically. The coloured dots represent the simulated data. The probability distribution was measured at $t/\tau_e = 10^2$ and averaged over 10^5 histories. (a) Small energy barrier $\Delta U = 3$. (b) Large energy barrier $\Delta U = 8$.

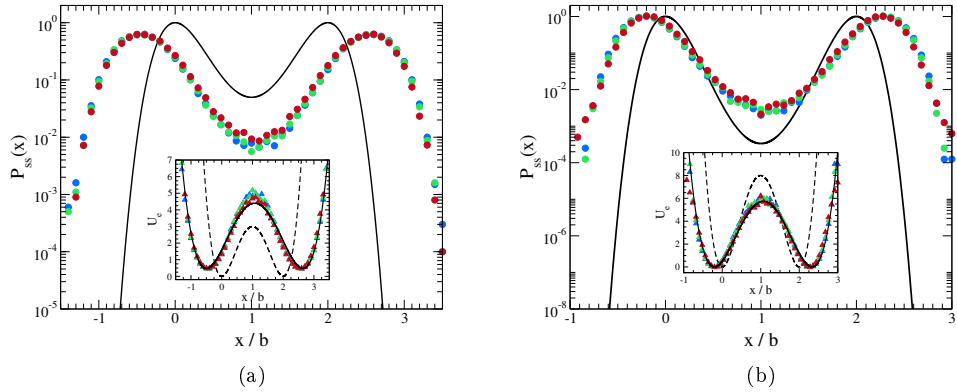


Figure 4.20: Log-lin plot of the steady state probability distribution of a particle in a double well ($b = 1$) surrounded by an active ($C = 10^3$, $\tau_A/\tau_e = 10^3$) viscoelastic bath ($\alpha = 0.4$ (red), 0.6 (green), 0.8 (blue), $k_B T = \gamma = 1$). The solid line in both figures represents the Boltzmann distribution. The coloured dots represent the simulated data. The distribution was measured at $t/\tau_e = 10^2$ and averaged over 10^5 histories. (a) Small energy barrier $\Delta U = 3$. (b) Large energy barrier $\Delta U = 8$. *Insets:* Show the effective energy landscape $U_e(x) = -k_B T \ln(P_{ss}(x))$. The dashed line is the original potential $U(x)$ and the coloured dots are generated from the simulation data of the main graphs. The full lines are a fit of $U_e(x) = \Delta U_e(((x/b_e) - 1)^2 - 1)^2$ through the data points, we have (a) $\Delta U_e = 3.93$, $b_e = 1.57$ and (b) $\Delta U_e = 5.74$, $b_e = 1.27$.

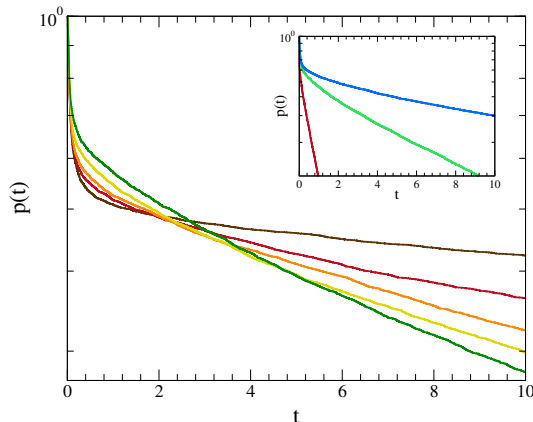


Figure 4.21: Log-lin plot of the survival probability as a function of time for a particle in a double well ($b = 1$), surrounded by an active ($C = 10^3$, $\tau_A/\tau_e = 10^3$) viscoelastic bath ($\alpha = 0.8$, $k_B T = \gamma = 1$). The coloured lines are the simulated data (averaged over $6 \cdot 10^3$ histories) for different ΔU values, they range from $\Delta U = 1, 3, 5, 8$ and 10 (from brown to green). The particle was initially “in equilibrium” in the left well. *Inset*: Log-lin plot of the survival probability as a function of time for a particle in a double well ($\Delta U = 8$) with the same parameters as the main graph, except $\alpha = 0.4$ (red), 0.6 (green) and 0.8 (blue).

the barrier compared to an equilibrated bath. The appropriate height for the energy barrier to induce this effect depends on the persistence and strength of the active forces.

The α -independency of the probability distribution when τ_A is large, strongly suggests that in that limit the distribution can be described in terms of an equilibrium-like distribution, albeit with a different potential $U_e(x)$ (when τ_A is small this argumentation is more difficult and we will not go into it here). This effective potential can be determined from the steady state distribution using the following definition

$$U_e(x) = -k_B T \ln(P_{ss}(x)), \quad (4.56)$$

where we dismissed the additive constant $-k_B T \ln(Z)$. The insets of Fig. 4.20 show the original potential energy $U(x)$ and the effective potential obtained from the main graph’s data. For both the low and high energy barrier, we see that the minima are shifted further apart. The height of the effective barrier is increased in the low ΔU case, while it is decreased for high ΔU . To quantify these changes, we try to fit the effective potential with the expression of the original potential, i.e. Eq (4.43). The two fitting parameters are, naturally, ΔU_e and b_e . As Fig. 4.20 shows, these fits work quite well and both fitting parameters are given in the caption of the figure. For the low energy barrier, we find $\Delta U_e/\Delta U = 1.31$ and $b_e/b = 1.57$. For the high energy barrier, we have $\Delta U_e/\Delta U = 0.72$ and $b_e/b = 1.27$. It would be interesting to develop an analytic approach that allows one to determine U_e from U as was recently done for other problems in the field of active matter [94].

The fact that we can associate an effective potential to this nonequilibrium process can have an interesting implication. One might be able to determine an equilibrium-like escape rate using Kramers' theory, applying it to the effective potential U_e . This promising implication is, however, quickly shattered since the simulated survival probabilities differ for different values of α , see the inset of Fig. 4.21. If a Kramers equilibrium-like escape rate would exist, all baths should display the same escape rate. This α -dependency suggests that the non-Markovian rate theory discussed above might prove a better candidate when applied with the effective potential. As we will soon see however, the behaviour of the escape rate in these active baths is too dissimilar from that in an equilibrated bath that there is little hope that our non-Markovian rate theory will offer solace. We can thus conclude that the effective potential is a neat characterising feature of bath with large τ_A , but it has no immediate practical use for describing the escape rate of this anomalous process.

If we investigate the survival probability for a particular α -value further, we discover a fascinating behaviour. Figure 4.21 shows this probability for $\alpha = 0.8$ and different values of the energy barrier height ΔU . Firstly, we see that the survival probability is no longer exponential. For short times it decreases rapidly, after which it shows a tail that does decay exponential. Secondly, whereas in equilibrium a high energy barrier would have a higher survival probability over the whole time range compared to a lower energy barrier (which is an intuitive result), for the nonequilibrium survival probability we find that this is no longer the case. In Fig. 4.21, we see that for short times this behaviour is still present, but for longer times the probability to be in the initial well is lower for a higher energy barrier. There is, in other words, a clear cross-over in the time profile of the survival probability. This curious behaviour can be traced back to the fact that, for large τ_A , the particle is mostly found on the steep edges of the potential. When ΔU is high, the margins of the potential increase much faster than when ΔU is low. The persistent active forces can push the particle up this slope and, when ΔU is high, the potential energy gained by the particle will thus be larger than when ΔU is low. It can then use this large potential energy to rapidly cross the energy barrier some time later. This process is thus a possible candidate to explain why, for long times, the particle is less likely to be in the initial well for high ΔU compared to when ΔU is low. This is, however, an effect that takes some time to reveal itself because it requires the particle to first ascend the leftmost slope (assuming the particle started in the left well). On shorter time-scales the dominant effect is the immediate crossing of the barrier to the right, which happens much faster when ΔU is low. This explains the short to long time cross-over.

4.3.3 Folding of DNA-hairpins

The overall structure of a macromolecule is not a fixed property, it can fluctuate between different configurations depending on external stimuli. Moreover, the function of a macromolecule often depends on its capability to alternate between two, or more, structural configurations. Understanding how macromolecules fold into these specific three-dimensional structures is one of the big open problems of biological physics. Such folding reactions are often described in terms of a reaction coordinate x (see Section 1.2) which moves stochastically in a free energy landscape $U(x)$. The reac-

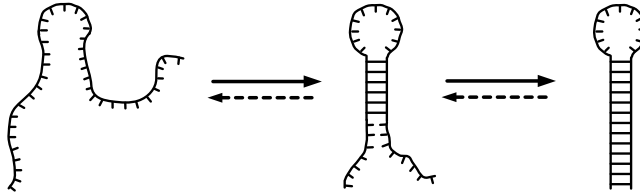


Figure 4.22: Schematic representation of three structural configurations of a DNA-hairpin. The left configuration is a fully unzipped hairpin, while the right one represents a hairpin in a fully zipped state. The intermediate configuration shows a partially zipped state. The full arrow indicates folding, while the dashed arrow represents unfolding.

tion coordinate is a slow variable like the end-to-end distance¹ of a polymer while $U(x)$ is obtained by integrating out the fast variables like the position of individual monomers. Since this averaging cannot easily be performed exactly it is often assumed that $U(x)$ has the shape of a double well whose minima correspond with two stable structural configurations. If one configuration is more stable than the other, its minimum will lie lower. When both configurations are equally stable, the wells will have equal depth. The two structural configurations are often referred to as the folded and unfolded state. The first state reflects the complex three-dimensional morphology that most polymers possess. The unfolded state occurs when external effects (e.g. high temperature) cause the polymer to lose its complex structure and reduce it to a freely fluctuating chain.

One of the simplest and best understood folding processes is that of the *zipping* of a DNA-hairpin (or RNA-hairpin). A DNA-hairpin consists of a single DNA-polymer-strand which has two regions (preferably at both ends of the strand) with complementary nucleotide sequences. It can therefore make weak intramolecular bonds when it folds back on itself. Some part of the DNA-polymer-strand, which has no complementary region, remains an unpaired loop. The relatively straight bounded region and loose loop region form a *stem-loop* profile that resembles the well known hair-clip, hence the origin of its name. Figure 4.22 shows a schematic representation of the (un)folding of a DNA-hairpin. Due to the sequential forming/breaking of bonds in a DNA-hairpin, the folding/unfolding is referred to as *zipping/unzipping*.

In recent years, much advance has been made in measuring various properties of

¹The end-to-end distance is the norm of the vector that connects the two endpoints of a linear polymer (see Chapter 5 for more information).

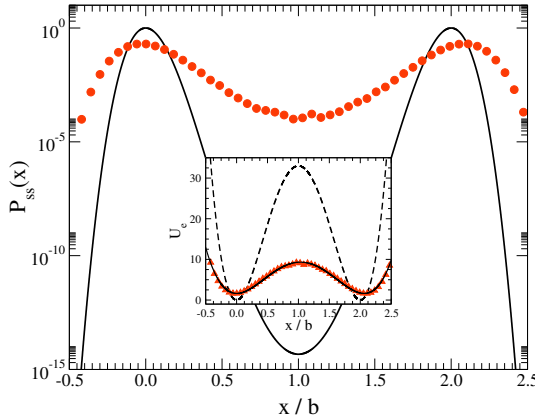


Figure 4.23: Log-linear plot of the steady state probability distribution of a particle in a double well ($\Delta U = 33$ pN nm, $b = 7.5$ nm) surrounded by an active ($C = 10$ pN², $\tau_A = 3$ s) viscoelastic bath ($\alpha = 3/4$, $k_B T = 4.14$ pN nm, $\gamma = 4.14 \cdot 10^{-5}$ pN s/nm). The solid line represents the Boltzmann distribution. The orange dots represent the simulated data. The distribution was measured at $t/\tau_e = 10^2$ and averaged over 10^5 histories. *Inset*: Shows the effective energy landscape $U_e(x) = -k_B T \ln(P_{ss}(x))$. The dashed line is the original potential $U(x)$ and the orange dots are generated from the simulation data of the main graphs. The full line is a fit of $U_e(x) = \Delta U_e(((x/b_e) - 1)^2 - 1)^2$ through the data points, we have $\Delta U_e = 7.69$ pN nm, $b_e = 7.7$ nm.

the zipping/unzipping of simple DNA and RNA structures, also at the single molecule level [95, 96]. In these latter experiments, the hairpins are held under tension by chemically connecting them to two beads that are in an optical trap. If the appropriate forces are applied, the free energy of the zipped and unzipped state are almost equal and the molecule continuously flips between the two states. From the measured dynamics, the free energy landscape for hairpins can then be determined. To good approximation, the folding or unfolding rate corresponds to the Kramers' rate of the reaction coordinate x to diffuse from one well to the other. Measured lifetimes of stable configurations are in the range from milliseconds to minutes, i.e. can be either shorter or longer in comparison with active forces. The characteristic transition times, i.e. the duration of actual structural change, are (until recently [97]) more difficult to observe experimentally but are believed to be of the order of microseconds.

As a simple model to investigate how crowding and nonequilibrium processes affect the zipped/unzipped transition for a hairpin under tension, we use the double well potential Eq. (4.43) in an active viscoelastic bath, as discussed in the previous section. It gives a reasonable description of the measured free energy landscapes of the hairpins 20TS06/T4 and 20TS10/T4 [97]. Using the results from this paper, we can estimate that for these hairpins we have: $\Delta U = 33$ pN nm, $b = 7.5$ nm and $\gamma = 4.14 \cdot 10^{-5}$ pN s/nm. From these parameters, with $\alpha = 3/4$, follows that the characteristic time of a well is $\tau_w = 8.8 \mu\text{s}$. Again we find that the biophysically interesting regime is $\tau_w \ll \tau_A$, since the persistence time is of the order of seconds, we take

$\tau_A = 3$ s. The thermal energy at room temperature is, as always, $k_B T = 4.14$ pN nm. Because we are in the large τ_A regime, we consider only one value of α since, as the previous sections showed, all viscoelastic baths yield the same steady state.

Figure 4.23 shows the steady state probability distribution of the system with the above described parameters in equilibrium (i.e. the Boltzmann distribution) and out-of-equilibrium with $C = 10$ pN². As was discussed previously, the system prefers to be at the edges of the potential (although this effect is less prominent here) and we see an increased probability to be on top of the energy barrier. The inset of this figure shows the effective potential derived from the data of the main graph. A decent fit with the original potential expression is again possible. Notice that the active fluctuations have greatly lowered the effective barrier between the two minima ($\Delta U_e/\Delta U = 0.23$) and at the same time have slightly increased the distance between them ($b_e/b = 1.03$). We can expect that the active forces will therefore considerably lower the time the hairpin spends in a zipped or unzipped state (effectively reducing the zipping/unzipping time of a hairpin) since the characteristic escape time from one of the wells of the effective potential will be substantially lower.

In order to quantify this result, we have numerically determined the survival probability in the potential well, both for the viscous passive case (which should yield Kramers' result) and for the active viscoelastic case. Figure 4.24 shows these survival probabilities. In a viscous passive bath ($\alpha = 1$, $C = 0$), we find that the simulation accurately retrieves Kramers' prediction. Notice that over the span of a thousand microseconds there will hardly be any transition from one state to the other. The characteristic time of being in one state is, according to Kramers Eq. (4.49), approximately 224.7 ms. This complies with the time-scale that was mentioned earlier. In an active viscoelastic environment ($\alpha = 3/4$, $C = 10$ pN²) the probability to change states over the same timespan is increased drastically. After a thousand microseconds, the chance to be in the other state is approximately 42%. Unfortunately, the time profile of the nonequilibrium case can not be fitted with an exponential function, so acquiring a characteristic lifetime of one state is not evident. However, from Fig. 4.24 we can identify that after ten microseconds the probability starts its steep decay. So we can suggest that the characteristic time, in a nonequilibrium bath, of lingering in one state is approximately 10μ s, which is 10^4 times smaller than that in equilibrium.

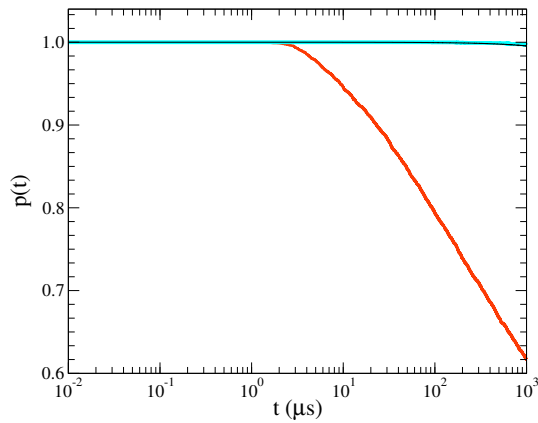


Figure 4.24: Lin-log plot of the survival probability as a function of microseconds for a particle in a double well ($\Delta U = 33$ pN nm, $b = 7.5$ nm), surrounded by an active ($C = 10$ pN², $\tau_A = 3$ s) viscoelastic bath ($\alpha = 3/4$, $k_B T = 4.14$ pN nm, $\gamma = 4.14 \cdot 10^{-5}$ pN s/nm). The orange line shows the simulated data, averaged over $6 \cdot 10^3$ histories. Also shown is the survival probability in a viscous passive bath ($\alpha = 1$, $C = 0$). The black line represents the analytic Kramers' prediction $p(t) = \exp(-R_K t)$, using Eq. (4.49). The blue line shows the simulated data, averaged over $6 \cdot 10^3$ histories. The particle was initially “in equilibrium” in the left well.

5 | Polymer Dynamics

The world is a dynamic mess of jiggling things.

Richard P. Feynman

In this chapter we will extend the model of one particle to describe a polymer in a nonequilibrium cellular environment. First, we discuss the Rouse model, which is perhaps the most widely used model to describe the dynamics of a polymer. This section is heavily based on chapters two and four from the book of M. Doi and S. F. Edwards [7]. Second, we explain how the Rouse model behaves in a viscoelastic bath. Thirdly, we investigate the transient behaviour of the viscoelastic Rouse model when it is subject to a constant force. Then, we replace the constant force with active forces and describe the resulting dynamics of the Rouse model as well as its nonequilibrium steady state. And lastly we introduce some modifications to the Rouse model in order to better mimic the characteristics of a real polymer. We discuss how these modifications alter the results of the previous sections. Most of the results in this chapter can also be found in two of our papers [98, 99].

5.1 The Rouse model

Polymers are very complex molecules that live in an even more complex environment, describing them mathematically is certainly an ambitious task. To tackle most problems, physicists try to model them as simple as possible without losing the key features. For a polymer, this characteristic feature is its linear elongated structure (see Section 1.2), whose configuration (or shape) should fluctuate due to the interaction with its thermal surroundings. This results in an immense amount of different configurations therefore requiring a statistical treatment. The simplest models that satisfy these requirements are the ideal chains. An ideal chain only interacts with the surrounding solvent and not with itself (apart from the local interactions that keep the chain together). The lack of this self-interaction will enable the chain to cross itself, therefore the term *phantom chain* is also used. Although this may not appear to be very physical, in some cases it is not far from reality. Enzymes such as topoisomerases are capable to cut and reseal the phosphate backbone of DNA, thereby allowing this polymer to temporarily cross itself. In the study of *chromosomal loci* it was indeed

found that the Rouse model could describe their motion [100]. A chromosomal locus is the specific location of a DNA-monomer sequence that defines one gene. Yet this observation does not take away the fact that the Rouse model is still a very plain model, not suited to describe all the intricacies of a real polymer. But it suffices to begin to understand the dynamics of a polymer, both in and out of equilibrium.

5.1.1 From random walk to Rouse model

The most straightforward way to create an equilibrium configuration of an ideal chain is with a three-dimensional random walk of $(N_0 - 1)$ steps of constant length b_0 . This will create a polymer with a contour length equal to $(N_0 - 1)b_0$ and with N_0 joints (which includes the two end points). This kind of ideal chain is called a *freely-jointed chain* because the direction of each step is completely uncorrelated with the previous step. Figure 5.1a shows a configuration of such a chain in two-dimensions. It is tempting to view the joints of this chain as the individual monomers of the polymer, but only rarely is the structure of a polymer uncorrelated on such a small scale. Yet on larger length scales the structure of a polymer loses its correlation, this length scale is called the *Kuhn length*. Therefore a step b_0 of the freely-jointed chain represents a Kuhn length segment of the polymer, often including a large number monomers. An ideal chain that is fully uncorrelated is called flexible. Ideal chains that maintain a certain correlation along their bonds are called semi-flexible, in Section 5.5 we will discuss how they can be modelled.

The freely-jointed chain can be defined by two different sets of vectors: The position vectors of the joints $\vec{Q}_n \in \{\vec{Q}_0, \vec{Q}_1, \dots, \vec{Q}_{N_0-1}\}$ or the bond vectors \vec{q}_n , defined by

$$\vec{q}_n = \vec{Q}_n - \vec{Q}_{n-1} \quad \text{with} \quad n = 1, 2, \dots, N_0 - 1. \quad (5.1)$$

Another vector that characterizes the chain, in a more global way, is the end-to-end vector $\vec{P} = \sum_n \vec{q}_n = \vec{Q}_{N_0-1} - \vec{Q}_0$. It connects both ends of the chain and is therefore a good measure for the physical extend of the polymer. We will show that the equilibrium distribution of the end-to-end vector is Gaussian.

Before we can calculate this distribution we first need to address the possibility to have a particular configuration $\{\vec{q}_n\} = (\vec{q}_1, \vec{q}_2, \dots, \vec{q}_{N_0-1})$ of the chain. Because all bond vectors are independent of each other, the conformational distribution is the product of the individual bond distributions

$$\Psi(\{\vec{q}_n\}) = \prod_{n=1}^{N_0-1} \psi(\vec{q}_n), \quad (5.2)$$

where $\psi(\vec{q}_n) = \delta(|\vec{q}_n| - b_0)/(4\pi b_0^2)$ is the normalised distribution of a random vector of length b_0 . The function $\delta(\cdot)$ represents the Dirac delta function.

To find the distribution $\Phi(\vec{P})$ of the end-to-end vector we need to integrate over all possible configurations of the chain while enforcing the sum over all bond vectors be equal to \vec{P} . The integration should also be weighted by the conformational distribution, leading to

$$\Phi(\vec{P}) = \int d\vec{q}_1 \int d\vec{q}_2 \dots \int d\vec{q}_{N_0-1} \delta\left(\vec{P} - \sum_{n=1}^{N_0-1} \vec{q}_n\right) \Psi(\{\vec{q}_n\}). \quad (5.3)$$

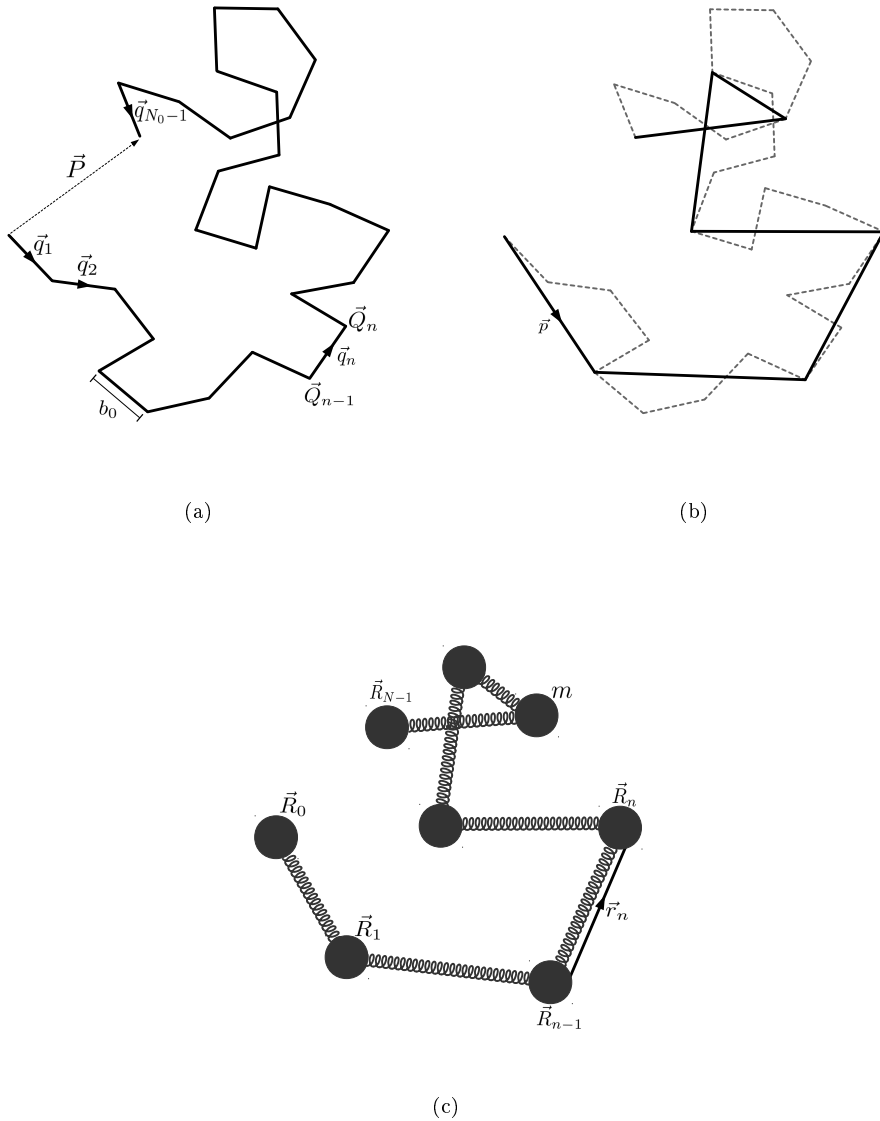


Figure 5.1: All three pictures are a two dimensional depiction of the chain they represent. (a) The freely-jointed chain, the end-to-end vector \vec{P} is shown as a dashed arrow. (b) The Gaussian chain, the original freely-jointed chain is shown in grey dashed lines while the end-to-end vectors \vec{p} of the sub-chains are the solid black lines. In this case $\mu = 7$. (c) The Rouse Chain, the black dots are the beads with mass m that are connected by harmonic springs.

When no integration interval is specified, it is assumed to range from minus infinity to plus infinity. In order to further work out this expression we use the following identity of the Dirac delta function

$$\delta(\vec{q}) = \frac{1}{(2\pi)^3} \int d\vec{\omega} e^{i\vec{\omega} \cdot \vec{q}}. \quad (5.4)$$

Using this equation and Eq. (5.2), it is easy to show that the end-to-end distribution can be written as

$$\Phi(\vec{P}) = \frac{1}{(2\pi)^3} \int d\vec{\omega} e^{i\vec{\omega} \cdot \vec{P}} \left[\int d\vec{q} e^{-i\vec{\omega} \cdot \vec{q}} \psi(\vec{q}) \right]^{N_0-1}. \quad (5.5)$$

The integration over \vec{q} to the power of $(N_0 - 1)$ comes from the fact that all the integrals over the bond vectors are identical after they decouple. This integration over \vec{q} is evaluated as follows

$$\frac{1}{4\pi b_0^2} \int_0^\infty dr r^2 \int_0^{2\pi} d\phi \int_0^\pi d\theta \sin(\theta) \exp(-i\omega r \cos(\theta)) \delta(r - b_0) = \frac{\sin(\omega b_0)}{\omega b_0}, \quad (5.6)$$

where $\omega = |\vec{\omega}|$. If $\omega b_0 \ll 1$, this result is approximated by $\exp(-\omega^2 b_0^2/6)$. This approximation also holds for large ωb_0 , since both expressions will be close to zero in that case. Then for large N_0 the end-to-end distribution becomes

$$\Phi(\vec{P}) = \frac{1}{(2\pi)^3} \int_{-\infty}^{+\infty} d\vec{\omega} \exp\left(i\vec{\omega} \cdot \vec{P} - \vec{\omega}^2 \frac{N_0 b_0^2}{6}\right). \quad (5.7)$$

After separating the three coordinate components, this Gaussian integral can be readily worked out using the standard techniques. The final result is

$$\Phi(\vec{P}) = \left(\frac{3}{2\pi N_0 b_0^2}\right)^{3/2} \exp\left(-\frac{3\vec{P}^2}{2N_0 b_0^2}\right). \quad (5.8)$$

Clearly, the distribution of the end-to-end vector is Gaussian. From this we find that the mean value of the end-to-end vector is zero, i.e. $\langle \vec{P} \rangle = 0$, and $\langle \vec{P}^2 \rangle = N_0 b_0^2$. These results are also easy to work out starting from the definition of the end-to-end vector and the fact that all bond vectors are uncorrelated, i.e. $\langle \vec{q}_n \cdot \vec{q}_m \rangle = 0$ when $n \neq m$. For large N_0 and using $\langle \vec{q}_n \rangle = 0$, one finds

$$\langle \vec{P} \rangle = \sum_{n=1}^{N_0-1} \langle \vec{q}_n \rangle = 0, \quad (5.9)$$

$$\langle \vec{P}^2 \rangle = \sum_{n,m=1}^{N_0-1} \langle \vec{q}_n \cdot \vec{q}_m \rangle = \sum_{n=1}^{N_0-1} \langle \vec{q}_n^2 \rangle \approx N_0 b_0^2, \quad (5.10)$$

The freely-jointed chain is well suited for the study of the equilibrium configurations of a polymer in solution. It does not, however, lend itself well to describe the dynamics of such polymers. It would be more beneficial to have an equation of motion that describes an ideal chain. By coarse-graining the freely-jointed chain it is

possible to arrive at such an equation, or rather set of equations. First notice that the ideal chain is self-similar, meaning that a smaller part of the chain resembles the full chain. To see this we divide the bond vectors into μ groups, called sub-chains. Each sub-chain has $(\tilde{N} - 1) = (N_0 - 1)/\mu$ bond vectors and \tilde{N} joints (see Fig. 5.1b). The end-to-end vector of a sub-chain is denoted by \vec{p} . If \tilde{N} is large, the distribution of \vec{p} is given by Eq. (5.8), where N_0 is interchanged by \tilde{N} . The sub-chains are thus similar to the global chain.

Using this characteristic we can transform the freely-jointed chain into a *Gaussian chain*. The bond vectors \vec{r}_n of this Gaussian chain are the end-to-end vectors of the freely-jointed sub-chains. Their length is not fixed but has a Gaussian distribution, this distribution is given by the following form

$$\psi(\vec{r}_n) = \left(\frac{3}{2\pi b^2}\right)^{3/2} \exp\left(-\frac{3\vec{r}_n^2}{2b^2}\right). \quad (5.11)$$

The mean of these Gaussian bond vectors is zero and $\langle \vec{r}_n^2 \rangle = b^2$, where b is of the order of the Kuhn length (since $b^2 \approx \tilde{N}b_0^2$). By combining many of the original bond vectors into one, we lose some properties of the local structure. But the global characteristics, Eq. (5.8), of the Gaussian chain are still identical to the freely-jointed chain. The fact that the bond vectors of the Gaussian chain do not have a constant length enables us to create a mechanical model of this chain. At every joint and at both ends of the Gaussian chain we place a mass m called a *bead*. Although one bead does not represent a single monomer, but a rigid group of monomers of Kuhn Length, we will sometimes refer to it as a monomer of the chain. The location of the n^{th} bead is given by the vector \vec{R}_n (see Fig. 5.1c), with n ranging from 0 to $(N - 1)$. In total there are N beads, with $N = \mu + 1$. These beads are connected by the Gaussian bond which we will interpret as a harmonic spring with spring constant k , obviously there are $(N - 1)$ springs. The potential energy stored in one such springs is

$$U_n = \frac{k}{2} \left[\vec{R}_n - \vec{R}_{n-1} \right]^2. \quad (5.12)$$

When the spring is thermalised in a heat bath at temperature T , its length is distributed according to the Boltzmann distribution, which is proportional to the Boltzmann factor $\exp(-U_n/k_B T)$. Normalizing this distribution and equating it to Eq. (5.11) gives a physical value to the spring constant, namely

$$k = \frac{3k_B T}{b^2}. \quad (5.13)$$

The total potential energy contained in a Gaussian chain is

$$U(\{\vec{R}_n\}) = \sum_{n=1}^{N-1} U_n. \quad (5.14)$$

If we now assume the Gaussian chain to be in contact with a heat bath (which is at temperature T), we can use the Langevin formalism (see Section 2.2) to find the evolution of \vec{R}_n . We assume the mass m of the beads to be very small and the heat bath to be a viscous fluid, with friction coefficient γ . Inserting the total potential

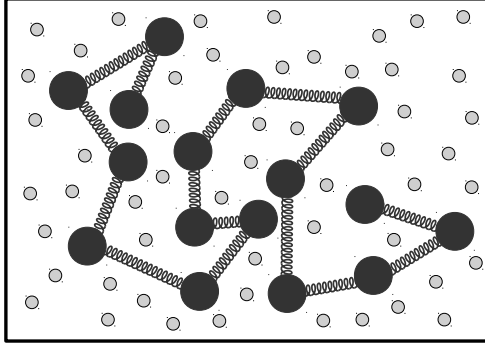


Figure 5.2: A cartoon of the Rouse model. The black spheres connected with springs are the Rouse chain. The small grey dots represent the particles of the surrounding viscous fluid.

energy, Eq. (5.14), into the overdamped Langevin equation, Eq. (2.29), yields the following equation of motion for the n^{th} bead (with $n = 0, 1, \dots, N - 1$)

$$\gamma \frac{d}{dt} \vec{R}_n(t) = -k \left(2\vec{R}_n(t) - \vec{R}_{n-1}(t) - \vec{R}_{n+1}(t) \right) + \vec{\xi}_{T,n}(t). \quad (5.15)$$

Where $\vec{\xi}_{T,n}$ represents the random thermal force on the n^{th} bead. These random thermal forces are Gaussian distributed and on average zero. From the fluctuation-dissipation relation, Eq. (2.22), we find their correlation. We also enforce that these forces are uncorrelated between different beads, we therefore have

$$\langle \vec{\xi}_{T,n}(t) \cdot \vec{\xi}_{T,m}(t') \rangle = 6\gamma k_B T \delta(t - t') \delta_{n,m}. \quad (5.16)$$

We also introduced two ghost beads, \vec{R}_{-1} and \vec{R}_N . They will ensure that Eq. (5.15) also holds for the beads at both ends of the chain, since they only have one neighbouring bead. They are defined as

$$\vec{R}_{-1} = \vec{R}_0 \quad \text{and} \quad \vec{R}_N = \vec{R}_{N-1}. \quad (5.17)$$

The set of N Langevin equations that Eq. (5.15) entails describes the overdamped dynamics of a thermalised Gaussian chain in a viscous fluid. This Langevin description of a polymer is called the Rouse model, devised by Prince E. Rouse in 1953 [101]. A schematic representation of his model is given in Fig. 5.2, where the grey dots depict the particles of the surrounding fluid.

5.1.2 Normal coordinates

Equation (5.15) is not straightforward to solve since it is a coupled differential equation. It is coupled in the sense that in order to solve it for the location of one bead, the location of the two neighbouring beads must also be known. It is however possible to decouple the equations by changing the coordinate system. These new coordinates \vec{X}_p , with $p = 0, 1, \dots, N - 1$, are called the normal coordinates and their motion

is independent of each other. The original coordinates \vec{R}_n we will refer to as the natural coordinates. The normal coordinates are a linear combination of all natural coordinates

$$\vec{X}_p(t) = \frac{1}{N} \sum_{n=0}^{N-1} C_n^p \vec{R}_n(t). \quad (5.18)$$

The transformation coefficients are given by the following expression

$$C_n^p = \cos\left(\frac{\pi p}{N} \left(n + \frac{1}{2}\right)\right). \quad (5.19)$$

In Chapter 6 we will give a more extensive explanation on how these coefficients are determined. Clearly, the normal coordinate with $p = 0$ is equivalent to the location of the centre of mass \vec{R}_{cm}

$$\vec{X}_0(t) = \frac{1}{N} \sum_{n=0}^{N-1} \vec{R}_n(t) = \vec{R}_{cm}(t). \quad (5.20)$$

For $p > 0$ the normal coordinates describe the internal vibrational modes of the chain, keeping the centre of mass fixed. Because of this we will also refer to \vec{X}_p as the p^{th} (Rouse) mode. It is also necessary to know the reverse transformation

$$\vec{R}_n(t) = \vec{X}_0(t) + 2 \sum_{p=1}^{N-1} C_n^p \vec{X}_p(t). \quad (5.21)$$

To understand that this is indeed the correct transformation, one can multiply both sides of Eq. (5.21) by C_n^q/N and do a summation over n . If the following orthogonal property of the transformation coefficients is used, then one arrives back at Eq. (5.18),

$$\sum_{n=0}^{N-1} C_n^p C_n^q = \frac{N}{2} (1 + \delta_{p,0}) \delta_{p,q}. \quad (5.22)$$

From Eq. (5.21) it is clear that the motion of one bead can be seen as the combination of two dynamical concepts: (1) The motion of the centre of mass. (2) All internal modes of vibration. The relevance of this property will become apparent later.

We can also write the evolution of the end-to-end vector in terms of normal coordinates, this vector can be written as

$$\vec{P}(t) = \vec{R}_{N-1}(t) - \vec{R}_0(t) = 2 \sum_{p=1}^{N-1} [C_{N-1}^p - C_0^p] \vec{X}_p(t), \quad (5.23)$$

we have that $C_{N-1}^p - C_0^p = ((-1)^p - 1)C_0^p$. This result is equal to zero if p is even and equal to $-2C_0^p$ if p is odd. We therefore find

$$\vec{P}(t) = -4 \sum_{p=1, \text{ odd}}^{N-1} C_0^p \vec{X}_p(t) \quad (5.24)$$

$$\approx -4 \sum_{p=1, \text{ odd}}^{N-1} \vec{X}_p(t). \quad (5.25)$$

The approximation in the second line holds when $N \gg 1$. For small p we have that C_0^p is close to one. For large p this transformation factor goes to zero, so it seems that the approximation does not hold. But we will soon find that the normal modes with high p vibrate on very short time scales and therefore contribute very little to overall dynamics of the end-to-end vector. Thus fully including them in approximation (5.25) does little harm. Naturally, the end-to-end vector does not depend on the motion of the centre of mass but only on the internal vibrations, as Eq. (5.24) shows.

We will now proceed to work out the decoupled differential equation of the normal coordinates. If we take the time-derivative of the normal coordinates and multiply it by γ , Eq. (5.18) becomes

$$\gamma \frac{d}{dt} \vec{X}_p(t) = \frac{\gamma}{N} \sum_{n=0}^{N-1} C_n^p \frac{d}{dt} \vec{R}_n(t). \quad (5.26)$$

Using Eq. (5.15) this can be rewritten as

$$\gamma \frac{d}{dt} \vec{X}_p(t) = -\frac{k}{N} \sum_{n=0}^{N-1} C_n^p \left(2\vec{R}_n(t) - \vec{R}_{n-1}(t) - \vec{R}_{n+1}(t) \right) + \frac{1}{N} \sum_{n=0}^{N-1} C_n^p \vec{\xi}_{T,n}(t). \quad (5.27)$$

Now we replace the natural coordinates in Eq. (5.27) with their linear combination, Eq. (5.21). The result, after some elementary calculations, is

$$\gamma \frac{d}{dt} \vec{X}_p(t) = -\frac{8k}{N} \sum_{q=1}^{N-1} \sin^2 \left(\frac{\pi q}{2N} \right) \vec{X}_q(t) \sum_{n=0}^{N-1} C_n^p C_n^q + \frac{1}{N} \sum_{n=0}^{N-1} C_n^p \vec{\xi}_{T,n}(t). \quad (5.28)$$

We can use property (5.22) of the transformation coefficients to arrive at the Langevin equation for the normal coordinates

$$\gamma \frac{d}{dt} \vec{X}_p(t) = -\frac{k_p}{2N} \vec{X}_p(t) + \vec{\xi}_{T,p}(t). \quad (5.29)$$

Two abbreviations were adopted. Firstly, we have the constant k_p , which can be interpreted as the harmonic constant of the p^{th} normal coordinate. It has the following expression

$$k_p = 8Nk \sin^2 \left(\frac{\pi p}{2N} \right) \approx \frac{2k \pi^2 p^2}{N}, \quad (5.30)$$

where the approximation holds for large N . Second, a new stochastic variable: the normal noise $\vec{\xi}_{T,p}$. It is a linear combination of the natural noises

$$\vec{\xi}_{T,p}(t) = \frac{1}{N} \sum_{n=0}^{N-1} C_n^p \vec{\xi}_{T,n}(t). \quad (5.31)$$

Because a linear combination of Gaussian variables is itself Gaussian distributed, the normal noise is a Gaussian variable. It is therefore fully characterized by its first and second moments. The first moment is clearly zero and the second is expressed by

$$\langle \vec{\xi}_{T,p}(t) \cdot \vec{\xi}_{T,q}(t') \rangle = \frac{3\gamma k_B T}{N} \delta(t-t') (1 + \delta_{p,0}) \delta_{p,q}, \quad (5.32)$$

where we used the orthogonal property of the transformation coefficients. Solving Eq. (5.29) gives

$$\vec{X}_p(t) = \vec{X}_p(0) e^{-t/\tau_p} + \frac{1}{\gamma} \int_0^t d\tau \vec{\xi}_{T,p}(t-\tau) e^{-\tau/\tau_p}. \quad (5.33)$$

Here we introduced the characteristic time τ_p of the p^{th} mode, with $\tau_p = 2\gamma N/k_p$. The largest of these time scales, i.e. τ_1 , is called the Rouse time τ_R , for large N it is equal to

$$\tau_R = \frac{\gamma N^2}{k\pi^2}. \quad (5.34)$$

Generally, the characteristic time of the p^{th} mode represents the independent relaxation time of a segment of N/p beads. So, τ_R gives the time-scale on which the entire chain relaxes. Next, the two halves of the chain (each containing $N/2$ beads) behave independently on a τ_2 time-scale. We can continue this reasoning, ending with $\tau_N = \gamma/4k$, which is the relaxation time of an individual bead. As promised we found here that modes with larger p have a shorter characteristic time, their features are thus quickly lost in time. Because the Rouse time depends quadratically on the polymer's length, this characteristic time can become very large when applied to values of real polymers. In many cases the Rouse time exceeds the lifetime of the cell, implying that a (long) polymer is never truly relaxed inside a cell.

5.1.3 Dynamic properties

We are now finally in a position to discuss the dynamical properties of the Rouse chain. Since Eq. (5.15) is a linear differential equation and the thermal noise is Gaussian, the position of a bead is Gaussian distributed. Determining its first and second moments will therefore fully describe its dynamics. Because the normal coordinates lie at the basis of the dynamics of the natural coordinates, it is instructive to first calculate how they evolve and fluctuate through time. The notation $\langle \cdot \rangle$ represents, as always, ensemble averages. Since the first moment of the normal noise is zero, the mean value of the p^{th} normal coordinate is

$$\langle \vec{X}_p(t) \rangle = \langle \vec{X}_p(0) \rangle e^{-t/\tau_p} = 0. \quad (5.35)$$

The second equality comes from the fact that we assume the polymer to be in equilibrium at $t = 0$, we therefore have the liberty to take $\langle \vec{X}_p(0) \rangle = 0$. Because there is no external forcing, the polymer will remain thermalised for all time. In equilibrium we can use the equipartition theorem (see Section 2.2) to find the expected value of a squared degree-of-freedom when it appears as a square in the total energy of the system. In our case this degree-of-freedom is \vec{X}_p . First we need to rewrite the total potential energy, Eq. (5.14), as a function of the normal coordinates. It is quite easy to show that the following relation holds

$$U(\{\vec{X}_p\}) = \sum_{p=1}^{N-1} \frac{k_p}{2} \vec{X}_p^2. \quad (5.36)$$

From this, the equipartition theorem gives us the following autocorrelation $\langle \vec{X}_p^2(t) \rangle = 3k_B T/k_p$. But we can write an even more general expression, since the different normal modes are independent, they are also uncorrelated. Therefore we have

$$\langle \vec{X}_p(t) \cdot \vec{X}_q(t) \rangle = \frac{3k_B T}{k_p} \delta_{p,q}. \quad (5.37)$$

It is also interesting to calculate the correlation between two normal coordinates at different times. We will focus first on the case where they have the same mode p (with $p \neq 0$), generalising to different modes is easy. Using Eq. (5.33) we can write

$$\begin{aligned} \langle \vec{X}_p(t) \cdot \vec{X}_p(t') \rangle &= \langle \vec{X}_p^2(0) \rangle e^{-(t+t')/\tau_p} \\ &+ \frac{1}{\gamma^2} \int_0^t d\tau \int_0^{t'} d\tau' \langle \vec{\xi}_{T,p}(t-\tau) \cdot \vec{\xi}_{T,p}(t'-\tau') \rangle e^{-(\tau+\tau')/\tau_p}, \end{aligned} \quad (5.38)$$

where we used the fact that the initial value of the normal coordinates is uncorrelated with the normal noise, i.e. $\langle \vec{X}_p(0) \cdot \vec{\xi}_{T,p}(t) \rangle = 0$. After inserting Eqs. (5.32) and (5.37) this expression becomes

$$\begin{aligned} \langle \vec{X}_p(t) \cdot \vec{X}_p(t') \rangle &= \frac{3k_B T}{k_p} e^{-(t+t')/\tau_p} \\ &+ \frac{3k_B T}{\gamma N} \int_0^t d\tau \int_0^{t'} d\tau' \delta(t-\tau-t'+\tau') e^{-(\tau+\tau')/\tau_p}. \end{aligned} \quad (5.39)$$

The double integral can be solved by temporarily assuming that $t' < t$, then the integral over τ should be worked out first. The result is $(\tau_p/2)(e^{-(t-t')/\tau_p} - e^{-(t+t')/\tau_p})$. If we, however, took $t < t'$ then the position of t and t' in this result should be interchanged. The general result, without assuming any relation between the two times is $(\tau_p/2)(e^{-|t-t'|/\tau_p} - e^{-(t+t')/\tau_p})$. Using this solution and the fact that different normal coordinates are uncorrelated, gives the final result (for $p \neq 0$)

$$\langle \vec{X}_p(t) \cdot \vec{X}_q(t') \rangle = \frac{3k_B T}{k_p} \exp(-|t-t'|/\tau_p) \delta_{p,q}. \quad (5.40)$$

For $t = t'$ we correctly retrieve Eq. (5.37). With the previously derived expressions we can calculate the dynamical properties of the Rouse chain. In the discussions to come, we use the following expression for the displacement at time t of a vector \vec{R} since $t = 0$: $\Delta \vec{R}(t) = \vec{R}(t) - \vec{R}(0)$. If the vector represents the location of a particle, $\Delta \vec{R}(t)$ can be seen as the total distance covered by the particle during the time interval $[0, t]$.

Centre of mass

We first look at the dynamics of the centre of mass. Remember that its location is equal to that of the zeroth mode \vec{X}_0 . From Eq. (5.33) we find that the position of the centre of mass obeys the following equation

$$\vec{R}_{cm}(t) = \vec{R}_{cm}(0) + \frac{1}{\gamma} \int_0^t d\tau \vec{\xi}_{T,p}(t-\tau). \quad (5.41)$$

Because the mean of the thermal noise is zero, it is clear that the mean displacement will also be zero, i.e. $\langle \Delta \vec{R}_{cm}(t) \rangle = 0$. The mean-squared displacement¹ of the centre of mass is expressed as $\Delta_{cm}^2(t) = \langle (\Delta \vec{R}_{cm}(t))^2 \rangle$. Squaring and averaging the second term Eq. (5.41) will give the mean-squared displacement of the centre of mass. Using Eq. (5.32), we obtain

$$\Delta_{cm}^2(t) = \frac{6k_B T}{\gamma N} t, \quad (5.42)$$

from this relation we can conclude that the centre of mass performs normal diffusion with diffusion constant $D^{cm} = k_B T / \gamma N$.

Single bead

Now we investigate the evolution of the n^{th} bead and in particular the middle bead with $n = N/2$. Because the dynamics of the middle bead is a good representation for all the other beads, we will always focus more on this particular bead. Finding the precise dynamics of the n^{th} bead is a trivial extension of the results of the middle bead. Again we find that the mean position is zero, this is achieved by averaging Eq. (5.21) and using Eq. (5.35). Therefore we have $\langle \Delta \vec{R}_n(t) \rangle = 0$. The mean-squared displacement, being $\Delta_n^2(t) = \langle (\Delta \vec{R}_n(t))^2 \rangle$, can be found employing Eq. (5.21). It reads

$$\Delta_n^2(t) = \langle \Delta \vec{X}_0^2(t) \rangle + 4 \sum_{p=1}^{N-1} C_n^{p^2} \langle \Delta \vec{X}_p^2(t) \rangle, \quad (5.43)$$

we used that different modes are uncorrelated to remove the cross-terms. The first term is identical to Eq. (5.42), i.e. the mean-squared displacement of the centre of mass. The second term can be evaluated when the square is first worked out. This will give three terms

$$\langle \vec{X}_p^2(t) \rangle + \langle \vec{X}_p^2(0) \rangle - 2 \langle \vec{X}_p(t) \vec{X}_p(0) \rangle. \quad (5.44)$$

The first two are identical and given by Eq. (5.37). The last term can be found using Eq. (5.40). The final result for the mean-squared displacement of the n^{th} bead is then

$$\Delta_n^2(t) = \frac{6k_B T}{\gamma N} t + \frac{12k_B T}{\gamma N} \sum_{p=1}^{N-1} C_n^{p^2} \tau_p \left[1 - e^{-t/\tau_p} \right]. \quad (5.45)$$

This expression is not very transparent, but we can determine the different regimes it holds. As mentioned before, we will focus on the middle bead ($n = N/2 = m$), but the other beads behave very similarly. For the middle bead we have

$$C_m^{p^2} = -\frac{1}{2} \left[((-1)^{p+1} - 1) \cos^2 \left(\frac{\pi p}{2N} \right) + ((-1)^p - 1) \sin^2 \left(\frac{\pi p}{2N} \right) \right], \quad (5.46)$$

¹A more complete measure of the dynamics would be the variance in the displacement, which is defined as $\sigma_{cm}^2(t) = \langle (\Delta \vec{R}_{cm}(t))^2 \rangle - \langle \Delta \vec{R}_{cm}(t) \rangle^2$. But since the mean displacement is zero, the variance is identical to the mean-squared displacement.

since p is integer. When p is small this expression is equal to one when p is even and zero when p is odd. For larger p this behaviour does not hold. But because τ_p goes to zero for high values of p , the behaviour of Eq. (5.46) for large p is irrelevant. We therefore have

$$\Delta_m^2(t) = \frac{6k_B T}{\gamma N} t + \frac{12k_B T}{\gamma N} \sum_{p=2, \text{even}}^{N-1} \tau_p \left[1 - e^{-t/\tau_p} \right]. \quad (5.47)$$

For very short times, $t \ll \tau_N$, we approximate the exponential to first order. The summation is then just done over t and thus becomes equal to $Nt/2$. We find that, for large N , the bead performs normal diffusion with a diffusion coefficient that obeys the Einstein relation $D = k_B T/\gamma$. This is the diffusion of a free bead. For early times the middle bead does not notice it is bounded by springs and therefore diffuses freely.

For short times, $t \ll \tau_R$, the summation in Eq. (5.47) will dominate. For large N , we can approximate this summation by an integral since its argument is a smooth continuous function. We take $1/N \rightarrow dx$ and $p/N \rightarrow x$. We should also add a factor one half to account for the fact that we only sum over the even modes. The approximation of the second term in Eq. (5.47) becomes

$$\frac{6k_B T}{\gamma} \int_0^\infty dx \frac{\gamma}{k\pi^2 x^2} \left[1 - e^{-tk\pi^2 x^2/\gamma} \right] = \frac{6k_B T}{\sqrt{\gamma k \pi}} t^{1/2}. \quad (5.48)$$

During this regime the middle beads feels the influence of the springs and is restricted by them. Therefore its diffusion is anomalous with exponent 1/2.

For long times, $t \gg \tau_R$, the first term in Eq. (5.47) will be dominant. Clearly, the middle bead then follows the diffusion of the centre of mass, which performs normal diffusion with diffusion coefficient $D^{cm} = k_B T/\gamma N$. It thus diffuses slower than for very short times. During these long time scales, the individual movements of the middle bead are overshadowed by the collective diffusion of all beads. This treatment of the diffusion of a bead reflects the statement we made earlier when we said that its dynamics is a combination of that of the centre of mass and the internal vibrations of the chain. To summarize we have the following sequence for the (approximate) mean-squared displacement through time

$$\Delta_m^2(t) = 6Dt \xrightarrow{\tau_N} \frac{6k_B T}{\sqrt{\gamma k \pi}} t^{1/2} \xrightarrow{\tau_R} 6D^{cm} t, \quad (5.49)$$

the value above the arrows indicates the time at which the transition happens.

End-to-end vector

Finally, we take a look at the autocorrelation of the end-to-end vector. Using Eq. (5.25) and Eq. (5.40), it is easy to find that

$$\langle \vec{P}(t) \cdot \vec{P}(t') \rangle = 16 \sum_{p,q=1, \text{odd}}^{N-1} \langle \vec{X}_p(t) \cdot \vec{X}_q(t') \rangle = \frac{24k_B T}{\gamma N} \sum_{p=1, \text{odd}}^{N-1} \tau_p e^{-|t-t'|/\tau_p}. \quad (5.50)$$

When $t = t'$ and N large we obtain

$$\langle \vec{P}^2(t) \rangle = \frac{3k_B T}{k} N, \quad (5.51)$$

to calculate this result we used $\sum_{p=0}^{\infty} (2p+1)^{-2} = \pi^2/8$. This quantity does not depend on time because the Rouse chain is equilibrated. Moreover, this result can therefore be understood using the equipartition theorem. We are dealing with $(N-1)$ thermalised harmonic springs, their average length squared is $3k_B T/k$. This we do $N(\approx N-1)$ times to acquire the average total length squared.

Now that we fully understand the original Rouse model, it is time we start expanding on it. First we will include memory effects to the surrounding medium. Thereafter we investigate two processes that will cause the polymer to leave equilibrium. Finally we propose some new internal potentials to increase the realism of the Rouse model.

5.2 The Rouse chain in a viscoelastic bath

The natural habitat of a biopolymer is the cytosol of a biological cell. The cytosol, or cytoplasmic matrix, is a complex mixture of densely packed substances dissolved in water. These substances include large amounts of macromolecules and concentration gradients of smaller molecules. Also present in the cytosol are the huge cell organelles and the grand structure of the cytoskeleton. This crowded environment will hinder the dynamics of a large biomolecule, such as a polymer. Its diffusion will therefore be restricted (see Section 2.4). For an equilibrated free particle (see Section 4.1), this subdiffusion is characterised by exponent α of the mean-squared displacement: $\Delta^2(t) \sim t^\alpha$. The value of α can be determined with rheological measurements. Estimates for the cytosol range from $\alpha \approx 0.2$ for eukaryotic cells [18] to $\alpha \approx 0.7$ for *Escherichia coli* [54].

As discussed in Section 2.4, the complex environment of the cytosol can be seen as a viscoelastic bath, which is described by the formalism of the generalised Langevin equation. Investigating how a Rouse chain behaves in a viscoelastic bath is therefore a meaningful study, which was first performed by A. Spakowitz *et al.* [16]. Based on the three-dimensional generalised Langevin equation from Section 2.6, we can rewrite the Langevin equations, Eq. (5.15), of the Rouse model to become generalised

$$\eta_\alpha {}_c\mathcal{D}^\alpha \vec{R}_n(t) = -k \left(2\vec{R}_n(t) - \vec{R}_{n-1}(t) - \vec{R}_{n+1}(t) \right) + \vec{\xi}_{T,n}(t), \quad (5.52)$$

with $\eta_\alpha = \gamma\Gamma(3-\alpha)$. As a reminder, ${}_c\mathcal{D}^\alpha$ stands for the Caputo fractional derivative, more information on this derivative can be found in Appendix A.7. The random thermal forces on the n^{th} bead also need to change to suit the fluctuation-dissipation relation. Because we assume them to be uncorrelated between beads, they become

$$\langle \vec{\xi}_{T,n}(t) \cdot \vec{\xi}_{T,m}(t') \rangle = 3k_B T K(|t-t'|) \delta_{n,m}, \quad (5.53)$$

with memory kernel $K(t)$ defined by Eq. (2.50)¹. Remember that the fractional derivative stands for a convolution between the memory kernel and the velocity profile. This description breaks down on short time-scales of the order of molecular collisions.

¹In calculations we will often use the following (equivalent) form of the memory kernel

$$K(t) = (2-\alpha)(1-\alpha)\gamma t^{-\alpha}. \quad (5.54)$$

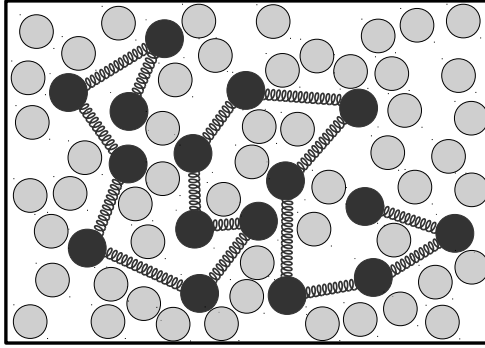


Figure 5.3: A cartoon of the Rouse model in a viscoelastic bath. The black spheres connected with springs are the Rouse chain. The large grey spheres represent the crowdedness of a viscoelastic bath (they are, for example, the macromolecules that are present in the cytosol).

An upper limit to these memory effects is put by the cellular lifetime, which is often much smaller than the largest relaxation time of viscoelastic baths.

The thermal noise is still a Gaussian variable and since Eq. (5.52) is linear, the position of the beads is also Gaussian distributed and therefore fully described by its first and second moments. Clearly, when $\alpha = 1$ we recover the original Rouse model. The two equations above fully describe a Rouse chain in a viscoelastic bath. A schematic representation of this model is shown in Fig. 5.3, where the surrounding fluid particles are larger than in Fig. 5.2 to represent the crowdedness of the bath.

Because Eq. (5.52) are still linear (fractional) differential equations, we can again use the normal coordinates to decouple them. It is easy to show that Eq. (5.29) becomes

$$\eta_\alpha {}_c\mathcal{D}^\alpha \vec{X}_p(t) = -\frac{k_p}{2N} \vec{X}_p(t) + \vec{\xi}_{T,p}(t). \quad (5.55)$$

The normal noise is still given by Eq. (5.31), i.e. a linear combination of the natural noises defined by Eq. (5.53). Its mean is zero and its correlation, using the orthogonal property of the transformation coefficients, reads

$$\langle \vec{\xi}_{T,p}(t) \cdot \vec{\xi}_{T,q}(t') \rangle = \frac{3k_B T}{2N} K(|t-t'|)(1 + \delta_{p,0})\delta_{p,q}. \quad (5.56)$$

To solve Eq. (5.55), notice that it closely resembles the equation of motion of a harmonic oscillator from the previous chapter, i.e. Eq. (4.19). Solving it is very analogous and yields a similar result for the evolution of the p^{th} normal mode

$$\begin{aligned} \vec{X}_p(t) &= \vec{X}_p(0) E_{\alpha,1} \left(- (t/\tau_{p,\alpha})^\alpha \right) \\ &+ \frac{1}{\eta_\alpha} \int_0^t d\tau \vec{\xi}_{T,p}(t-\tau) \tau^{\alpha-1} E_{\alpha,\alpha} \left(- (\tau/\tau_{p,\alpha})^\alpha \right). \end{aligned} \quad (5.57)$$

The Mittag-Leffler function $E_{\alpha,\beta}(\cdot)$ appears in this expression, we refer to Appendix A.1 for more information on this function. We introduced the characteristic time $\tau_{p,\alpha}$

of the p^{th} mode in a viscoelastic bath, with $\tau_{p,\alpha} = (\Gamma(3 - \alpha)\tau_p)^{1/\alpha}$, clearly we have $\tau_p = \tau_{p,1}$. From this we define the generalised Rouse time to be $\tau_{R,\alpha} = \tau_{1,\alpha}$, it has the following form

$$\tau_{R,\alpha} = \left(\frac{\eta_\alpha N^2}{k\pi^2} \right)^{1/\alpha}, \quad (5.58)$$

for large N . The dependence on N as $N^{2/\alpha}$ implies that for the small α -values reported for cells, this time scale can become quite large. The smallest characteristic time (which is that of a single bead) is again denoted by $\tau_{N,\alpha} \sim (\gamma/k)^{1/\alpha}$. Just as we have done in the previous section, we can use the evolution of the normal coordinates to find the dynamics of the natural coordinates.

Centre of mass

If $p = 0$ in Eq. (5.57) we get the equation of motion for the centre of mass. Because of property (A.3), this simply becomes

$$\vec{R}_{cm}(t) = \vec{R}_{cm}(0) + \frac{1}{\Gamma(\alpha)\eta_\alpha} \int_0^t d\tau \vec{\xi}_{T,0}(t - \tau) \tau^{\alpha-1}. \quad (5.59)$$

From this it is clear that the mean displacement of the centre of mass is zero, $\langle \Delta \vec{R}_{cm}(t) \rangle = 0$. The mean-squared displacement is given by $\Delta_{cm}^2(t) = \langle (\Delta \vec{R}_{cm}(t))^2 \rangle$ and its expression can be found by squaring and averaging the second term of Eq. (5.59). Applying Eq. (5.56) and using some convenient notation for later, we find

$$\Delta_{cm}^2(t) = \frac{3k_B T(2 - \alpha)(1 - \alpha)}{\gamma N G_\alpha^2} \int_0^t d\tau \int_0^t d\tau' \frac{\tau^{\alpha-1} \tau'^{\alpha-1}}{|\tau - \tau'|^\alpha}, \quad (5.60)$$

with $G_\alpha = \Gamma(\alpha)\Gamma(3 - \alpha)$. We already solved the double integral in Eq. (4.8). Using this result, the final result for the mean-squared displacement is then

$$\Delta_{cm}^2(t) = \frac{6 D_\alpha^{cm}}{\Gamma(\alpha + 1)} t^\alpha. \quad (5.61)$$

We have associated a generalised diffusion constant to this process, namely $D_\alpha^{cm} = k_B T / \eta_\alpha N$. When $\alpha = 1$ we recover the viscous result of Eq. (5.42) where the centre of mass diffuses normally. When $\alpha < 1$ the centre of mass performs subdiffusion.

Single bead

For the same reasons as the previous section, the mean displacement of the n^{th} bead is zero. Its mean-squared displacement is given by Eq. (5.43). In order to work out this expression we need to find the generalised version of Eq. (5.40). From Eq. (5.57) we obtain

$$\begin{aligned} \langle \vec{X}_p(t) \cdot \vec{X}_p(t') \rangle &= \langle \vec{X}_p^2(0) \rangle E_{\alpha,1} \left(- (t/\tau_{p,\alpha})^\alpha \right) E_{\alpha,1} \left(- (t'/\tau_{p,\alpha})^\alpha \right) \\ &+ \frac{1}{\eta_\alpha^2} \int_0^t d\tau \int_0^{t'} d\tau' \langle \vec{\xi}_{T,p}(t - \tau) \cdot \vec{\xi}_{T,p}(t' - \tau') \rangle \tau^{\alpha-1} \tau'^{\alpha-1} \\ &\times E_{\alpha,\alpha} \left(- (\tau/\tau_{p,\alpha})^\alpha \right) E_{\alpha,\alpha} \left(- (\tau'/\tau_{p,\alpha})^\alpha \right). \end{aligned} \quad (5.62)$$

The fact that the bath is viscoelastic will change the dynamics of the Rouse chain, it will not however change its equilibrium properties. This is ensured by the fluctuation-dissipation relation Eq. (5.53). Therefore the equipartition result for the normal coordinates, i.e. Eq. (5.37), still holds. We can use this for the first term of this expression. Also applying Eq. (5.56) brings us to the following result (for $p \neq 0$)

$$\begin{aligned} \langle \vec{X}_p(t) \cdot \vec{X}_p(t') \rangle &= \frac{3k_B T}{k_p} E_{\alpha,1} \left(- (t/\tau_{p,\alpha})^\alpha \right) E_{\alpha,1} \left(- (t'/\tau_{p,\alpha})^\alpha \right) \\ &\quad + \frac{3\gamma k_B T}{N\eta_\alpha^2} \int_0^t d\tau \int_0^{t'} d\tau' (2-\alpha)(1-\alpha) \frac{\tau^{\alpha-1} \tau'^{\alpha-1}}{|\tau - \tau'|^\alpha} \\ &\quad \times E_{\alpha,\alpha} \left(- (\tau/\tau_{p,\alpha})^\alpha \right) E_{\alpha,\alpha} \left(- (\tau'/\tau_{p,\alpha})^\alpha \right). \end{aligned} \quad (5.63)$$

The double integral in this expression can be evaluated using property (A.10) of the Mittag-Leffler functions. Because two different modes are uncorrelated, the final relation is

$$\langle \vec{X}_p(t) \cdot \vec{X}_q(t') \rangle = \frac{3k_B T}{k_p} E_{\alpha,1} \left(- \left(\frac{|t-t'|}{\tau_{p,\alpha}} \right)^\alpha \right) \delta_{p,q}. \quad (5.64)$$

When $t = t'$, the equipartition result is recovered, as it should. Also notice that when $\alpha = 1$, this becomes the viscous result Eq. (5.40). Now the first term of Eq. (5.43) is simply the mean-squared displacement of the centre of mass, being Eq. (5.61). The second term is found by filling in Eq. (5.44). The mean-squared displacement of the n^{th} bead is then

$$\Delta_n^2(t) = \frac{6D_\alpha^{cm}}{\Gamma(\alpha+1)} t^\alpha + \frac{12k_B T}{\gamma N} \sum_{p=1}^{N-1} C_n^{p^2} \tau_p \left[1 - E_{\alpha,1} \left(- (t/\tau_{p,\alpha})^\alpha \right) \right]. \quad (5.65)$$

If we want the expression for the middle bead ($n = N/2 = m$), the transformation coefficients C_n^p can be omitted but the summation should then only go over the even modes (as was explained in the previous section). Just as in the viscous case, to which it reduces when $\alpha = 1$, we can identify three time regimes from this expression. For very short times, $t \ll \tau_{N,\alpha}$, the bead subdiffuses as a free particle since it has not yet had the time to feel the influence of the springs. Approximating the second term in Eq. (5.65) to first order (see Appendix A.1), one finds $\Delta_m^2(t) = (6k_B T/\gamma\alpha G_\alpha) t^\alpha$. For short times, $t \ll \tau_{R,\alpha}$, the summation can be approximated by an integral. Using a very analogue reasoning as for Eq. (5.48), leads us to

$$\frac{6k_B T}{\gamma} \int_0^\infty dx \frac{\gamma}{k\pi^2 x^2} \left[1 - E_{\alpha,1} \left(- \frac{k\pi^2 t^\alpha}{\eta_\alpha} x^2 \right) \right] = \frac{6k_B T I_\alpha}{\sqrt{\eta_\alpha k \pi^2}} t^{\alpha/2}, \quad (5.66)$$

with $I_\alpha = \int_0^\infty dx x^{-2} (1 - E_{\alpha,1}(-x^2))$ which only depends on α . We have that $I_0 = \pi/2$ and $I_1 = \sqrt{\pi}$, for all other α -values (for $0 < \alpha < 1$) I_α lies between these limits. One finds that the mean-squared displacement goes as: $\Delta_m^2(t) \sim t^{\alpha/2}$, so it becomes even more subdiffusive due to the restricting springs. For long times, $t \gg \tau_{R,\alpha}$, the first term in Eq. (5.65) dominates. So again the bead follows the collective motion of the entire chain. We thus find that in a viscoelastic bath ($\alpha < 1$), the bead always

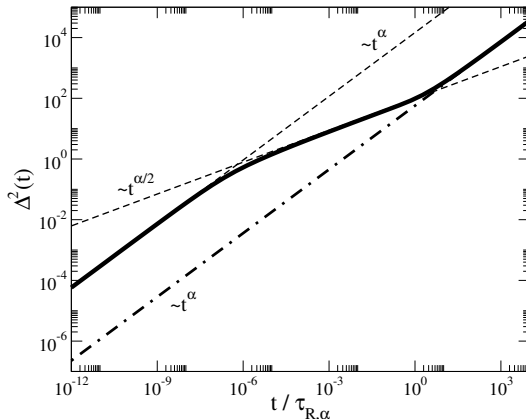


Figure 5.4: Log-log plot of the mean-squared displacement of the middle bead $\Delta_m^2(t)$ (solid line) and of the centre of mass $\Delta_{cm}^2(t)$ (dashed-dotted line). For $\alpha = 0.7$, $k_B T = \gamma = 1$, $k = 3$ and $N = 256$. The approximate mean-squared displacements of Eq. (5.67) are plotted in dashed lines.

displays a subdiffusion. These three time regimes, together with the diffusion of the centre of mass, are shown in Fig. 5.4. The sequence of the approximate regimes of Δ_n^2 , with $n = N/2$, is summarized as

$$\Delta_m^2(t) = \frac{6D_\alpha}{\Gamma(\alpha + 1)} t^\alpha \xrightarrow{\tau_{N,\alpha}} \frac{6k_B T I_\alpha}{\sqrt{\eta_\alpha k \pi^2}} t^{\alpha/2} \xrightarrow{\tau_{R,\alpha}} \frac{6D_\alpha^{cm}}{\Gamma(\alpha + 1)} t^\alpha. \quad (5.67)$$

Notice that this sequence reduces to that of Eq. (5.49) when $\alpha = 1$.

End-to-end vector

The autocorrelation of the end-to-end vector is found using the same technique as in Eq. (5.50). In a viscoelastic bath this autocorrelation becomes

$$\langle \vec{P}(t) \cdot \vec{P}(t') \rangle = \frac{24k_B T}{\gamma N} \sum_{p=1, \text{odd}}^{N-1} \tau_p E_{\alpha,1} \left(- \left(\frac{|t - t'|}{\tau_{p,\alpha}} \right)^\alpha \right). \quad (5.68)$$

We already mentioned that the equilibrium properties should still hold in a viscoelastic bath. We see that this is indeed the case since for $t = t'$ we recover the equipartition result of Eq. (5.51), i.e. $\langle \vec{P}^2(t) \rangle = 3k_B T N/k$.

5.3 Dragging through a viscoelastic bath

The inside of a cell is certainly not a passive place but is under constant agitation. Many processes are involved in keeping the cell from reaching equilibrium, as was discussed in Section 1.3. Small molecules such as gases and glucose can diffuse to

where they are needed. Large molecules, however, can not easily diffuse to their destination through the crowded cytosol. Therefore, the workings of a cell depend heavily on the active displacement of polymers. For example, during cell division, the chromosomes are pulled to opposite sides of the cell by the mitotic spindle. This restructuring inside a cell is also often done by molecular motors such as the actin-myosin complex. These motors are able to drag a polymer through the cytosol in a well defined direction. These cellular processes all involve applying a (constant) force on a particular place of the polymer. The strength of these forces is of the order of pico-Newtons. Because the cytosol is a viscoelastic medium, it is interesting to study how the Rouse chain behaves in a viscoelastic bath when such a constant force is applied on its first bead. This situation is not only relevant for polymers in a cellular environment but also in an *in vitro* situation. Nowadays, it is possible to manipulate a single macromolecule using optical tweezers as was, for example, done with the bacterial nucleoid [102]. Notice that this set-up is completely equivalent to that where the first monomer is held fixed and the polymer is subjected to a uniform flow [103–106]. This section is based on our research which was published in [98].

We assume that the polymer is thermalised at $t = 0$ when we turn on the constant force. Because this force is conservative, i.e. it can be derived from a potential, the system will, for long times, again reach an equilibrated state. Although we will study some quantities in this new equilibrated state, the main focus of this section will be on the transient, nonequilibrium behaviour the Rouse chain exhibits between its two equilibrium states. This transient behaviour will depend on the viscoelasticity of the bath while the equilibrium states will not. The generalised Langevin equation of the Rouse model, Eq. (5.52), that includes a constant force on the first bead is written as

$$\eta_{\alpha c} \mathcal{D}^\alpha \vec{R}_n(t) = -k \left(2\vec{R}_n(t) - \vec{R}_{n-1}(t) - \vec{R}_{n+1}(t) \right) + \vec{\xi}_{T,n}(t) + \vec{f}_n(t). \quad (5.69)$$

The thermal forces are still defined by Eq. (5.53). The last term in this equation represents the constant force of strength f . It is given by the following formula

$$\vec{f}_n(t) = f \delta_{n,0} H(t) \hat{e}_x, \quad (5.70)$$

where $H(t)$ is the Heaviside function (see Eq. (4.3)) that ensures the force is turned on at $t = 0$. Although not necessary, we will assume $f > 0$. Without loss of generality, we arbitrarily choose the direction of the force to be along the x -axis, hence the inclusion of unit vector \hat{e}_x . A schematic representation of this model is given by Fig. 5.5. When $f = 0$ we should, naturally, retrieve the results of the previous section. Because, in essence, $\vec{f}_n(t)$ is a constant, it will only affect the mean value of the natural coordinates. It will not change the fluctuations around this value, therefore the variance in the displacement is given by the results of the previous section where they represented the mean-squared displacement since there the mean value was zero.

We again invoke the normal coordinates to solve Eq. (5.69), they are still defined by Eq. (5.18). The generalised Langevin equation of the normal coordinates can be found quite easily by using Eq. (5.55) and it reads

$$\eta_{\alpha c} \mathcal{D}^\alpha \vec{X}_p(t) = -\frac{k_p}{2N} \vec{X}_p(t) + \vec{\xi}_{T,p}(t) + \vec{f}_p(t), \quad (5.71)$$

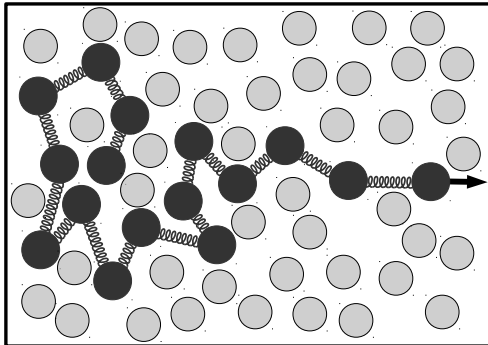


Figure 5.5: A cartoon of the Rouse model in a viscoelastic bath with a constant force applied to its first bead. The black spheres connected with springs are the Rouse chain. The large grey spheres represent the crowdedness of a viscoelastic bath (they are, for example, the macromolecules that are present in the cytosol). The black arrow is the constant force (originating from, for example, molecular motors).

with

$$\vec{f}_p(t) = \frac{f}{N} C_0^p H(t) \hat{e}_x. \quad (5.72)$$

Using the same techniques as in the previous section we find the evolution of the p^{th} Rouse mode. A more rapid derivation can be achieved, however, by interchanging $\vec{\xi}_{T,p}$ with $\vec{\xi}_{T,p} + \vec{f}_p$ in Eq. (5.57). If then the integral property Eq. (A.9) is used the final result becomes

$$\begin{aligned} \vec{X}_p(t) = & \vec{X}_p(0) E_{\alpha,1} \left(- (t/\tau_{p,\alpha})^\alpha \right) \\ & + \frac{1}{\eta_\alpha} \int_0^t d\tau \vec{\xi}_{T,p}(t-\tau) \tau^{\alpha-1} E_{\alpha,\alpha} \left(- (\tau/\tau_{p,\alpha})^\alpha \right) \\ & + \frac{C_0^p f}{\eta_\alpha N} t^\alpha E_{\alpha,\alpha+1} \left(- (t/\tau_{p,\alpha})^\alpha \right) \hat{e}_x. \end{aligned} \quad (5.73)$$

Using this expression we can calculate the dynamic properties of the dragged polymer.

5.3.1 Mean position

Without loss of generality, we take $\langle \vec{R}_{cm}(0) \rangle = 0$. Because the thermalised Rouse chain is fully symmetric around its centre of mass, we also have $\langle \vec{R}_n(0) \rangle = 0$. And since the normal coordinates are a linear combination of the natural coordinates we have $\langle \vec{X}_p(0) \rangle = 0$. Taking the average of Eq. (5.73) gives the following expression for the mean of the p^{th} mode

$$\langle \vec{X}_p(t) \rangle = \frac{C_0^p f}{\eta_\alpha N} t^\alpha E_{\alpha,\alpha+1} \left(- (t/\tau_{p,\alpha})^\alpha \right) \hat{e}_x. \quad (5.74)$$

Since the directed force breaks the rotational symmetry of the Rouse chain the before mentioned averages will become non-zero when $t > 0$.

Centre of mass

The zeroth mode corresponds to the position of the centre of mass, as Eq. (5.20) showed. Taking $p = 0$ in Eq. (5.74) gives

$$\langle \vec{R}_{cm}(t) \rangle = \frac{f \hat{e}_x}{\gamma N \alpha G_\alpha} t^\alpha. \quad (5.75)$$

From this we can conclude that the centre of mass moves sub-ballistically. Such motion has indeed been observed in experiments with molecular motors that move under their own generated force [80].

Single bead

The linear combination of normal coordinates that defines the position of the n^{th} bead is given by Eq. (5.21). Taking the average of this expression and using Eq. (5.74) results in

$$\langle \vec{R}_n(t) \rangle = \frac{f \hat{e}_x}{\gamma N \alpha G_\alpha} t^\alpha \left[1 + 2\Gamma(\alpha + 1) \sum_{p=1}^{N-1} C_n^p C_0^p E_{\alpha, \alpha+1} \left(- (t/\tau_{p, \alpha})^\alpha \right) \right]. \quad (5.76)$$

For long times, $t \gg \tau_{R, \alpha}$, the n^{th} bead will display the same sub-ballistic motion as the centre of mass, since the second term between the brackets goes to zero for this time limit. The polymer then performs a steady collective motion. To understand the short time behaviour, $t \ll \tau_{R, \alpha}$, of the beads, we refer to Fig. 5.6. The displacement of the first beads is instantaneous since the beads have no inertia (because we work in the overdamped limit). Their mean position is initially much further than that of the centre of mass and grows as $t^{\alpha/2}$ (for the calculation of this regime we refer to the very analogue calculations in the section about the velocity of a bead). That is because the last beads are lagging behind while the first spring are extending. This energy absorption of the force delays its immediate transmission to the end of the chain. Only when all beads have increased their mean position will they all move according to the centre of mass.

5.3.2 Shape of the polymer

The springs that are closer in the chain to the first bead will absorb more of the force's energy than the springs at the end of the chain. The average extension of the springs will thus increase the closer one gets to the first bead. And since the end of the chain will lag behind due to the friction force, the polymer will have an elongated shape. The rotational symmetry of the polymer is broken by the force. Because the influence of the force decreases along the chain, the thermal fluctuations will have more effect on the beads further down the chain. Therefore the thermal swelling of the polymer will be different depending on the location of the chain. It will be larger when one moves to the end of the chain. These features of the polymer will be discussed in this section and are crudely sketched in Fig. 5.5.

From the position of the n^{th} bead, Eq. (5.76), we can gain information on the elongation of the polymer through time. This elongation, in the direction of the

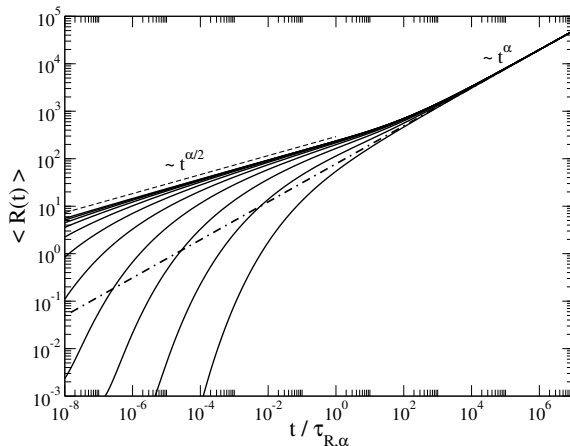


Figure 5.6: Log-log plot of the mean position (where $\langle R(t) \rangle = |\langle \vec{R}(t) \rangle|$) of the n^{th} bead $\langle \vec{R}_n(t) \rangle$ (solid lines) and of the centre of mass $\langle \vec{R}_{cm}(t) \rangle$ (dashed-dotted line) with $n = 0, 2^i, 1023$ and $i = 0, 1, \dots, 9$. For $\alpha = 0.4$, $k_B T = \gamma = 1$, $k = 3$, $f = 2$ and $N = 1024$. The higher the n value, the lower the curve lies. The long time regime is indicated and the dashed line indicates the early $t^{\alpha/2}$ regime.

force, has an average length $L(t)$. It is defined through the end-to-end vector

$$L(t) = |\langle \vec{P}(t) \rangle| = |\langle \vec{R}_{N-1}(t) \rangle - \langle \vec{R}_0(t) \rangle|. \quad (5.77)$$

Using Eq. (5.76) and $C_{N-1}^p - C_0^p = ((-1)^p - 1)C_0^p$, we find the following expression for the average length. This result can also be attained when Eq. (5.74) is plugged in Eq. (5.24).

$$L(t) = \frac{4f}{\eta_\alpha N} t^\alpha \sum_{p=1, \text{odd}}^{N-1} C_0^{p^2} E_{\alpha, \alpha+1} \left(- (t/\tau_{p,\alpha})^\alpha \right). \quad (5.78)$$

Asymptotically in time the length grows to a steady value $L^* = L(t \rightarrow \infty)$. Using the asymptotic behaviour of the Mittag-Leffler functions (see Appendix A.1), we find

$$L^* = \frac{4fN}{k\pi^2} \sum_{p=1, \text{odd}}^{N-1} \frac{C_0^{p^2}}{p^2} = \frac{fN}{2k}, \quad (5.79)$$

where the second equation holds for large N . This result is of course independent of the viscoelasticity of the bath (or α) since it is an equilibrium property, it was already calculated for a viscous medium [14]. The transient regime that leads up to the steady length is, however, dependent on the viscoelasticity of the medium where it occurs. For very small times, $t \ll \tau_{N,\alpha}$, the Mittag-Leffler function in Eq. (5.78) can be approximated by $1/\Gamma(\alpha + 1)$. If we then apply $\sum_{p=1, \text{odd}}^{N-1} C_0^{p^2} = N/4$, we find that the length grows as $L(t) = ft^\alpha/\gamma\alpha G_\alpha$. To discover how the transient regime behaves for larger times we first drop the $C_0^{p^2}$ factor from Eq. (5.78). We can do this

because for small p it is close to one and the terms with large p are suppressed by their small characteristic time τ_p . For times smaller than the Rouse time $\tau_{R,\alpha}$ and $N \rightarrow \infty$, we can approximate the summation by an integral, because its argument is a smooth continuous function. We should take $1/N \rightarrow dx$ and $p/N \rightarrow x$. Because the summation is only over odd p , we multiply the integral by one half. This leads to

$$L(t) \approx \frac{2f}{\eta_\alpha} t^\alpha \int_0^\infty dx E_{\alpha,\alpha+1} \left(-\frac{k\pi^2 t^\alpha}{\eta_\alpha} x^2 \right) = \frac{2f I_\alpha}{\pi \sqrt{\eta_\alpha k}} t^{\alpha/2}, \quad (5.80)$$

where $I_\alpha = \int_0^\infty dx E_{\alpha,\alpha+1}(-x^2) = \int_0^\infty dx x^{-2}(1 - E_{\alpha,1}(-x^2))$ as it was introduced in the previous section. The numeric value of I_α lies between $\pi/2$ and $\sqrt{\pi}$ for $0 < \alpha \leq 1$. From this it is clear that the length grows as a power-law of $\alpha/2$. In Fig. 5.7 we plot $L(t)/L^*$ as a function of time for various α -values. We clearly see the predicted behaviour: after an initial t^α regime, the length grows as $t^{\alpha/2}$ and then reaches its limiting value after $\tau_{R,\alpha}$. The sequence of regimes for the length through time is

$$L(t) = \frac{f}{\gamma \alpha G_\alpha} t^\alpha \xrightarrow{\tau_{N,\alpha}} \frac{2f I_\alpha}{\pi \sqrt{\eta_\alpha k}} t^{\alpha/2} \xrightarrow{\tau_{R,\alpha}} \frac{fN}{2k}. \quad (5.81)$$

Because $\tau_{R,\alpha} \sim N^{2/\alpha}$, for small values of α it can take a very long time before the steady length L^* is reached.

It is experimentally possible to pull a polymer through a medium using optical tweezers [102]. The shape of that polymer can be studied if it is made fluorescent [107, 108]. In this way, it can in principle be possible to determine the length of the polymer as a function of time. From such measurements it would be possible to get an independent estimate of the intrinsic exponent α of the medium. This can be seen as a new active microrheological approach which complements existing techniques where α is determined from (passive) measurements of the subdiffusion of a particle immersed in the environment or from (active) measurements of the response to a periodic perturbation [109].

Next, we investigate the density profile, how it evolves in time and what its equilibrium configuration is. We know, from [110], that a fixed polymer in a constant flow displays a trumpet shape (characterized by an ever increasing density profile, very small at the start and diverging at the end). Since the dragging of a polymer through a fluid is equivalent to a fixed polymer in a constant flow, we also expect to find the trumpet shape for our dragged polymer. Because the Rouse chain is infinity extendible, the trumpet shape is the only possible density profile available. For a finite extendible polymer (which we will discuss later) the stem-flower shape can also be assumed for strong forces [104]. We define \mathcal{X} as the average distance (in the direction of the force) between the n^{th} and the first bead

$$\mathcal{X}(n, t) = |\langle \vec{R}_n(t) \rangle - \langle \vec{R}_0(t) \rangle|, \quad (5.82)$$

we clearly have that $\mathcal{X}(N-1, t) = L(t)$. Using Eq. (5.76) one finds

$$\mathcal{X}(n, t) = \frac{2f}{\eta_\alpha N} t^\alpha \sum_{p=1}^{N-1} (C_0^p - C_n^p) C_0^p E_{\alpha,\alpha+1} \left(- (t/\tau_{p,\alpha})^\alpha \right). \quad (5.83)$$

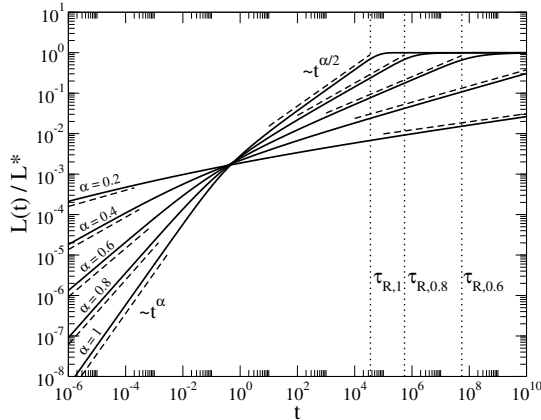


Figure 5.7: Log-log plot of the ratio of the length to the equilibrium length as a function of time for $\alpha = 0.2, 0.4, 0.6, 0.8$ and 1.0 (as indicated in the figure). All curves are for $k_B T = \gamma = 1$, $k = 3$, $f = 2$ and $N = 1024$. The Rouse time for various α -values are indicated by a vertical dotted line (for $\alpha = 0.2$ and $\alpha = 0.4$ these times lay outside the figure). The dashed lines indicate the local power-law.

If this function is inverted to $n(\mathcal{X}, t)$, we get an expression that gives the bead index n as a function of the average distance from the first bead. If we then take the \mathcal{X} -derivative of this expression we obtain a measure for the density of beads as a function of distance from the first bead, we thus have $\rho(\mathcal{X}, t) = dn(\mathcal{X}, t)/d\mathcal{X}$. For arbitrary times this calculation has to be done numerically. But in the steady state ($t \rightarrow \infty$) we can get analytic results. Taking the asymptotic behaviour of the Mittag-Leffler function (see Appendix A.1) and plugging that into Eq. (5.83) we get

$$\mathcal{X}(n, t \rightarrow \infty) = \frac{2f}{\gamma N} \sum_{p=1}^{N-1} (C_0^p - C_n^p) C_0^p \tau_p. \quad (5.84)$$

This summation can be worked out (the calculation is given at the end of this section) and gives the following result

$$\mathcal{X}(n, t \rightarrow \infty) = \frac{f}{k} \left[n - \frac{n}{2N} - \frac{n^2}{2N} \right] \approx \frac{f}{k} \left[n - \frac{n^2}{2N} \right], \quad (5.85)$$

where the approximation holds for large N . Inverting this expression gives the following two relations for n

$$n(\mathcal{X}, t \rightarrow \infty) = N \left(1 \pm \sqrt{1 - \frac{2k}{fN} \mathcal{X}} \right). \quad (5.86)$$

Only the solution with the minus-symbol is realistic because if $\mathcal{X} = 0$ we should get $n = 0$, not $n = 2N$ (since the first monomer has no distance from itself). Also notice

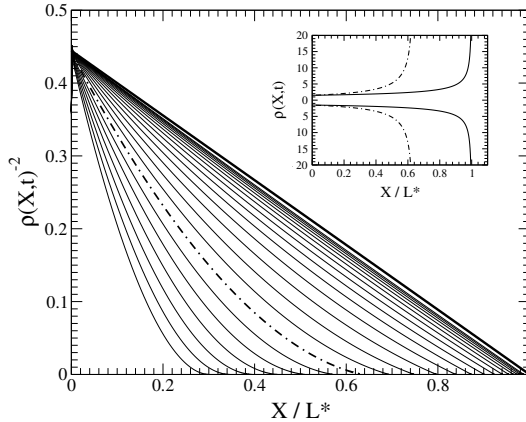


Figure 5.8: Time evolution of the density profile for a medium with $\alpha = 0.4$. We plot $\rho(\mathcal{X}, t)^{-2}$ for different times (increasing from left to right). For $\alpha = 0.4$, $k_B T = \gamma = 1$, $k = 3$, $f = 2$, and $N = 1024$. The thick solid line gives the steady state shape, Eq. (5.87). The different curves give the density at times $t = 2^i \tau_{R,\alpha}$ with $i = -6, -5, \dots, 13, 14$. *Inset:* Density of beads versus distance from the first monomer for a medium with $\alpha = 0.4$. The full line gives the steady state shape, the dashed-dotted line gives the density at the Rouse time $\tau_{R,\alpha}$. The density is also shown reflected on the \mathcal{X} -axis to display the trumpet shape.

that in this formula the steady length $L^* = fN/2k$ appears. Taking the \mathcal{X} -derivative gives the density profile at long times

$$\rho(\mathcal{X}, t \rightarrow \infty) = \frac{k}{f\sqrt{1 - \mathcal{X}/L^*}}. \quad (5.87)$$

This function, which diverges at L^* , is the famous trumpet shape of a polymer in a steady flow. Notice that this result is again independent of the properties of the viscoelastic medium and therefore also holds for the Rouse model in a viscous medium. We thus find that the polymer adopts the trumpet shape when it is being dragged through a viscoelastic medium. As was stated before, the transient density profile can only be found numerically. Figure 5.8 shows the density at different moments in time. Because of the form of Eq. (5.87) it is convenient to plot $\rho(\mathcal{X}, t)^{-2}$ as a function of \mathcal{X} which in the steady state is a linear function that becomes zero at $\mathcal{X} = L^*$. For finite times, $\rho(\mathcal{X}, t)$ diverges at $L(t)$ though the precise function relation is unknown. Yet, as the inset of Fig. 5.8 shows, during these earlier times the density has a short trumpet shape, that elongates through time to meet up with Eq. (5.87).

As promised, we will give here the derivation of Eq. (5.85). We need to work out the following expression

$$\frac{2fN}{k\pi^2} \sum_{p=1}^{\infty} \left[\frac{C_0^p{}^2}{p^2} - \frac{C_n^p C_0^p}{p^2} \right], \quad (5.88)$$

where we took N large. Writing the cosine as exponentials, $\cos(x) = (e^{-ix} + e^{ix})/2$, yields

$$\frac{fN}{2k\pi^2} \sum_{p=1}^{\infty} \left[\frac{\exp^p \left(-\frac{i\pi}{N} \right)}{p^2} + \frac{\exp^p \left(\frac{i\pi}{N} \right)}{p^2} + \frac{2}{p^2} - \frac{\exp^p \left(-\frac{i\pi(n+1)}{N} \right)}{p^2} \right. \\ \left. - \frac{\exp^p \left(\frac{i\pi(n+1)}{N} \right)}{p^2} - \frac{\exp^p \left(-\frac{i\pi n}{N} \right)}{p^2} - \frac{\exp^p \left(\frac{i\pi n}{N} \right)}{p^2} \right]. \quad (5.89)$$

Here we use the formalism of the polylogarithm (see Appendix A.5). The relation $\sum_{p=1}^{\infty} p^{-2} = \pi^2/6$ is also used. The expression becomes

$$\frac{fN}{2k\pi^2} \left[\mathcal{L}_2 \left(\exp \left(-\frac{i\pi}{N} \right) \right) + \mathcal{L}_2 \left(\exp \left(\frac{i\pi}{N} \right) \right) + \frac{\pi^2}{3} - \mathcal{L}_2 \left(\exp \left(-\frac{i\pi(n+1)}{N} \right) \right) \right. \\ \left. - \mathcal{L}_2 \left(\exp \left(\frac{i\pi(n+1)}{N} \right) \right) - \mathcal{L}_2 \left(\exp \left(-\frac{i\pi n}{N} \right) \right) - \mathcal{L}_2 \left(\exp \left(\frac{i\pi n}{N} \right) \right) \right]. \quad (5.90)$$

If we then apply property (A.35), we obtain

$$\frac{fN}{4k\pi^2} \left[\pi^2 - \ln^2 \left(-\exp \left(-\frac{i\pi}{N} \right) \right) + \ln^2 \left(-\exp \left(-\frac{i\pi(n+1)}{N} \right) \right) + \ln^2 \left(-\exp \left(-\frac{i\pi n}{N} \right) \right) \right]. \quad (5.91)$$

Notice that $\ln^2(-e^{-ix}) = -(\pi - x)^2$ for $x > 0$. Using this relation yields

$$\frac{fN}{4k} \left[1 + \left(1 - \frac{1}{N} \right)^2 - \left(1 - \frac{(n+1)}{N} \right)^2 - \left(1 - \frac{n}{N} \right)^2 \right]. \quad (5.92)$$

Working out the squares and doing some elementary calculus will give Eq. (5.85).

5.3.3 Mean velocity

Taking the time derivative of the mean position will yield the mean velocity. The mean velocity will provide information on how the Rouse chain gradually responds to the constant force. From this response we can, in the next section, derive the front propagation through the chain.

Centre of mass

Deriving Eq. (5.75) with respect to time gives the mean velocity of the centre of mass. It reads

$$\langle \vec{V}_{cm}(t) \rangle = \frac{f \hat{e}_x}{\gamma N G_\alpha} t^{\alpha-1}. \quad (5.93)$$

For $\alpha < 1$, this quantity decreases as a power-law. This implies that the polymer practically comes to a rest for large t . Only in the viscous case, $\alpha = 1$, will the polymer keep moving. Its velocity will then be constant, and given by $\langle \vec{V}_{cm} \rangle = (f/\gamma N) \hat{e}_x$. As was already derived in [14].

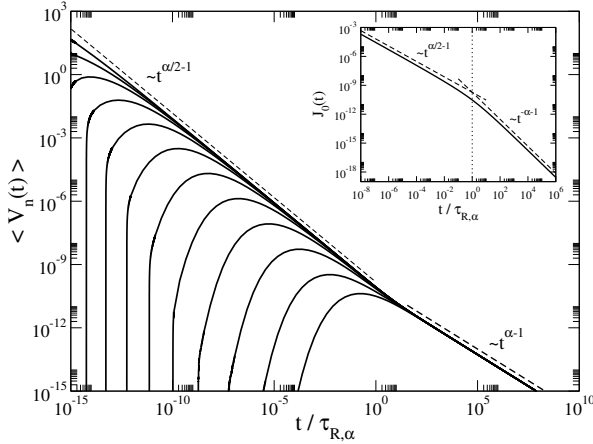


Figure 5.9: Log-log plot of the mean velocity (where $\langle V(t) \rangle = |\langle \vec{V}(t) \rangle|$) of the n^{th} bead, with $n = 0, 2^i, 1023$ and $i = 0, 1, \dots, 9$. For $\alpha = 0.4$, $k_B T = \gamma = 1$, $k = 3$, $f = 2$ and $N = 1024$. The higher the n value, the lower the curve lies. The dashed lines indicate the power-law behaviour. *Inset*: Log-log plot of the difference between the velocity of the first bead and the centre of mass versus time, with $J_0 = |\vec{J}_0|$. The dashed lines indicate the early and late time behaviour.

Single bead

The time derivative of Eq. (5.76) gives the mean velocity of each individual bead. Using the derivative of a Mittag-Leffler function (see Appendix A.1) gives the mean velocity of the n^{th} bead

$$\langle \vec{V}_n(t) \rangle = \frac{f \hat{e}_x}{\gamma N G_\alpha} t^{\alpha-1} \left[1 + 2\Gamma(\alpha) \sum_{p=1}^{N-1} C_n^p C_0^p E_{\alpha,\alpha} \left(- (t/\tau_{p,\alpha})^\alpha \right) \right]. \quad (5.94)$$

In Fig. 5.9 we plot the mean velocity of a few beads as a function of time. The first beads start to move immediately (since the beads have no inertia) and as time goes on other beads join the movement. When the influence of the force reaches a bead, it rapidly increases its velocity up to some maximum, which lies somewhat lower than the current velocity of the moving beads. Thereafter the velocity starts decreasing with the collective velocity as $t^{\alpha/2-1}$. After the Rouse time, all beads move with the velocity of the centre of mass (up to a power-law correction), which goes as $t^{\alpha-1}$.

We will now discuss how these power-laws are established. We focus on the first bead, $n = 0$, but the calculation and subsequent behaviour of the other beads is very similar. Investigating Eq. (5.94) reveals that the first term is just the mean velocity of the centre of mass. The second term, i.e. the summation, we will denote by $\vec{J}_n(t) = \langle \vec{V}_n(t) \rangle - \langle \vec{V}_{cm}(t) \rangle$. This term quantifies the difference in velocity between a given bead and the centre of mass. For the first bead, and large N , it is given by

$$\vec{J}_0(t) = \frac{2f \hat{e}_x}{\eta_\alpha N} t^{\alpha-1} \sum_{p=1}^{N-1} E_{\alpha,\alpha} \left(- (t/\tau_{p,\alpha})^\alpha \right). \quad (5.95)$$

We approximated $\mathcal{C}_0^{p^2}$ by one, which is correct for small p and large N . It is not, however, correct for larger p . But since $\tau_{p,\alpha}$ is very small in that case, the Mittag-Leffler function will be nearly zero and thus the approximation holds. In the viscous case, $\alpha = 1$, this quantity goes to zero exponentially fast after the Rouse time. In the viscoelastic case, $\alpha < 1$, this transient term dies out much slower. Asymptotically in time, only the Rouse mode with $p = 1$ survives, using Eq. (A.6) we find that for long times \vec{J}_0 decays as

$$\vec{J}_0(t \rightarrow \infty) = -\frac{2\eta_\alpha N^3 f \hat{e}_x}{\pi^4 k^2 \Gamma(-\alpha)} t^{-\alpha-1}, \quad (5.96)$$

this quantity will be positive because $\Gamma(-\alpha) < 0$ for $0 < \alpha \leq 1$. When $\alpha = 1$, it is equal to zero, as it should be for an exponential decay. For small times, we approximate the summation in Eq. (5.95) by an integral. We should take $1/N \rightarrow dx$ and $p/N \rightarrow x$. It becomes

$$\frac{2f \hat{e}_x}{\eta_\alpha} t^{\alpha-1} \int_0^\infty dx E_{\alpha,\alpha} \left(-\frac{k\pi^2 t^\alpha}{\eta_\alpha} x^2 \right) = \frac{2f Y_\alpha \hat{e}_x}{\pi \sqrt{\eta_\alpha k}} t^{\alpha/2-1}, \quad (5.97)$$

with $Y_\alpha = \int_0^\infty dx E_{\alpha,\alpha}(-x^2)$. We have that $Y_1 = \sqrt{\pi}/2$ and Y_α decreases to zero when α decreases. If we plug this result into Eq. (5.95), we find the $t^{\alpha/2-1}$ time dependence. The predicted short and long time regimes of \vec{J}_0 are shown in the inset of Fig. 5.9, where Eq. (5.95) is plotted. We can summarize the sequence of regimes as follows

$$\vec{J}_0(t) = \frac{2f Y_\alpha \hat{e}_x}{\pi \sqrt{\eta_\alpha k}} t^{\alpha/2-1} \xrightarrow{\tau_{R,\alpha}} -\frac{2\eta_\alpha N^3 f \hat{e}_x}{\pi^4 k^2 \Gamma(-\alpha)} t^{-\alpha-1}. \quad (5.98)$$

Combining these regimes of \vec{J}_0 with the velocity of the centre of mass gives the behaviour discussed in Fig. 5.9.

5.3.4 Front propagation

The curves in Fig. 5.9 suggests that as we pull on the first bead, a front moves through the chain that gradually sets into motion all other beads. This front is realised by each subsequent spring that adsorbs some energy of the force, thus creating tension in the chain. In order to further characterise the motion of this front, we determined numerically the time T_n at which the n^{th} bead reaches its maximum velocity. One can say that at this time, the response to the force is maximal. In Fig. 5.10 we plot these times as a function of n in a log-log scale for $\alpha = 0.4$. Clearly, the front propagates as a power-law $T_n \sim n^z$. From a fit of the data, we find $z \approx 4.92$. This estimate is consistent with the prediction $z = 2/\alpha$ as can be expected from the scaling of the mean length $L(t)$, since that is closely related to the front propagation in the chain. The inset of Fig. 5.10 shows that this expectation is indeed in agreement with the numerical results for the whole range of α -values. Sakaue *et al.* already derived, using a scaling approach [14], the front propagation through a pulled polymer in a viscous bath. They found the following scaling law for the time of response of the n^{th} bead $n \sim (t/\tau_R)^{1/2}$. This result complies with ours, i.e. $n \sim T_n^{\alpha/2}$, since for a viscous bath we have $\alpha = 1$.

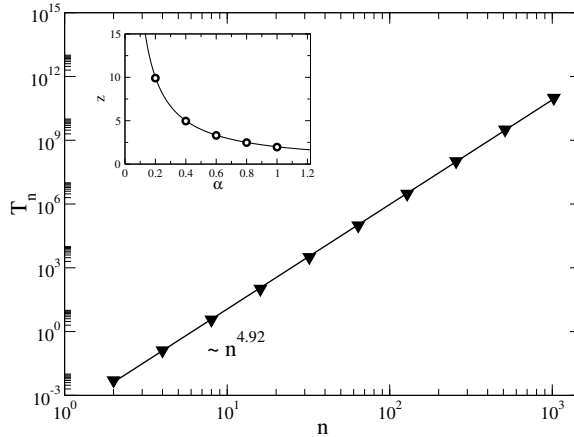


Figure 5.10: Log-log plot of time T_n at which the n^{th} beads has a maximal velocity versus n . For $\alpha = 0.4$, $k_B T = \gamma = 1$, $k = 3$, $f = 2$, and $N = 1024$. The straight line shows a best linear fit through the numerical data points. *Inset*: Lin-lin plot of the estimates of the exponent z versus α . The full line is $z = 2/\alpha$.

5.4 Dynamics in an active viscoelastic bath

In the previous section we investigated the response of a polymer subjected to a constant force. Although there are some specific cellular processes that can be modelled as such, the natural (i.e. most occurring) “habitat” of a polymer does not include such a constant force. This, however, does not imply that there is no driving on the polymer in the cellular environment. In the cytosol, the polymer is constantly agitated by fluctuating forces that are not only thermal in nature. These non-thermal random forces are, among other processes, responsible for keeping the internal structure of a cell away from equilibrium (which is essential for the survival of a cell, as was discussed in Section 1.3). It does so by facilitating the transport of, for example, polymers that would be much slower when left to thermal diffusion alone. In Section 2.5, we already discussed the origin of these *active processes*, as they are called. In short, they come about through the interplay between the myosin-II molecular motors and the actin filaments of the cytoskeleton. The active process they create introduces these non-thermal random forces that persist in a particular (yet random) direction for some characteristic (average) time. Together with viscoelasticity, the active processes capture the most important features of the cytosol. In this section, we investigate how a Rouse chain behaves in an active viscoelastic bath since this mimics the natural environment of a polymer. We will find that a rich diffusive profile emerges from it, which does not exist in an unnatural non-active viscous bath. The results in this section were published in one of our papers [99].

As always, we assume the system to be in equilibrium at $t = 0$, after which we turn on the active forces (experimentally this can be done by providing the cell with ATP at $t = 0$, of which it was previously deprived). These forces will add an extra stochastic term to the generalised Langevin equation of the Rouse model, Eq. (5.52).

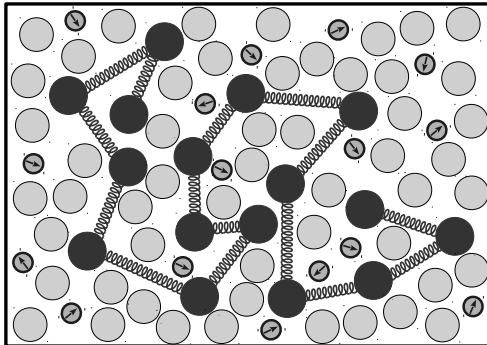


Figure 5.11: A cartoon of the Rouse model in an active and viscoelastic bath. The black spheres connected with springs are the Rouse chain. The large grey spheres represent the crowdedness of a viscoelastic bath (they are, for example, the macromolecules that are present in the cytosol). The small grey spheres depict (no physical representation) the active bath, their persistent motion is indicated by an arrow.

The equation of motion of the n^{th} bead in an active and viscoelastic bath thus becomes

$$\eta_{\alpha} c \mathcal{D}^{\alpha} \vec{R}_n(t) = -k \left(2\vec{R}_n(t) - \vec{R}_{n-1}(t) - \vec{R}_{n+1}(t) \right) + \vec{\xi}_{T,n}(t) + \vec{\xi}_{A,n}(t) H(t), \quad (5.99)$$

where $H(t)$ is the Heaviside function (see Eq. (4.3)). We still consider the thermal noise $\vec{\xi}_{T,n}$ to be Gaussian distributed with zero mean and a coloured correlation equal to Eq. (5.53). The characteristics of the active noise $\vec{\xi}_{A,n}$ were provided by Levine and MacKintosh [111]. They are discussed at length in Section 2.5. The active noise is also a Gaussian random variable with average zero and an exponential correlation that is uncorrelated between different beads

$$\langle \vec{\xi}_{A,n}(t) \cdot \vec{\xi}_{A,m}(t') \rangle = 3C \exp(-|t - t'|/\tau_A) \delta_{n,m}. \quad (5.100)$$

The strength of the active forces is thus measured by \sqrt{C} and their direction persists over a characteristic persistence time τ_A . This time-scale was found to be of the order of seconds and therefore much smaller than the cellular lifetime, thus $\tau_A \ll \tau_{R,\alpha}$. Both noise terms, thermal and active, in Eq. (5.99) are coloured. But only the thermal noise has a corresponding friction term, to which it is connected by the fluctuation-dissipation relation. The active noise does not have such a friction term and therefore lacks a fluctuation-dissipation relation. Because of this, these active forces will pull the system away from equilibrium. Figure 5.11 shows a schematic representation of our model for the Rouse chain in an active viscoelastic bath. It does not, however, reflect the real biological situation but rather gives an interpretation of Eq. (5.99). We see a Rouse chain surrounded by two different baths. One is depicted by the large grey spheres, it is the heat bath which is viscoelastic in nature. The second bath is represented by the small dark grey spheres, they show their persistent motion with an arrow. This is the active bath which has no dissipative property.

The addition of a stochastic term that is on average zero will not change the mean of the variable, therefore we still have $\langle \vec{R}_n(t) \rangle = 0$, as was the case in Section

5.2. Furthermore, if we would add the constant force, Eq. (5.72), of the previous section to our current model, the results of that section would not change. What will change is the mean-squared displacement we calculated in Section 5.2. The active stochastic term in Eq. (5.99) has no influence on the linearity of the generalised Langevin equation of the n^{th} bead. Therefore this equation can again be solved by applying the normal coordinates, Eq. (5.18). The generalised Langevin equation of the normal coordinates becomes

$$\eta_{\alpha} c \mathcal{D}^{\alpha} \vec{X}_p(t) = -\frac{k_p}{2N} \vec{X}_p(t) + \vec{\xi}_{T,p}(t) + \vec{\xi}_{A,p}(t), \quad (5.101)$$

with

$$\vec{\xi}_{A,p}(t) = \frac{1}{N} \sum_{n=0}^{N-1} \mathcal{C}_n^p \vec{\xi}_{A,n}(t), \quad (5.102)$$

the normal active noise. Since it is a linear combination of the natural active noises, it is Gaussian distributed with zero mean and a correlation of

$$\langle \vec{\xi}_{A,p}(t) \cdot \vec{\xi}_{A,q}(t') \rangle = \frac{3C}{2N} \exp(-|t-t'|/\tau_A) (1 + \delta_{p,0}) \delta_{p,q}, \quad (5.103)$$

where we used the orthogonal property of the transformation coefficients. The normal thermal noise $\vec{\xi}_{T,p}$ is given by Eq. (5.56). If we interchange $\vec{\xi}_{T,p}$ with $\vec{\xi}_{T,p} + \vec{\xi}_{A,p}$ in Eq. (5.57), we find the time evolution of the p^{th} mode, it reads

$$\begin{aligned} \vec{X}_p(t) &= \vec{X}_p(0) E_{\alpha,1} \left(-(t/\tau_{p,\alpha})^{\alpha} \right) \\ &+ \frac{1}{\eta_{\alpha}} \int_0^t d\tau \vec{\xi}_{T,p}(t-\tau) \tau^{\alpha-1} E_{\alpha,\alpha} \left(-(\tau/\tau_{p,\alpha})^{\alpha} \right) \\ &+ \frac{1}{\eta_{\alpha}} \int_0^t d\tau \vec{\xi}_{A,p}(t-\tau) \tau^{\alpha-1} E_{\alpha,\alpha} \left(-(\tau/\tau_{p,\alpha})^{\alpha} \right). \end{aligned} \quad (5.104)$$

From this expression it is clear that the mean value of the normal coordinates through time is zero. From Eq. (5.21) we find that the same is true for the natural coordinates, which we already argued would be the case. Using Eq. (5.104) we can obtain properties of the diffusion of the polymer and the fluctuation of its physical extension.

5.4.1 Anomalous diffusion

In Chapter 4, we found that a particle in an active viscoelastic bath can display all kinds of anomalous diffusion through time. Due to the active forces, it can even perform superdiffusion. Because of its higher complexity, a Rouse chain will, naturally, show more diversity in its diffusive profile than a single particle could. Therefore, we investigate the emerging anomalous diffusion of the centre of mass and of a single bead in a Rouse chain submerged in an active viscoelastic bath.

Centre of mass

Taking $p = 0$ in Eq. (5.104) will give us the equation of motion for the centre of mass

$$\vec{R}_{cm}(t) = \vec{R}_{cm}(0) + \frac{1}{\eta_{\alpha} \Gamma(\alpha)} \int_0^t d\tau \left(\vec{\xi}_{T,p}(t-\tau) + \vec{\xi}_{A,p}(t-\tau) \right) \tau^{\alpha-1}. \quad (5.105)$$

Squaring and averaging the second term will give us the mean-squared displacement of the centre of mass, $\Delta_{cm}^2(t) = \langle (\Delta R_{cm}(t))^2 \rangle$. Using Eq. (5.56) and Eq. (5.103) results in

$$\begin{aligned} \Delta_{cm}^2(t) &= \frac{3k_B T(2-\alpha)(1-\alpha)}{\gamma N G_\alpha^2} \int_0^t d\tau \int_0^t d\tau' \frac{\tau^{\alpha-1} \tau'^{\alpha-1}}{|\tau - \tau'|^\alpha} \\ &\quad + \frac{3C}{\gamma^2 N G_\alpha^2} \int_0^t d\tau \int_0^t d\tau' \exp(-|\tau - \tau'|/\tau_A) \tau^{\alpha-1} \tau'^{\alpha-1}, \end{aligned} \quad (5.106)$$

where we used the fact that the different noises are uncorrelated, implying that $\langle \vec{\xi}_{T,p}(t) \cdot \vec{\xi}_{A,q}(t') \rangle = 0$. The first term in this equation we already worked out, it is equal to the right-hand side of Eq. (5.61). The second term is added by the active forces and can not be fully solved into a closed form. It can be simplified in the same way as Eq. (4.9), using the difference of two incomplete gamma-functions (see Appendix A.2). The mean-squared displacement of the centre of mass then becomes

$$\Delta_{cm}^2(t) = \frac{6 D_\alpha^{cm}}{\Gamma(\alpha+1)} t^\alpha + \frac{6 \tau_A^{2\alpha} C}{\Gamma^2(\alpha) \eta_\alpha^2 N} \mathcal{A}_\alpha(t/\tau_A), \quad (5.107)$$

with $\mathcal{A}_\alpha(t)$ defined by Eq. (4.11). When $C = 0$ we clearly find the subdiffusion of the centre of mass in a non-active viscoelastic bath from Section 5.2. The second term in Eq. (5.107) is the active addition.

For very early times, $t \ll \tau_{N,\alpha}$, the non-active term in Eq. (5.107) will dominate, because $\mathcal{A}_\alpha(t \rightarrow 0)$ goes faster to zero. After this initial non-active-like subdiffusion the active forces will take effect, the resulting diffusion can be split up into two regimes. One before the persistence time and one after, to characterise these we need to approximate the active addition. These approximations were already done in Section 4.1, we can therefore readily apply them here.

For times smaller than the persistence time, $t \ll \tau_A$, the active addition becomes

$$\frac{3C}{\Gamma^2(\alpha+1) \eta_\alpha^2 N} t^{2\alpha}. \quad (5.108)$$

When $\alpha > 1/2$ we thus find that the centre of mass performs a superdiffusion for times shorter than the persistence time τ_A . Yet when α is smaller than one half, the motion remains subdiffusive. For $\alpha = 1$, we observe that the centre of mass displays a ballistic motion $\Delta_{cm}^2(t) \sim t^2$.

For times longer than the persistence time, $t \gg \tau_A$, the active addition behaves as

$$\frac{6\tau_A C}{(2\alpha-1)\Gamma^2(\alpha)\eta_\alpha^2 N} t^{2\alpha-1}. \quad (5.109)$$

This $t^{2\alpha-1}$ evolution is slower than the non-active diffusion that goes as t^α , so asymptotically in time the centre of mass will display the non-active subdiffusion i.e. the first term in Eq. (5.107). When $\alpha < 1/2$, the exponent of time is negative and therefore this regime dies out very fast, leading quickly to the non-active behaviour. This can be seen in Fig. 5.12 where we plot the mean-squared displacement for $\alpha = 0.4$ and different values of $\tau_A/\tau_{R,\alpha}$. When $\alpha > 1/2$ and $C\tau_A$ is large compared to $\gamma k_B T$, the behaviour of Eq. (5.109) will dominate over several orders of magnitude in time.

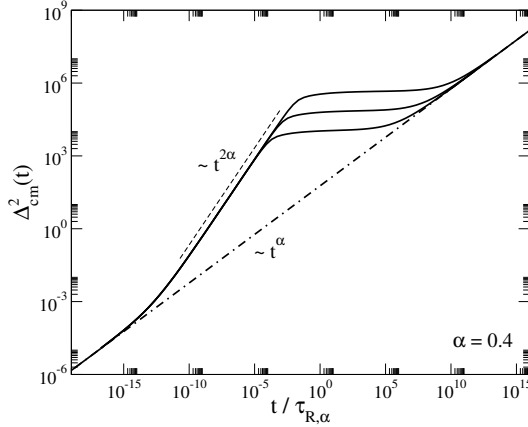


Figure 5.12: Log-log plot of the squared distance travelled by the centre of mass as a function of $t/\tau_{R,\alpha}$ for a Rouse chain ($N = 256$, $k = 3$) in a viscoelastic medium ($\alpha = 0.4$, $k_B T = \gamma = 1$) in the presence of active forces with $C = 10^2$ and $\tau_A/\tau_{R,\alpha} = 10^{-2}, 10^{-3}, 10^{-4}$ (full lines, top to bottom) compared to that without active forces (dashed-dotted line). Power-law behaviour is indicated with dashed lines.

The centre of mass will still show a subdiffusion as in the non-active case but with exponent $(2\alpha - 1)$, not α . If this time regime corresponds to the experimental one, not taking into account active forces could lead to a wrong estimate of α , and hence to a wrong characterisation of the rheological properties of the medium. Figure 5.13 shows this behaviour for $\alpha = 0.7$ and several values for $\tau_A/\tau_{R,\alpha}$. Results like that of Fig. 5.13 are under the assumption that our model is realistic for all t . When comparing with experimental data, one has to take into account that, as already discussed in Section 5.2, the model will break down on small and large time scales. Because the persistence time τ_A is much smaller than the lifetime of a cell (as discussed in Section 4.1), we expect that only the superdiffusive and $(2\alpha - 1)$ subdiffusive behaviour can be observed. In the viscous case, $\alpha = 1$, the centre of mass diffuses normally but with a diffusion constant that is enhanced by a factor $(1 + C\tau_A/\gamma k_B T)$. It will therefore never rejoin with the non-active diffusion. This can be seen in Fig. 5.14. The general sequence of diffusion regimes for the centre of mass is

$$\Delta_{cm}^2(t) = \frac{6 D_\alpha^{cm}}{\Gamma(\alpha + 1)} t^\alpha \xrightarrow{\tau_\downarrow} \frac{3C}{\Gamma^2(\alpha + 1)\eta_\alpha^2 N} t^{2\alpha} \xrightarrow{\tau_A} \frac{6\tau_A C}{(2\alpha - 1)\Gamma^2(\alpha)\eta_\alpha^2 N} t^{2\alpha - 1} \xrightarrow{\tau_\uparrow} \frac{6 D_\alpha^{cm}}{\Gamma(\alpha + 1)} t^\alpha. \quad (5.110)$$

Notice that the behaviour of the centre of mass is $3/N$ times that of the free particle from Section 4.1. This factor comes from the fact that we are here dealing with three dimensions and that there are, in fact, N particles inside the centre of mass.

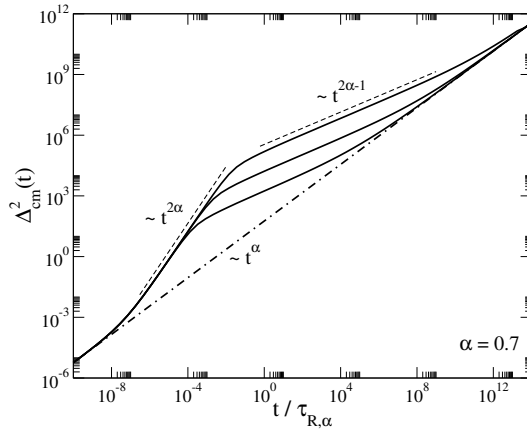


Figure 5.13: Log-log plot of the squared distance travelled by the centre of mass as a function of $t/\tau_{R,\alpha}$ for a Rouse chain ($N = 256$, $k = 3$) in a viscoelastic medium ($\alpha = 0.7$, $k_B T = \gamma = 1$) in the presence of active forces with $C = 10^2$ and $\tau_A/\tau_{R,\alpha} = 10^{-2}, 10^{-3}, 10^{-4}$ (full lines, top to bottom) compared to that without active forces (dashed-dotted line). Power-law behaviour is indicated with dashed lines.

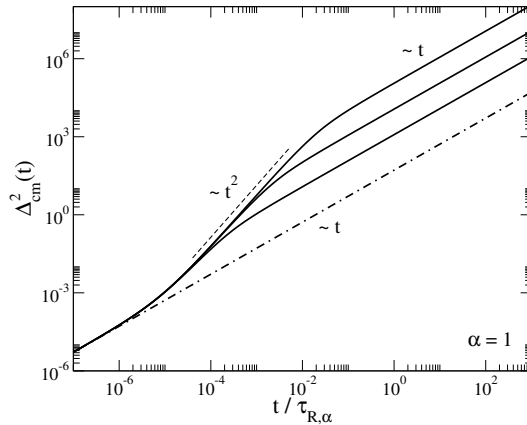


Figure 5.14: Log-log plot of the squared distance travelled by the centre of mass as a function of $t/\tau_{R,\alpha}$ for a Rouse chain ($N = 256$, $k = 3$) in a viscous medium ($\alpha = 1$, $k_B T = \gamma = 1$) in the presence of active forces with $C = 10^2$ and $\tau_A/\tau_{R,\alpha} = 10^{-2}, 10^{-3}, 10^{-4}$ (full lines, top to bottom) compared to that without active forces (dashed-dotted line). Power-law behaviour is indicated with dashed lines.

Single bead

Now we will turn to the motion of an individual monomer. From an experimental point of view, this quantity is the most interesting one, since it can be determined using fluorescence techniques. In order to find the mean-squared displacement of the n^{th} bead, we need to calculate Eq. (5.43) using the normal coordinates we derived in Eq. (5.104). The first term in Eq. (5.43) is precisely the mean-squared displacement of the centre of mass we just calculated. The summation in Eq. (5.43) will be a bit more difficult to calculate. First notice that the argument of the summation, $\langle \Delta \vec{X}_p^2(t) \rangle$, can be written as the three terms in Eq. (5.44). To find an expression for these, we should use Eq. (5.104). Taking into account that the initial value of the normal coordinates, the thermal noise and the active noise do not correlate with each other leads to the following expression

$$\begin{aligned}
\langle \vec{X}_p(t) \cdot \vec{X}_p(t') \rangle &= \langle \vec{X}_p^2(0) \rangle E_{\alpha,1} \left(- (t/\tau_{p,\alpha})^\alpha \right) E_{\alpha,1} \left(- (t'/\tau_{p,\alpha})^\alpha \right) \\
&+ \frac{1}{\eta_\alpha^2} \int_0^t d\tau \int_0^{t'} d\tau' \langle \vec{\xi}_{T,p}(t-\tau) \cdot \vec{\xi}_{T,p}(t'-\tau') \rangle \tau^{\alpha-1} \tau'^{\alpha-1} \\
&\quad \times E_{\alpha,\alpha} \left(- (\tau/\tau_{p,\alpha})^\alpha \right) E_{\alpha,\alpha} \left(- (\tau'/\tau_{p,\alpha})^\alpha \right) \\
&+ \frac{1}{\eta_\alpha^2} \int_0^t d\tau \int_0^{t'} d\tau' \langle \vec{\xi}_{A,p}(t-\tau) \cdot \vec{\xi}_{A,p}(t'-\tau') \rangle \tau^{\alpha-1} \tau'^{\alpha-1} \\
&\quad \times E_{\alpha,\alpha} \left(- (\tau/\tau_{p,\alpha})^\alpha \right) E_{\alpha,\alpha} \left(- (\tau'/\tau_{p,\alpha})^\alpha \right). \quad (5.111)
\end{aligned}$$

The first two terms were already calculated in Section 5.2 where the Rouse chain is equilibrated in the viscoelastic bath. Together they become Eq. (5.64). For the third term we fill in the correlation of the normal active noise Eq. (5.103). If we then use the $A_\alpha(t, t'; \tau_1, \tau_2)$ from Section 4.2 (see Eq. (4.28)) and the fact that different modes are uncorrelated, the correlation between the normal coordinates in an active viscoelastic bath becomes

$$\langle \vec{X}_p(t) \cdot \vec{X}_q(t') \rangle = \left[\frac{3k_B T}{k_p} E_{\alpha,1} \left(- \left(\frac{|t-t'|}{\tau_{p,\alpha}} \right)^\alpha \right) + \frac{6CN}{k_p^2} A_\alpha(t, t'; \tau_{p,\alpha}, \tau_A) \right] \delta_{p,q}. \quad (5.112)$$

Using this to complete Eq. (5.44) gives

$$\frac{6k_B T}{k_p} \left[1 - E_{\alpha,1} \left(- (t/\tau_{p,\alpha})^\alpha \right) \right] + \frac{6CN}{k_p^2} A_\alpha(t; \tau_{p,\alpha}, \tau_A), \quad (5.113)$$

where $A_\alpha(t; \cdot, \cdot) = A_\alpha(t, t; \cdot, \cdot)$. Then using this result together with Eq. (5.107), plugging it into Eq. (5.43) gives the mean-squared displacement of the n^{th} bead in an active viscoelastic bath.

$$\begin{aligned}
\Delta_n^2(t) &= \frac{6 D_\alpha^{cm}}{\Gamma(\alpha+1)} t^\alpha + \frac{12k_B T}{\gamma N} \sum_{p=1}^{N-1} C_n^{p^2} \tau_p \left[1 - E_{\alpha,1} \left(- (t/\tau_{p,\alpha})^\alpha \right) \right] \\
&+ \frac{6 \tau_A^{2\alpha} C}{\Gamma^2(\alpha) \eta_\alpha^2 N} \mathcal{A}_\alpha(t/\tau_A) + \frac{6C}{\gamma^2 N} \sum_{p=1}^{N-1} C_n^{p^2} \tau_p^2 A_\alpha(t; \tau_{p,\alpha}, \tau_A). \quad (5.114)
\end{aligned}$$

The first line of this expression represents the dynamics of a thermalised Rouse chain in a viscoelastic bath, which we already found in Section 5.2 (see Eq. (5.65)). The second line is the active addition that pulls the polymer out of equilibrium. The first and the third terms originate from the motion of the centre of mass, while the second and fourth terms tracks the internal vibrations of the chain. We now turn our attention to the middle bead. As we said before, the results we find for this bead are representable for the other beads. To convert Eq. (5.114) to the expression that describes the middle bead we need to drop the transformation coefficients and let the summations go only over the even modes

$$\begin{aligned} \Delta_m^2(t) &= \frac{6D_\alpha^{cm}}{\Gamma(\alpha+1)} t^\alpha + \frac{12k_B T}{\gamma N} \sum_{p=2, \text{even}}^{N-1} \tau_p \left[1 - E_{\alpha,1} \left(- (t/\tau_{p,\alpha})^\alpha \right) \right] \\ &+ \frac{6\tau_A^{2\alpha} C}{\Gamma^2(\alpha)\eta_\alpha^2 N} \mathcal{A}_\alpha(t/\tau_A) + \frac{6C}{\gamma^2 N} \sum_{p=2, \text{even}}^{N-1} \tau_p^2 A_\alpha(t; \tau_{p,\alpha}, \tau_A). \end{aligned} \quad (5.115)$$

The behaviour of most of these terms was already discussed in previous sections, only the last term we did not yet explore. For times shorter than the persistence time, $t \ll \tau_A$, we have that the exponential in $A_\alpha(t; \tau_{p,\alpha}, \tau_A)$ is approximately equal to one. When we remove it from the expression the integrals in $A_\alpha(t; \tau_{p,\alpha}, \tau_A)$ decouple and are identical. Therefore this term reduces to

$$\frac{6C}{\gamma^2 N} \sum_{p=2, \text{even}}^{N-1} \tau_p^2 \left[\int_0^{t/\tau_{p,\alpha}} dx x^{\alpha-1} E_{\alpha,\alpha}(-x^\alpha) \right]^2. \quad (5.116)$$

Using property (A.9) to work out the integral gives the following approximation for times smaller than the persistence time

$$\frac{6C}{\eta_\alpha^2 N} t^{2\alpha} \sum_{p=2, \text{even}}^{N-1} E_{\alpha,\alpha+1}^2 \left(- (t/\tau_{p,\alpha})^\alpha \right). \quad (5.117)$$

For very early times, $t \approx \tau_{N,\alpha}$, we can approximate the Mittag-Leffler function as $1/\Gamma(\alpha+1)$. The sum then contributes a factor $N/2$, leading to the following power law

$$\frac{3C}{\Gamma^2(\alpha+1)\eta_\alpha^2} t^{2\alpha}. \quad (5.118)$$

For somewhat longer times (but still smaller than τ_A) and N very large, we can approximate the summation in Eq. (5.117) by an integral since its argument is a smooth continuous function. We take $1/N \rightarrow dx$ and $p/N \rightarrow x$. We should also add a factor one half to account for the fact that we only sum over the even modes. The integration becomes

$$\frac{3C}{\eta_\alpha^2} t^{2\alpha} \int_0^\infty dx E_{\alpha,\alpha+1}^2 \left(- \frac{k\pi^2 t^\alpha}{\eta_\alpha} x^2 \right) = \frac{3CI'_\alpha}{\sqrt{k\pi^2\eta_\alpha^3}} t^{3\alpha/2}, \quad (5.119)$$

with $I'_\alpha = \int_0^\infty dx E_{\alpha,\alpha+1}^2(-x^2)$ that only depends on α . For long times longer than the persistence time the term will go to a constant, which we will derive in the next

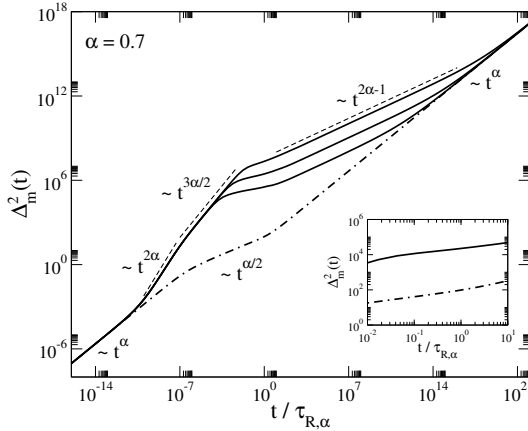


Figure 5.15: Log-log plot of the squared distance travelled by the middle bead as a function of $t/\tau_{R,\alpha}$ for a Rouse chain ($N = 256$, $k = 3$) in a viscoelastic medium ($\alpha = 0.7$, $k_B T = \gamma = 1$) in the presence of active forces with $C = 10^4$ and $\tau_A/\tau_{R,\alpha} = 10^{-2}, 10^{-3}, 10^{-4}$ (full lines, top to bottom) compared to that without active forces (dashed-dotted line). Power-law behaviour is indicated with dashed lines. *Inset:* The mean-squared displacement of the middle bead in a smaller time window, in the absence (dashed-dotted line) and presence (full line) of active forces. All parameters are the same as in the main graph, apart from $C = 1$ and $\tau_A/\tau_{R,\alpha} = 10^{-2}$.

section. Now that we know all the power law behaviours of the terms in Eq. (5.115), we can evaluate the full range of regimes the motion of the middle bead displays.

Figure 5.15 shows the mean-squared displacement of the middle bead in an active viscoelastic bath with $\alpha = 0.7$ and various values for the persistence time τ_A . First notice that we also plotted the non-active mean-squared displacement given by Eq. (5.65) (or the first two terms of Eq. (5.115)) as the dashed-dotted line. It is exactly the same curve as in Fig. 5.4 and has three regimes of subdiffusion, given by Eq. (5.67). When the active forces are added we see in Fig. 5.15 that a whole range of power law regimes emerge from it. After an initial regime where the active forces did not yet take effect, we find that two 2α regimes compete with each other. Namely Eq. (5.108) from the motion of the centre of mass and Eq. (5.118) from the internal vibrations. The latter will dominate because its prefactor is N times larger than the former. The bead will thus perform a superdiffusion when $\alpha > 1/2$. After this regime, when $t \approx \tau_{N,\alpha}$, we find that the $3\alpha/2$ power law of Eq. (5.119) takes over, if α isn't larger than $2/3$ the system will fall back to subdiffusion, otherwise it will maintain a superdiffusive motion. This regime ends around $t \approx \tau_A$, thereafter the mean-squared displacement tends to become constant. Very recently superdiffusive motion of chromosomal loci has indeed been observed [19]. It is not clear whether these rapid chromosomal movements (as [19] calls it) are due to active processes or to stress relaxation. Our results, however, quantify better the response to active forces and could therefore help in discriminating the real origin of the observed motion.

When time grows larger than the Rouse time $\tau_{R,\alpha}$, the middle bead will first follow

the $(2\alpha - 1)$ subdiffusion of the centre of mass. This regime will persist over many orders of magnitude in time as Fig. 5.15 shows. But eventually the centre of mass's α subdiffusion takes over. However, most of the $(2\alpha - 1)$ regime and the crossover to the α exponent may not be observable for chromosomal loci since the time window at which they appear lies well beyond the lifetime of a cell. The full sequence of the mean-squared displacement of the middle bead in an active viscoelastic bath reads

$$\begin{aligned} \Delta_m^2(t) &= \frac{6D_\alpha}{\Gamma(\alpha + 1)} t^\alpha \xrightarrow{\tau_\downarrow} \frac{3C}{\Gamma^2(\alpha + 1)\eta_\alpha^2} t^{2\alpha} \xrightarrow{\tau_{N,\alpha}} \frac{3CI'_\alpha}{\sqrt{k\pi^2\eta_\alpha^3}} t^{3\alpha/2} \xrightarrow{\tau_A} \text{constant} \\ &\xrightarrow{\tau_{R,\alpha}} \frac{6\tau_A C}{(2\alpha - 1)\Gamma^2(\alpha)\eta_\alpha^2 N} t^{2\alpha-1} \xrightarrow{\tau_\uparrow} \frac{6D_\alpha^{cm}}{\Gamma(\alpha + 1)} t^\alpha. \end{aligned} \quad (5.120)$$

For certain values of C and τ_A , there is a time regime (see inset of Fig. 5.15) where, on a log-log scale, the lines of $\Delta_m^2(t)$ in the presence and absence of active forces run parallel. This scenario resembles, at least qualitatively, the experimental one, where after ATP synthesis with sodium azide and 2-deoxyglucose, the exponent of the loci's subdiffusion hardly changed but the diffusion coefficient decreased [112].

5.4.2 Swelling of the polymer

Here we will discuss how the overall shape of the polymer reacts to the active component in a viscoelastic bath. Because the active forces do not have a preferred direction, we do not expect that the rotational symmetry of the polymer will change. What we can expect is that the physical extend of the polymer will be influenced by the active forces. A measure for this is the end-to-end vector \vec{P} . We already calculated in Section 5.1 that the average squared length of this vector in equilibrium is equal to b^2N . Here we will denote this average squared length of the end-to-end vector as $\mathcal{P}^2(N, t) = \langle \vec{P}^2(t) \rangle$, where we explicitly include the N dependency which will be important later. For very long polymers we know that the end-to-end vector is defined by Eq. (5.25) and from Eq. (5.50) we find that

$$\mathcal{P}^2(N, t) = 16 \sum_{p,q=1, \text{odd}}^{N-1} \langle \vec{X}_p(t) \cdot \vec{X}_q(t) \rangle. \quad (5.121)$$

Then inserting the correlation of the normal coordinates in an active viscoelastic bath, Eq. (5.112), leads to

$$\mathcal{P}^2(N, t) = 16 \sum_{p=1, \text{odd}}^{N-1} \left[\frac{3k_B T}{k_p} + \frac{6CN}{k_p^2} A_\alpha(t; \tau_{p,\alpha}, \tau_A) \right]. \quad (5.122)$$

The first term is exactly the one of the equilibrium case, Eq. (5.51), it is evaluated in the same way, yielding b^2N . The second term is the active addition, we find

$$\mathcal{P}^2(N, t) = b^2N + 96CN \sum_{p=1, \text{odd}}^{N-1} k_p^{-2} A_\alpha(t; \tau_{p,\alpha}, \tau_A). \quad (5.123)$$

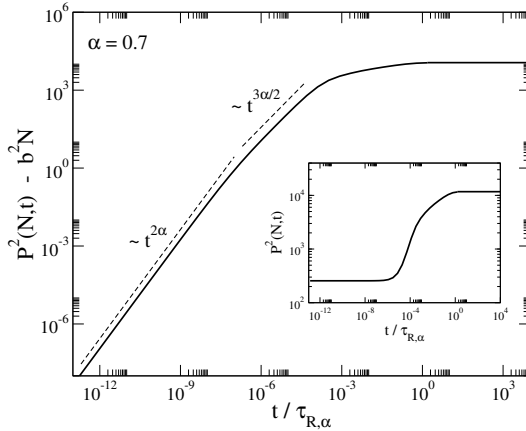


Figure 5.16: Log-log plot of the active addition to the average squared end-to-end vector as a function of $t/\tau_{R,\alpha}$ for a Rouse chain ($N = 256$, $k = 3$) in a viscoelastic medium ($\alpha = 0.7$, $k_B T = \gamma = 1$) in the presence of active forces with $C = 10^4$ and $\tau_A/\tau_{R,\alpha} = 10^{-4}$. Power-law behaviour is indicated with dashed lines. *Inset*: This shows the same data as the main graph plus b^2N , so it is the true average squared end-to-end vector that is shown.

Investigating the definition of $A_\alpha(t; \tau_{p,\alpha}, \tau_A)$ will quickly reveal that it is strictly positive and increases with time. This implies that the active addition raises the value of the average squared end-to-end vector through time. The interpretation of this is that the length of the springs fluctuates more since they acquire extra energy from the active forces, which will make the polymer swell from its equilibrium configuration. As we will soon see, this swelling is characterised by the nature of the viscoelastic bath, i.e. the value of α . This is quite interesting since the viscoelasticity does not have influence on the equilibrium shape of the polymer while it does on the swelling due to active forces, therefore this swelling becomes a measure for the value of α .

In Fig. 5.16 we plotted the active addition to the average length of the end-to-end vector (i.e. the second term in Eq. (5.123)) as a function of time for $\alpha = 0.7$. It is clear that this quantity shows two power law regimes, first with exponent 2α and second with $3\alpha/2$. These can be understood by the approximations made in the previous section. Since the second term in Eq. (5.123) and the fourth term in Eq. (5.115) are very similar, we can reuse the approximations that were done on this fourth term. In Fig. 5.16 we see that for times longer than the Rouse time, the active addition becomes constant. Or in other words, the swelling reaches a nonequilibrium steady state (nss) value: $\mathcal{P}_{nss}^2(N) = \mathcal{P}^2(N, t \rightarrow \infty)$. The sequence of the active addition to the average length of the end-to-end vector through time is

$$\mathcal{P}^2(N, t) - b^2N = \frac{12C}{\Gamma^2(\alpha + 1)\eta_\alpha^2} t^{2\alpha} \xrightarrow{\tau_{N,\alpha}} \frac{12CI'_\alpha}{\sqrt{k\pi^2\eta_\alpha^3}} t^{3\alpha/2} \xrightarrow{\tau_{R,\alpha}} nss. \quad (5.124)$$

The inset of Fig. 5.16 shows how the original equilibrium average squared length at $t = 0$ increases and saturates to the nonequilibrium steady state. This nonequilibrium

steady state has an interesting N dependence. Notice that $A_\alpha(t \rightarrow \infty; \tau_{p,\alpha}, \tau_A)$ only depends on the ratio $\tau_{p,\alpha}/\tau_A$, for a constant value of α . The active addition in full for long times is

$$\sum_{p=1, \text{odd}}^{N-1} \frac{96 CN}{k_p^2} \int_0^\infty dx \int_0^\infty dy e^{-|x-y|/\epsilon} x^{\alpha-1} y^{\alpha-1} E_{\alpha,\alpha}(-x^\alpha) E_{\alpha,\alpha}(-y^\alpha), \quad (5.125)$$

where we took $\epsilon = \tau_A/\tau_{p,\alpha}$. This epsilon goes to zero when $N \rightarrow \infty$ (this only holds for small p , but large p 's are suppressed by k_p^{-2}). In this limit we can use a well known representation of the Dirac Delta function,

$$\delta(x) = \lim_{\epsilon \rightarrow 0} \frac{1}{2\epsilon} \exp(-|x|/\epsilon), \quad (5.126)$$

to rewrite the active addition into the following form

$$\frac{12 C \tau_A N^{3-2/\alpha}}{\eta_\alpha^{1/\alpha} (k \pi^2)^{2-1/\alpha}} h(\alpha) \sum_{p=1, \text{odd}}^{N-1} p^{2/\alpha-4}, \quad (5.127)$$

where $h(\alpha)$ is twice the double integral in Eq. (5.125) with the exponential replaced by $\delta(x-y)$. This function was already introduced and discussed in Section 4.2. The summation in Eq. (5.127) diverges when $\alpha < 2/3$ and converges when $\alpha > 2/3$. In the latter case it can be written more neatly

$$\sum_{p=1, \text{odd}}^\infty p^{2/\alpha-4} = \sum_{p=0}^\infty (2p+1)^{2/\alpha-4} = 2^{2/\alpha-4} \zeta(4 - \frac{2}{\alpha}, \frac{1}{2}), \quad (5.128)$$

where $\zeta(\cdot, \cdot)$ is the Hurwitz zeta function (see Appendix A.4). It has a finite value for $\alpha > 2/3$, independent of N . Therefore the active addition, Eq. (5.127), will go as $N^{3-2/\alpha}$ for $\alpha > 2/3$. When $\alpha < 2/3$, the summation in Eq. (5.127) does not go to a definite value for increasing N but scales with it as $N^{2/\alpha-3}$. A numeric verification of this behaviour is shown in Fig. 5.17. The $N^{3-2/\alpha}$ term in Eq. (5.127) will compensate for this N dependence of the sum, leaving the active addition independent of N for $\alpha < 2/3$. For large N , the swelling due to the active forces will therefore be neglectable compared to the equilibrium shape (i.e. $b^2 N$). For $\alpha < 2/3$, we thus state that no considerable swelling occurs.

The nonequilibrium steady state value of the average squared length of the end-to-end vector for large N thus shows two regimes

$$\mathcal{P}_{nss}^2(N) = b^2 N \quad \text{if } \alpha < 2/3, \quad (5.129)$$

$$\mathcal{P}_{nss}^2(N) = b^2 N + \frac{12 C \tau_A h(\alpha) \zeta(4 - \frac{2}{\alpha}, \frac{1}{2})}{\eta_\alpha^{1/\alpha} (4k \pi^2)^{2-1/\alpha}} N^{3-2/\alpha} \quad \text{if } \alpha > 2/3. \quad (5.130)$$

In a viscous medium, $\alpha = 1$, we have that $h(1) = 1$ and $\zeta(2, 1/2) = \pi^2/2$. We thus find that when the swelling saturates, it is proportional to N

$$\mathcal{P}_{nss}^2(N) = \left(1 + \frac{C \tau_A}{\gamma k_B T}\right) b^2 N. \quad (5.131)$$

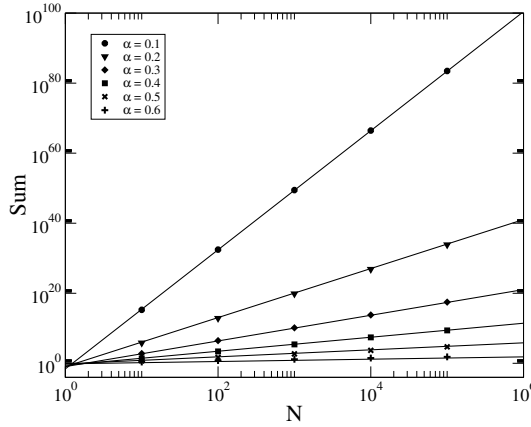


Figure 5.17: Log-log plot of the sum $\sum_{p=1, \text{odd}}^{N-1} p^{2/\alpha-4}$ as a function of N for different values of α . The symbols present a numeric evaluation of the summation and the full lines are lines that go as $N^{2/\alpha-3}$.

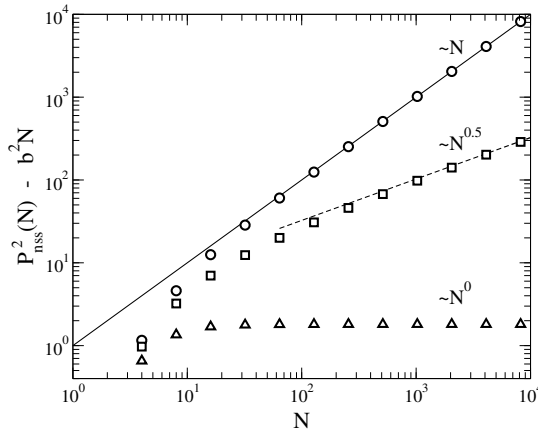


Figure 5.18: Log-log plot of the active addition in the nonequilibrium steady state as a function of N for $\alpha = 1$ (circles), 0.8 (squares) and 0.4 (triangles). Other parameters are $k_B T = \gamma = 1$, $k = 3$, $C = \tau_A = 1$. The symbols are the result of a numerical evaluation of Eq. (5.123) for $t \rightarrow \infty$. The full line is a plot of Eq. (5.131) minus b^2N and the dashed line of Eq. (5.130) minus b^2N .

This result is exactly what could be expected from an extension [17] of the equipartition theorem to harmonic oscillators in an active viscous medium (see Section 4.2).

Figure 5.18 shows the numeric solution of the second term in Eq. (5.123) as a function of N for $\alpha = 1, 0.8$ and 0.4 . Also shown are expressions (5.130) and (5.131) that show excellent agreement for large N . From this figure it is clear that when $\alpha < 2/3$, the active addition does not increase with increasing N . So larger polymers will not swell more than shorter ones, and even not much more than a thermalised polymer in a non-active bath. When $\alpha > 2/3$, we see that indeed the polymer swells more for larger values of α while the swelling is also dependent on the length of the polymer. This threshold at $\alpha = 2/3$ is an interesting one in the context of storing large polymers and influencing their effectiveness. The small nucleus of a cell has to contain large chromosomes, so it is advised that its viscoelasticity is lower than $2/3$. This could be experimentally tested. On the other hand, the function of a polymer can depend greatly on its expansion. The cell could therefore adjust the value of α to increase or decrease the swelling of its polymers when α is larger than $2/3$. All this is of course only possible when active forces are present, in a non-active environment all polymers of equal length swell the same amount.

5.5 Toward a more realistic model

The previous sections all used the pure Rouse model which portrays the polymer as an ideal chain, where the only interactions are with neighbouring beads. The simplicity of this model allowed us to perform an analytic treatment. But the Rouse model is quite far from realistic. If we would like to investigate how a real polymer behaves under the circumstances of the previous sections, we should introduce more realistic – though more complicated – features. We will not, however, change the overall idea of the Rouse model. There are models that describe the very intricate structure of a polymer down to individual atomic interactions [113–115], this is too specific for our study. The general make-up of the Rouse model, being connected beads in a heat-bath, will not be altered. The new features will come in the form of potentials added to the existing equation of motion, Eq. (5.52). These potentials can be subdivided into short or long range interactions, where short range means between neighbouring or almost-neighbouring beads and long range between beads that are well separated along the chain. Note there that the long range interactions still work physically over short distances, but they are called long range because they come into play when distant parts of the chain physically meet. This induces long range correlations inside the chain, hence the name. These monomer-monomer interactions should swell the (thermalised) polymer at high temperatures and cause the polymer to collapse at low temperatures (below the theta temperature) [116]. Another extension to the Rouse model that we should mention here, although we will not use it, is the Zimm model [117]. This model includes hydrodynamic interactions and including these would be a natural extension to our work. More information on this can be found in [7].

When we introduce new potentials to the Rouse chain, we depart from the ideal chain description and can call it a real chain (although this is still an overstatement). The downside of this realism is that we can no longer find analytical exact solutions to interesting (dynamical) quantities. We will have to fall back to approximate scaling

arguments and/or simulations. Yet comparing these with the exact results of the ideal chain can give important insights into the behaviour and inner workings of the real chain. The results in this section remain, at the time of writing, unpublished.

5.5.1 Potentials

In order to modify the original generalised Rouse model we write Eq. (5.52) with the total interaction potential U^{tot} between the different beads unspecified

$$\eta_{\alpha} c \mathcal{D}^{\alpha} \vec{R}_n(t) = -\vec{\nabla} U^{tot}(\{\vec{R}_n\}) + \vec{\xi}_{T,n}(t), \quad (5.132)$$

later we can include several potentials in U^{tot} to made our chain more realistic. If we want to regain the original Rouse model we choose Eqs. (5.12)-(5.14) for U^{tot} . Now we will discuss the four potentials we will use, three of them are short range interactions and one is long range.

Harmonic springs

The Rouse model uses harmonic (Hookean) springs with a resting length equal to zero. But this need not be the case, we can also assume a non-zero resting length. Neighbouring beads are then, on average, separated. The potential to achieve this is

$$U_n^{harm} = \frac{k}{2} (|\vec{r}_n| - a)^2, \quad (5.133)$$

with $\vec{r}_n = \vec{R}_n - \vec{R}_{n-1}$. The strength of the springs is characterised by k and their resting length by a . If k is chosen very large and $a \neq 0$, the bonds can be seen as rigid rods. We take

$$U^{harm}(\{\vec{R}_n\}) = \sum_{n=1}^{N-1} U_n^{harm}. \quad (5.134)$$

When $a = 0$ and $U^{tot} = U^{harm}$ we arrive back at the Rouse model. The harmonic spring is obviously a short range interaction.

FENE springs

The harmonic springs in the Rouse model can be infinitely extended, this is a rather unphysical property. The covalent bonds that hold a real polymer together give it a finite extension, therefore we will introduce new springs that reflect this property. The *finite extensible nonlinear elastic* (FENE) springs, introduced by K. Kremer *et al.* [118], are defined by the following potential, where again $\vec{r}_n = \vec{R}_n - \vec{R}_{n-1}$

$$U_n^{fene} = -\frac{kR_0^2}{2} \ln \left[1 - \left(\frac{\vec{r}_n}{R_0} \right)^2 \right], \quad (5.135)$$

when $|\vec{r}_n| \leq R_0$ and $U_n^{fene} = 0$, when $|\vec{r}_n| > R_0$. Here we have that k is the strength of the springs and R_0 their maximum extension. When we do a Taylor expansion on Eq. (5.135) for $|\vec{r}_n|/R_0 \ll 1$, we find that $U_n^{fene} = U_n^{harm}$ with $a = 0$. So for

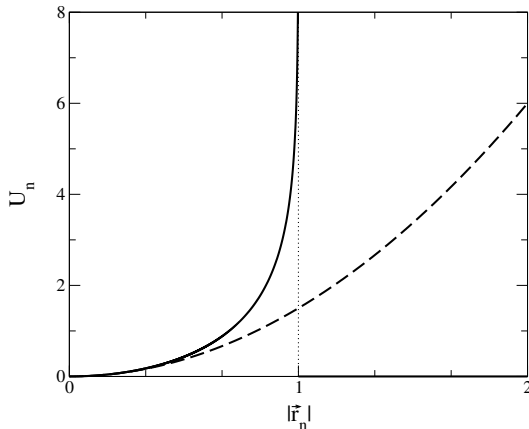


Figure 5.19: Plot of the harmonic spring potential U_n^{harm} (dashed line) and the FENE spring potential U_n^{fene} (full line) as a function of spring extension $|\vec{r}_n| = |\vec{R}_n - \vec{R}_{n-1}|$. Given by Eq. (5.133) and Eq. (5.135) respectively. The maximum extension of the FENE spring is indicated by a dotted line. We used $a = 0$, $k = 3$ and $R_0 = 1$.

small spring excitations, they should behave like the ordinary harmonic springs of the Rouse model. Yet when FENE springs absorb a lot of energy, they can reach their maximum extension whereas harmonic springs can just extend infinitely. Figure 5.19 shows this behaviour. We take

$$U^{fene}(\{\vec{R}_n\}) = \sum_{n=1}^{N-1} U_n^{fene}. \quad (5.136)$$

This interaction has clearly a short range.

Lennard-Jones potential

The original Rouse model describes a phantom chain because all beads can pass through each other without any energy penalty. To remedy this we can introduce an interaction between all beads, not just neighbouring beads. A standard potential that fulfils this task is the Lennard-Jones potential which approximates the interaction between a pair of neutral atoms or molecules. It combines the Pauli repulsion, which is a quantum mechanical effect between identical particles, and the attractive van der Waals forces, which are the residual attractive (or repulsive) forces between molecules that do not originate from a covalent bond or electrostatic interaction between ions. As the distance \vec{r} between two molecules increases, the repulsive forces will decay as $1/|\vec{r}|^{12}$ while the attractive forces will decay as $1/|\vec{r}|^6$. The full Lennard-Jones expression between the n^{th} and m^{th} bead is

$$U_{nm}^{LJ} = 4\epsilon \left[\left(\frac{\sigma}{|\vec{r}_{nm}|} \right)^{12} - \left(\frac{\sigma}{|\vec{r}_{nm}|} \right)^6 \right], \quad (5.137)$$

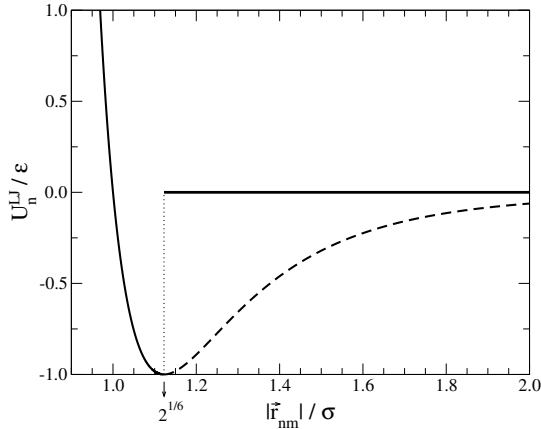


Figure 5.20: Plot of the Lennard-Jones potential U_n^{LJ} (dashed line) and the purely repulsive Lennard-Jones potential (full line) as a function of the distance between beads $|\vec{r}_{nm}| = |\vec{R}_n - \vec{R}_m|$. Given by Eq. (5.137).

with $\vec{r}_{nm} = \vec{R}_n - \vec{R}_m$ the vector from bead n to bead m . We have that ϵ is the strength of the potential and σ characterises its range. While the attractive term has a clear physical origin, the repulsive term has not. It is used due to its good approximation of the Pauli repulsion and because of its computational pleasing form (since it is the square of the sixth power of the attractive term). The Lennard-Jones potential gives each bead a certain volume that is inaccessible to the other beads, this volume is proportional to σ and inversely proportional to temperature. Often, the Lennard-Jones is reduced to its purely repulsive form. Then it satisfies Eq. (5.137) when $|\vec{r}_{nm}| \leq r_{min}$ and it is equal to zero when $|\vec{r}_{nm}| > r_{min}$, where $r_{min} = 2^{1/6}\sigma$ is the location of the minimum of the potential, $U_n^{LJ}(r_{min}) = -\epsilon$. The purely repulsive Lennard-Jones potential is used to reduce the computation time because the potential will only influence beads that are close by. Also when temperatures are high, the attractive term will be overshadowed by the kinetic motion, leaving it irrelevant. The Lennard-Jones potential and its purely repulsive alternative are shown in Fig. (5.20). We take

$$U^{LJ}(\{\vec{R}_n\}) = \sum_{n=0}^{N-1} \sum_{m>n}^{N-1} U_{nm}^{LJ}. \quad (5.138)$$

Notice that the second summation avoids counting each pair twice and also excludes a possible self-interaction. Because any bead can interact with any other bead, no matter how far apart they are in the chain, this interaction is obviously long range.

Bending rigidity

As was mentioned before, the Rouse model is an example of a completely flexible chain, meaning that the orientation of the springs is totally uncorrelated. Yet real polymers have a stiffness to them, on small length scales they maintain their orientation. Some

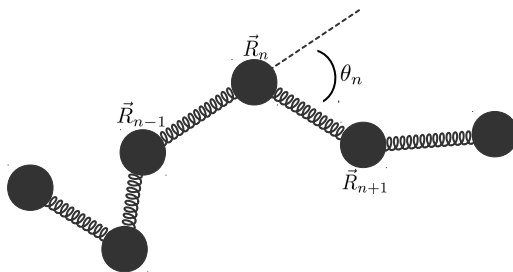


Figure 5.21: Schematic representation of the bond angle $\theta_n = \cos^{-1}(\hat{r}_n \cdot \hat{r}_{n+1})$.

polymers, such as microtubules, even resist bending on very long length scales, making them quite straight and rigid. If we define the following unit vector $\hat{r}_n = \vec{r}_n/|\vec{r}_n|$, then the potential that gives rise to bending rigidity is

$$U_n^{bend} = -\kappa(\hat{r}_n \cdot \hat{r}_{n+1}) = -\kappa \cos(\theta_n), \quad (5.139)$$

where κ is the strength of the potential and θ_n the angle between bond \vec{r}_n and bond \vec{r}_{n+1} . Figure 5.21 clarifies how θ_n is defined. If κ is large, the chain will be very stiff and therefore almost straight. Subsequently the angles between bonds will be small, therefore the potential is often approximated by $U_n^{bend} \approx \kappa \theta_n^2/2$ when κ is large. We take

$$U^{bend}(\{\vec{R}_n\}) = \sum_{n=1}^{N-2} U_n^{bend}. \quad (5.140)$$

Due to the bending rigidity potential a bead is influenced by its two nearest neighbours on both sides, it is therefore a short range interaction.

5.5.2 Dragging a real chain

Here we will consider the problem of Section 5.3 – where we applied a constant force on the first bead – but with a more realistic chain. We will replace the harmonic springs with FENE springs and add self-avoidance through the Lennard-Jones potential. The motion of the beads will be governed by

$$\eta_{\alpha} c \mathcal{D}^{\alpha} \vec{R}_n(t) = -\vec{\nabla} U^{tot}(\{\vec{R}_n\}) + \vec{\xi}_{T,n}(t) + \vec{f}_n(t), \quad (5.141)$$

with

$$U^{tot} = U^{fene} + U^{LJ}. \quad (5.142)$$

Two important properties of this real chain need to be addressed. First, due to the FENE springs, the chain has a maximum length. This is obviously equal to

$L_M = (N - 1)R_0$. Second, because it is a self-avoiding chain, the volume a bead occupies is not accessible to the rest of the chain causing excluded volume effects to arise that swell the polymer. The end-to-end vector \vec{P} , Eq. (5.23), is the quantity we use to determine the physical extend of the polymer. For a phantom chain we found, Eq. (5.51), that in equilibrium (irrespective of the value of α) we have $\mathcal{P}^2 = \langle \vec{P}^2 \rangle = b^2N$. But since a self-avoiding chain should swell, this relation can not hold for such a chain. More generally we state

$$\mathcal{P}^2 \simeq b^2N^{2\nu}, \quad (5.143)$$

with ν the Flory exponent that characterises the fractality of the equilibrium polymer coil. For a phantom chain (or random walk) in any dimension we have $\nu = 1/2$. For a self-avoiding chain in a good solvent we have $\nu \simeq 3/(d+2)$, where d is the dimension. So since we work in three dimensions, our chain has $\nu \approx 3/5$ (numerical analysis suggests a more accurate value: $\nu = 0.588\dots$).

The quantity we will investigate is the average thermalised length (the average length is defined by Eq. (5.77)) due to the constant force f . In other words, we study $L^* = L(t \rightarrow \infty)$. Because the viscoelasticity of the solvent, or in other words the value of α , does not influence equilibrated quantities we will take $\alpha = 1$ in (5.141). This will make the numeric calculations much easier. We solved Eq. (5.141) using a standard technique for numerically integrating an ordinary Langevin equation (see [69] for more details). To determine if the simulation performed properly we simulated the length as a function of time for the original Rouse chain, so $U^{tot} = U^{harm}$ with $a = 0$. The result should conform with the exact solution Eq. (5.78) with $\alpha = 1$. Of course, this output will be different if $\alpha \neq 1$ but we did not execute such a simulation. It is clear from Fig. 5.22 that the simulation performs very well, since the simulated data lies perfectly on top of the analytic result for almost every time-scale. Also shown in this figure is the same transient average length but for the real chain. It lies above that of the ideal chain but its dynamics is also proportional to $t^{1/2}$, as was predicted in [13] and [14] using scaling arguments. The real chain reaches its equilibrium state around the same time as the ideal chain, i.e. $t \approx \tau_R$. For this particular value of the dragging force, $f = 2$, the equilibrium state of the length is higher than that of the Rouse chain, which is a characteristic we will discuss below.

Before we go into the discussion of the average thermalised length of the real chain, we should argue that there are different force regimes. When the force is very weak it will not disturb the equilibrium conformation of the polymer. The upper limit for this weak force can be found by relating the largest length scale of the polymer with the thermal energy $k_B T$. The largest length scale is surely the length of the average end-to-end vector, we have $\mathcal{P} \sim N^\nu$. Therefore the upper limit for the weak forces is $f_w \sim k_B T / N^\nu$. Very strong forces, on the other hand, will stretch the polymer almost to its full extend. To find the threshold for these strong forces we relate the thermal energy with the smallest length scale of the system. For this length we take the average distance b between two beads in an ideal chain. We therefore find that the regime of the strong forces starts at $f_s \sim k_B T / b$. We have thus three force scales: weak forces $f < f_w$, intermediate forces $f_w < f < f_s$ and strong forces $f > f_s$.

Now we turn to the discussion of the equilibrium length L^* as a function of the dragging force f . In the case of the ideal chain, the relation is simple and linear. From Eq. (5.79) we have $L^* = (N/2k)f$. Figure 5.23 shows the simulated results

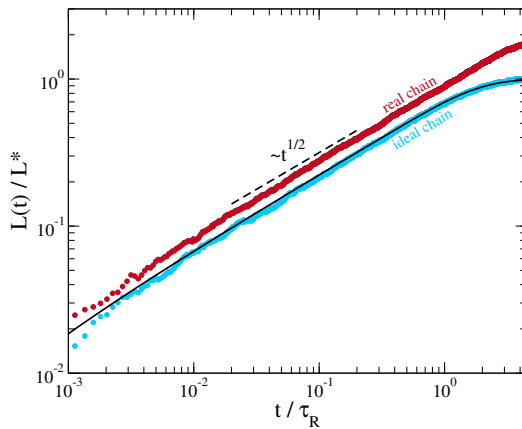


Figure 5.22: Log-log plot of the ratio of the length to the equilibrium length as a function of time. The solid black line is the analytic result from Eq. (5.78) and the coloured dots are the simulations results with blue being the ideal chain and red the real chain. The dashed line indicates the power-law behaviour. The simulations were performed starting with an equilibrated chain. The parameters are $f = 2$, $N = 256$, $k_B T = \gamma = 1$, $k = 3$, $\epsilon = \sigma = R_0 = 1$, $\Delta t = 10^{-4}$. The results are averaged over 10^2 histories.

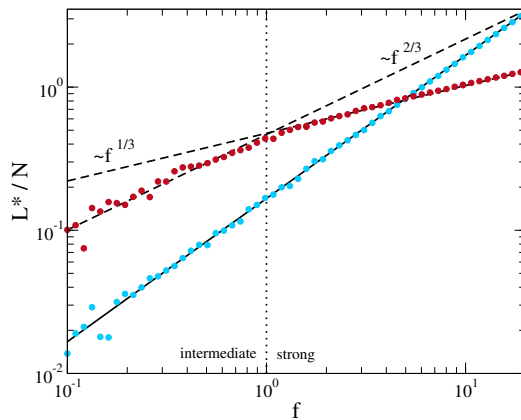


Figure 5.23: Log-log plot of the equilibrium length-force relation. The solid black line is the analytic result for ideal chains $L^*/N = f/2k$ and the coloured dots are the simulations results with blue being the ideal chain and red the real chain. The dashed lines indicate the local power-law behaviour. The dotted line divides the force spectrum into intermediate and strong forces. The length was measured after enough time had passed to reach equilibrium. The parameters are $N = 128$, $k_B T = \gamma = 1$, $k = 3$, $\epsilon = \sigma = 1$, $R_0 = 2$, $\Delta t = 10^{-4}$. The results are averaged over $3.5 \cdot 10^4$ histories.

for a chain with $N = 128$. From this it is clear that, for the ideal chain, simulation and analytic results perfectly agree over several force regimes. Concerning these force regimes: for a real chain (with $k_B T = b = 1$, $N = 128$ and $\nu \approx 3/5$) the upper limit of the weak forces lies approximately at $f_w \approx 0.05$ while the threshold for the strong forces is $f_s \approx 1$. So the data of a real chain in Fig. 5.23 starts in the intermediate force regime (lower forces are of little interest since they will not deform the equilibrium conformation of the polymer). For intermediate forces, Sakaue derived an approximate expression for the length-force relation [14]. It reads

$$L^* \simeq bN \left(\frac{bf}{k_B T} \right)^{(1-\nu)/\nu}. \quad (5.144)$$

For self-avoiding chains in three dimensions we had $\nu \approx 3/5$. Therefore we should find that, in the intermediate force regime, the equilibrium length should go as $L^* \sim f^{2/3}$. This is indeed what the simulations yield for $f < f_s = 1$, see Fig. 5.23. For strong forces the average equilibrium length should eventually reach the maximum length L_M when all the FENE springs adopt their ultimate extension. From our simulation data we find that the climb to this maximum length goes as $L^* \sim f^{1/3}$. We do not have a satisfying explanation for this exponent. We do, however, know that this regime is characterised by a “stem-flower” shape rather than a trumpet shape of the polymer, see [104]. A stem-flower configuration is rod-like (stem) close to the pulled monomer. At the end of the rod-like structure is an elongated fluctuating coil (flower).

Notice that over the full force range, the equilibrium length of the ideal and real chain differ (except at one particular crossing point). For intermediate forces we find that the real chain is more swollen than the ideal chain (as is the case in the non-dragging case). While for large forces, the length of the real chain is limited by its finite extensibility, yielding a shorter equilibrium length than the ideal chain. This shows that adding more realistic features to the model will drastically change the properties of the chain and hopefully better mimic a real polymer.

5.5.3 Semi-flexible polymer in an active viscoelastic bath

In Section 5.4 we investigated how a Rouse chain in a viscoelastic bath reacts to the presence of active forces. Two important results were achieved, namely that the monomers performed both sub- and superdiffusion, and that the polymer swells due to these active forces. But real polymers are not nearly as flexible as a Rouse chain, over short length scales they resist bending and appear to be stiff. This characteristic could very well influence the results of Section 5.4. The orientation of individual springs in the Rouse chain is completely uncorrelated with the other springs. This we would like to change and make the orientation dependent on the local collective orientation. To do so we introduce the following potentials

$$U^{tot} = U^{harm} + U^{bend}, \quad (5.145)$$

with $k \gg 1$ and $a \neq 0$. In doing so, the bonds (of length a) between the beads become practically incompressible/inextensible and the only important feature will be the bending rigidity. Notice that we did not include the self-avoidance potential. The chain can therefore not be regarded as a real chain, it is still an ideal one. Chains

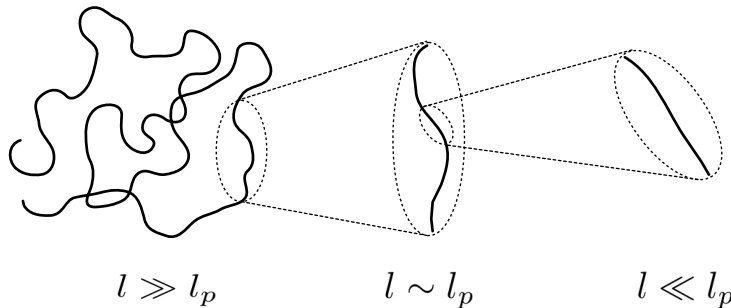


Figure 5.24: Illustration of how thermal fluctuations determine the global orientation of a chain on different length scales l compared to the persistence length l_p . We have: $l \gg l_p \rightarrow$ flexible, $l \sim l_p \rightarrow$ semi-flexible and $l \ll l_p \rightarrow$ rigid.

with these characteristic can however be classified as *worm-like chains* (or Kratky-Porod chains) [119]. A special case of semi-flexible chains is when $\kappa = 0$, then there is no energy cost in bending the chain. Such a chain is called a freely-jointed chain (see Section 5.1) because we have stiff, rod-like, springs whose orientation is uncorrelated.

An important quantity to describe the flexibility of a polymer is the persistence length l_p . It is the length scale on which the polymer forgets its original orientation due to thermal fluctuations. When we consider segments of the polymer (of length l) that are much larger than the persistence length, $l \gg l_p$, they can be considered as flexible, in the sense of the Rouse chain. On the other hand, when the length of the segment is shorter than the persistence length, $l \ll l_p$, the segment will maintain one direction. This we call a rigid rod. The intermediate case where $l \sim l_p$ is called semi-flexible, their orientation is overall consistent but undergoes some minor deviations due to thermal agitations. In Fig. (5.24) these three length scales are clarified. A good everyday example to illustrate the persistence length is spaghetti. Uncooked, spaghetti has a very long persistence length, $l_p \approx 10^{18}$ m, i.e. it is very hard to bend. As a fun fact: one would need a dry spaghetti with a length comparable to the diameter of our Milky Way galaxy to consider it a flexible object at room temperature (by which we mean that thermal fluctuations are able to bend it). A cooked spaghetti, on the other hand, has a very short persistence length of a few centimetres, which we clearly recognize by its curled-up shape when immersed in water. A more biologically relevant example is DNA with $l_p \approx 35$ nm [120]. Microtubules are one of the stiffest polymers, with a persistence length of $l_p \approx 0.24$ mm [121]. Before we go into the simulation results of a semi-flexible chain in an active viscoelastic bath, we first discuss briefly the equilibrium properties of a semi-flexible worm-like chain.

Equilibrium properties of a semi-flexible chain

Just as for the (flexible) Rouse model, we can calculate some interesting properties of a thermalised semi-flexible chain. Here we will assume that the bonds have a constant length a (or $|\vec{r}_n| = a$) and the energy stored in a bended joint is given by U_n^{bend} . First, we would like to find an expression for the persistence length since it is a defining quantity for a worm-like chain. The persistence length is defined as the characteristic length scale over which the correlation in the orientation of the bonds decays along the chain. We will soon show that this decay is exponential, we thus have

$$\langle \hat{r}_n \cdot \hat{r}_{n+m} \rangle = e^{-a|m|/l_p}. \quad (5.146)$$

We should now work out the average correlation on the left-hand side of this relation. Luckily, this calculation was already performed in 1963 in a completely different field. In his paper on "*Magnetism in one-dimensional systems - the Heisenberg model for infinite spin*" [122], Michael E. Fisher calculated, among other things, the average correlation in a linear chain of spins that can orient themselves in three dimensions. The interaction between the spins (which, for us, represent the unit bond vectors \hat{r}_n) was the nearest-neighbour isotropic Heisenberg coupling, which happens to have the exact same form as our bending rigidity potential U^{bend} . Using our notation, he found

$$\langle \hat{r}_n \cdot \hat{r}_{n+m} \rangle = \left[\coth \left(\frac{\kappa}{k_B T} \right) - \frac{k_B T}{\kappa} \right]^{|m|}, \quad (5.147)$$

equating this with Eq. (5.146) one finds

$$l_p = -a \ln^{-1} \left[\coth \left(\frac{\kappa}{k_B T} \right) - \frac{k_B T}{\kappa} \right] \approx \frac{a\kappa}{k_B T}, \quad (5.148)$$

where the approximation is correct when $\kappa \gg k_B T$. When κ is much larger than $k_B T$, then there is not enough thermal energy to significantly bend the chain. The angle θ_n between two bonds will therefore be quite small, remember $\cos(\theta_n) = \hat{r}_n \cdot \hat{r}_{n+1}$. We can therefore do the following expansions (for small θ_n due to large κ)

$$\langle \cos(\theta_n) \rangle = 1 - \frac{1}{2} \langle \theta_n^2 \rangle + \mathcal{O}(\langle \theta_n^4 \rangle), \quad (5.149)$$

$$e^{-a/l_p} = 1 - \frac{a}{l_p} + \mathcal{O}((a/l_p)^2). \quad (5.150)$$

We therefore find (approximately) that $\langle \theta_n^2 \rangle = 2k_B T/\kappa$. From symmetry considerations we also have that $\langle \theta_n \rangle = 0$. Next, we calculate the average of the squared end-to-end distance $\mathcal{P}^2 = \langle \vec{P}^2 \rangle$, we have

$$\mathcal{P}^2 = \left\langle \sum_{n=1}^{N-1} \vec{r}_n \cdot \sum_{m=1}^{N-1} \vec{r}_m \right\rangle = a^2 \sum_{n=1}^{N-1} \sum_{m=1}^{N-1} e^{-a|n-m|/l_p}, \quad (5.151)$$

remember that for this discussion we took $|\vec{r}_n| = a$, therefore $\vec{r}_n = a\hat{r}_n$. For long chains ($a \ll N$) we can replace the summation with an integral, we should take

$a \rightarrow dx$ and $an \rightarrow x$. Then the integration boundaries are from zero to $a(N-1)$, this last value is the contour length of the chain $L_M \approx aN$. We get

$$\mathcal{P}^2 = \int_0^{L_M} dx \int_0^{L_M} dy e^{-|x-y|/l_p}. \quad (5.152)$$

Working out this integral is rather elementary [123], the final result is

$$\mathcal{P}^2 = 2l_p L_M - 2l_p^2 \left[1 - \exp\left(-\frac{L_M}{l_p}\right) \right]. \quad (5.153)$$

When the total length of the chain greatly exceeds the persistence length $L_M \gg l_p$, we should find that the end-to-end distance behaves like that of a flexible chain. Indeed if we approximate Eq. (5.153) accordingly we get $\mathcal{P}^2 \approx 2l_p L_M$. This complies with a flexible chain for which we have, using Eq. (5.51) and the fact¹ that $L_M = bN$, $\mathcal{P}^2 = b L_M$. We therefore find that the Kuhn length is two times the persistence length $b = 2l_p$, which fits with its definition as the length scale over which the orientation of the chain loses its correlation. When the total length of the chain is much shorter than the persistence length $L_M \ll l_p$, we find that the leading term of the approximation is $\mathcal{P}^2 \approx L_M^2$. This is exactly what was to be expected from a rigid rod.

When simulating a worm-like chain, it is often important that the initial configuration of the chain is one that is drawn from an equilibrium distribution. It is possible to construct such a thermalised chain using its main (equilibrium) characteristics. In Appendix D we show the construction protocol and check that the obtained chain indeed possesses the equilibrium properties discussed above. To simulate the evolution of the polymer in an active viscoelastic bath we use the algorithm revealed in Chapter 3. This algorithm can deal with fractional differential equations and non-white noise.

Testing the algorithm

Before we go into the simulation results of the semi-flexible chain in an active viscoelastic bath, we must verify that the algorithm performs well by comparing simulations of an ordinary Rouse chain with the analytic results of Section 5.4. Figures 5.25 and 5.26 show the simulation results for the diffusion of the centre of mass and the middle bead respectively. The initial configuration of the chain was drawn from an equilibrium distribution. The analytic curves in these figures are the exact same as in Figs. 5.13 and 5.15. It is immediately clear that the results are in complete agreement with the theory, both for active and non-active baths. A downside to the algorithm is that it can not simulate a large amount of time-steps in a reasonable amount of time due to the ever increasing history that needs to be convoluted with all previous results to calculate the next time-step. This, combined with the need for a small time-step, restricts the maximum time which we can reach (in a reasonable computation time). That is the reason why the figures only compare the analytic results with the simulated data for early times, later times are out of our reach. Both figures have an inset that shows which part of the original (analytic) plot is shown in the main figure.

¹The Rouse chain, of course, does not have a maximum length. We interpret L_M here as the average contour length, i.e. approximately N springs with an average length b .

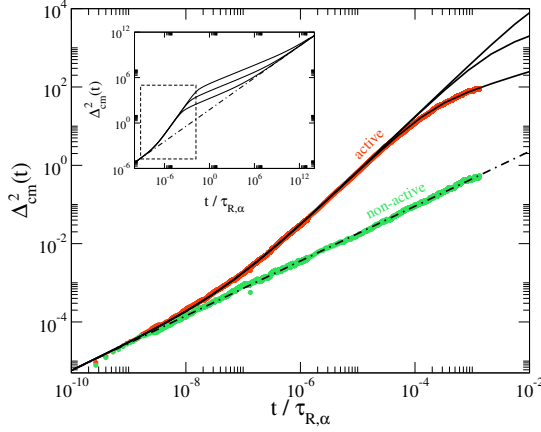


Figure 5.25: Log-log plot of the squared distance travelled by the centre of mass as a function of $t/\tau_{R,\alpha}$ for a Rouse chain ($N = 256$, $k = 3$) in a viscoelastic medium ($\alpha = 0.7$, $k_B T = \gamma = 1$) in the presence of active forces with $C = 10^2$ and $\tau_A/\tau_{R,\alpha} = 10^{-2}, 10^{-3}, 10^{-4}$ (full lines, top to bottom) compared to that without active forces (dashed-dotted line). Also shown, in coloured dots, are the simulated data (total number of time steps: 10^4 , $\Delta t = 10^{-5}, 10^{-2}$ and averaged over 10^2 histories) with green being the non-active bath and orange the active bath ($\tau_A/\tau_{R,\alpha} = 10^{-4}$). *Inset*: a copy of Fig. 5.13 with an indication of the region that the main graph displays.

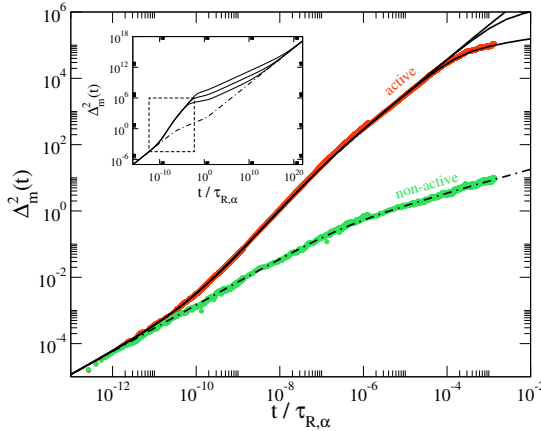


Figure 5.26: Log-log plot of the squared distance travelled by the middle bead as a function of $t/\tau_{R,\alpha}$ for a Rouse chain ($N = 256$, $k = 3$) in a viscoelastic medium ($\alpha = 0.7$, $k_B T = \gamma = 1$) in the presence of active forces with $C = 10^4$ and $\tau_A/\tau_{R,\alpha} = 10^{-2}, 10^{-3}, 10^{-4}$ (full lines, top to bottom) compared to that without active forces (dashed-dotted line). Also shown, in coloured dots, are the simulated data (total number of time steps: 10^4 , $\Delta t = 10^{-8}, 10^{-5}, 10^{-2}$ and averaged over 10^2 histories) with green being the non-active bath and orange the active bath ($\tau_A/\tau_{R,\alpha} = 10^{-4}$). *Inset*: a copy of Fig. 5.15 with an indication of the region that the main graph displays.

Simulation results

These simulations were performed starting with an equilibrated chain (as described in Appendix D). The values for k and κ were chosen as large as the accuracy of the simulation allowed. A large value for the spring constant k will make sure that the bonds do not deviate much from their resting length a . The length of the chains in the simulations is much shorter than we previously used, the reason for this is twofold: first because long chains take much more computation time to simulate and second because the length of the chain should not greatly exceed the persistence length otherwise the chain can again be considered flexible. Before we show the actual results, we will reveal a possible theory that can explain our findings.

An approximate theory can be produced if we assume the springs to be completely rigid, i.e. $|\vec{r}_n| = a$. The only potential energy that can be stored in the chain is in the bending of the chain. The total potential energy is thus $U^{tot} = U^{bend} = -\kappa \sum_{n=1}^{N-2} \hat{r}_n \cdot \hat{r}_{n+1}$. Because adding a constant to the potential will not change the resulting force we can also write the total potential energy as

$$U^{tot} = \kappa \sum_{n=1}^{N-2} (1 - \hat{r}_n \cdot \hat{r}_{n+1}) = \frac{\kappa}{2a^2} \sum_{n=1}^{N-2} \left(2\vec{R}_n - \vec{R}_{n-1} - \vec{R}_{n+1} \right)^2, \quad (5.154)$$

where we used $\hat{r}_n = (\vec{R}_n - \vec{R}_{n-1})/a$. To find the dynamics of a bead in a semi-flexible chain in an active viscoelastic bath we substitute this energy into Eq. (5.132) and add active noise. After some elementary calculations one finds

$$\begin{aligned} \eta_\alpha c \mathcal{D}^\alpha \vec{R}_n(t) = & -\frac{\kappa}{a^2} \left(6\vec{R}_n(t) - 4\vec{R}_{n-1}(t) - 4\vec{R}_{n+1}(t) + \vec{R}_{n-2}(t) + \vec{R}_{n+2}(t) \right) \\ & + \vec{\xi}_{T,n}(t) + \vec{\xi}_{A,n}(t). \end{aligned} \quad (5.155)$$

It is important to note here that this equation does not fully portrait the dynamics of a bead in a semi-flexible chain with rigid springs. That is because it contains no information of the fact that the beads should, at all times, be at a distance a from each other. It is common to enforce this constraint through the use of a *Lagrange multiplier*¹ which gives rise to an extra term in the energy. We will not go into this more difficult model and use Eq. (5.155) as an approximation to the exact dynamics. From the above (linear) expression it is easy to find the equation of motion of the normal coordinates. Following very analogous steps as in Section 5.1.2, we arrive at

$$\eta_\alpha c \mathcal{D}^\alpha \vec{X}_p(t) = -\frac{k'_p}{2N} \vec{X}_p(t) + \vec{\xi}_{T,p}(t) + \vec{\xi}_{A,p}(t). \quad (5.156)$$

The two normal noise terms are defined as before, but k'_p is defined differently

$$k'_p = \frac{32\kappa N}{a^2} \sin^4 \left(\frac{\pi p}{2N} \right) \approx \frac{2\kappa \pi^4 p^4}{a^2 N^3}. \quad (5.157)$$

It is now proportional to p^4 and will yield different characteristic times. These are again defined as $\tau'_{p,\alpha} = (2\eta_\alpha N/k'_p)^{1/\alpha}$. The vibrations of different parts of the chain

¹The method of Lagrange multipliers is an optimisation technique that can be used to determine the extrema of a multivariate function subject to a specific constraint. For more information on this technique see [124].

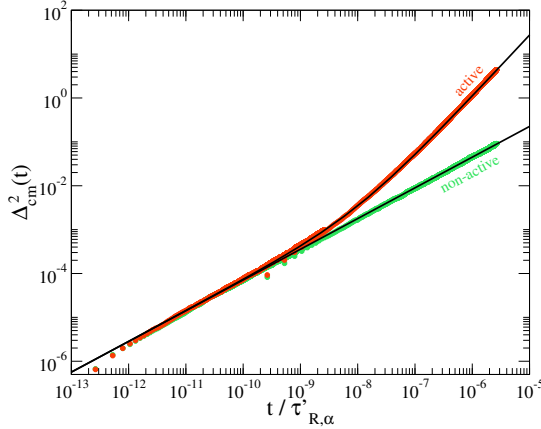


Figure 5.27: Log-log plot of the squared distance travelled by the centre of mass as a function of $t/\tau'_{R,\alpha}$ for a semi-flexible chain ($N = 64$, $k = 100$, $\kappa = 100$, $a = 2$) in a viscoelastic medium ($\alpha = 0.7$, $k_B T = \gamma = 1$) with active forces ($C = 10^2$, $\tau_A/\tau'_{R,\alpha} = 10^{-2}$) and without active forces. Also shown, in coloured dots, is the simulated data with green being the non-active bath and orange the active bath (total number of time steps: 10^4 , $\Delta t = 10^{-7}$, 10^{-4} and averaged over 10^3 histories).

are thus different from those of a Rouse chain due to the stiffness of the worm-like chain. The generalised “Rouse” time for a semi-flexible chain is

$$\tau'_{R,\alpha} = \left(\frac{\eta_\alpha a^2 N^4}{\kappa \pi^4} \right)^{1/\alpha}. \quad (5.158)$$

Because Eq. (5.156) has exactly the same form as the one in the case of the flexible Rouse chain, Eq. (5.101), it allows us to recycle all results from Section 5.4 provided we use the characteristic times $\tau'_{p,\alpha}$ of the semi-flexible chain, instead of $\tau_{p,\alpha}$.

The first quantity we will discuss is the mean-squared displacement of the centre of mass, it is given by Eq. (5.107). This expression is clearly not dependent on $\tau_{p,\alpha}$ and therefore the centre of mass of a semi-flexible chain should diffuse exactly like that of a Rouse chain. This is not surprising since the collective motion of a chain should not be influenced by simple internal interactions. Figure 5.27 shows the simulation results together with Eq. (5.107). It is clear that for both the active and the non-active baths the centre of mass of the semi-flexible chain follows the predicted behaviour.

Next we investigate the mean-squared displacement of the middle bead. We will first do this for a non-active bath, where the diffusion is governed by Eq. (5.65). The first term is not dependent on $\tau_{p,\alpha}$ and will therefore behave exactly the same for a semi-flexible chain as for a Rouse chain. The second term however does depend on the characteristic times and will thus yield different dynamics when we use $\tau'_{p,\alpha}$ instead of $\tau_{p,\alpha}$. The approximation for very short times, $t \ll \tau'_{N,\alpha}$, can be done in the same manner as for Eq. (5.65) and will yield the same result $\Delta_m^2(t) = (6k_B T/\gamma\alpha G_\alpha)t^\alpha$. So for these very early times the bead does not yet feel the influence of its fellow beads and will diffuse as a free particle, as was the case for the Rouse chain. For somewhat

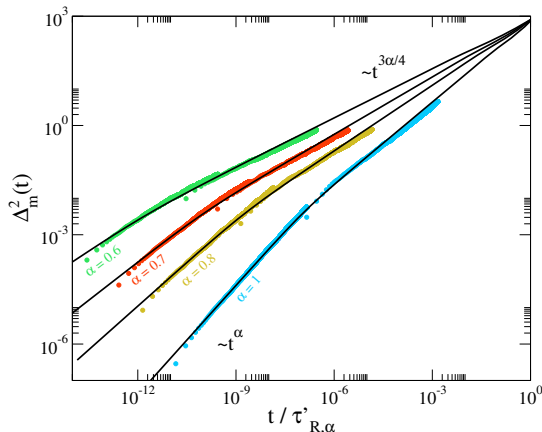


Figure 5.28: Log-log plot of the squared distance travelled by the middle bead as a function of $t/\tau'_{R,\alpha}$ for a semi-flexible chain ($N = 64$, $k = 100$, $\kappa = 100$, $a = 2$) in a viscoelastic medium ($\alpha = 0.6, 0.7, 0.8$ and 1 , $k_B T = \gamma = 1$) without active forces (full lines). Also shown, in coloured dots, is the simulated data (total number of time steps: 10^4 , $\Delta t = 10^{-7}$, 10^{-3} and averaged over 10^3 histories). The time regimes are indicated.

longer times, $t \ll \tau'_{R,\alpha}$, we can approximate the summation by an integral. With very similar reasoning as for Eq. (5.66), we find

$$\frac{6k_B T}{\gamma} \int_0^\infty dx \frac{\gamma a^2}{\kappa \pi^4 x^4} \left[1 - E_{\alpha,1} \left(-\frac{\kappa \pi^4 t^\alpha}{\eta_\alpha a^2} x^4 \right) \right] = \frac{6k_B T a^{1/2} I''_\alpha}{\eta_\alpha^{3/4} \kappa^{1/4} \pi} t^{3\alpha/4}, \quad (5.159)$$

with $I''_\alpha = \int_0^\infty dx x^{-4} (1 - E_{\alpha,1}(-x^4))$ which only depends on α . This approximation makes it clear that the mean-squared displacement goes as: $\Delta_m^2(t) \sim t^{3\alpha/4}$, which is always subdiffusive and faster than in the case of the Rouse chain with the same α . Since the first term of Eq. (5.65) remains unchanged for a semi-flexible chain, the long time behaviour also doesn't change. We therefore find the following sequence of approximate regimes of Δ_m^2 for a semi-flexible chain

$$\Delta_m^2(t) = \frac{6 D_\alpha}{\Gamma(\alpha + 1)} t^\alpha \xrightarrow{\tau'_{N,\alpha}} \frac{6k_B T a^{1/2} I''_\alpha}{\eta_\alpha^{3/4} \kappa^{1/4} \pi} t^{3\alpha/4} \xrightarrow{\tau'_{R,\alpha}} \frac{6 D_\alpha^{cm}}{\Gamma(\alpha + 1)} t^\alpha. \quad (5.160)$$

Remember that this analytic model for the semi-flexible chain is by no means complete, deviations from it are expected. In Fig. 5.28 the early time mean-squared displacement of the middle bead is plotted for $\alpha = 0.6, 0.7, 0.8$ and 1 . The analytic curves are given by Eq. (5.65) with $\tau_{p,\alpha}$ substituted by $\tau'_{p,\alpha}$. The t^α and $t^{3\alpha/4}$ behaviour is indicated. Also shown in this figure are the simulation results, for early times they agree well with the analytic solutions. After an initial agreement with the $t^{3\alpha/4}$ regime, the simulation appears to slightly deviate from it. As mentioned earlier, our simulations can not reach long times. It was therefore not possible to investigate whether the semi-flexible chain would follow the predicted behaviour for all times.

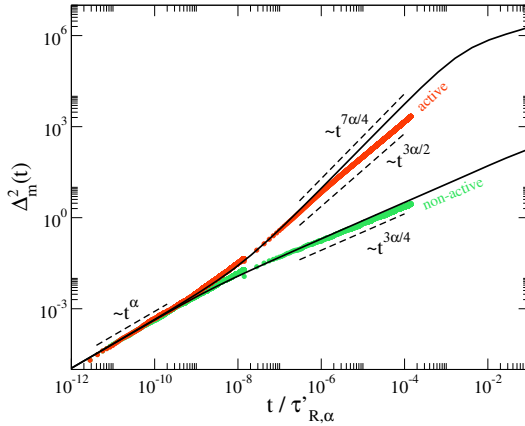


Figure 5.29: Log-log plot of the squared distance travelled by the middle bead as a function of $t/\tau'_{R,\alpha}$ for a semi-flexible chain ($N = 64$, $k = 100$, $\kappa = 100$, $a = 2$) in a viscoelastic medium ($\alpha = 0.8$, $k_B T = \gamma = 1$) with active forces ($C = 10^3$, $\tau_A/\tau'_{R,\alpha} = 10^{-3}$) and without active forces. Also shown, in coloured dots, is the simulated data with green being the non-active bath and orange the active bath (total number of time steps: 10^4 , $\Delta t = 10^{-7}$, 10^{-3} and averaged over $5 \cdot 10^2$ histories). The time regimes are indicated.

Now we will look at the mean-squared displacement of the middle bead when active forces are present. Again, if we substitute $\tau'_{p,\alpha}$ into Eq. (5.115), we find the predicted behaviour. The first and third terms are not affected by this change. We already discussed above how the second term is altered. It yields a t^α behaviour for very early times and a $t^{3\alpha/4}$ behaviour for times thereafter. The approximation of the fourth term will yield the same $t^{2\alpha}$ behaviour for very early times (see Eq. (5.118)). But performing the integration for longer times, i.e. Eq. (5.119), with $\tau'_{p,\alpha}$ will yield a time dependence of $t^{7\alpha/4}$. The reason why we discuss this behaviour so briefly is because, as Fig. 5.29 shows, the simulated results deviate quite strongly from the analytic model. The model shows its shortcomings when active forces are present. For early times we do find the t^α behaviour, but for longer times the predicted $t^{7\alpha/4}$ regime is abandoned in favour of a $t^{3\alpha/2}$ regime. Whether this $3\alpha/2$ exponent stems from the diffusion of the middle bead in a Rouse chain, Eq. (5.119), is not clear. Again, the long-time diffusion was out of our simulation reach.

The most important conclusion from these results is that it is crucial to know the flexibility of a polymer when performing experiments with it. That is because, as we have seen, semi-flexible polymers can exhibit different anomalous diffusion than flexible polymers, in active and non-active bath alike. In other words, when determining the viscoelasticity (i.e. the value of α) of the cytosol by rheological measurements, one should use the correct exponent of time that corresponds to the polymer's flexibility.

We will briefly discuss how the end-to-end distance of a semi-flexible chain (in a viscoelastic bath) is influenced by active forces. We saw that, for a flexible Rouse chain, the average squared end-to-end distance \mathcal{P}^2 always increased in an active viscoelastic

bath, effectively swelling the polymer. We will soon see that, for a semi-flexible chain, not only swelling but also shrinking can occur. Figure 5.30 shows some simulation results for different lengths of the chain and for different characteristics of the active forces. All simulations were done in a viscoelastic bath with $\alpha = 0.8$. From these figures it is clear that the end-to-end distance has a rich variety of responses to the active forces. Our research on this subject was, at the time of writing, still in its infancy. We can therefore not give it a full and quantitative treatment here, but some general observations can be made. First, notice that for all lengths a non-active simulation was performed. This should of course stay (on average) constant at all time and comply with Eq. (5.153). This behaviour is clearly met and gives a good comparison for the results of the active bath (since all polymers started from an equilibrium configuration). A second observation is that the initial response to the active forces is always a shrinking of the polymer. This shrinking can be explained by the fact that the active forces provide enough energy to bend the polymer more strongly than the thermal forces could. Due to these larger kinks, the chain will be more compact. After this initial response we observe a large variety of different behaviours, no clear qualitative trend reveals itself from these preliminary simulations. Many polymers keep shrinking, others start swelling and some appear to find a steady state (which can be both above or below the value of a non-active bath). The nature of these responses can vary strongly between the values of N , C and τ_A . More research should be done to better understand the behaviour of the end-to-end distance of a semi-flexible chain in an active viscoelastic bath. Mainly simulations that go further in time are essential, in order to reach the steady state for all investigated polymers.

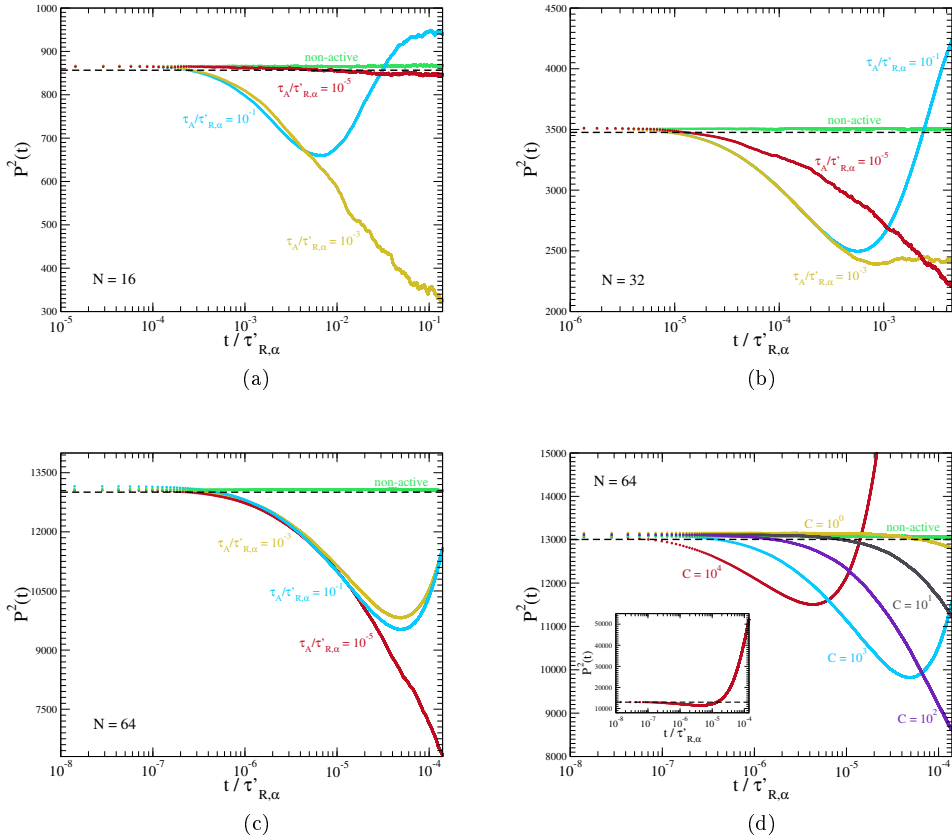


Figure 5.30: Lin-log plots of the simulated data of the squared end-to-end distance as a function of $t/\tau'_{R,\alpha}$ for a semi-flexible chain ($N = 16, 32, 64, k = 100, \kappa = 100, a = 2$) in a viscoelastic medium ($\alpha = 0.8, k_B T = \gamma = 1$) with active forces (where it is not indicated we have $C = 10^3$ and $\tau_A/\tau'_{R,\alpha} = 10^{-3}$) and without active forces. Also shown is the analytic equilibrium value in a non-active bath (dashed line). (The total number of time steps: $10^4, \Delta t = 10^{-3}$ and averaged over 10^3 histories). *Inset:* Shows the same red data points as the main graph but over a longer P^2 range.

6 | Generalised Langevin Equation: Middle Bead

Never mistake motion for action.

Ernest Hemingway

The procedure to obtain a generalised Langevin equation involves the projection of many fast moving degrees-of-freedom of an ensemble (or bath) onto just a few slow moving, which we call the system. By doing so one acquires the reduced dynamics of the system. Generally speaking the projection introduces three terms in the equation of motion of the system: an effective potential, a non-Markovian friction force and a non-white effective noise. The latter two are governed by a memory kernel, which connects them through the fluctuation-dissipation relation (see Section 2.3 for a more rigorous explanation on the projection of fast degrees-of-freedom). Here we will try to find the generalised Langevin equation of the middle bead in a chain of beads that are interconnected by harmonic springs (i.e. the middle bead of a Rouse chain). The chain is also surrounded by a heat-bath. Later we will also introduce some driving agent and see how the generalised Langevin equation deals with nonequilibrium circumstances. As a warning, this chapter is a technical one. Mainly focussed on the procedure of how a generalised Langevin equation is constructed. The first three sections, and part of the fourth, are partly based on works by W. Briels [125], D. Panja [126] and T. Sakaue [127]. We provide a detailed revision of their calculations. Section 6.4, however, deals with nonequilibrium situations and is original work by the author, published in [128].

6.1 System plus bead-bath

While for many models the projection process can be quite difficult, in the case of the Rouse model it only involves eliminating variables from a set of linear differential equations. In this section we will perform this elimination process.

To construct a generalised Langevin equation of the middle bead, also referred to as the system, we need to integrate out all degrees-of-freedom of the other beads that are not of interest. These beads we will refer to as the bead-bath. Suppose the chain has length $N = 2M + 1$, then the middle bead is on both sides connected to a chain of

length M . The coordinates of the middle bead are $\vec{r} = \vec{R}_{M+1}$ while the coordinates that need to be projected on \vec{r} are $\mathcal{R} = \{\vec{R}_1, \vec{R}_2, \dots, \vec{R}_M, \vec{R}_{M+2}, \dots, \vec{R}_{2M}, \vec{R}_N\}$. Notice that the bead-labelling here differs from that of the previous chapter, where the first bead was labelled as zero. This is just a matter of notation and beneficial to the calculations that lie ahead. As is usual with a Rouse chain we introduce two ghost beads to take care of the boundary conditions: $\vec{R}_0 = \vec{R}_1$ and $\vec{R}_{N+1} = \vec{R}_N$. To describe this system we need to write down the total potential energy that arises from the harmonic springs (which have spring constant k) between neighbouring beads. Between bead i and bead $i + 1$, this potential is given by $k(\vec{R}_{i+1} - \vec{R}_i)^2/2$. To find the total potential energy we sum over all $(N - 1)$ springs, we find

$$\begin{aligned} \mathcal{U}(\vec{r}, \mathcal{R}) = & \frac{k}{2} (\vec{r} - \vec{R}_M)^2 + \frac{k}{2} (\vec{R}_{M+2} - \vec{r})^2 \\ & + \frac{k}{2} \left[\sum_{i=1}^{M-1} (\vec{R}_{i+1} - \vec{R}_i)^2 + \sum_{i=M+2}^{N-1} (\vec{R}_{i+1} - \vec{R}_i)^2 \right]. \end{aligned} \quad (6.1)$$

This expression can be rewritten to identify three components in the total potential energy. One term only involves the system coordinate \vec{r} which we will call $V(\vec{r})$, another term describes the coupling between the system and the bead-bath $\mathcal{U}_{bs}(\vec{r}, \mathcal{R})$ and yet another term gives the interaction between the bead-bath particles $\mathcal{U}_{bb}(\mathcal{R})$. So we can write the total potential energy as follows

$$\mathcal{U}(\vec{r}, \mathcal{R}) = V(\vec{r}) + \mathcal{U}_{bs}(\vec{r}, \mathcal{R}) + \mathcal{U}_{bb}(\mathcal{R}), \quad (6.2)$$

with

$$V(\vec{r}) = k\vec{r}^2, \quad (6.3)$$

$$\mathcal{U}_{bs}(\vec{r}, \mathcal{R}) = -k\vec{r} \left(\vec{R}_M + \vec{R}_{M+2} \right), \quad (6.4)$$

$$\mathcal{U}_{bb}(\mathcal{R}) = \frac{k}{2} \left[\vec{R}_M^2 + \vec{R}_{M+2}^2 + \sum_{i=1}^{M-1} (\vec{R}_{i+1} - \vec{R}_i)^2 + \sum_{i=M+2}^{N-1} (\vec{R}_{i+1} - \vec{R}_i)^2 \right]. \quad (6.5)$$

6.1.1 Eigenvectors of the bath-bath coupling

From the (bead) bath-bath coupling Eq. (6.5) we can define two coupling-matrices, one for the left chain and one for the right. \hat{H}^L and \hat{H}^R , respectively. These are $M \times M$ matrices and they are defined as follows

$$\hat{H}^L = \begin{bmatrix} 1 & -1 & 0 & 0 & \cdots & 0 & 0 & 0 & 0 & 0 \\ -1 & 2 & -1 & 0 & \cdots & 0 & 0 & 0 & 0 & 0 \\ 0 & -1 & 2 & -1 & \cdots & 0 & 0 & 0 & 0 & 0 \\ \vdots & \vdots & \vdots & \vdots & & \vdots & \vdots & \vdots & \vdots & \vdots \\ 0 & 0 & 0 & 0 & \cdots & 0 & -1 & 2 & -1 & 0 \\ 0 & 0 & 0 & 0 & \cdots & 0 & 0 & -1 & 2 & -1 \\ 0 & 0 & 0 & 0 & \cdots & 0 & 0 & 0 & -1 & 2 \end{bmatrix}, \quad (6.6)$$

$$\hat{H}^R = \begin{bmatrix} 2 & -1 & 0 & 0 & \cdots & 0 & 0 & 0 & 0 & 0 \\ -1 & 2 & -1 & 0 & \cdots & 0 & 0 & 0 & 0 & 0 \\ 0 & -1 & 2 & -1 & \cdots & 0 & 0 & 0 & 0 & 0 \\ \vdots & \vdots & \vdots & \vdots & & \vdots & \vdots & \vdots & \vdots & \vdots \\ 0 & 0 & 0 & 0 & \cdots & 0 & -1 & 2 & -1 & 0 \\ 0 & 0 & 0 & 0 & \cdots & 0 & 0 & -1 & 2 & -1 \\ 0 & 0 & 0 & 0 & \cdots & 0 & 0 & 0 & -1 & 1 \end{bmatrix}. \quad (6.7)$$

We also define the vector-of-vectors

$$\mathbf{R}^L = (\vec{R}_1, \vec{R}_2, \dots, \vec{R}_M) \quad \text{and} \quad \mathbf{R}^R = (\vec{R}_{M+2}, \vec{R}_{M+3}, \dots, \vec{R}_N), \quad (6.8)$$

that hold the bead-bath coordinates of the left and right chains. With these vectors and matrices we can rewrite the bath-bath coupling as

$$\mathcal{U}_{bb}(\mathcal{R}) = \frac{k}{2} \left[\mathbf{R}^L \hat{H}^L \mathbf{R}^{L^T} + \mathbf{R}^R \hat{H}^R \mathbf{R}^{R^T} \right], \quad (6.9)$$

where the superscript T stand for the transpose of the vector. We will now proceed by calculating the eigenvalues and eigenvectors of the \hat{H} -matrices (\hat{H}^L and \hat{H}^R). Finding these will greatly simplify the expression of $\mathcal{U}_{bb}(\mathcal{R})$. Notice that the \hat{H} -matrices are hermitian ($\hat{H} = \hat{H}^\dagger$) and therefore also normal ($\hat{H}\hat{H}^\dagger = \hat{H}^\dagger\hat{H}$). This implies that \hat{H} is diagonalisable by a unitary matrix \hat{U} , meaning that there exists a diagonal matrix \hat{D} which is given by $\hat{D} = \hat{U}^{-1}\hat{H}\hat{U}$. Because \hat{H} is a normal matrix, its eigenvectors are an orthonormal set that span the entire space, i.e. they form a complete basis. The columns of \hat{U} are in fact the M eigenvectors of \hat{H} , while its M eigenvalues λ_i can be found on the diagonal of \hat{D} . We can thus write $\hat{U} = [\vec{U}_1 \ \vec{U}_2 \ \dots \ \vec{U}_M]$ and $D_{ii} = \lambda_i$ for $i = 1, 2, \dots, M$. Furthermore, we define the normal coordinates as the vector-of-vectors $\mathbf{X} = \mathbf{R}\hat{U}$, which is a linear transformation of the natural coordinates \vec{R}_n toward the basis of the eigenvectors of \hat{H} . In full we have $\mathbf{X}^L = (\vec{X}_1^L, \vec{X}_2^L, \dots, \vec{X}_M^L)$ and $\mathbf{X}^R = (\vec{X}_1^R, \vec{X}_2^R, \dots, \vec{X}_M^R)$. Using $\hat{U}\hat{U}^{-1} = \hat{I}$ and $\hat{U}^{-1} = \hat{U}^T$, we can write Eq. (6.9) as

$$\mathcal{U}_{bb}(\mathcal{R}) = \frac{k}{2} \left[\mathbf{R}^L \hat{U}^L \hat{D}^L \hat{U}^{L^{-1}} \mathbf{R}^{L^T} + \mathbf{R}^R \hat{U}^R \hat{D}^R \hat{U}^{R^{-1}} \mathbf{R}^{R^T} \right] \quad (6.10)$$

$$= \frac{k}{2} \left[\mathbf{X}^L \hat{D}^L \mathbf{X}^{L^T} + \mathbf{X}^R \hat{D}^R \mathbf{X}^{R^T} \right] \quad (6.11)$$

$$= \frac{k}{2} \sum_{i=1}^M \left[\lambda_i^L \vec{X}_i^{L^2} + \lambda_i^R \vec{X}_i^{R^2} \right]. \quad (6.12)$$

Now we will proceed to find the eigenvectors and eigenvalues of \hat{H}^L and \hat{H}^R . Because the calculation for both the left and right eigenvectors is completely analogue, we will only focus on calculating the left chain. The solutions of the right are given in the end. We also agree on some indices notation, an eigenvector is labelled by p , while a component of an eigenvector is labelled by q . Thus $U_{p,q}^L$ is the q -th component of the

p -th left eigenvector with eigenvalue λ_p^L . Solving the matrix equation $\hat{U}^L \hat{D}^L = \hat{H}^L \hat{U}^L$ gives the following set of equations

$$\begin{cases} U_{p,1}^L - U_{p,2}^L = \lambda_p^L U_{p,1}^L \\ -U_{p,q-1}^L + 2U_{p,q}^L - U_{p,q+1}^L = \lambda_p^L U_{p,q}^L & \text{for } q = 2, 3, \dots, M-1 \\ -U_{p,M-1}^L + 2U_{p,M}^L = \lambda_p^L U_{p,M}^L \end{cases} \quad (6.13)$$

We can reduce these three different types of equations into one. First remember that at the start of this section we introduced two ghost beads, in particular $\vec{R}_0 = \vec{R}_1$. Because $U_{p,q}^L$ defines a linear transformation of \vec{R}_n , we have that $U_{p,0}^L = U_{p,1}^L$. Also, since we can approach this problem from the rest frame of the middle bead, we are free to take $\vec{R}_{M+1} = 0$. Again due to its linear nature we have $U_{p,M+1}^L = 0$. Using these constraints we can write a single formula for all the components of the p^{th} left eigenvector

$$U_{p,q-1}^L + U_{p,q+1}^L = (2 - \lambda_p^L) U_{p,q}^L. \quad (6.14)$$

As a solution for this equation we propose the following form

$$U_{p,q}^L = A \cos(aq + b). \quad (6.15)$$

The ghost bead imposes the equation $\cos(b) = \cos(a + b)$. This has the solution $a = 0$, which is not desirable. Another solution is $b = -a/2$, which we will use. From $U_{p,M+1}^L = 0$ we get $\cos(a(M+1) - a/2) = 0$. This is satisfied if $a(M+1) - a/2 = (p-1/2)\pi$ or $a = (2p-1)\pi/N$ with $p = 1, 2, \dots, M$. The eigenvectors are therefore

$$U_{p,q}^L = A \cos\left(\frac{2p-1}{N} \left(q - \frac{1}{2}\right) \pi\right). \quad (6.16)$$

To find the eigenvalues we plug this equation into Eq. (6.14). Using $\cos(x) + \cos(y) = 2 \cos((x-y)/2) \cos((x+y)/2)$ and performing some elementary calculations leads to

$$\lambda_p^L = 4 \sin^2\left(\frac{2p-1}{2N} \pi\right). \quad (6.17)$$

Completely analogous we find the eigenvalues and eigenvectors of \hat{H}^R . They are

$$U_{p,q}^R = A \cos\left(\frac{2p-1}{N} \left(q - M - \frac{1}{2}\right) \pi\right) \quad (6.18)$$

and

$$\lambda_p^R = 4 \sin^2\left(\frac{2p-1}{2N} \pi\right). \quad (6.19)$$

The final thing that we need to do is find a value for the constant A . For this we enforce the fact that \hat{U}^L and \hat{U}^R should be unitary, to ensure that we have

$$\hat{U}^L \hat{U}^{L^T} + \hat{U}^R \hat{U}^{R^T} = 2\hat{I}. \quad (6.20)$$

The p -th diagonal element of the matrix on the left-hand side is in fact a summation over the components of the p -th eigenvector and should be equal to two

$$\sum_{q=1}^M A^2 \cos^2 \left(\frac{2p-1}{N} \left(q - \frac{1}{2} \right) \pi \right) + \sum_{q=1}^M A^2 \cos^2 \left(\frac{2p-1}{N} \left(q - M - \frac{1}{2} \right) \pi \right) = 2. \quad (6.21)$$

Changing the indices of the second sum gives

$$\sum_{q=1}^M \cos^2 \left(\frac{2p-1}{N} \left(q - \frac{1}{2} \right) \pi \right) + \sum_{q=M+2}^N \cos^2 \left(\frac{2p-1}{N} \left(q - N - \frac{1}{2} \right) \pi \right) = 2A^{-2}. \quad (6.22)$$

Now we can put both summations together (remember $U_{p,M+1}^L = 0$)

$$\sum_{q=1}^N \cos^2 \left(\frac{2p-1}{N} \left(q - \frac{1}{2} \right) \pi \right) = 2A^{-2}. \quad (6.23)$$

Using $\cos^2(x) = (1 + \cos(2x))/2$ gives

$$\sum_{q=1}^N \left[1 + \cos \left(\frac{2p-1}{N} \left(q - \frac{1}{2} \right) 2\pi \right) \right] = 4A^{-2}. \quad (6.24)$$

Doing the summation with the use of Lagrange's trigonometric identities gives

$$N + \frac{1}{2} \frac{\sin(4p\pi)}{\sin((2p-1)\pi/N)} = 4A^{-2}. \quad (6.25)$$

It is clear that the second term is zero when $p = 1, 2, \dots, M$. Therefore the value of A is simply

$$A = \frac{2}{\sqrt{N}}. \quad (6.26)$$

6.1.2 Normal coordinates

Now that we have the full expression of the eigenvectors, we can write the normal coordinates as a linear combination of the natural coordinates. Using $\mathbf{X}^L = \mathbf{R}^L \hat{U}^L$

$$\vec{X}_p^L = \sum_{q=1}^M U_{p,q}^L \vec{R}_q = A \sum_{q=1}^M \cos \left(\frac{2p-1}{N} \left(q - \frac{1}{2} \right) \pi \right) \vec{R}_q, \quad (6.27)$$

for $p = 1, 2, \dots, M$. Using $\mathbf{X}^R = \mathbf{R}^R \hat{U}^R$

$$\begin{aligned} \vec{X}_p^R &= \sum_{q=1}^M U_{p,q}^R \vec{R}_{q+M+1} = A \sum_{q=1}^M \cos \left(\frac{2p-1}{N} \left(q - M - \frac{1}{2} \right) \pi \right) \vec{R}_{q+M+1} \\ &= -A \sum_{q=M+2}^N \cos \left(\frac{2p-1}{N} \left(q - \frac{1}{2} \right) \pi \right) \vec{R}_q, \end{aligned} \quad (6.28)$$

for $p = 1, 2, \dots, M$. The inverse linear transformation is also easy to find, we have $\mathbf{R}^L = \mathbf{X}^L \hat{U}^{LT}$

$$\vec{R}_i = \sum_{j=1}^M U_{j,i}^L \vec{X}_j^L = A \sum_{j=1}^M \cos \left(\frac{2j-1}{N} \left(i - \frac{1}{2} \right) \pi \right) \vec{X}_j^L, \quad (6.29)$$

for $i = 1, 2, \dots, M$. We also have $\mathbf{R}^R = \mathbf{X}^R \hat{U}^{RT}$, so for $i = M+2, M+3, \dots, N$ we get

$$\begin{aligned} \vec{R}_i &= \sum_{j=1}^M U_{j,i-M-1}^R \vec{X}_j^R = A \sum_{j=1}^M \cos \left(\frac{2j-1}{N} \left(i - N - \frac{1}{2} \right) \pi \right) \vec{X}_j^R \\ &= -A \sum_{j=1}^M \cos \left(\frac{2j-1}{N} \left(i - \frac{1}{2} \right) \pi \right) \vec{X}_j^R. \end{aligned} \quad (6.30)$$

6.1.3 Overview

To simplify the coming calculations, it is convenient to introduce the following notation

$$C_q^p = \cos \left(\frac{2p-1}{N} \left(q - \frac{1}{2} \right) \pi \right). \quad (6.31)$$

Notice that this is very similar, but not equal, to the C_n^p of Chapter 5. Although not completely analogous to Eq. (5.19) it is now clear how these transformation coefficients can be calculated. The normal coordinates are (for $p = 1, 2, \dots, M$)

$$\vec{X}_p^L = \frac{2}{\sqrt{N}} \sum_{n=1}^M C_n^p \vec{R}_n, \quad (6.32)$$

$$\vec{X}_p^R = -\frac{2}{\sqrt{N}} \sum_{n=M+2}^N C_n^p \vec{R}_n. \quad (6.33)$$

The natural coordinates are (for $n = 1, 2, \dots, M$ and $n' = M+2, M+3, \dots, N$)

$$\vec{R}_n = \frac{2}{\sqrt{N}} \sum_{p=1}^M C_n^p \vec{X}_p^L, \quad (6.34)$$

$$\vec{R}_{n'} = -\frac{2}{\sqrt{N}} \sum_{p=1}^M C_{n'}^p \vec{X}_p^R. \quad (6.35)$$

And finally the total potential energy, Eq. (6.2), has the following terms

$$V(\vec{r}) = k\vec{r}^2, \quad (6.36)$$

$$\mathcal{U}_{bs}(\vec{r}, \mathcal{R}) = \frac{2k\vec{r}}{\sqrt{N}} \sum_{p=1}^M (-1)^p S^p \left(\vec{X}_p^L + \vec{X}_p^R \right), \quad (6.37)$$

$$\mathcal{U}_{bb}(\mathcal{R}) = \frac{k}{2} \sum_{p=1}^M \lambda_p \left[\vec{X}_p^{L^2} + \vec{X}_p^{R^2} \right]. \quad (6.38)$$

where

$$\lambda_p = \lambda_p^L = \lambda_p^R = 4 \sin^2 \left(\frac{2p-1}{2N} \pi \right). \quad (6.39)$$

We used $C_M^p = -(-1)^p S^p$ and $C_{M+2}^p = (-1)^p S^p$ where $S^p = \sin((2p-1)\pi/N)$.

6.2 Equation of motion

In this section we will construct the reduced dynamics of the middle bead, doing this will require the equation of motion of the normal coordinates. Before we go further however we should admit that in the previous section we cheated quite a bit, we said we would project all degrees-of-freedom of the bath onto the system of interest. But we only projected the coordinates of the beads (the bead-bath) onto the middle bead, we completely discarded the degrees-of-freedom of the surrounding medium. This surrounding medium consists of particles (which we will call the heat-bath) that interact with the system, their coordinates should also be integrated out. Yet for these we fall back to the original Langevin formalism, where their projection has already been accounted for by a Markovian friction force and a white random noise term (see Section 2.2). The motion of the middle bead should thus obey the following (overdamped) Langevin equation

$$\gamma \frac{d\vec{r}(t)}{dt} = \vec{\xi}_T(t) - \vec{\nabla}U(\vec{r}, \mathcal{R}), \quad (6.40)$$

where γ is the friction coefficient of the medium, $\vec{\xi}_T(t)$ the thermal noise and $U(\vec{r}, \mathcal{R})$ the total potential energy of \vec{r} . The thermal noise is characterised by the fluctuation-dissipation relation, thus its mean is zero and its correlation is given by Eq. (2.22), i.e. $\langle \vec{\xi}_T(t) \vec{\xi}_T(t') \rangle = 6\gamma k_B T \delta(t-t')$, with k_B Boltzmann's constant and T the temperature of the medium. Using Eq. (6.36)-(6.38) the equation of motion becomes

$$\gamma \frac{d\vec{r}(t)}{dt} = \vec{\xi}_T(t) - 2k\vec{r}(t) - \frac{2k}{\sqrt{N}} \sum_{p=1}^M (-1)^p S^p \left(\vec{X}_p^L(t) + \vec{X}_p^R(t) \right). \quad (6.41)$$

6.2.1 Motion of the normal coordinates

Before we can go any further we should know how the normal coordinates evolve in time. To find their equation of motion, we note that the heat-bath couples to the bead-bath the same way it coupled to the middle bead, i.e. through the original Langevin formalism. A bead from the bead-bath also feels the harmonic force of its neighbouring bead(s). In the overdamped limit we have (see Section 5.1)

$$\gamma \frac{d\vec{R}_n(t)}{dt} = \vec{\xi}_{T,n}(t) - k \left(2\vec{R}_n(t) - \vec{R}_{n+1}(t) - \vec{R}_{n-1}(t) \right), \quad (6.42)$$

with $\langle \vec{\xi}_{T,n}(t) \vec{\xi}_{T,m}(t') \rangle = 6\gamma k_B T \delta(t-t') \delta_{n,m}$, because the thermal forces between two different beads are uncorrelated. To calculate the motion of the normal coordinates

we write down the following

$$\gamma \frac{d\vec{X}_p^L(t)}{dt} = \frac{2\gamma}{\sqrt{N}} \sum_{n=1}^M C_n^p \frac{d\vec{R}_n}{dt}. \quad (6.43)$$

Filling in Eq. (6.42) gives

$$\gamma \frac{d\vec{X}_p^L(t)}{dt} = \frac{2k}{\sqrt{N}} \sum_{n=1}^M C_n^p \left(\vec{R}_{n+1}(t) + \vec{R}_{n-1}(t) - 2\vec{R}_n(t) \right) + \vec{f}_p^L(t), \quad (6.44)$$

where

$$\vec{f}_p^L(t) = \frac{2}{\sqrt{N}} \sum_{n=1}^M C_n^p \vec{\xi}_{T,n}(t). \quad (6.45)$$

Using Eq. (6.32) the equation of motion becomes

$$\gamma \frac{d\vec{X}_p^L(t)}{dt} = -2k\vec{X}_p^L(t) + \frac{2k}{\sqrt{N}} \sum_{n=1}^M C_n^p \left(\vec{R}_{n+1}(t) + \vec{R}_{n-1}(t) \right) + \vec{f}_p^L(t). \quad (6.46)$$

The summation of the second term on the right-hand side can be written as

$$\sum_{n=2}^{M+1} C_{n-1}^p \vec{R}_n(t) + \sum_{n=0}^{M-1} C_{n+1}^p \vec{R}_n(t). \quad (6.47)$$

Extracting some terms from the sums results in

$$\sum_{n=2}^M C_{n-1}^p \vec{R}_n(t) + C_M^p \vec{r}(t) + C_0^p \vec{R}_1(t) + \sum_{n=1}^{M-1} C_{n+1}^p \vec{R}_n(t), \quad (6.48)$$

here we used the fact that $\vec{R}_0 = \vec{R}_1$. Now we add the third term to the first summation and add a term that is zero ($C_{M+1}^p = 0$)

$$\sum_{n=1}^M C_{n-1}^p \vec{R}_n(t) + C_M^p \vec{r}(t) + \sum_{n=1}^{M-1} C_{n+1}^p \vec{R}_n(t) + C_{M+1}^p \vec{R}_M(t). \quad (6.49)$$

Adding the last term to the second summation gives us

$$C_M^p \vec{r}(t) + \sum_{n=1}^M [C_{n-1}^p + C_{n+1}^p] \vec{R}_n(t). \quad (6.50)$$

Using $\cos(x) + \cos(y) = 2 \cos((x-y)/2) \cos((x+y)/2)$

$$C_M^p \vec{r}(t) + 2C_{3/2}^p \sum_{n=1}^M C_n^p \vec{R}_n(t). \quad (6.51)$$

Here we recognise Eq. (6.32)

$$C_M^p \vec{r}(t) + \sqrt{N} C_{3/2}^p \vec{X}_p^L(t). \quad (6.52)$$

Putting this back into Eq. (6.46) gives

$$\gamma \frac{d\vec{X}_p^L(t)}{dt} = -2k\vec{X}_p^L(t) + \frac{2k}{\sqrt{N}} C_M^p \vec{r}(t) + 2k C_{3/2}^p \vec{X}_p^L(t) + \vec{f}_p^L(t). \quad (6.53)$$

Finally we notice that $2(C_{3/2}^p - 1) = -\lambda_p$ and use S^p to find

$$\gamma \frac{d\vec{X}_p^L(t)}{dt} = -k\lambda_p \vec{X}_p^L(t) - (-1)^p \frac{2k}{\sqrt{N}} S^p \vec{r}(t) + \vec{f}_p^L(t). \quad (6.54)$$

A very analogous calculation gives the motion of the right normal coordinates

$$\gamma \frac{d\vec{X}_p^R(t)}{dt} = -k\lambda_p \vec{X}_p^R(t) - (-1)^p \frac{2k}{\sqrt{N}} S^p \vec{r}(t) + \vec{f}_p^R(t), \quad (6.55)$$

with

$$\vec{f}_p^R(t) = -\frac{2}{\sqrt{N}} \sum_{n=M+2}^N C_n^p \vec{\xi}_{T,n}(t). \quad (6.56)$$

Solving these differential equations gives us the motion of the normal coordinates

$$\vec{X}_p^L(t) = \vec{X}_p^L(0) e^{-t/\tau_p} + \frac{1}{\gamma} \int_0^t d\tau \vec{f}_p^L(\tau) e^{(\tau-t)/\tau_p} - (-1)^p \frac{2k}{\gamma\sqrt{N}} S^p \int_0^t d\tau \vec{r}(\tau) e^{(\tau-t)/\tau_p}, \quad (6.57)$$

$$\vec{X}_p^R(t) = \vec{X}_p^R(0) e^{-t/\tau_p} + \frac{1}{\gamma} \int_0^t d\tau \vec{f}_p^R(\tau) e^{(\tau-t)/\tau_p} - (-1)^p \frac{2k}{\gamma\sqrt{N}} S^p \int_0^t d\tau \vec{r}(\tau) e^{(\tau-t)/\tau_p}, \quad (6.58)$$

with $\tau_p = \gamma/(k\lambda_p)$.

6.2.2 Motion of the middle bead

Putting the evolution of the normal coordinates into Eq. (6.41) gives

$$\begin{aligned} \gamma \frac{d\vec{r}(t)}{dt} &= \vec{\xi}_T(t) - 2k\vec{r}(t) - \frac{2k}{\sqrt{N}} \sum_{p=1}^M (-1)^p S^p \left[\left(\vec{X}_p^L(0) + \vec{X}_p^R(0) \right) e^{-t/\tau_p} \right. \\ &\quad \left. + \frac{1}{\gamma} \int_0^t d\tau \left(\vec{f}_p^L(\tau) + \vec{f}_p^R(\tau) \right) e^{(\tau-t)/\tau_p} - (-1)^p \frac{4k}{\gamma\sqrt{N}} S^p \int_0^t d\tau \vec{r}(\tau) e^{(\tau-t)/\tau_p} \right]. \end{aligned} \quad (6.59)$$

The last integral can be rewritten using integration by parts

$$\int_0^t d\tau \vec{r}(\tau) e^{(\tau-t)/\tau_p} = \tau_p \vec{r}(t) - \tau_p \vec{r}(0) e^{-t/\tau_p} - \tau_p \int_0^t d\tau e^{(\tau-t)/\tau_p} \frac{d\vec{r}(\tau)}{dt}. \quad (6.60)$$

When we put this back into the equation of motion, we can group some terms and identify them in the context of the generalised Langevin equation. We get

$$\gamma \frac{d\vec{r}(t)}{dt} = \vec{\xi}_T(t) - \vec{\nabla} W(\vec{r}) - \int_0^t d\tau K(t-\tau) \frac{d\vec{r}(\tau)}{dt} + \vec{\Phi}(t). \quad (6.61)$$

The effective potential

$$W(\vec{r}) = k \left(1 - \frac{4k}{\gamma N} \sum_{p=1}^M \tau_p S^{p^2} \right) \vec{r}^2(t). \quad (6.62)$$

The memory kernel

$$K(t) = \frac{8k^2}{\gamma N} \sum_{p=1}^M \tau_p S^{p^2} e^{-t/\tau_p}. \quad (6.63)$$

The effective noise term

$$\begin{aligned} \vec{\Phi}(t) = -\frac{2k}{\sqrt{N}} \sum_{p=1}^M (-1)^p S^p e^{-t/\tau_p} \left[\vec{X}_p^L(0) + \vec{X}_p^R(0) + (-1)^p \frac{4k}{\sqrt{N}} \tau_p S^p \vec{r}(0) \right. \\ \left. + \frac{1}{\gamma} \int_0^t d\tau \left(\vec{f}_p^L(\tau) + \vec{f}_p^R(\tau) \right) e^{\tau/\tau_p} \right]. \quad (6.64) \end{aligned}$$

To have a complete generalised Langevin description, we need to take a closer look at these three terms.

Effective potential

The effective potential can be simplified greatly

$$W(\vec{r}) = k \left(1 - \frac{4}{N} \sum_{p=1}^M \frac{\sin^2((2p-1)\pi/N)}{4 \sin^2((2p-1)\pi/2N)} \right) \vec{r}(t)^2 \quad (6.65)$$

$$= k \left(1 - \frac{4}{N} \sum_{p=1}^M \cos^2 \left(\frac{2p-1}{2N} \pi \right) \right) \vec{r}(t)^2 \quad (6.66)$$

$$= k \left(1 - \frac{4}{N} \frac{N}{4} \right) \vec{r}(t)^2 = 0. \quad (6.67)$$

So $W(\vec{r})$ appears to be a harmonic oscillator, yet it proves to be equal to zero when the summation is evaluated. The effective potential therefore vanishes.

Memory kernel

Now we look at the memory kernel. First notice that we can simplify the expression if τ_p and S^p are written in full

$$K(t) = \frac{8k}{N} \sum_{p=1}^M C_0^{p^2} e^{-t/\tau_p}. \quad (6.68)$$

We can not make this expression simpler but we can approximate it for $N \rightarrow \infty$. In full we have

$$K(t) = \frac{8k}{N} \sum_{p=1}^M \cos^2 \left(\frac{(2p-1)\pi}{2N} \right) \exp \left(-\frac{4kt}{\gamma} \sin^2 \left(\frac{(2p-1)\pi}{2N} \right) \right). \quad (6.69)$$

If we let N become very big, we take $\sin(x/N) \approx x/N$ and $\cos(x/N) \approx 1$. This is of course only correct when p is small, but when p approaches M the cosine comes close to zero, making the tail of the summation non-essential anyway.

$$K(t) = \frac{8k}{N} \sum_{p=1}^{\infty} \exp \left(-\frac{k\pi^2 t}{\gamma N^2} (2p-1)^2 \right) \quad (6.70)$$

$$= \frac{8k}{N} e^{-k\pi^2 t/\gamma N} \sum_{p=1}^{\infty} \exp \left(-\frac{4k\pi^2 t}{\gamma N^2} (p^2 - p) \right). \quad (6.71)$$

If we take $1/N \rightarrow dx$ and $p/N \rightarrow x$, we can convert the summation into an integration over x . The term $-x/N$ this will create, we neglect. The integration goes as follows

$$K(t) = 8k e^{-k\pi^2 t/\gamma N} \int_0^{\infty} dx \exp \left(-\frac{4k\pi^2 t}{\gamma} x^2 \right). \quad (6.72)$$

This is a Gaussian integral which will produce the following kernel for large N

$$K(t) = \sqrt{\frac{4k\gamma}{\pi}} \exp \left(-\frac{k\pi^2 t}{\gamma N^2} \right) t^{-1/2}. \quad (6.73)$$

Effective noise

Finally we take a look at the effective noise $\vec{\Phi}(t)$. It essentially consists of the initial configuration of the chain and the thermal random forces of the heat-bath. Because this is a linear combination of constants and Gaussian variables, it itself is a Gaussian variable. Therefore we need to find its mean and correlation to fully describe it. We clearly have $\langle \vec{f}_p^L(t) \rangle = \langle \vec{f}_p^R(t) \rangle = 0$, we thus find

$$\langle \vec{\Phi}(t) \rangle = -\frac{2k}{\sqrt{N}} \sum_{p=1}^M (-1)^p S^p e^{-t/\tau_p} \left[\langle \vec{X}_p^L(0) \rangle + \langle \vec{X}_p^R(0) \rangle + (-1)^p \frac{4k}{\sqrt{N}} \tau_p S^p \langle \vec{r}(0) \rangle \right]. \quad (6.74)$$

The mean of the initial values on the right-hand side are not trivial to determine. However, we can assume that, for long times, the system and the bead-bath will go

to equilibrium, irrespective of their specific initial values. We therefore determine the mean and correlation after a long time, when equilibrium has certainly been reached. We have $\langle \vec{\Phi}(t) \rangle_{eq} = \langle \vec{\Phi}(t \rightarrow \infty) \rangle$. Because the mean of the initial values is surely independent of time, the only time dependent factor is e^{-t/τ_p} which will go to zero for large times. Therefore

$$\langle \vec{\Phi}(t) \rangle_{eq} = 0. \quad (6.75)$$

Now we calculate $\langle \vec{\Phi}(t)\vec{\Phi}(t') \rangle_{eq}$, which should obey the fluctuation-dissipation relation. It is clear from Eq. (6.64) that writing down the product of $\vec{\Phi}(t)$ and $\vec{\Phi}(t')$ will become a very lengthy expression. Therefore we first notice that all cross-terms with the normal noise will be zero (because neither the initial position nor the random forces are mutually correlated), we will not write them down.

$$\begin{aligned} \langle \vec{\Phi}(t)\vec{\Phi}(t') \rangle &= \frac{4k^2}{N} \sum_{p,q=1}^M (-1)^{p+q} S^p S^q e^{-t/\tau_p} e^{-t'/\tau_q} \left[\langle \vec{X}_p^L(0)\vec{X}_q^L(0) \rangle + \langle \vec{X}_p^L(0)\vec{X}_q^R(0) \rangle \right. \\ &+ (-1)^q \frac{4k}{\sqrt{N}} \tau_q S^q \langle \vec{X}_p^L(0)\vec{r}(0) \rangle + \langle \vec{X}_p^R(0)\vec{X}_q^R(0) \rangle + \langle \vec{X}_p^R(0)\vec{X}_q^L(0) \rangle \\ &+ (-1)^q \frac{4k}{\sqrt{N}} \tau_q S^q \langle \vec{X}_p^R(0)\vec{r}(0) \rangle + (-1)^p \frac{4k}{\sqrt{N}} \tau_p S^p \langle \vec{r}(0)\vec{X}_q^L(0) \rangle \\ &+ (-1)^p \frac{4k}{\sqrt{N}} \tau_p S^p \langle \vec{r}(0)\vec{X}_q^R(0) \rangle + (-1)^{p+q} \frac{8k^2}{N} \tau_p \tau_q S^p S^q \langle \vec{r}(0)^2 \rangle \\ &\left. + \frac{1}{\gamma^2} \int_0^t d\tau \int_0^{t'} d\tau' \langle (\vec{f}_p^L(\tau) + \vec{f}_p^R(\tau)) (\vec{f}_q^L(\tau') + \vec{f}_q^R(\tau')) \rangle e^{\tau/\tau_p} e^{\tau'/\tau_q} \right]. \end{aligned} \quad (6.76)$$

We again examine this formula for very large times, when thermalisation is achieved. For $t \rightarrow \infty$ and $t' \rightarrow \infty$, the two exponential functions will go to zero. Many terms in the summation are not functions of t or t' , they all go to zero due to the exponentials. The only term that could possibly withstand these exponentials is the last term. We can therefore write

$$\begin{aligned} \langle \vec{\Phi}(t)\vec{\Phi}(t') \rangle_{eq} &= \frac{4k^2}{\gamma^2 N} \sum_{p,q=1}^M (-1)^{p+q} S^p S^q e^{-t/\tau_p} e^{-t'/\tau_q} \int_0^t d\tau \int_0^{t'} d\tau' \left(\langle \vec{f}_p^L(\tau)\vec{f}_q^L(\tau') \rangle \right. \\ &\left. + \langle \vec{f}_p^L(\tau)\vec{f}_q^R(\tau') \rangle + \langle \vec{f}_p^R(\tau)\vec{f}_q^L(\tau') \rangle + \langle \vec{f}_p^R(\tau)\vec{f}_q^R(\tau') \rangle \right) e^{\tau/\tau_p} e^{\tau'/\tau_q}. \end{aligned} \quad (6.77)$$

To go any further we need to know what the correlation of the normal forces is. A short calculation will give the following result

$$\langle \vec{f}_p^a(t)\vec{f}_q^b(t') \rangle = 6\gamma k_B T \delta(t-t') \delta_{p,q} \delta_{a,b}. \quad (6.78)$$

Therefore

$$\langle \vec{\Phi}(t)\vec{\Phi}(t') \rangle_{eq} = \frac{48k_B T k^2}{\gamma N} \sum_{p=1}^M S^{p^2} e^{-(t+t')/\tau_p} \int_0^t d\tau \int_0^{t'} d\tau' \delta(\tau - \tau') e^{\tau/\tau_p} e^{\tau'/\tau_p} \quad (6.79)$$

$$= \frac{48k_B T k^2}{\gamma N} \sum_{p=1}^M S^{p^2} e^{-(t+t')/\tau_p} \int_0^{\min(t,t')} d\tau e^{2\tau/\tau_p} \quad (6.80)$$

$$= \frac{24k_B T k^2}{\gamma N} \sum_{p=1}^M \tau_p S^{p^2} \left(e^{-(t+t'-2\min(t,t'))/\tau_p} - e^{-(t+t')/\tau_p} \right) \quad (6.81)$$

$$= \frac{24k_B T k^2}{\gamma N} \sum_{p=1}^M \tau_p S^{p^2} \left(e^{-|t-t'|/\tau_p} - e^{-(t+t')/\tau_p} \right). \quad (6.82)$$

In the last step we used $|t - t'| = t + t' - 2 \min(t, t')$. Because we let time become very large, the second term will approach zero. The absolute difference between the large times t and t' can definitely be a finite value, therefore the first term is the only one that will not vanish when we thermalise. If we also evaluate $\tau_p S^{p^2}$, we get

$$\langle \vec{\Phi}(t)\vec{\Phi}(t') \rangle_{eq} = \frac{24k_B T k}{N} \sum_{p=1}^M C_0^{p^2} e^{-|t-t'|/\tau_p} \quad (6.83)$$

$$= 3k_B T K(|t - t'|), \quad (6.84)$$

which is exactly what we need for the fluctuation-dissipation relation to hold. Now we are ready to fully present the generalised Langevin equation of the middle bead.

6.3 Generalised Langevin equation

Consider a chain of $N = 2M + 1$ beads that are interconnected by harmonic springs (with spring constant k) and submerged in a heat-bath at temperature T and with friction coefficient γ . Suppose we project all degrees-of-freedom of this ensemble onto the middle bead of the chain to obtain its reduced dynamics. The projection of the heat-bath was done using the original Langevin description, while the projection of the chain was performed using the generalised Langevin description. The reduced dynamics of the bead $\vec{r}(t)$ obeys the following generalised Langevin equation

$$\gamma \frac{d\vec{r}(t)}{dt} = \vec{\xi}_T(t) - \vec{\nabla} W(\vec{r}) - \int_0^t d\tau K(t - \tau) \frac{d\vec{r}(\tau)}{dt} + \vec{\Phi}(t). \quad (6.85)$$

The terms on the right-hand side are interpreted in the following way:

The random thermal forces originating from the heat-bath

$$\langle \vec{\xi}_T(t) \rangle = 0, \quad (6.86)$$

$$\langle \vec{\xi}_T(t)\vec{\xi}_T(t') \rangle = 6\gamma k_B T \delta(t - t'). \quad (6.87)$$

The effective potential

$$W(\vec{r}) = 0. \quad (6.88)$$

The memory kernel

$$K(t) = \frac{8k}{N} \sum_{p=1}^M \cos^2 \left(\frac{2p-1}{N} \frac{\pi}{2} \right) e^{-t/\tau_p} \quad (6.89)$$

$$\approx \sqrt{\frac{4k\gamma}{\pi}} \exp \left(-\frac{k\pi^2 t}{\gamma N^2} \right) t^{-1/2}. \quad (6.90)$$

The characteristic time

$$\tau_p = \frac{\gamma}{4k \sin^2((2p-1)\pi/2N)} \quad (6.91)$$

$$\approx \frac{\gamma N^2}{k\pi^2(2p-1)^2}. \quad (6.92)$$

The effective noise in equilibrium

$$\langle \vec{\Phi}(t) \rangle_{eq} = 0, \quad (6.93)$$

$$\langle \vec{\Phi}(t) \vec{\Phi}(t') \rangle_{eq} = 3k_B T K(|t-t'|). \quad (6.94)$$

The approximations are considered for $N \rightarrow \infty$.

6.4 Extension to driven baths

In this chapter we take a look at two cases where the heat-bath possesses some driving force that will take our system away from equilibrium. These driving forces are, in fact, the ones from Section 5.3 and Section 5.4. First we look at a constant force applied on the first bead. For long times the system will regain thermalisation, but during the transient regime where the chain responds to the new force the system will not be in equilibrium. In the second case the heat-bath exerts, apart from the thermal forces, random active forces on the chain.

6.4.1 Constant force

If we add a constant force of strength f to the first bead in the x direction, we need to change Eq. (6.42) into

$$\gamma \frac{d\vec{R}_n(t)}{dt} = \vec{\xi}_{T,n}(t) - k \left(2\vec{R}_n(t) - \vec{R}_{n+1}(t) - \vec{R}_{n-1}(t) \right) + \vec{f}_n(t), \quad (6.95)$$

with $\vec{f}_n(t) = f\delta_{n,0}H(t)\vec{e}_x$ and $H(t)$ the Heaviside function (see Eq. (4.3)). After some simple calculations one finds that this will add a term in the motion of the left normal coordinates $\vec{X}_p^L(t)$. To Eq. (6.57) we need to add $(2f/\gamma\sqrt{N})C_0^p\tau_p [1 - e^{-t/\tau_p}] H(t)\vec{e}_x$,

which on its turn adds a term to the generalised Langevin equation of the middle bead. It becomes

$$\gamma \frac{d\vec{r}(t)}{dt} = \vec{\xi}_T(t) - \vec{\nabla}W(\vec{r}) - \int_0^t d\tau K(t-\tau) \frac{d\vec{r}(\tau)}{dt} + \vec{\Phi}(t) + \vec{\mathcal{F}}(t). \quad (6.96)$$

The last term in this expression can be seen as an effective force on the middle bead, originating from the constant force on the first bead. It has the following expression

$$\vec{\mathcal{F}}(t) = \frac{2f}{N} \sum_{p=1}^M (-1)^p \cos\left(\frac{2p-1}{N} \frac{\pi}{2}\right) \cot\left(\frac{2p-1}{N} \frac{\pi}{2}\right) \left[e^{-t/\tau_p} - 1\right] H(t) \vec{e}_x. \quad (6.97)$$

It is clear that when $t \ll \tau_M$ the extra force on the middle bead is essentially zero. The force has not yet had time to propagate through the chain to the middle bead, leaving this bead unaware of its presence. When it does reach the bead, the bead will undergo a transient phase where the extra force on it will build up to a constant value at $t \rightarrow \infty$. Then the system is back in equilibrium, which is expected for a conservative driving force. This constant value should be equal to the original constant force since it has fully propagated the chain. We indeed find this in our model for large N

$$\vec{\mathcal{F}}(t \rightarrow \infty) = -\frac{2f}{N} \sum_{p=1}^M (-1)^p \cos\left(\frac{2p-1}{N} \frac{\pi}{2}\right) \cot\left(\frac{2p-1}{N} \frac{\pi}{2}\right) \vec{e}_x \quad (6.98)$$

$$= -\frac{2f}{N} (-M) \vec{e}_x = f \vec{e}_x. \quad (6.99)$$

Figure 6.1 shows the time-evolution of the effective force's magnitude compared to that of the constant force. It is a numerical evaluation of Eq. (6.97). As expected, the effective force is, for early times, zero and for long times it is equal to f . It reaches about half of its final value at the longest characteristic time τ_1 . In fact, in Section 5.3 it was shown that the effect of the force diffuses through the chain, so that the time to reach the middle bead is of the order $(N/2)^2$, which on its term is of the order of the longest characteristic time τ_1 .

6.4.2 Active forces

Now assume that the heat-bath contains a property that will, after integrating out its fast moving variables, inflict an extra random force on the bead-bath. We change the equation of motion of the beads, Eq. (6.42), into

$$\gamma \frac{d\vec{R}_n(t)}{dt} = \vec{\xi}_{T,n}(t) - k \left(2\vec{R}_n(t) - \vec{R}_{n+1}(t) - \vec{R}_{n-1}(t) \right) + \vec{\xi}_{A,n}(t). \quad (6.100)$$

We first consider a general case where the new random force is Gaussian distributed with zero mean and a correlation that is a function of the absolute difference in time and uncorrelated between beads

$$\langle \vec{\xi}_{A,n}(t) \rangle = 0, \quad (6.101)$$

$$\langle \vec{\xi}_{A,n}(t) \vec{\xi}_{A,m}(t') \rangle = F(|t-t'|) \delta_{n,m}. \quad (6.102)$$

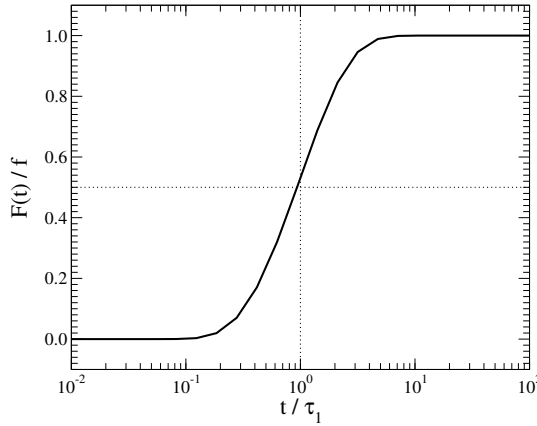


Figure 6.1: Lin-log plot of the relative magnitude of the effective force to the constant force as a function of time. We have $F(t) = |\vec{F}(t)|$. The vertical dotted line indicates the longest characteristic time τ_1 . The horizontal dotted line is drawn at $F = f/2$. The length of the chain is $N = 1025$, the remaining parameters are $\gamma = 1$ and $k = 3$.

We assume that the active random forces do not couple to the middle bead in Eq. (6.40), extending the model to one where they do couple is trivial and does not yield conceptually different results. If we write the normal random forces as follows we can keep much of the previous calculations unchanged

$$\vec{f}_p^L(t) = \frac{2}{\sqrt{N}} \sum_{n=1}^M C_n^p \left(\vec{\xi}_{T,n}(t) + \vec{\xi}_{A,n}(t) \right), \quad (6.103)$$

$$\vec{f}_p^R(t) = -\frac{2}{\sqrt{N}} \sum_{n=M+2}^N C_n^p \left(\vec{\xi}_{T,n}(t) + \vec{\xi}_{A,n}(t) \right). \quad (6.104)$$

Notice that we now have

$$\langle \vec{f}_p^a(t) \vec{f}_q^b(t') \rangle = 6\gamma k_B T \delta(t-t') \delta_{p,q} \delta_{a,b} + F(|t-t'|) \delta_{p,q} \delta_{a,b}. \quad (6.105)$$

This will seriously affect the original equilibrium correlation of the effective noise (its mean remains zero though). We again take t and t' large, but we clearly do not regain the equilibrium result. Therefore we call this the nonequilibrium effective noise

$$\langle \vec{\Phi}(t) \vec{\Phi}(t') \rangle_{neq} = 3k_B T \left(K(|t-t'|) + K_+(t, t') \right), \quad (6.106)$$

with

$$K_+(t, t') = \frac{8k^2}{3\gamma^2 k_B T N} \sum_{p=1}^M S^{p^2} \int_0^t d\tau \int_0^{t'} d\tau' F(|\tau - \tau'|) e^{-(t-\tau)/\tau_p} e^{-(t'-\tau')/\tau_p}. \quad (6.107)$$

This result is precisely what C. Maes predicts in [129]. The nonequilibrium effective random noise now consists of an entropic term that obeys the fluctuation-dissipation relation and a term that doesn't, this term is called the frenetic contribution. The expression for the frenetic $K_+(t, t')$ can be solved for some specific forms of the correlation of the new random force $F(|t - t'|)$. Here we will present the case where the driving force is characterised by an exponential autocorrelation

$$F(|t - t'|) = 3C \exp(-|t - t'|/\tau_A), \quad (6.108)$$

i.e. the form we used for the active forces in the previous chapter. After a lengthy calculation, which is given in Appendix E, one finds

$$K_+(|t - t'|) = \frac{8Ck^2}{\gamma^2 k_B T N} \sum_{p=1}^M \frac{\tau_p^2 S^{p^2}}{1 - (\tau_p/\tau_A)^2} \left[e^{-|t-t'|/\tau_A} - (\tau_p/\tau_A) e^{-|t-t'|/\tau_p} \right]. \quad (6.109)$$

Just as the equilibrium kernel, K_+ is a sum over exponentials and only a function of the absolute difference in time, i.e. $|t - t'|$. We can approximate this expression when we allow some assumptions to be made.

Large persistence time

First consider $\tau_A \gg \tau_1$, then we find a very simple form

$$K_+(|t - t'|) = \frac{CN}{k_B T} \exp(-|t - t'|/\tau_A), \quad (6.110)$$

we used $\sum_{p=1}^M (S^p \tau_p)^2 = \gamma^2 N^2 / 8k^2$ for large N . This expression can be understood in the following way: in the previous section, on the constant force, we found that a force on a bead needs a duration of order τ_1 to fully reach the middle bead (see Fig. 6.1). Because the persistence in one direction of these active forces is indeed much longer than τ_1 , they act like a constant force for a considerable amount of time. Therefore, all beads fully transpose the active force on them to the middle bead, yielding N times Eq. (6.108). The nonequilibrium effective noise subsequently becomes

$$\langle \vec{\Phi}(t) \vec{\Phi}(t') \rangle_{neq} = 3k_B T K(|t - t'|) + N F(|t - t'|). \quad (6.111)$$

One can interpret this result as two distinct effective noises. The first are the equilibrium thermal random forces, governed by memory kernel $K(t)$. The second are the original active forces that act on every bead, but enhanced by a factor N . This result is general for any function F that decays with a typical time scale $\tau_A \gg \tau_1$.

Small persistence time

When we take $\tau_A \ll \tau_M$ in Eq. (6.109), we can do the following

$$K_+(|t - t'|) = -\frac{8Ck^2}{\gamma^2 k_B T N} \sum_{p=1}^M S^{p^2} \tau_A^2 \left[e^{-|t-t'|/\tau_A} - (\tau_p/\tau_A) e^{-|t-t'|/\tau_p} \right] \quad (6.112)$$

$$= -\frac{2\tau_A^2 C k^2}{\gamma^2 k_B T} e^{-|t-t'|/\tau_A} + \frac{\tau_A C}{\gamma k_B T} K(|t - t'|), \quad (6.113)$$

where we used the definition of the memory kernel and the fact that $\sum_{p=1}^M \mathcal{S}^{p^2} \approx N/4$ for large N . The first term can be neglected since τ_A is very small. The nonequilibrium effective noise becomes

$$\langle \vec{\Phi}(t) \vec{\Phi}(t') \rangle_{neq} = 3k_B T_* K(|t - t'|), \quad (6.114)$$

with $k_B T_* = k_B T + \tau_A C / \gamma$. We thus find an effective noise that has an equilibrium expression but with a higher effective temperature than in the case where no active forces are present. The system will therefore appear to thermalise under this new temperature. The reason for this behaviour is because the active forces, with very small τ_A , mimic the thermal noise $\vec{\xi}_{T,n}$ on the beads. The correlation of the active forces, Eq. (6.102) together with Eq. (6.108), indeed becomes approximately¹ equal to $6\tau_A C \delta(t - t') \delta_{n,m}$. The two Gaussian white noises, thermal and active, can thus be combined into one $\vec{\xi}_n = \vec{\xi}_{T,n} + \vec{\xi}_{A,n}$. Naturally, this new random force is also Gaussian distributed with zero mean. Its autocorrelation is

$$\langle \vec{\xi}_n(t) \cdot \vec{\xi}_m(t') \rangle = 6\gamma \left[k_B T + \frac{\tau_A C}{\gamma} \right] \delta(t - t') \delta_{n,m}. \quad (6.116)$$

When using this noise in Eq. (6.42) instead of $\vec{\xi}_{T,n}$, it is clear that we can redo the equilibrium calculations, but with the effective temperature $k_B T_*$. This will also yield the nonequilibrium effective noise, Eq. (6.114), derived above.

Figure 6.2 shows the numerical evaluation of $K(t)$ and $K_+(t)$, Eq. (6.89) and Eq. (6.109) respectively. For very early times, the equilibrium memory kernel is constant. Thereafter, for times up to τ_1 , this kernel shows a power-law decay after which it decays exponentially, as approximation (6.90) predicts. The behaviour of the frenetic contribution correctly shows a dependency on the value of τ_A . In Fig. 6.3a we demonstrate that for small τ_A the frenetic contribution is indeed equal to the equilibrium memory kernel multiplied by $\tau_A C / \gamma k_B T$. For large τ_A , Fig. 6.3b shows that the equilibrium memory kernel is not exponential for early times while the frenetic contribution is for all times, corresponding nicely with Eq. (6.110). The maximum value of the frenetic contribution never exceeds $CN/k_B T$, which Fig. 6.2 clearly shows.

To find the time-evolution of the middle bead, one should solve Eq. (6.85) using the nonequilibrium version of the fluctuation-dissipation relation (6.106). Since the equation is linear, this can be done using Laplace transform methods. Alternatively, one could solve the set of equations of motion (6.100). This alternative derivation was already performed in Section 5.4. In that section, the more general case of a Rouse chain moving in a viscoelastic environment and in the presence of active forces was studied. Little attention was paid to the viscous limit.

Using result (5.115) or by direct solution of Eq. (6.85) it is possible to obtain the mean-squared displacement $\Delta_m^2(t) \equiv \langle (\vec{r}(t) - \vec{r}(0))^2 \rangle$ of the middle bead for the case

¹We used here the following definition of the Dirac delta function

$$\delta(x) = \lim_{\epsilon \rightarrow 0} \frac{1}{2\epsilon} \exp(-|x|/\epsilon). \quad (6.115)$$

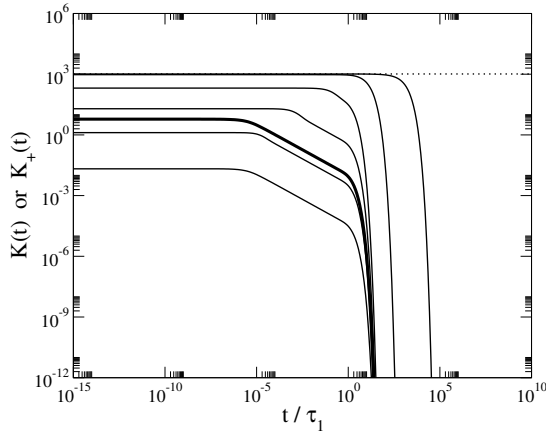


Figure 6.2: Log-log plot of the two kernels as a function of time for $N = 1025$. The solid black line represents $K(t)$, while the other thin lines are $K_+(t)$. With $\tau_A/\tau_1 = 10^{-7}, 10^{-5}, 10^{-3}, 10^{-1}, 10^1$ and 10^3 . The higher the value of τ_A/τ_1 , the higher the line lies. The other parameters are $k_B T = \gamma = C = 1$ and $k = 3$. The straight dotted line is drawn at $CN/k_B T$.

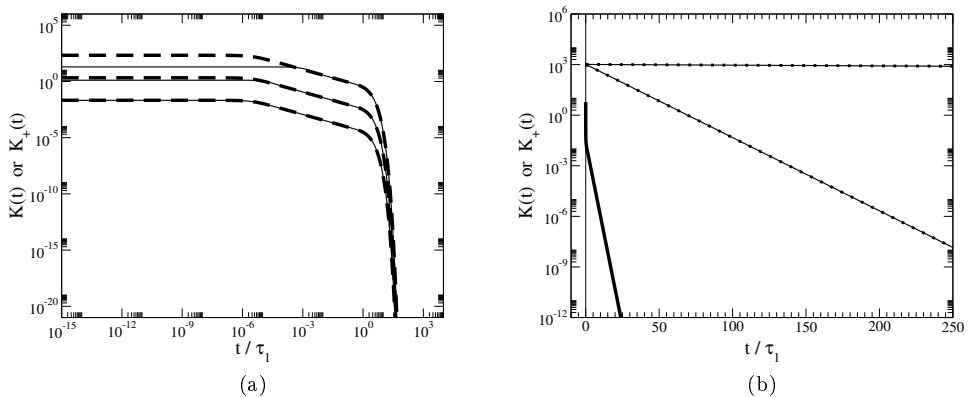


Figure 6.3: (a) Log-log plot that shows the same three lowest $K_+(t)$ curves from Fig. 6.2, with $\tau_A/\tau_1 = 10^{-7}, 10^{-5}$ and 10^{-3} . Also shown in dashed lines are the weighted equilibrium memory kernels, i.e. $(\tau_A C/\gamma k_B T)K(t)$. (b) Log-linear plot of the two upper $K_+(t)$ curves from Fig. 6.2, with $\tau_A/\tau_1 = 10^1$, and 10^3 . Also shown are $K(t)$ (solid black line) and Eq. (6.110) (dotted lines).

of exponentially correlated active noise. The result is (taking $\alpha = 1$ in Eq. (5.115))

$$\begin{aligned} \Delta_m^2(t) = & \frac{6}{\gamma N} \left(k_B T + \frac{\tau_A C}{\gamma} \right) t \\ & + \frac{12 k_B T}{\gamma N} \sum_{p=2, \text{even}}^{N-1} \tilde{\tau}_p \left(1 - \exp(-t/\tilde{\tau}_p) \right) + \frac{6 \tau_A^2 C}{\gamma^2 N} \left(\exp(-t/\tau_A) - 1 \right) \\ & + \frac{12 C}{\gamma^2 N} \sum_{p=2, \text{even}}^{N-1} \frac{\tau_A \tilde{\tau}_p^2}{\tau_A - \tilde{\tau}_p} \left[\frac{\tau_A}{\tau_A + \tilde{\tau}_p} \left(1 - \exp(-(\tau_A^{-1} + \tilde{\tau}_p^{-1})t) \right) \right. \\ & \left. + \frac{1}{2} \left(\exp(-2t/\tilde{\tau}_p) - 1 \right) \right], \quad (6.117) \end{aligned}$$

with $\tilde{\tau}_p = \tau_{(p+1)/2}$. In absence of active forces ($C = 0$) only two terms survive. It is well known that for that case there are three time regimes (see Section 5.2). For $t < \tau_M$, the bead doesn't feel the effect of the neighbouring beads yet, and it diffuses, i.e. $\Delta_m^2(t) \sim t$. For $t > \tau_1$ the bead follows the diffusion of the chain as a whole, i.e. we have again $\Delta_m^2(t) \sim t$ but with a diffusion constant that is a factor N smaller. Finally, in the intermediate time regime $\tau_M < t < \tau_1$ the bead feels that it is inside a chain leading to the subdiffusion $\Delta_m^2(t) \sim t^{1/2}$. This behaviour is shown in Fig. 6.4.

In the presence of active forces the motion is more complicated. Remember that a free particle in presence of thermal and exponentially correlated active forces (see Section 4.1), initially diffuses until $t \approx \tau_A$. Thereafter it superdiffuses with exponent 2, after which it again diffuses. If the particle is part of a chain we expect that, as was the case in the absence of active forces, its motion will be modified in the time regime $\tau_M < t < \tau_1$. In fact, in Section 5.4 we have shown that the bead will then superdiffuse but with an exponent $3/2$.

We can now envisage two scenarios. When persistence times are large, i.e. $\tau_A \gg \tau_1$, then the bead will, for early times, behave like a free particle. So it will first diffuse and then superdiffuse with exponent 2. Then the following intermediate time-scale is dominated by the influence of the chain, the bead will superdiffuse with exponent $3/2$. For long times the bead again acts like a free particle, first superdiffusing with exponent 2 after which it will continue to diffuse for all time. This behaviour is shown in Fig. 6.4 for $\tau_A = 10\tau_1$. When persistence times are small, i.e. $\tau_A \ll \tau_1$, the bead will show the behaviour described above only up to τ_A after which it moves like a bead in a chain with only thermal noise. It therefore yields the same profile as the dynamics in a non-active bath but with a larger pre-factor. This is in agreement with what we learned from the frenetic contribution where, for $\tau_A \ll \tau_1$, the behaviour of the bead could be described in terms of an effective temperature. This behaviour is shown in Fig. 6.4 for $\tau_A = 10^{-7}\tau_1$.

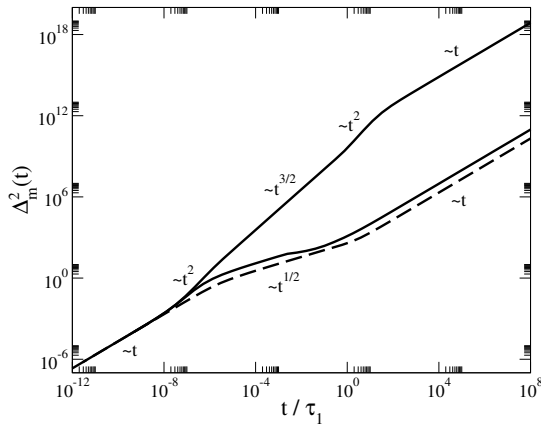


Figure 6.4: Log-log plot of the the mean-squared displacement of the middle bead in a Rouse chain ($N = 1025$, $k = 3$) as a function of time. The dashed line represents the dynamics in a passive viscous bath with $k_B T = \gamma = 1$. The full lines include active forces with $C = 10^3$ and $\tau_A/\tau_1 = 10$ for the top line and $\tau_A/\tau_1 = 10^{-7}$ for the bottom line. Also indicated are the different regimes of diffusive, subdiffusive and superdiffusive behaviour.

7 | Conclusion and Perspective

*Your perceived failure can
become a catalyst for profound reinvention.*

Conan O'Brien

In a recent article [130], Jennifer Ross argued that cell biology experiences a similar problem as the field of cosmology. In cosmology, *dark matter* is an undefined type of matter that makes up about 27% of the mass and energy of the observable universe. This dark matter can, with current experiments, not be observed directly but its properties can be studied through its gravitational effects on detectable entities. Ross states that cell biology has an equivalent “dark matter” paradigm. In a cell, there are many important species of macromolecules that we can not observe with fluorescent or dynamic reporters. However, they interact weakly with many cellular processes, resulting in important biochemical effects. Through experiments on strongly interacting cellular species, we can indirectly determine the characteristics of this “dark matter”. An example that nicely fits with our research is that of the speed of kinesin motors inside a living cell. Experiments [85, 86, 131] have shown that their speed is lower *in vitro* than in the complex interior of a cell. However, naively one might expect the opposite to be true. Such discrepancies, Ross argues, can be explained by the influence of this “dark matter”. She urges researchers to study these weak and transient interactions to shine some light on this “dark matter”, which will generate a more profound understanding of the complexities of the cell. We hope that our work on biological processes in active viscoelastic baths can contribute to this endeavour.

In Chapter 2, we constructed a generalised Langevin equation that could be used as a model for the dynamics in an active viscoelastic bath. The following chapters showed that, when applied to a whole range of specific systems, this equation can often be solved exactly. It is therefore a tractable tool to describe many cellular processes. Further work can be done to extend our model to include more complex features of a cell, yielding an even more realistic model for the dynamics in the cytosol. A first possible extension is the application of non-Gaussian active noise.

In Chapter 3, we combined existing numerical schemes to construct an algorithm that can cope with the non-trivial generalised Langevin equation of Chapter 2. The simulation results presented in this document proved that our numerical scheme produces accurate data. It can therefore be readily used to simulate systems that were

not considered in our work. We do believe that the algorithm can be optimized quite extensively, both in the context of memory usage as that of a kernel cut-off.

In Chapter 4, we investigated how a particle behaves in a particular potential when it is surrounded by an active viscoelastic bath. We found that a free particle acquires two new anomalous diffusion regimes on top of the t^α regime from a non-active bath, where $0 \leq \alpha \leq 1$ characterises the viscoelasticity of the bath. The new exponents are 2α and $2\alpha - 1$, superdiffusion is therefore possible for a free particle. We also found that, in a viscous bath, the diffusion coefficient becomes enhanced. These results can, qualitatively at least, explain the cross-over in time exponents found in the anomalous diffusion of tracer particles in living cells [80]. They can also explain the decrease of the exponent when the activity of the cell is decreased [20, 82]. The persistence time of the active forces in a cell could be estimated to be of the order of seconds. A harmonic oscillator showed the same time behaviour as a free particle for early times. For long times, it reached a nonequilibrium steady state. This steady state does not depend on α when the persistence time is large, but does when this time is small. An effective temperature could be calculated for these steady states. When applying this theory to the dynamics of kinesin molecular motors, we found that the motor showed overall faster dynamics in an active bath. This resulted in a higher probability for performing the next step. These results suggest an increased speed of the kinesin motor in a living active cell (which could explain Ross' example given above). More experiments could be done to understand the dependence on the activity of the motor's speed. For a particle in a double well surrounded by a non-active viscoelastic bath, we empirically found a generalised escape rate for $\alpha > 0.5$. More simulations are required to test the applicability of this escape rate, especially simulations that find the survival probability for long times. Although this is a long-standing problem, a generalised escape rate should also be derived analytically. For active viscoelastic baths, we found that the steady state probability distribution of the particle was dependent on α when the persistence time is small. When, however, it is large, all viscoelastic baths will yield the same distribution. For these large persistence time baths, we discovered that they can provide an effective potential which has the same expression as the original potential. This effective potential can not, however, be used to describe the non-intuitive behaviour of the survival probability. This quantity was on the contrary different for different values of α , and showed an interesting cross-over when the height of the energy barrier is varied. The model of the double well was used to investigate the folding dynamics of DNA-hairpins in an active and complex environment. It was found that the effective potential drastically lowered the effective energy barrier and that the folding times are considerably reduced in these baths.

In Chapter 5, we first discussed the Rouse model and showed how this simple polymer model behaves in a viscoelastic bath. Then, applying a constant force on the first bead, we found that the transient length is α dependent, yielding a new experimental technique to measure the viscoelasticity of the cytosol. We found that the polymer displays an increasing trumpet shape in the transient regime, while also providing an analytic expression for this shape in equilibrium. From the mean velocity of the middle bead, we discovered how the force-front propagates through the polymer, it goes as $n^{2/\alpha}$ where n is the monomer number. Including self-avoidance and finite extendible springs in this model, we found, through simulations, two new length-force relations. One of which was already predicted by Sakaue [14], the other still needs a

theoretical explanation. Simulations where $\alpha \neq 1$ should also be performed for this system. Finally, we introduced active forces to the Rouse model in a viscoelastic bath. The centre of mass behaved like a free particle with a smaller diffusion coefficient. For the middle bead, we found that its diffusion displays many time-regimes, some of them can result in superdiffusion. We showed that the polymer swells in an active bath with $\alpha > 2/3$, when $\alpha < 2/3$ it does not. This prediction should be experimentally verified. To understand how a real polymer reacts to the activity of a viscoelastic bath, we simulated semi-flexible chains in such an environment. Before doing so we argued that an approximate theory can be constructed from the original (Rouse) theory. We found that the diffusion of the centre of mass of a semi-flexible chain does not deviate from that of a flexible chain. The dynamics of the middle bead in a non-active viscoelastic bath appeared to be well described by the approximate theory (at least for the time scales that we tested), yielding new time exponents. When the bath was active, however, the approximate theory failed since it did not predict the simulated data correctly for long times. More work can be done to refine this approximate theory. We also performed some preliminary simulations on the end-to-end distance of a semi-flexible chain in an active viscoelastic bath. A diverse response, that included both shrinking and swelling of the polymer, emerged. We gave some predictions on the possible mechanics behind this behaviour but more analytic research should be done. Simulations that reach the steady state of the end-to-end distance are also essential to understand these mechanics.

In Chapter 6, we reviewed how one finds the generalised Langevin equation of the middle bead in a Rouse chain. We extended this calculation to one where the surrounding bath has a driving agent. This yielded a nonequilibrium version of the generalised Langevin equation. We derived the time-response of the middle bead that resulted from a constant force on the first bead. We also found the frenetic contribution for a heat-bath with an extra random force. When this random force had the form of active forces, this frenetic contribution could be simplified greatly for two limiting cases. We provided an interpretation for both cases. Many other driving agents can be introduced to this system. The resulting generalised Langevin equation is an interesting topic for theoretical research.

In the light of our attempt to explain some biological phenomena through physical concepts, we like to conclude with a quote by Richard P. Feynman: *“There’s so much distance between the fundamental rules and the final phenomenon, that it’s almost unbelievable that the final variety of phenomena can come from such a steady operation of such simple rules.”* It nicely summarises the connection between the “invisible” microscopic world and the “visible” macroscopic world it creates.

A | Functions and Transformations

Mathematics is the gate and key to the sciences.

Roger Bacon

A.1 Mittag-Leffler function

The Mittag-Leffler function $E_{\alpha,\beta}(x)$ is, most generally, defined as the following series

$$E_{\alpha,\beta}(x) = \sum_{k=0}^{\infty} \frac{x^k}{\Gamma(\alpha k + \beta)}, \quad (\text{A.1})$$

with $\alpha, \beta, x \in \mathbb{C}$, $\Re(\alpha) > 0$ and $\Re(\beta) > 0$. Where $\Gamma(\cdot)$ represents the gamma function (see Appendix A.2). When α and β are real and positive, the Mittag-Leffler function converges for all values of x . The ordinary case, where $\beta = 1$, was first introduced by Gösta Mittag-leffler in 1903 [132] in connection with his method of summation of some divergent series. The general case first appeared in the work of Adders Wiman in 1905 [133]. The Mittag-Leffler function arises naturally in the solution of fractional order integral equations or fractional order differential equations, which we will discuss in Appendix A.7. The ordinary and generalised Mittag-Leffler functions interpolate between a purely exponential law and power-law like behaviour. For a full treatment of the Mittag-Leffler functions we refer to [134].

This function can be seen as a generalisation of the exponential function, to which it reduces when $\alpha = \beta = 1$. But the exponential function is not the only function of closed form that can be produced by the Mittag-Leffler functions. Some other examples are

$$\begin{aligned} E_{0,1}(x) &= (1-x)^{-1}, \quad |x| < 1 & E_{1/2,1}(x) &= e^{x^2} \operatorname{erfc}(-x) \\ E_{1,1}(x) &= e^x & E_{2,1}(-x^2) &= \cos(x) \\ E_{2,1}(x) &= \cosh(\sqrt{x}) & E_{2,2}(x) &= \sinh(\sqrt{x})x^{-1/2} \\ E_{1,2}(x) &= (e^x - 1)x^{-1} & E_{1,3}(x) &= (e^x - x - 1)x^{-2} \end{aligned} \quad (\text{A.2})$$

It is clear from Eq. (A.1) that for $x = 0$ we have

$$E_{\alpha,\beta}(0) = \frac{1}{\Gamma(\beta)}. \quad (\text{A.3})$$

The asymptotic expansion of the Mittag-Leffler function when $0 < \alpha \leq 1$, $|x| \rightarrow \infty$ and $\arg(x) = \pi$ is given by

$$E_{\alpha,\beta}(x) = - \sum_{r=1}^{N^*} \frac{x^{-r}}{\Gamma(\beta - \alpha r)} + \mathcal{O} \left[\frac{1}{x^{N^*+1}} \right], \quad (\text{A.4})$$

with $N^* \in \mathbb{N}$, $N^* \neq 1$ (more general constraints on α and x are possible but not relevant here). Therefore the leading term of the expansion for large x and $\alpha \neq \beta$ is

$$E_{\alpha,\beta}(x) \approx - \frac{x^{-1}}{\Gamma(\beta - \alpha)}. \quad (\text{A.5})$$

When $\alpha = \beta$, the leading term is

$$E_{\alpha,\alpha}(x) \approx - \frac{x^{-2}}{\Gamma(-\alpha)}. \quad (\text{A.6})$$

When $\alpha = \beta = 1$, this becomes, evidently, zero since the Mittag-Leffler function will decay exponentially fast. Some interesting recurrence relations of the Mittag-Leffler functions are

$$E_{\alpha,\beta}(x) = x E_{\alpha,\alpha+\beta}(x) + \frac{1}{\Gamma(\beta)}, \quad (\text{A.7})$$

$$\frac{d}{dx} E_{\alpha,\beta}(x) = \frac{E_{\alpha,\beta-1}(x) - (\beta-1)E_{\alpha,\beta}(x)}{\alpha x}. \quad (\text{A.8})$$

The following integral can easily be proved using the definition of the Mittag-Leffler function and property Eq. (A.20) of the gamma function

$$\int_0^t dx x^{\alpha-1} E_{\alpha,\alpha}(ax^\alpha) = t^\alpha E_{\alpha,\alpha+1}(at^\alpha). \quad (\text{A.9})$$

Figure A.1 shows the Mittag-Leffler functions $E_{\alpha,1}(-x^\alpha)$, $E_{\alpha,\alpha}(-x^\alpha)$ and $E_{\alpha,\alpha+1}(-x^\alpha)$ that often reoccur in our work. Notice here the early and late time behaviour that was discussed above. Finally we state the following property of the Mittag-Leffler functions

$$\begin{aligned} \frac{a}{\Gamma(1-\alpha)} \int_0^t dy \int_0^{t'} dy' |y-y'|^{-\alpha} y^{\alpha-1} y'^{\alpha-1} E_{\alpha,\alpha}(-ay^\alpha) E_{\alpha,\alpha}(-ay'^\alpha) \\ = E_{\alpha,1}(-a|t-t'|^\alpha) - E_{\alpha,1}(-at^\alpha) E_{\alpha,1}(-at'^\alpha). \end{aligned} \quad (\text{A.10})$$

To derive this relation, we start with the following Mittag-Leffler function

$$E_{\alpha,1}(-a|t-t'|^\alpha), \quad (\text{A.11})$$

with a a constant and t and t' variable. The Laplace transform (see Appendix A.6) of this function to both its arguments is

$$\int_0^\infty dt \int_0^\infty dt' e^{-st} e^{-s't'} E_{\alpha,1}(-a|t - t'|^\alpha). \quad (\text{A.12})$$

Because we are dealing with the absolute value of the difference of the two variables, we divide the integral up in the following two parts

$$\begin{aligned} & \int_0^\infty dt \int_t^\infty dt' e^{-st} e^{-s't'} E_{\alpha,1}(-a(t' - t)^\alpha) \\ & + \int_0^\infty dt' \int_{t'}^\infty dt e^{-st} e^{-s't'} E_{\alpha,1}(-a(t - t')^\alpha). \end{aligned} \quad (\text{A.13})$$

Introducing the substitutions $u = t' - t$ and $w = t - t'$ decouples the integrals

$$\begin{aligned} & \int_0^\infty dt e^{-(s+s')t} \int_0^\infty du e^{-s'u} E_{\alpha,1}(-au^\alpha) \\ & + \int_0^\infty dt' e^{-(s+s')t'} \int_0^\infty dw e^{-s'w} E_{\alpha,1}(-aw^\alpha). \end{aligned} \quad (\text{A.14})$$

The first integral in both terms is easily evaluated, the second is just the Laplace transform of a Mittag-Leffler function which is given by Eq. (A.42)

$$\frac{1}{s + s'} \left[s'^{-1} (1 + as'^{-\alpha})^{-1} + s^{-1} (1 + as^{-\alpha})^{-1} \right]. \quad (\text{A.15})$$

After some elementary algebra this expression can be rewritten as

$$\begin{aligned} & s^{-1} s'^{-1} (1 + as^{-\alpha})^{-1} (1 + as'^{-\alpha})^{-1} \\ & + as^{-\alpha} s'^{-\alpha} (1 + as^{-\alpha})^{-1} (1 + as'^{-\alpha})^{-1} \frac{s^{\alpha-1} + s'^{\alpha-1}}{s + s'}. \end{aligned} \quad (\text{A.16})$$

The first term is not coupled and thus the inverse Laplace transform is readily evaluated, it gives

$$E_{\alpha,1}(-at^\alpha) E_{\alpha,1}(-at'^\alpha). \quad (\text{A.17})$$

To invert the second term, we observe that it is a product of two known double Laplace transforms. We recognise two Mittag-Leffler function transforms and transformation (A.43). Using Eq. (A.45), we find a convolution after the inversion to time-space. Combining this with Eq. (A.11) and Eq. (A.17), and rearranging some terms we finally come to Eq. (A.10).

A.2 Gamma function

The gamma function $\Gamma(x)$ is defined for all complex numbers except the non-positive integers. For complex numbers with a positive real part, it is defined via a convergent improper integral

$$\Gamma(x) = \int_0^\infty dt t^{x-1} e^{-t}. \quad (\text{A.18})$$

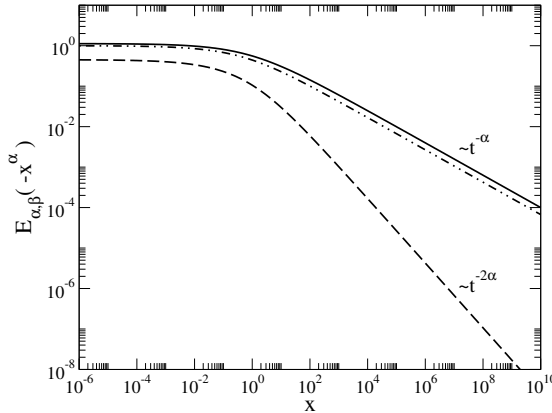


Figure A.1: Numeric evaluation of some Mittag-Leffler functions $E_{\alpha,\beta}(-x^\alpha)$. With $\alpha = 0.4$ and $\beta = 1$ (dashed-dotted line), α (dashed line) and $\alpha + 1$ (full line). The long time behaviour of Eqs. (A.5) and (A.6) is indicated.

The gamma function can be seen as an extension to real and complex numbers of the factorial function with its argument shifted down by one

$$\Gamma(n) = (n - 1)!, \quad (\text{A.19})$$

with n is a positive integer. Figure A.2 shows the gamma function as a function of its argument, it is clear that non-positive integers are not defined by the gamma function. Building on the same property as the factorial function one can prove using integration by parts

$$\Gamma(x + 1) = \int_0^\infty dt t^x e^{-t} = -t^x e^{-t} \Big|_0^\infty + \int_0^\infty dt x t^{x-1} e^{-t} = x \Gamma(x). \quad (\text{A.20})$$

If the lower integration bound in Eq. (A.18) is not taken zero we have an upper incomplete gamma function. It is defined as

$$\Gamma(x; y) = \int_y^\infty dt t^{x-1} e^{-t}. \quad (\text{A.21})$$

When we want both integration bounds in Eq. (A.18) to be different we take the difference between two incomplete gamma functions

$$\Gamma(x; y_1, y_2) = \Gamma(x; y_1) - \Gamma(x; y_2) = \int_{y_1}^{y_2} dt t^{x-1} e^{-t}. \quad (\text{A.22})$$

A particularly interesting asymptotic behaviour of the incomplete gamma function is when y becomes large

$$\lim_{y \rightarrow \infty} \frac{\Gamma(x; y)}{y^{x-1} e^{-y}} = 1. \quad (\text{A.23})$$

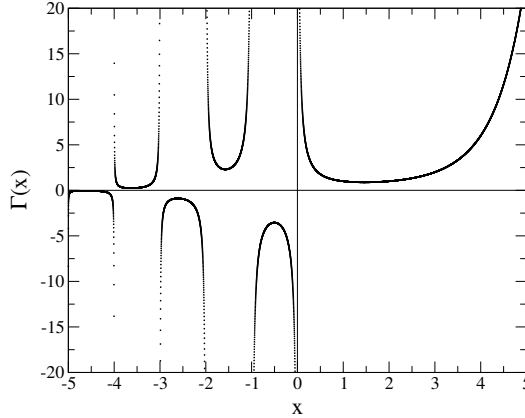


Figure A.2: Numeric evaluation of the gamma function $\Gamma(x)$.

A.3 Beta function

The beta function $\mathcal{B}(x, y)$, also called the Euler integral of the first kind, is a special function defined by

$$\mathcal{B}(x, y) = \int_0^1 dt t^{x-1} (1-t)^{y-1}, \quad (\text{A.24})$$

with $\text{Re}(x), \text{Re}(y) > 0$. The beta function is symmetric, i.e. $\mathcal{B}(x, y) = \mathcal{B}(y, x)$. One of its important features is its relation to the gamma function

$$\mathcal{B}(x, y) = \frac{\Gamma(x)\Gamma(y)}{\Gamma(x+y)}. \quad (\text{A.25})$$

To see this consider, using Eq. (A.18)

$$\Gamma(x)\Gamma(y) = \int_0^\infty du \int_0^\infty dv e^{-u-v} u^{x-1} v^{y-1} \quad (\text{A.26})$$

$$= \int_0^\infty dz \int_0^1 dt e^{-z} (zt)^{x-1} (z(1-t))^{y-1} |J(z, t)| \quad (\text{A.27})$$

$$= \int_0^\infty dz e^{-z} z^{x+y-1} \int_0^1 dt t^{x-1} (1-t)^{y-1} \quad (\text{A.28})$$

$$= \Gamma(x+y)\mathcal{B}(x, y). \quad (\text{A.29})$$

In the second line we changed the variables to $u = f(z, t) = zt$ and $v = g(z, t) = z(1-t)$. Here $|J(z, t)| = z$ is the absolute value of the Jacobian determinant of $f(z, t)$ and $g(z, t)$.

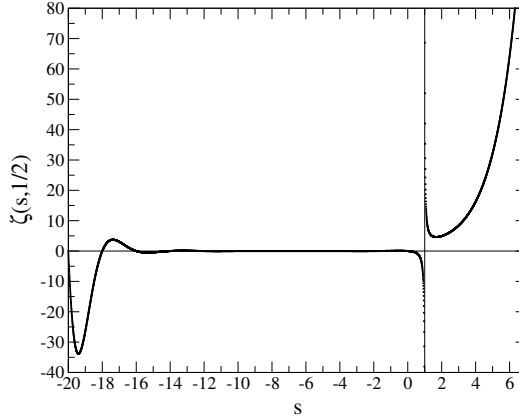


Figure A.3: Numeric evaluation of the Hurwitz zeta function $\zeta(s, \frac{1}{2})$.

A.4 Hurwitz zeta function

A zeta function $\zeta(s)$ is a function analogous to the original example, i.e. the Riemann zeta function

$$\zeta(s) = \sum_{n=1}^{\infty} \frac{1}{n^s}, \quad (\text{A.30})$$

which converges when the real part of s is greater than one. The Hurwitz zeta function $\zeta(s, q)$, named after Adolf Hurwitz, is one of many zeta function. It is formally defined for complex arguments s with $\text{Re}(s) > 1$ and q with $\text{Re}(q) > 0$ by

$$\zeta(s, q) = \sum_{n=0}^{\infty} \frac{1}{(q+n)^s}. \quad (\text{A.31})$$

This series is absolutely convergent for the given values of s and q . Clearly the Hurwitz zeta function reduces to the Riemann zeta function when $q = 1$. We also have that

$$\zeta(s, \frac{1}{2}) = (2^s - 1)\zeta(s). \quad (\text{A.32})$$

In Fig. A.3 we plot the Hurwitz zeta function for $q = 1/2$ and s variable, since this case is most relevant in our work.

A.5 Polylogarithm

The polylogarithm, also known as Jonquière's function, is a special function $\mathcal{L}_s(x)$ of order s and argument x . The polylogarithm function is defined by an infinite sum

$$\mathcal{L}_s(x) = \sum_{k=1}^{\infty} \frac{x^k}{k^s}, \quad (\text{A.33})$$

with $s \in \mathbb{C}$ and for all complex arguments x with $|x| < 1$. It can be extended to $|x| \geq 1$ by the process of analytic continuation. When $s = 1$, the polylogarithm reduces to the ordinary natural logarithm $\mathcal{L}_1(x) = -\ln(1-x)$. When $s = 2$ we call it the dilogarithm or Spence's function. Naturally for $s = 3$ it is called the trilogarithm. The origin of the name of this function comes from the fact that it is a repeated integral of itself

$$\mathcal{L}_{s+1}(x) = \int_0^x dt \frac{\mathcal{L}_s(t)}{t}. \tag{A.34}$$

Therefore the dilogarithm is an integral of the logarithm, the trilogarithm of the dilogarithm, and so on. A special identity of the Spence's function is

$$\mathcal{L}_2(x) + \mathcal{L}_2(x^{-1}) = -\frac{\pi^2}{6} - \frac{1}{2} \ln^2(-x). \tag{A.35}$$

A.6 Laplace transform

The Laplace transform \mathfrak{L} is an integral transform named after its discoverer Pierre-Simon Laplace. It transforms a function of a positive real variable t (often time) to a function of a complex variable s (frequency). Its use in solving physical problems is widespread. The (unilateral) Laplace transform of a function $f(t)$ is defined as

$$\mathfrak{L}[f(t), s] = \int_0^\infty dt e^{-st} f(t), \tag{A.36}$$

where $f(t)$ is defined for $t \geq 0$. To shorten the notation, the Laplace transform of function $f(t)$ is written as $\tilde{f}[s]$. Some specific Laplace transformations that are relevant in our research are given here (where $H(t)$ is the Heaviside function, Eq. (4.3))

Laplace transform of a constant c

$$cH(t) \xrightarrow{\mathfrak{L}} cs^{-1} \tag{A.37}$$

Laplace transform of the q^{th} power

$$t^q H(t) \xrightarrow{\mathfrak{L}} \Gamma(q+1) s^{-q-1} \tag{A.38}$$

Laplace transform of a linear combination (a and b constant)

$$af(t) + bg(t) \xrightarrow{\mathfrak{L}} a\tilde{f}[s] + b\tilde{g}[s] \tag{A.39}$$

Laplace transform of the n^{th} derivative

$$f^{(n)}(t) \xrightarrow{\mathfrak{L}} s^n \tilde{f}[s] - \sum_{k=1}^n s^{n-k} f^{(k-1)}(0) \tag{A.40}$$

Laplace transform of the Caputo fractional derivative of order α (with $m = \lceil \alpha \rceil$)

$${}_c\mathcal{D}^\alpha f(t) \xrightarrow{\mathfrak{L}} s^{\alpha-m} \mathfrak{L}[f^{(m)}(t), s] \tag{A.41}$$

Laplace transform of the Mittag-Leffler function

$$t^{\beta-1} E_{\alpha,\beta}(at^\alpha) \xrightarrow{\mathfrak{L}} s^{-\beta}(1 - as^{-\alpha})^{-1} \quad (\text{A.42})$$

Double Laplace transform of the absolute difference in times to the $-q^{\text{th}}$ power

$$|t - t'|^{-q} \xrightarrow{\mathfrak{L}} \Gamma(1 - q)(s^{q-1} + s'^{q-1})(s + s')^{-1} \quad (\text{A.43})$$

One can also introduce the inverse Laplace transform \mathfrak{L}^{-1} , it satisfies the following property

$$\mathfrak{L}^{-1}[\tilde{f}[s], t] = f(t). \quad (\text{A.44})$$

An important inverse Laplace transformation is that of the product of two functions in Laplace space that become a convolution in time space

$$\mathfrak{L}^{-1}[\tilde{f}[s]\tilde{g}[s], t] = \int_0^t dt' f(t - t')g(t'). \quad (\text{A.45})$$

A.7 Fractional derivative

The concept of fractional derivative [135, 136] is a rather old one, but it has only recently attracted the attention of the mainstream science. Already in 1695, Leibniz introduced the derivative of order $1/2$, and in 1832 the foundations of the formalism were laid out by Liouville. Fractional derivatives have a great appeal due to their non-local nature which is ideal for describing complex phenomena with a long memory. To understand the concept of fractional derivatives, first consider the ordinary differentiation operator $\mathcal{D} = d/dx$. Performing this operation n times gives the n^{th} derivative, this corresponds to taking the (integer) n^{th} power of the operator: \mathcal{D}^n . A fractional derivative assumes a real positive power a of the differentiation operator. If two fractional derivatives, of order a and b , are applied. And if $a + b$ is a positive integer, then we should retrieve an ordinary derivative. For example, $\mathcal{D}^{1/2}\mathcal{D}^{1/2} = d/dx$.

To construct the fractional derivative, we first produce a fractional integral. Let $f(x)$ be a function that is defined for $x > 0$. The definite integral operator \mathcal{I} from 0 to x is

$$\mathcal{I}f(x) = \int_0^x dt f(t). \quad (\text{A.46})$$

It is relatively easy to show that if one performs this operation multiple (integer) times, one arrives at the Cauchy formula for repeated integration

$$\mathcal{I}^n f(x) = \frac{1}{(n-1)!} \int_0^x dt (x-t)^{n-1} f(t). \quad (\text{A.47})$$

This formula suggests a natural candidate for the fractional integration. We generalise n to a real value a and use the gamma function $\Gamma(\cdot)$ to replace the discrete factorial function. This yields the (left) Riemann-Liouville type fractional integral of order a

$$\mathcal{I}^a f(x) = \frac{1}{\Gamma(a)} \int_0^x dt (x-t)^{a-1} f(t). \quad (\text{A.48})$$

This is a well-behaved operator. Using this definition one can construct a fractional derivative \mathcal{D}^a of order a . For physical processes the most commonly used fractional derivative is the one in the Caputo sense, introduced in 1967 [137]. The reason for this is that when solving fractional differential equations involving Caputo's definition, it is not necessary to define fractional order initial conditions, which are ill defined in a physical world. The Caputo fractional derivative is defined as

$${}_c\mathcal{D}^a f(x) = \mathcal{I}^{m-a} f^{(m)}(x), \quad (\text{A.49})$$

where the superscript (m) stands for the ordinary m^{th} derivative with m the value of a rounded up to the nearest integer, thus $m = \lceil a \rceil$. When $0 < a \leq 1$, we have $m = 1$ and the fractional derivative gets the following form

$${}_c\mathcal{D}^a f(x) = \frac{1}{\Gamma(1-a)} \int_0^x dt (x-t)^{-a} f'(t). \quad (\text{A.50})$$

From this definition it is clear that a fractional derivative of a function f at a point x is not a local property (only when a is integer is it local), meaning it is not only dependent on the values of f very close to x . One could state that it requires peripheral vision to produce the result.

B | Derivation of $\langle \xi(t)\xi(0) \rangle$

*Nothing is more intolerable
than to have admit to yourself your own errors.*

Ludwig van Beethoven

This derivation was provided to us by Karel Proesmans. First consider the random force at $t = 0$, it is given by

$$\xi(0) = - \sum_i \epsilon_i \left(x_i(0) + x(0) \frac{\epsilon_i}{m_i \omega_i^2} \right). \quad (\text{B.1})$$

Multiplying this by $\xi(t)$ and taking the ensemble average gives

$$\langle \xi(t)\xi(0) \rangle = - \sum_i \epsilon_i \left(\langle \xi(t)x_i(0) \rangle + \langle \xi(t)x(0) \rangle \frac{\epsilon_i}{m_i \omega_i^2} \right). \quad (\text{B.2})$$

In the main text we argued that the second term in this expression should be equal to zero. So the autocorrelation of the random force becomes

$$\langle \xi(t)\xi(0) \rangle = - \sum_i \epsilon_i \langle \xi(t)x_i(0) \rangle, \quad (\text{B.3})$$

and when we substitute the expression for $\xi(t)$, this becomes (where we dropped the explicit $t = 0$ dependence of the variables)

$$\langle \xi(t)\xi(0) \rangle = \sum_i \sum_j \epsilon_i \epsilon_j \left(\left(\langle x_j x_i \rangle + \langle x_j x \rangle \frac{\epsilon_i}{m_i \omega_i^2} \right) \cos(\omega_i t) + \langle x_j p_i \rangle \frac{\sin(\omega_i t)}{m_i \omega_i} \right). \quad (\text{B.4})$$

Because the position and momentum coordinates are uncorrelated, the last term is equal to zero

$$\langle \xi(t)\xi(0) \rangle = \sum_i \sum_j \epsilon_i \epsilon_j \left(\langle x_j x_i \rangle + \langle x_j x \rangle \frac{\epsilon_i}{m_i \omega_i^2} \right) \cos(\omega_i t). \quad (\text{B.5})$$

Now we first evaluate $\langle x_i x_j \rangle$ when $i \neq j$. To find this expected value we use the total Hamiltonian: $H = H_s + H_b + H_c$, given by Eqs. (2.30), (2.31) and (2.32). If we

take Z to be the partition function for the harmonic-bath Hamiltonian we get (with $\beta = 1/k_B T$)

$$\langle x_i x_j \rangle = \frac{1}{Z} \int dx dp \prod_k dx_k dp_k x_i x_j e^{-\beta H_s} e^{-\beta H_b} e^{-\beta H_c}. \quad (\text{B.6})$$

Notice that if we isolate the following part from the total integral we can rewrite it using standard techniques for solving integrals

$$\int dx_i x_i e^{-\beta \left(\frac{m_i \omega_i^2}{2} x_i^2 + x \epsilon_i x_i \right)} = -\frac{x \epsilon_i}{m_i \omega_i^2} \int dx_i e^{-\beta \left(\frac{m_i \omega_i^2}{2} x_i^2 + x \epsilon_i x_i \right)}. \quad (\text{B.7})$$

Substituting this result back into the original expression immediately gives us the following relation

$$\langle x_i x_j \rangle = -\frac{\epsilon_i}{m_i \omega_i^2} \langle x_j x \rangle. \quad (\text{B.8})$$

From this result it is clear that Eq. (B.5) is equal to zero when $i \neq j$, therefore we have

$$\langle \xi(t) \xi(0) \rangle = \sum_i \epsilon_i^2 \left(\langle x_i^2 \rangle + \langle x_i x \rangle \frac{\epsilon_i}{m_i \omega_i^2} \right) \cos(\omega_i t). \quad (\text{B.9})$$

Very analogous to the calculation of Eq. (B.8) we can derive

$$\langle x_i x \rangle = -\frac{\epsilon_i}{m_i \omega_i^2} \langle x^2 \rangle. \quad (\text{B.10})$$

Next we find $\langle x_i x_j \rangle$ when $i = j$, thus $\langle x_i^2 \rangle$. we have that

$$\langle x_i^2 \rangle = \frac{1}{Z} \int dx dp \prod_k dx_k dp_k x_i^2 e^{-\beta H_s} e^{-\beta H_b} e^{-\beta H_c}. \quad (\text{B.11})$$

Again we isolate the relevant integral

$$\int dx_i x_i^2 e^{-\beta \left(\frac{m_i \omega_i^2}{2} x_i^2 + x \epsilon_i x_i \right)} = \frac{\beta x^2 \epsilon_i^2 + m_i \omega_i^2}{\beta m_i^2 \omega_i^4} \int dx_i e^{-\beta \left(\frac{m_i \omega_i^2}{2} x_i^2 + x \epsilon_i x_i \right)}. \quad (\text{B.12})$$

We thus obtain

$$\langle x_i^2 \rangle = \frac{\epsilon_i^2}{m_i^2 \omega_i^4} \langle x^2 \rangle + \frac{k_B T}{m_i \omega_i^2}. \quad (\text{B.13})$$

When we now plug Eqs. (B.10) and (B.13) into Eq. (B.9), we arrive at the following relation

$$\langle \xi(t) \xi(0) \rangle = \sum_i \frac{\epsilon_i^2 k_B T}{m_i \omega_i^2} \cos(\omega_i t). \quad (\text{B.14})$$

Using the expression for the memory kernel K , Eq. (2.42), brings us to the final result

$$\langle \xi(t) \xi(0) \rangle = k_B T K(t). \quad (\text{B.15})$$

C | Velocity Correlation

The years really do speed by.

David Bowie

In Section 4.2 we derived the Laplace transform of the velocity of a harmonic oscillator in an active viscoelastic bath. It reads

$$\tilde{v}[s] = -\frac{k s^{-\alpha}}{\eta_\alpha} x(0) \left[1 + \frac{k}{\eta_\alpha} s^{-\alpha}\right]^{-1} + \frac{s^{1-\alpha}}{\eta_\alpha} \left(\tilde{\xi}_T[s] + \tilde{\xi}_A[s]\right) \left[1 + \frac{k}{\eta_\alpha} s^{-\alpha}\right]^{-1}. \quad (\text{C.1})$$

Taking the ensemble average of this quantity times $\tilde{v}[w]$ is

$$\begin{aligned} \langle \tilde{v}[s] \tilde{v}[w] \rangle &= \frac{k^2}{\eta_\alpha^2} \langle x^2(0) \rangle s^{-\alpha} w^{-\alpha} \left[1 + \frac{k}{\eta_\alpha} s^{-\alpha}\right]^{-1} \left[1 + \frac{k}{\eta_\alpha} w^{-\alpha}\right]^{-1} \\ &+ \frac{1}{\eta_\alpha^2} \langle \tilde{\xi}_T[s] \tilde{\xi}_T[w] \rangle s^{1-\alpha} w^{1-\alpha} \left[1 + \frac{k}{\eta_\alpha} s^{-\alpha}\right]^{-1} \left[1 + \frac{k}{\eta_\alpha} w^{-\alpha}\right]^{-1} \\ &+ \frac{1}{\eta_\alpha^2} \langle \tilde{\xi}_A[s] \tilde{\xi}_A[w] \rangle s^{1-\alpha} w^{1-\alpha} \left[1 + \frac{k}{\eta_\alpha} s^{-\alpha}\right]^{-1} \left[1 + \frac{k}{\eta_\alpha} w^{-\alpha}\right]^{-1}. \quad (\text{C.2}) \end{aligned}$$

Here we already dismissed the cross-terms because they all are equal to zero. The last term in this expression, we will write as $\Phi(s, w)$, because we can not simplify it with this Laplace technique. Using the equipartition theorem (see Section 2.2), we find that $\langle x^2(0) \rangle = k_B T / k$. The Laplace transform of $\langle \xi_T(t) \xi_T(t') \rangle$ is done as follows

$$\langle \tilde{\xi}_T[s] \tilde{\xi}_T[w] \rangle = \int_0^\infty dt \int_0^\infty dt' e^{-st} e^{-wt'} \langle \xi_T(t) \xi_T(t') \rangle \quad (\text{C.3})$$

$$= \frac{\eta_\alpha k_B T}{\Gamma(1-\alpha)} \int_0^\infty dt \int_0^\infty dt' \frac{e^{-st} e^{-wt'}}{|t-t'|^\alpha}. \quad (\text{C.4})$$

The double integral is a Laplace transform defined by Eq. (A.43). Applying this yields

$$\langle \tilde{\xi}_T[s] \tilde{\xi}_T[w] \rangle = \eta_\alpha k_B T (s^{\alpha-1} + w^{\alpha-1}) (s+w)^{-1}. \quad (\text{C.5})$$

Plugging this into expression (C.2) we get

$$\begin{aligned}
\langle \tilde{v}[s]\tilde{v}[w] \rangle &= \frac{k k_B T}{\eta_\alpha^2} s^{-\alpha} w^{-\alpha} \left[1 + \frac{k}{\eta_\alpha} s^{-\alpha} \right]^{-1} \left[1 + \frac{k}{\eta_\alpha} w^{-\alpha} \right]^{-1} \\
&\quad + \frac{k_B T}{\eta_\alpha} (s^{1-\alpha} + w^{1-\alpha})(s+w)^{-1} \left[1 + \frac{k}{\eta_\alpha} s^{-\alpha} \right]^{-1} \left[1 + \frac{k}{\eta_\alpha} w^{-\alpha} \right]^{-1} \\
&\quad + \Phi(s, w).
\end{aligned} \tag{C.6}$$

After some algebra, one can find that the following holds for the right-hand side

$$\frac{k_B T}{\eta_\alpha} \left[\frac{[1 + (ks^{-\alpha}/\eta_\alpha)]^{-1} s^{1-\alpha}}{s+w} + \frac{[1 + (kw^{-\alpha}/\eta_\alpha)]^{-1} w^{1-\alpha}}{s+w} \right] + \Phi(s, w). \tag{C.7}$$

If one calculates the double Laplace transform of $|t-t'|^{\alpha-2} E_{\alpha, \alpha-1}(-k/\eta_\alpha)|t-t'|^\alpha$, the solution will be what is between the large brackets in the above expression. The inverse Laplace transform of the first term can thus be performed. To transform the second term, $\Phi(s, w)$, back to the time domain, we rely on the inverse transform of $\tilde{v}[s]$. With very similar techniques as were used in Chapter 4, one can find $v(t)$. With this $\langle v(t)v(t') \rangle$ can be calculated. This will give the inverse transform of $\Phi(s, w)$, together with the inverse transform of the first term, which we could simplify greatly using Laplace space. The correlation of the velocity at times t and t' is thus given by the following expression

$$\begin{aligned}
\langle v(t)v(t') \rangle &= \frac{k_B T}{\eta_\alpha} |t-t'|^{\alpha-2} E_{\alpha, \alpha-1} \left(-\frac{k}{\eta_\alpha} |t-t'|^\alpha \right) \\
&\quad + \frac{C}{\eta_\alpha^2} \int_0^t dx \int_0^{t'} dy \left(\frac{E_{\alpha, \alpha-1} \left(-\frac{k}{\eta_\alpha} x^\alpha \right) E_{\alpha, \alpha-1} \left(-\frac{k}{\eta_\alpha} y^\alpha \right)}{x^{2-\alpha} y^{2-\alpha}} \right) e^{-\frac{|t-x-t'+y|}{\tau_A}}.
\end{aligned} \tag{C.8}$$

D | Thermalised Worm-like Chain

*Yes, I think it can be easily done,
just take everything down to Highway 61.*

Bob Dylan

Here we will discuss how one can construct a thermalised semi-flexible worm-like chain. We will also show that the obtained chain is indeed equilibrated. Remember that for a worm-like chain we take $\kappa \gg 1$, $k \gg 1$ and $a \neq 0$ (see Section 5.5).

First, place the first bead in the origin

$$R_{0,x} = R_{0,y} = R_{0,z} = 0. \quad (\text{D.1})$$

Then we place the second bead at a distance a' from the first, this distance is equal to a plus the appropriate fluctuation $3k_B T/k$. We have $a' = |a + N(0, 3k_B T/k)|$, where $N(\mu, \sigma^2)$ is a normal distribution with mean μ and variance σ^2 . We choose to put the first bond along the x -axis, this is of course arbitrary

$$R_{1,x} = a', \quad (\text{D.2})$$

$$R_{1,y} = R_{1,z} = 0. \quad (\text{D.3})$$

Placing the third bead will force us to make sure that the angle θ between the bonds is correct. We know that $\theta = N(0, 2k_B T/\kappa)$. Because of the rotational symmetry of the problem we also need to generate a second angle α , which is uniformly distributed between zero and π . So we have $\alpha \in [0, \pi]$. Figure D.1 clarifies how θ and α are defined. The third bead is thus placed at

$$R_{2,x} = a' \cos(\theta) + R_{1,x}, \quad (\text{D.4})$$

$$R_{2,y} = a' \sin(\theta) \cos(\alpha), \quad (\text{D.5})$$

$$R_{2,z} = a' \sin(\theta) \sin(\alpha). \quad (\text{D.6})$$

Placing the following beads \vec{R}_n , with $n > 2$, is a bit more tricky because the orientation of the previous bond always changes and does not lie neatly along the x -axis. We will therefore first find the location of the next bead as if the previous bead \vec{R}_{n-1} was located in the origin and the previous bond was along the (negative) x -axis. This implies that the second previous bead \vec{R}_{n-2} lies on the negative x -axis. Thereafter

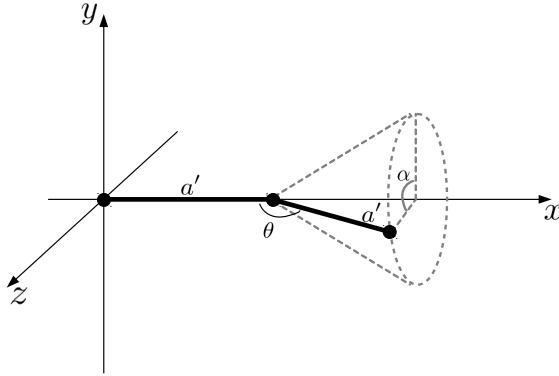


Figure D.1: Illustration of the angles θ and α .

we will translate the bead to its correct position. So, pretending the previous bond lies along the x -axis with the previous bead in the origin, for the n^{th} bead \vec{R}_n we do

$$X = a' \cos(\theta), \quad (\text{D.7})$$

$$Y = a' \sin(\theta) \cos(\alpha), \quad (\text{D.8})$$

$$Z = a' \sin(\theta) \sin(\alpha). \quad (\text{D.9})$$

Now to get this point to where the bead should be, we first need to rotate the new bond so that the imaginary previous bond on the x -axis has the same direction as the actual previous bond. We use Rodrigues' rotation formula¹ to achieve this. The actual previous bond is given by $\vec{r} = (R_{n-1,x} - R_{n-2,x}, R_{n-1,y} - R_{n-2,y}, R_{n-1,z} - R_{n-2,z})$. First, we define the angle β between the x -axis and the previous bond, with $\hat{u} = (\hat{e}_x \times \vec{r}) / |\hat{e}_x \cdot \vec{r}|$ the axis of rotation (our new bond should be rotated about β)

$$\beta = \arccos\left(\frac{r_x}{|\vec{r}|}\right), \quad (\text{D.10})$$

also take $s = \sin(\beta)$, $c = 1 - \cos(\beta)$ and $n = (r_y^2 + r_z^2)^{-1/2}$. The transformation is

$$X' = (1 - c) X - snr_y Y - snr_z Z, \quad (\text{D.11})$$

$$Y' = snr_y X + (1 - cn^2 r_y^2) Y - cn^2 r_y r_z Z, \quad (\text{D.12})$$

$$Z' = snr_z X - cn^2 r_y r_z Y + (1 - cn^2 r_z^2) Z. \quad (\text{D.13})$$

Now we only need to translate the point to the end of the chain

$$R_{n,x} = X' + R_{n-1,x}, \quad (\text{D.14})$$

$$R_{n,y} = Y' + R_{n-1,y}, \quad (\text{D.15})$$

$$R_{n,z} = Z' + R_{n-1,z}. \quad (\text{D.16})$$

¹Suppose \vec{v} is a vector to be rotated over an angle ϕ according to the right-hand rule. The axis of rotation is defined by unit vector \hat{u} , then $\vec{v}_{rot} = \cos(\phi)\vec{v} + \sin(\phi)(\hat{u} \times \vec{v}) + (1 - \cos(\phi))\hat{u}(\hat{u} \cdot \vec{v})$.

Doing this until $n = N - 1$ creates a thermalised worm-like chain. To prove this statement we measure two equilibrium properties of the chain. First the bond-bond correlation, according to Eq. (5.146) we should find that $\langle \hat{r}_n \cdot \hat{r}_{n+m} \rangle = \exp(-k_B T |m| / \kappa)$. In Fig. D.2 we plot this correlation starting from the middle of the chain, so $n = N/2$. We indeed find that, on average, it agrees with the formula for different values of the temperature. The second quantity we check is the average end-to-end distance squared, which is given by formula Eq. (5.153). The simulated results again produce the correct output over a large range of chain lengths, see Fig. D.3. An interesting quantity we can also simulate is the distribution of the end-to-end distance $|\vec{P}|$. For a freely-jointed chain ($\kappa = 0$) this distribution can be derived (see Eq. (5.8) or [123]). The probability distribution Φ in the spherical coordinate system is

$$\Phi(|\vec{P}|) 4\pi |\vec{P}|^2 d|\vec{P}| = 4\pi \left(\frac{3}{2\pi a^2 N} \right)^{3/2} \exp\left(-\frac{3|\vec{P}|^2}{2a^2 N}\right) |\vec{P}|^2 d|\vec{P}|, \quad (\text{D.17})$$

this is the probability of finding the end-to-end vector in the spherical shell with radius between $|\vec{P}|$ and $|\vec{P}| + d|\vec{P}|$, where the centre of the shell is one of the chains ends. When we have a worm-like chain with high κ , it is obvious that the distribution will be heavily peaked close to the maximum extension $L_M = a(N - 1)$. Figure D.4 shows that for $\kappa = 0$ we indeed find the distribution Eq. (D.17). For $\kappa \gg 1$ we also find that the distribution behaves as we expected. The figure also shows the distributions for chain with intermediate values of κ .

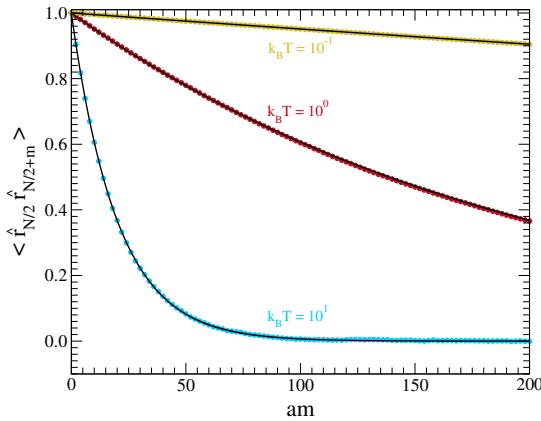


Figure D.2: Lin-lin plot of the bond correlation from the middle of the chain as a function of length down the chain am . The solid lines are the analytic expression, Eq. (5.146), and the coloured dots are the simulated results. The parameters are $N = 256$, $k_B T = 10^{-1}$ (yellow), 10^0 (red), 10^1 (blue), $k = \kappa = 100$ and $a = 2$. The results are averaged over 10^5 histories.

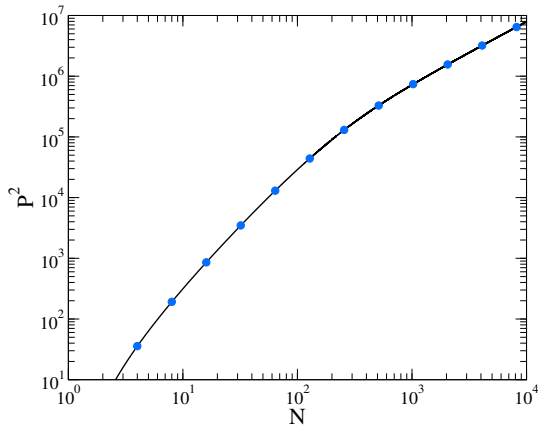


Figure D.3: Log-log plot of the average end-to-end distance squared as a function of number of beads N . The solid line is the analytic formula, Eq. (5.153), and the coloured dots are the simulated results. The parameters are $N = 256$, $k_B T = 1$, $k = \kappa = 100$ and $a = 2$. The results are averaged over 10^5 histories.

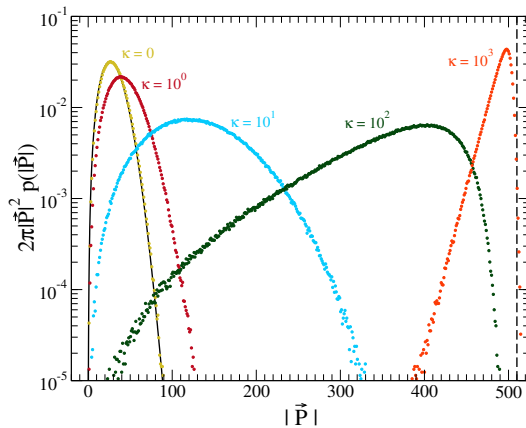


Figure D.4: Log-lin plot of the distribution of the end-to-end distance. The solid line is the analytic formula, Eq. (D.17), the dashed line represents the maximum extension L_M and the coloured dots are the simulated results. The parameters are $N = 256$, $\kappa = 0$ (yellow), 10^0 (red), 10^1 (blue), 10^2 (green), 10^3 (orange), $k_B T = 1$, $k = 100$ and $a = 2$. The results are averaged over 10^6 histories.

E | Derivation of K_+

*Success is a science;
if you have the conditions, you get the result.*

Oscar Wilde

First we will evaluate the integrals in Eq. (6.107). We have

$$3C \int_0^t d\tau \int_0^{t'} d\tau' e^{-|\tau-\tau'|/\tau_A} e^{(\tau+\tau')/\tau_P}. \quad (\text{E.1})$$

Without loss of generality we assume $t > t'$. To deal with the absolute value function we divide the integrals using the diagram in Fig. E.1. We thus find

$$\begin{aligned} 3C \int_0^{t'} d\tau' \int_0^{\tau'} d\tau e^{-(\tau'-\tau)/\tau_A} e^{(\tau+\tau')/\tau_P} + 3C \int_0^{t'} d\tau \int_0^{\tau} d\tau' e^{-(\tau-\tau')/\tau_A} e^{(\tau+\tau')/\tau_P} \\ + 3C \int_{t'}^t d\tau \int_0^{t'} d\tau' e^{-(\tau-\tau')/\tau_A} e^{(\tau+\tau')/\tau_P}. \end{aligned} \quad (\text{E.2})$$

Notice that the first two integrals are actually identical. After some reordering we

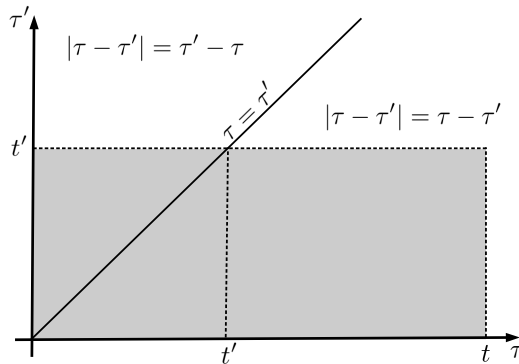


Figure E.1: Illustration of the double integral over a function of $|\tau - \tau'|$, with $t > t'$.

find

$$6C \int_0^{t'} d\tau e^{\omega-\tau} \int_0^\tau d\tau' e^{\omega+\tau'} + 3C \int_{t'}^t d\tau e^{\omega-\tau} \int_0^{t'} d\tau' e^{\omega+\tau'}, \quad (\text{E.3})$$

where we introduced

$$\omega_\pm = \frac{1}{\tau_p} \pm \frac{1}{\tau_A}. \quad (\text{E.4})$$

Solving gives

$$\begin{aligned} & \frac{6C}{\omega_+(\omega_+ + \omega_-)} \left[e^{(\omega_+ + \omega_-)t'} - 1 \right] - \frac{6C}{\omega_+\omega_-} \left[e^{\omega_- t'} - 1 \right] \\ & + \frac{3C}{\omega_+\omega_-} \left[e^{\omega_- t + \omega_+ t'} - e^{\omega_- t} - e^{(\omega_+ + \omega_-)t'} + e^{\omega_- t'} \right]. \end{aligned} \quad (\text{E.5})$$

Remember that we took $t > t'$, so more generally we can say

$$\begin{aligned} & \frac{3C\tau_p}{\omega_+} \left[e^{2\min(t,t')/\tau_p} - 1 \right] - \frac{6C}{\omega_+\omega_-} \left[e^{\omega_- \min(t,t')} - 1 \right] \\ & + \frac{3C}{\omega_+\omega_-} \left[e^{\omega_- \max(t,t') + \omega_+ \min(t,t')} - e^{\omega_- \max(t,t')} - e^{2\min(t,t')/\tau_p} + e^{\omega_- \min(t,t')} \right], \end{aligned} \quad (\text{E.6})$$

where we used $(\omega_+ + \omega_-) = 2/\tau_p$. Working toward Eq. (6.107) we need to multiply by $e^{-(t+t')/\tau_p}$ or $e^{-(\omega_+ + \omega_-)(t+t')/2}$, depending on what suits best

$$\begin{aligned} & \frac{3C\tau_p}{\omega_+} \left[e^{-(t+t'-2\min(t,t'))/\tau_p} - e^{-(t+t')/\tau_p} \right] \\ & - \frac{6C}{\omega_+\omega_-} \left[e^{\omega_- \min(t,t') - (\omega_+ + \omega_-)(t+t')/2} - e^{-(t+t')/\tau_p} \right] \\ & + \frac{3C}{\omega_+\omega_-} \left[e^{\omega_- \max(t,t') + \omega_+ \min(t,t') - (\omega_+ + \omega_-)(t+t')/2} \right. \\ & \quad \left. - e^{\omega_- \max(t,t') - (\omega_+ + \omega_-)(t+t')/2} - e^{-(t+t'-2\min(t,t'))/\tau_p} \right. \\ & \quad \left. + e^{\omega_- \min(t,t') - (\omega_+ + \omega_-)(t+t')/2} \right] \end{aligned} \quad (\text{E.7})$$

and

$$\begin{aligned} & \frac{3C\tau_p}{\omega_+} \left[e^{-(t+t'-2\min(t,t'))/\tau_p} - e^{-(t+t')/\tau_p} \right] \\ & - \frac{6C}{\omega_+\omega_-} \left[e^{-\omega_- (t+t'-2\min(t,t'))/2} e^{-\omega_+ (t+t')/2} - e^{-(t+t')/\tau_p} \right] \\ & + \frac{3C}{\omega_+\omega_-} \left[e^{-\omega_- (t+t'-2\max(t,t'))/2} e^{-\omega_+ (t+t'-2\min(t,t'))/2} \right. \\ & \quad \left. - e^{-\omega_- (t+t'-2\max(t,t'))/2} e^{-\omega_+ (t+t')/2} - e^{-(t+t'-2\min(t,t'))/\tau_p} \right. \\ & \quad \left. + e^{-\omega_- (t+t'-2\min(t,t'))/2} e^{-\omega_+ (t+t')/2} \right]. \end{aligned} \quad (\text{E.8})$$

Now we use $|t - t'| = t + t' - 2 \min(t, t')$ and $-|t - t'| = t + t' - 2 \max(t, t')$.

$$\begin{aligned} & \frac{3C\tau_p}{\omega_+} \left[e^{-|t-t'|/\tau_p} - e^{-(t+t')/\tau_p} \right] \\ & - \frac{6C}{\omega_+\omega_-} \left[e^{-\omega_-|t-t'|/2} e^{-\omega_+(t+t')/2} - e^{-(t+t')/\tau_p} \right] \\ & + \frac{3C}{\omega_+\omega_-} \left[e^{\omega_-|t-t'|/2} e^{-\omega_+|t-t'|/2} - e^{\omega_-|t-t'|/2} e^{-\omega_+(t+t')/2} \right. \\ & \quad \left. - e^{-|t-t'|/\tau_p} + e^{-\omega_-|t-t'|/2} e^{-\omega_+(t+t')/2} \right]. \end{aligned} \quad (\text{E.9})$$

As always we let $t \rightarrow \infty$ and $t' \rightarrow \infty$ to reach the steady state. Many terms drop out since $\omega_+ > 0$. Also using $(\omega_- - \omega_+) = -2/\tau_A$ gives

$$\frac{3C}{\omega_+} \left[\tau_p e^{-|t-t'|/\tau_p} + \frac{1}{\omega_-} \left(e^{-|t-t'|/\tau_A} - e^{-|t-t'|/\tau_p} \right) \right]. \quad (\text{E.10})$$

Inserting $1/\omega_{\pm} = \tau_p/(1 \pm (\tau_p/\tau_A))$ brings us to

$$\frac{3C\tau_p}{1 + (\tau_p/\tau_A)} \left[\tau_p e^{-|t-t'|/\tau_p} + \frac{\tau_p}{1 - (\tau_p/\tau_A)} \left(e^{-|t-t'|/\tau_A} - e^{-|t-t'|/\tau_p} \right) \right]. \quad (\text{E.11})$$

Putting $\tau_p/(1 - (\tau_p/\tau_A))$ outside the brackets

$$\frac{3C\tau_p^2}{1 - (\tau_p/\tau_A)^2} \left[(1 - (\tau_p/\tau_A)) e^{-|t-t'|/\tau_p} + e^{-|t-t'|/\tau_A} - e^{-|t-t'|/\tau_p} \right] \quad (\text{E.12})$$

and finally

$$\frac{3C\tau_p^2}{1 - (\tau_p/\tau_A)^2} \left[e^{-|t-t'|/\tau_A} - (\tau_p/\tau_A) e^{-|t-t'|/\tau_p} \right]. \quad (\text{E.13})$$

Completing Eq. (6.107) gives

$$K_+(t, t') = \frac{24Ck^2}{\gamma^2 N} \sum_{p=1}^M \frac{\tau_p^2 \mathcal{S}^{p^2}}{1 - (\tau_p/\tau_A)^2} \left[e^{-|t-t'|/\tau_A} - (\tau_p/\tau_A) e^{-|t-t'|/\tau_p} \right]. \quad (\text{E.14})$$

Publications and Presentations

Publications

- Hans Vandebroek and Carlo Vanderzande. Transient behaviour of a polymer dragged through a viscoelastic medium. *The Journal of Chemical Physics*, 141(11):114910, 2014.
- Hans Vandebroek and Carlo Vanderzande. Dynamics of a polymer in an active and viscoelastic bath. *Physical Review E*, 92(6):060601, 2015.
- Hans Vandebroek and Carlo Vanderzande. On the generalized Langevin equation for a Rouse bead in a nonequilibrium bath. Submitted to *Journal of Statistical Physics* in October 2016. *arXiv:1610.07433*, 2016.
- Hans Vandebroek and Carlo Vanderzande. The effect of active fluctuations on the dynamics of particles, motors and hairpins. Submitted to *Soft Matter* in November 2016. *arXiv:1611.02123*, 2016.

Poster presentations

- *Dynamics of a polymer pulled through a viscous medium*. Venice meeting on fluctuations in small complex systems II, Venice, 10-13 October 2014.
- *Dynamics of a polymer in an active and viscoelastic bath*. Topical research meeting on physical principles of biological and active systems, Edinburgh, 6-7 January 2016.
- *Dynamics of a polymer in an active and viscoelastic bath*. StatPhys26, Lyon, 18-22 July 2016.

Talks

- *Polymer dynamics in viscoelastic active baths*. Annual Scientific Meeting of the Belgian Physical Society, Liège, 13 May 2015.
- *Active processes*. Theory at Sea, Oostende, 25-26 May 2016.

Bibliography

- [1] Isaac Newton. *Philosophiæ naturalis principia mathematica*, london 1687. *English translation: Sir Isaac Newton's Mathematical Principles*, Univ. of Calif. Press, Berkeley, 1966.
- [2] Pierre Simon Laplace and Pierre Simon. A philosophical essay on probabilities, translated from the 6th french edition by frederick wilson truscott and frederick lincoln emory, 1951.
- [3] Robert E Ulanowicz. *Growth and Development: Ecosystems phenomenology*. Springer Science & Business Media, 1986.
- [4] Benjamin Lewin. *Cells*. Jones & Bartlett Learning, 2007.
- [5] Paul J Flory. *Principles of polymer chemistry*. Cornell University Press, 1953.
- [6] Pierre-Gilles De Gennes. *Scaling concepts in polymer physics*. Cornell university press, 1979.
- [7] M. Doi and Edwards S. F. *The Theory of Polymer Dynamics*. Oxford University, New York, 1986.
- [8] A Yu Grosberg and AR Khokhlov. *Statistical mechanics of macromolecules*. AIP: Woodbury, NY, 1994.
- [9] Charles Darwin. The origin of species by means of natural selection, or, the preservation of favored races in the struggle for life. vol. 1. *International Science Library*, 1897.
- [10] James D Watson, Francis HC Crick, et al. Molecular structure of nucleic acids. *Nature*, 171(4356):737–738, 1953.
- [11] M Cristina Marchetti, Yaouen Fily, Silke Henkes, Adam Patch, and David Yllanes. Structure and mechanics of active colloids. *arXiv preprint arXiv:1510.00425*, 2015.
- [12] I Goychuk and P Hänggi. Anomalous escape governed by thermal 1/f noise. *Physical review letters*, 99(20):200601, 2007.

- [13] Payam Rowghanian and Alexander Y Grosberg. Propagation of tension along a polymer chain. *Physical Review E*, 86(1):011803, 2012.
- [14] Takahiro Sakaue, Takuya Saito, and Hirofumi Wada. Dragging a polymer in a viscous fluid: Steady state and transient. *Physical Review E*, 86(1):011804, 2012.
- [15] A Ghosh and NS Gov. Dynamics of active semiflexible polymers. *Biophysical journal*, 107(5):1065–1073, 2014.
- [16] Stephanie C Weber, Julie A Theriot, and Andrew J Spakowitz. Subdiffusive motion of a polymer composed of subdiffusive monomers. *Physical Review E*, 82(1):011913, 2010.
- [17] Claudio Maggi, Matteo Paoluzzi, Nicola Pellicciotta, Alessia Lepore, Luca Angelani, and Roberto Di Leonardo. Generalized energy equipartition in harmonic oscillators driven by active baths. *Physical review letters*, 113(23):238303, 2014.
- [18] Nikta Fakhri, Alok D Wessel, Charlotte Willms, Matteo Pasquali, Dieter R Klopfenstein, Frederick C MacKintosh, and Christoph F Schmidt. High-resolution mapping of intracellular fluctuations using carbon nanotubes. *Science*, 344(6187):1031–1035, 2014.
- [19] Avelino Javer, Nathan J Kuwada, Zhicheng Long, Vincenzo G Benza, Kevin D Dorfman, Paul A Wiggins, Pietro Cicuta, and Marco Cosentino Lagomarsino. Persistent super-diffusive motion of escherichia coli chromosomal loci. *Nature communications*, 5, 2014.
- [20] Diana Goldstein, Tal Elhanan, Maria Aronovitch, and Daphne Weihs. Origin of active transport in breast-cancer cells. *Soft Matter*, 9(29):7167–7173, 2013.
- [21] Clifford P Brangwynne, Gijsje H Koenderink, Frederick C MacKintosh, and David A Weitz. Nonequilibrium microtubule fluctuations in a model cytoskeleton. *Physical review letters*, 100(11):118104, 2008.
- [22] Venkataraman Balakrishnan. *Elements of Nonequilibrium Statistical Mechanics*. Ane Books, 2008.
- [23] Thijs Becker. *Diffusion of interacting particle in confined geometries: a random walk approach*. Hasselt University, 2015.
- [24] W Coffey, Yu P Kalmykov, and JT Waldron. The langevin equation: with applications to stochastic problems in physics. *Chemistry and Electrical Engineering. World Scientific*, 2004.
- [25] Stephen G Brush. The kind of motion we call heat. 1976.
- [26] Robert Zwanzig. *Nonequilibrium statistical mechanics*. Oxford University Press, 2001.
- [27] Mark Tuckerman. *Statistical mechanics: theory and molecular simulation*. Oxford University Press, 2010.

- [28] Robert Brown. XXVII. a brief account of microscopical observations made in the months of june, july and august 1827, on the particles contained in the pollen of plants; and on the general existence of active molecules in organic and inorganic bodies. *Philosophical Magazine Series 2*, 4(21):161–173, 1828.
- [29] Francis Darwin. *Charles Darwin: his life told in an autobiographical chapter, and in a selected series of his published letters*. 1908.
- [30] Wiener Christian. *Ann. Phys. [2]*, 118(79), 1863.
- [31] Cantoni Giovanni. *Reale Istituto Lombardo di Scienze e Lettere (Milano), Rendiconti [2]*, 1(56), 1868.
- [32] Albert Einstein. Über die von der molekularkinetischen theorie der wärme geforderte bewegung von in ruhenden flüssigkeiten suspendierten teilchen. *Annalen der physik*, 322(8):549–560, 1905.
- [33] Albert Einstein. Über einen die erzeugung und verwandlung des liches betreffenden heuristischen gesichtspunkt. *Annalen der physik*, 322(6):132–148, 1905.
- [34] Albert Einstein. Zur elektrodynamik bewegter körper. *Annalen der physik*, 322(10):891–921, 1905.
- [35] Albert Einstein. Ist die trägheit eines körpers von seinem energieinhalt abhängig? *Annalen der Physik*, 323(13):639–641, 1905.
- [36] Paul Arthur Schilpp, GÃ Kurt, et al. Albert einstein: philosopher-scientist. page 161, 1949.
- [37] Tongcang Li, Simon Kheifets, David Medellin, and Mark G Raizen. Measurement of the instantaneous velocity of a brownian particle. *Science*, 328(5986):1673–1675, 2010.
- [38] Louis Bachelier. Théorie de la spéculation. *Annales Scientifiques de l'École Normale Supérieure*, 3(17):21–86, 1900.
- [39] Marian Von Smoluchowski. Zur kinetischen theorie der brownischen molekularebewegung und der suspensionen. *Annalen der physik*, 326(14):756–780, 1906.
- [40] Paul Langevin. Sur la théorie du mouvement brownien. *CR Acad. Sci. Paris*, 146(530-533):530, 1908.
- [41] Theodor Svedberg. *Studien zur Lehre von den kolloiden Lösungen*. Akademische Buchdruckerei, 1907.
- [42] Victor Henri. Étude cinématographique des mouvements browniens. *Comptes rendus hebdomadaires des séances de l'académie des sciences*, 146:1024–1026, 1908.
- [43] Jean Perrin. La loi de stokes et le mouvement brownien. *Comptes rendus*, 147:475–476, 1908.

- [44] M Chaudesaigues. Le mouvement brownien et la formule d'Einstein. *CR*, 147: 1044–1046, 1908.
- [45] Ralph Howard Fowler. *Statistical Mechanics: The Theory of the Properties of Matter in Equilibrium; Based on an Essay Awarded the Adams Prize in the University of Cambridge, 1923-24*. The University Press, 1929.
- [46] Rep Kubo. The fluctuation-dissipation theorem. *Reports on progress in physics*, 29(1):255, 1966.
- [47] NG Van Kampen. Stochastic processes in chemistry and physics. *Amsterdam: North Holland*, 1, 1981.
- [48] Edward M Purcell. Life at low reynolds number. *Am. J. Phys*, 45(1):3–11, 1977.
- [49] AO Caldeira and AJ Leggett. Quantum tunnelling in a dissipative system. *Annals of Physics*, 149(2):374–456, 1983.
- [50] Richard Phillips Feynman and Frank Lee Vernon. The theory of a general quantum system interacting with a linear dissipative system. *Annals of physics*, 24:118–173, 1963.
- [51] Steven H Strogatz. *Nonlinear dynamics and chaos: with applications to physics, biology, chemistry, and engineering*. Westview press, 2014.
- [52] Matthias Weiss, Markus Elsner, Fredrik Kartberg, and Tommy Nilsson. Anomalous subdiffusion is a measure for cytoplasmic crowding in living cells. *Biophysical journal*, 87(5):3518–3524, 2004.
- [53] Iva Marija Tolić-Nørrelykke, Emilia-Laura Munteanu, Genevieve Thon, Lene Oddershede, and Kirstine Berg-Sørensen. Anomalous diffusion in living yeast cells. *Physical Review Letters*, 93(7):078102, 2004.
- [54] Ido Golding and Edward C Cox. Physical nature of bacterial cytoplasm. *Physical review letters*, 96(9):098102, 2006.
- [55] Matthias Weiss. Single-particle tracking data reveal anticorrelated fractional brownian motion in crowded fluids. *Physical Review E*, 88(1):010101, 2013.
- [56] Jae-Hyung Jeon and Ralf Metzler. Fractional brownian motion and motion governed by the fractional langevin equation in confined geometries. *Physical Review E*, 81(2):021103, 2010.
- [57] J. Clerk Maxwell. On the dynamical theory of gases. *Philosophical Transactions of the Royal Society of London*, 157:49–88, 1867.
- [58] Igor Goychuk. Viscoelastic subdiffusion: Generalized langevin equation approach. *Advances in Chemical Physics*, 150:187, 2012.
- [59] Andrew Gemant. A method of analyzing experimental results obtained from elasto-viscous bodies. *Journal of Applied Physics*, 7(8):311–317, 1936.

- [60] Kenneth S Cole and Robert H Cole. Dispersion and absorption in dielectrics I. alternating current characteristics. *The Journal of chemical physics*, 9(4): 341–351, 1941.
- [61] Govindan Rangarajan and Mingzhou Ding. *Processes with long-range correlations: Theory and applications*, volume 621. Springer Science & Business Media, 2003.
- [62] J Gladrow, N Fakhri, FC MacKintosh, CF Schmidt, and CP Broedersz. Broken detailed balance of filament dynamics in active networks. *Physical Review Letters*, 116(24):248301, 2016.
- [63] Fred C MacKintosh and Alex J Levine. Nonequilibrium mechanics and dynamics of motor-activated gels. *Physical review letters*, 100(1):018104, 2008.
- [64] Marina Soares e Silva, Björn Stuhmann, Timo Betz, and Gijsje H Koenderink. Time-resolved microrheology of actively remodeling actomyosin networks. *New Journal of Physics*, 16(7):075010, 2014.
- [65] Björn Stuhmann, Marina Soares e Silva, Martin Depken, Frederick C MacKintosh, and Gijsje H Koenderink. Nonequilibrium fluctuations of a remodeling in vitro cytoskeleton. *Physical Review E*, 86(2):020901, 2012.
- [66] Toshihiro Toyota, David A Head, Christoph F Schmidt, and Daisuke Mizuno. Non-gaussian athermal fluctuations in active gels. *Soft Matter*, 7(7):3234–3239, 2011.
- [67] Adar Sonn-Segev, Anne Bernheim-Groswasser, and Yael Roichman. Scale dependence of mechanics and dynamics of active gels with increasing motor concentration. *arXiv:1609.04163*, 2016.
- [68] Yaouen Fily and M Cristina Marchetti. Athermal phase separation of self-propelled particles with no alignment. *Physical review letters*, 108(23):235702, 2012.
- [69] AC Brańka and David M Heyes. Algorithms for brownian dynamics computer simulations: multivariable case. *Physical Review E*, 60(2):2381, 1999.
- [70] Andrei Nikolaevitch Kolmogorov. The wiener spiral and some other interesting curves in hilbert space. In *Dokl. Akad. Nauk SSSR*, volume 26, pages 115–118, 1940.
- [71] Benoit B Mandelbrot and John W Van Ness. Fractional brownian motions, fractional noises and applications. *SIAM review*, 10(4):422–437, 1968.
- [72] Jonathan RM Hosking. Modeling persistence in hydrological time series using fractional differencing. *Water resources research*, 20(12):1898–1908, 1984.
- [73] Ronald F Fox, Ian R Gatland, Rajarshi Roy, and Gautam Vemuri. Fast, accurate algorithm for numerical simulation of exponentially correlated colored noise. *Physical review A*, 38(11):5938, 1988.

- [74] Varsha Daftardar-Gejji and Hossein Jafari. Analysis of a system of nonautonomous fractional differential equations involving caputo derivatives. *Journal of Mathematical Analysis and Applications*, 328(2):1026–1033, 2007.
- [75] Ernst Hairer, SP Norsett, and G Wanner. *Solving Ordinary Differential Equations I Springer*. Berlin, 1993.
- [76] G Wanner and E Hairer. *Solving ordinary differential equations II*, volume 1. Springer-Verlag, Berlin, 1991.
- [77] Kai Diethelm, Neville J Ford, and Alan D Freed. A predictor-corrector approach for the numerical solution of fractional differential equations. *Nonlinear Dynamics*, 29(1-4):3–22, 2002.
- [78] Varsha Daftardar-Gejji, Yogita Sukale, and Sachin Bhalekar. A new predictor-corrector method for fractional differential equations. *Applied Mathematics and Computation*, 244:158–182, 2014.
- [79] Hans Vandebroek and Carlo Vanderzande. The effect of active fluctuations on the dynamics of particle, motors and hairpins. *arXiv:1611.02123*, 2016.
- [80] Avi Caspi, Rony Granek, and Michael Elbaum. Enhanced diffusion in active intracellular transport. *Physical Review Letters*, 85(26):5655, 2000.
- [81] Naama Gal and Daphne Weihs. Intracellular mechanics and activity of breast cancer cells correlate with metastatic potential. *Cell biochemistry and biophysics*, 63(3):199–209, 2012.
- [82] Julia F Reverey, Jae-Hyung Jeon, Han Bao, Matthias Leippe, Ralf Metzler, and Christine Selhuber-Unkel. Superdiffusion dominates intracellular particle motion in the supercrowded cytoplasm of pathogenic *acanthamoeba castellanii*. *Scientific Reports*, 5, 2015.
- [83] William O Hancock. The kinesin-1 chemomechanical cycle: Stepping toward a consensus. *Biophysical journal*, 110(6):1216–1225, 2016.
- [84] Matthew L Kutys, John Fricks, and William O Hancock. Monte carlo analysis of neck linker extension in kinesin molecular motors. *PLoS Comput Biol*, 6(11):e1000980, 2010.
- [85] Dawen Cai, Kristen J Verhey, and Edgar Meyhöfer. Tracking single kinesin molecules in the cytoplasm of mammalian cells. *Biophysical Journal*, 92(12):4137–4144, 2007.
- [86] David B Hill, MJ Plaza, K Bonin, and G Holzwarth. Fast vesicle transport in pc12 neurites: velocities and forces. *European Biophysics Journal*, 33(7):623–632, 2004.
- [87] Srabanti Chaudhury and Binny J Cherayil. Complex chemical kinetics in single enzyme molecules: Kramers’s model with fractional gaussian noise. *The Journal of chemical physics*, 125(2):024904, 2006.

- [88] Hendrik Anthony Kramers. Brownian motion in a field of force and the diffusion model of chemical reactions. *Physica*, 7(4):284–304, 1940.
- [89] Peter Hänggi, Peter Talkner, and Michal Borkovec. Reaction-rate theory: fifty years after kramers. *Reviews of modern physics*, 62(2):251, 1990.
- [90] Richard F Grote and James T Hynes. The stable states picture of chemical reactions. II. rate constants for condensed and gas phase reaction models. *The Journal of Chemical Physics*, 73(6):2715–2732, 1980.
- [91] Eli Pollak. Theory of activated rate processes: A new derivation of kramers' expression. *The Journal of chemical physics*, 85(2):865–867, 1986.
- [92] Wei Min and X Sunney Xie. Kramers model with a power-law friction kernel: Dispersed kinetics and dynamic disorder of biochemical reactions. *Physical Review E*, 73(1):010902, 2006.
- [93] Igor Goychuk. Viscoelastic subdiffusion: from anomalous to normal. *Physical Review E*, 80(4):046125, 2009.
- [94] Étienne Fodor, Cesare Nardini, Mike E Cates, Julien Tailleur, Paolo Visco, and Frédéric van Wijland. How far from equilibrium is active matter? *arXiv preprint arXiv:1604.00953*, 2016.
- [95] Alessandro Borgia, Philip M Williams, and Jane Clarke. Single-molecule studies of protein folding. *Annu. Rev. Biochem.*, 77:101–125, 2008.
- [96] Michael T Woodside, Cuauhtémoc García-García, and Steven M Block. Folding and unfolding single rna molecules under tension. *Current opinion in chemical biology*, 12(6):640–646, 2008.
- [97] Krishna Neupane, Dustin B Ritchie, Hao Yu, Daniel AN Foster, Feng Wang, and Michael T Woodside. Transition path times for nucleic acid folding determined from energy-landscape analysis of single-molecule trajectories. *Physical review letters*, 109(6):068102, 2012.
- [98] Hans Vandebroek and Carlo Vanderzande. Transient behaviour of a polymer dragged through a viscoelastic medium. *The Journal of chemical physics*, 141(11):114910, 2014.
- [99] Hans Vandebroek and Carlo Vanderzande. Dynamics of a polymer in an active and viscoelastic bath. *Physical Review E*, 92(6):060601, 2015.
- [100] Jian Liu. The ghost in the machine: is the bacterial chromosome a phantom chain? *Biophysical journal*, 108(1):20–21, 2015.
- [101] Prince E Rouse Jr. A theory of the linear viscoelastic properties of dilute solutions of coiling polymers. *The Journal of Chemical Physics*, 21(7):1272–1280, 1953.

- [102] Vivek V Thacker, Krystyna Bromek, Benoit Meijer, Jurij Kotar, Bianca Sclavi, Marco Cosentino Lagomarsino, Ulrich F Keyser, and Pietro Cicuta. Bacterial nucleoid structure probed by active drag and resistive pulse sensing. *Integrative Biology*, 6(2):184–191, 2014.
- [103] F Brochard-Wyart. Europhys lett 23: 105. *Brochard-Wyart F, Hervet H, Pincus P (1994) Europhys Lett*, 26:511, 1993.
- [104] Francoise Brochard-Wyart. Polymer chains under strong flows: stems and flowers. *EPL (Europhysics Letters)*, 30(7):387, 1995.
- [105] Thomas T Perkins, Douglas E Smith, and Steven Chu. Single polymer dynamics in an elongational flow. *Science*, 276(5321):2016–2021, 1997.
- [106] RG Larson, TT Perkins, DE Smith, and S Chu. The hydrodynamics of a DNA molecule in a flow field. In *Flexible Polymer Chains in Elongational Flow*, pages 259–282. Springer, 1999.
- [107] Thomas T Perkins, Douglas E Smith, Ronald G Larson, and Steven Chu. Stretching of a single tethered polymer in a uniform flow. *Science*, 268(5207):83, 1995.
- [108] R. G. Larson, T. T. Perkins, D. E. Smith, and S. Chu. Hydrodynamics of a dna molecule in a flow field. *Physical Review E*, 55:1794, 1997.
- [109] Damien Robert, Thi-Hanh Nguyen, François Gallet, and Claire Wilhelm. In vivo determination of fluctuating forces during endosome trafficking using a combination of active and passive microrheology. *PLoS one*, 5(4):e10046, 2010.
- [110] F Brochard-Wyart. Deformations of one tethered chain in strong flows. *EPL (Europhysics Letters)*, 23(2):105, 1993.
- [111] Alex J Levine and FC MacKintosh. The mechanics and fluctuation spectrum of active gels. *The Journal of Physical Chemistry B*, 113(12):3820–3830, 2009.
- [112] Stephanie C Weber, Andrew J Spakowitz, and Julie A Theriot. Nonthermal atp-dependent fluctuations contribute to the in vivo motion of chromosomal loci. *Proceedings of the National Academy of Sciences*, 109(19):7338–7343, 2012.
- [113] Alberto Pérez, F Javier Luque, and Modesto Orozco. Frontiers in molecular dynamics simulations of dna. *Accounts of chemical research*, 45(2):196–205, 2011.
- [114] Martin Karplus and J Andrew McCammon. Molecular dynamics simulations of biomolecules. *Nature Structural & Molecular Biology*, 9(9):646–652, 2002.
- [115] Alexander D Mackerell and Nilesh K Banavali. All-atom empirical force field for nucleic acids: II. application to molecular dynamics simulations of dna and rna in solution. *Journal of Computational Chemistry*, 21(2):105–120, 2000.
- [116] Carlo Vanderzande. *Lattice models of polymers*, volume 11. Cambridge University Press, 1998.

- [117] Bruno H Zimm. Dynamics of polymer molecules in dilute solution: viscoelasticity, flow birefringence and dielectric loss. *The journal of chemical physics*, 24(2):269–278, 1956.
- [118] Gary S Grest and Kurt Kremer. Molecular dynamics simulation for polymers in the presence of a heat bath. *Physical Review A*, 33(5):3628, 1986.
- [119] Chase P Broedersz and Fred C MacKintosh. Modeling semiflexible polymer networks. *Reviews of Modern Physics*, 86(3):995, 2014.
- [120] Sanneke Brinkers, Heidelinde RC Dietrich, Frederik H de Groot, Ian T Young, and Bernd Rieger. The persistence length of double stranded dna determined using dark field tethered particle motion. *The Journal of chemical physics*, 130(21):215105, 2009.
- [121] MGL Van Den Heuvel, S Bolhuis, and C Dekker. Persistence length measurements from stochastic single-microtubule trajectories. *Nano letters*, 7(10):3138–3144, 2007.
- [122] Michael E Fisher. Magnetism in one-dimensional systems - the heisenberg model for infinite spin. *American Journal of Physics*, 32(5):343–346, 1964.
- [123] M Rubinstein and Ralph H Colby. Polymer physics. 2003. *NEW YORK: Oxford University*.
- [124] Robert Alexander Adams. *Calculus*. Addison-Wesley, 1991.
- [125] WJ Briels. Theory of polymer dynamics. *Lecture Notes; Uppsala University: Uppsala, Sweden*, 1994.
- [126] Debabrata Panja. Generalized langevin equation formulation for anomalous polymer dynamics. *Journal of Statistical Mechanics: Theory and Experiment*, 2010(02):L02001, 2010.
- [127] Takahiro Sakaue. Memory effect and fluctuating anomalous dynamics of a tagged monomer. *Physical Review E*, 87(4):040601, 2013.
- [128] Hans Vandebroek and Carlo Vanderzande. On the generalized langevin equation for a rouse bead in a nonequilibrium bath. *arXiv:1610.07433*, 2016.
- [129] Christian Maes. On the second fluctuation–dissipation theorem for nonequilibrium baths. *Journal of Statistical Physics*, 154(3):705–722, 2014.
- [130] Jennifer L Ross. The dark matter of biology. *Biophysical Journal*, 111(5):909–916, 2016.
- [131] Koret Hirschberg, Chad M Miller, Jan Ellenberg, John F Presley, Eric D Siggia, Robert D Phair, and Jennifer Lippincott-Schwartz. Kinetic analysis of secretory protein traffic and characterization of golgi to plasma membrane transport intermediates in living cells. *The Journal of cell biology*, 143(6):1485–1503, 1998.
- [132] GM Mittag-Leffler. Sur la nouvelle fonction $E_\alpha(x)$. *CR Acad. Sci. Paris*, 137:554–558, 1903.

- [133] Adders Wiman. Über den fundamentalsatz in der theorie der funktionen $E_\alpha(x)$. *Acta Mathematica*, 29(1):191–201, 1905.
- [134] Hans J Haubold, Arak M Mathai, and Ram K Saxena. Mittag-leffler functions and their applications. *Journal of Applied Mathematics*, 2011, 2011.
- [135] Agnieszka Malinowska and Delfim Torres. Fractional calculus of variations for a combined caputo derivative. *Fractional Calculus and Applied Analysis*, 14(4): 523–537, 2011.
- [136] Bruce J West. Colloquium: Fractional calculus view of complexity: A tutorial. *Reviews of Modern Physics*, 86(4):1169, 2014.
- [137] Michele Caputo. Linear models of dissipation whose Q is almost frequency independent-II. *Geophysical Journal International*, 13(5):529–539, 1967.